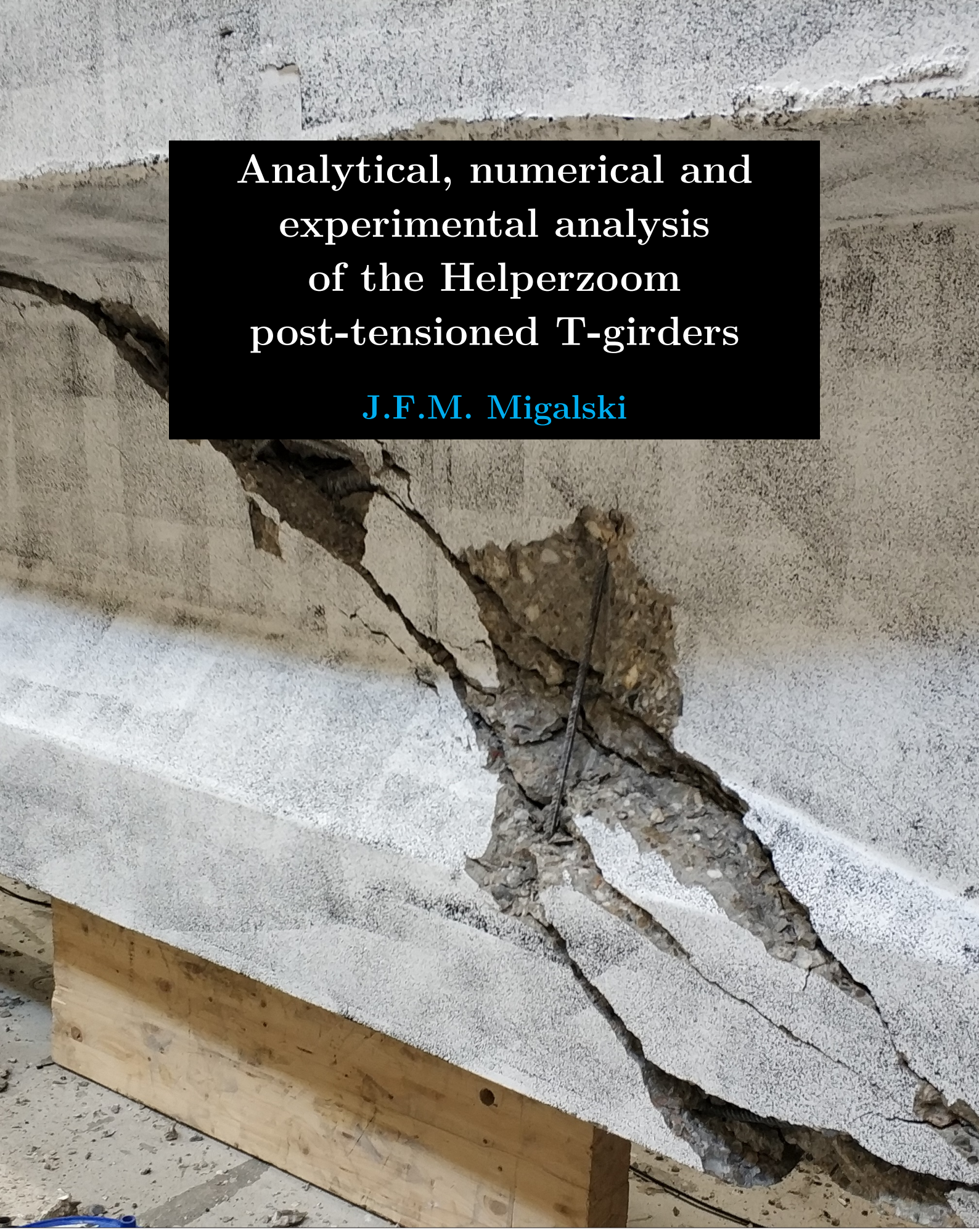

Analytical, numerical and experimental analysis of the Helperzoom post-tensioned T-girders

J.F.M. Migalski

TU Delft Delft University of Technology

Challenge the future

Analytical, Numerical and Experimental Analysis of the Helperzoom Post-Tensioned T-Girders

Analyzing the shear capacity and failure mode of thin-webbed post-tensioned bulb-T-shaped girders with non-code-compliant stirrups

by

J.F.M. Migalski

to obtain the degree of Master of Science

at the Delft University of Technology,

to be defended publicly on Friday February 21, 2020 at 3:00 PM.

Student number:	4102177	
Project duration:	March 1, 2019 – February, 2020	
Thesis committee:	Dr. ir. M.A.N. Hendriks,	TU Delft
	Dr. ir. Y. Yang,	TU Delft
	Dr. ir. E.O.L. Lantsoght,	TU Delft
	Ir. J.M. Houben,	TU Delft

TU Delft

Preface

During my study I gained experience, motivation and interest in civil structures and in particular concrete structures. I followed a mid-term internship with the construction combination BAM-TBI, where I worked on a connection road between Goes and Gent by means of an excavation tunnel. My bachelor graduation project I worked on a simply supported prestressed deck, which was my first experience with prestressed concrete. The relationship between models and practice appeals to me and will be present in this thesis.

First of all I want to thank Cor van der Veen for giving me the opportunity to carry out this research. This was the first topic he suggested and while finishing up my thesis in this final step of my study I am glad I took it.

Furthermore, I would like to thank my graduation committee and in particular Eva Lantsoght for the great effort and motivation she gave me with her feedback and meetings. This really helped me through this difficult time of my study.

I also want to thank my parents for giving me the opportunity to follow a master track at TU Delft and for the financial support during my time in Delft and my fellow students for the great time and studying together during the my pre-master "Structural Engineering" and master track "Concrete Structures".

J.F.M. Migalski
Delft, January 2020

Abstract

The Helperzoom bridge is one of few existing prestressed slab-between-girder bridges that is being managed by Rijkswaterstaat. These bridges are built before 1980 and do not comply with the current standards. To evaluate the structural safety and capacity these bridges are being assessed. A total of four girders were taken from the Helperzoom bridge, named HPZ1 through HPZ4, and have been destructively tested at TU Delft to determine the shear capacity and failure mode. The first two experiments, HPZ1 and HPZ2, have been considered in this research. Shear-tension failure is one of the failure modes that was being looked for and where the experiments were based on.

The most important results of HPZ1 and HPZ2 have been combined and summarized in the experimental analysis, such as the failure load, the failure mechanism, the load at which the first inclined crack occurred, the cracking angles of the observed cracks, the calculated inclinations of the compression field from the LVDT measurements, the contribution of the shear reinforcement and the contribution of the prestressing cables to the shear capacity. Remarkably, the outcome of the test resulted in shear-compression/flexure-shear failure instead of the predicted shear-tension failure. The purpose of this thesis is to check whether the observed shear capacity and failure mode from HPZ1 and HPZ2 can be validated with existing models that are currently used by (inter)national standards and numerical programs.

The Euler-Bernoulli beam theory and five (inter)national codes: ACI 318-14 (American Concrete Institute), AASHTO 8th Edition (American Association of State Highway and Transportation Officials), NEN-EN 1992-1-1:2011 (Eurocode 2), RBK 1.1:2013 (Richtlijnen Bestaande Kunstwerken) and EC2 draft 2018 (prEN 1992-1-1:2018 D3), have been used to calculate the shear capacity and if possible the failure mode of the Helperzoom girders. Next to the nominal shear resistance, failure of the compression field is considered for three codes: AASHTO, EC2 and EC2 draft 2018. For the two Eurocodes the value of the inclination of the compression field can be chosen by the user: the EC2 has a lower limit of $\theta = 21.8°$, the lower limit of the EC2 draft 2018 (based on state of strains) is reached when θ is chosen such that failure of the compression field occurs simultaneously with yielding of the stirrups. For the EC2 draft 2018 different ways have been used to determine the longitudinal strain: with the expression given in the code, analytically determined with a sectional analysis and with the results of the LVDTs in the two experiments. In addition to the analytical calculations, a non-linear finite element program `Response-2010` has been used, with which a cross-sectional analysis was made with two values for the prestressing force. With this program it is easy to determine the maximum shear capacity, the failure mechanism and many other results per loading step, such as the inclination θ, acting and maximum compressive- and tensile stresses, strains, etc. The maximum shear capacity is divided into components: the contribution of the uncracked concrete, cracked concrete, transverse reinforcement and a vertical prestressing force.

Four different shear capacities have been calculated: the inclined cracking load, the nominal shear resistance according to the general procedures of the design codes, failure of the compression field and the moment that failure of the compression field occurs simultaneously with yielding of the stirrups. The Euler-Bernoulli beam theory, ACI (flexure-shear) and `Response-2010` show that the load for the first inclined crack are close to the results of HPZ1 and HPZ2. For the nominal shear capacity, none of the codes nor `Response-2010` are in line with the results of the two tests: all shear capacities are underestimated. The AASHTO overestimates the shear capacity for failure of the compression field, because the inclination θ is not included in the expression. The EC2 overestimates failure of the compression field due to limitation of $\theta = 21.8°$. The EC2 draft 2018 allows for lower values for θ, when the longitudinal strains are based on the state of strains with $\theta \leq 19.08°$. The results for the shear capacity and inclination of the compression field of the latter design code are much more in line with the observed failure loads and inclinations calculated from the LVDTs. The lower limit for the shear capacity is when failure of the compression field occurs simultaneously with yielding of the stirrups. With this limit, the shear capacity is underestimated and the inclination of the compression field is lower than the inclination calculated from the LVDTs.

The results between the three analyses have been compared with each other and it was concluded that there are major differences between the analyses for the calculated shear capacities, internal lever arms, critical positions and the inclinations of the compression field. None of the results from the codes match the observed failure load in the experiments. Considering the expressions given for failure of the compression field, the EC draft 2018 based on the state of strains were closest to the test results for both the shear capacity and the calculated inclinations of the compression field from the LVDTs. The moment that yielding of the stirrups occurs simultaneously with failure of the compression field, the EC2 draft 2018 gave too low values for the shear capacity. For the numerical results, `Response-2010` gave a representative shear force for the first inclined crack and failure mechanism, but not for the ultimate shear capacity. After the onset of the first inclined crack, the girder did not build up extra capacity as was observed in the experiments. The critical position was also not in line with the results from the test. It can be concluded that the results should always be looked at from a critical point of view and that no clear answer can be given as to which analysis is the "best" to determine the shear capacity of (prestressed) concrete T-girders. For the Helperzoom girders the EC2 draft 2018 based on the state of strains with $\theta \leq 19.08°$ gave the best results for the shear capacity.

Table of Contents

List of Figures

List of Tables

List of Notations

Roman lower case

a	shear span
a_{cs}	effective shear span with respect to the control section
a_g	maximum aggregate size
a_i	perpendicular distance to the centroid of a considered element to the neutral axis
a_v	clear shear span or mechanical shear span
b	width of the beam
b_{cf} , b_{tfl}	width of compression- / top flange
b_D	width of the compressive strut
b_n	clear width of the beam
b_w , b_v	web width
$b_{w,gem}$	average width of the beam
c	distance between the neutral axis and the extreme compression fibre
d	effective depth of a cross-section
d_{dg}	factor for the failure zone roughness and aggregate properties for the concrete type
d_e	average effective depth of a cross-section for prestressed and nonprestressed steel in the most tension side
d_{mean}	average effective depth of a cross-section
d_p	effective depth of the prestressing steel
d_s , d	effective depth of the longitudinal tension reinforcement
d'_s	effective depth of the longitudinal compression reinforcement
d_v	effective shear depth between the tensile and compressive forces due to flexure
e_p	eccentricity of the prestressing tendons
f_c	compressive strength of concrete
$f_{c,red}$	reduced compressive strength of concrete
f'_c	specified compressive strength of concrete at 28 days
f_{cd}	design compressive strength of concrete
f_{ck}	characteristic compressive cylinder strength of concrete at 28 days
$f_{ck,cube}$	characteristic compressive cubic strength of concrete at 28 days
f_{cm}	mean value of concrete cylinder compressive strength
$f_{cm,cube}$	mean value of concrete cubic compressive strength
f_{cr}	cracking strength of concrete
f_{ct}	tensile strength of concrete
f_{ctd}	design axial tensile strength of concrete
f_{ctk}	characteristic axial tensile strength of concrete
$f_{ctk,0.05}$	5% fractile for characteristic axial tensile strength of concrete
f_{ctm}	mean value of axial tensile strength of concrete
$f_{ctm,sp}$	mean value of splitting tensile strength of concrete
f_{pd}	design tensile strength of prestressing steel
f_{pk}	characteristic tensile strength of prestressing steel
$f_{p0.1k}$	characteristic 0.1% proof-stress of prestressing steel
f_{po}	value for the difference in stress in the prestressing steel and concrete
f_{ps}	average stress in prestressing steel
f_{pu}	specified or ultimate tensile strength of the prestressing steel
f_{py}	yield strength of the prestressing steel
f_r	modulus of rupture of concrete
f_s	average stress in longitudinal tension reinforcement
f'_s	average stress in longitudinal compression reinforcement

f_y	yield strength of reinforcement
f_{yd}	design yield strength of reinforcement
f_{yk}	characteristic yield strength of reinforcement
f_{ym}	average yield strength of reinforcement
f_{ywm}	average yield strength of transversal reinforcement
f_{yx}	stress in the longitudinal reinforcement
f_{yz}	stress in the transversal reinforcement
f_{ywd} , f_{yt}	design yield strength of shear reinforcement
h	height
h_f , h_{tfl}	height of the compression- / top flange
k	factor for the stress in prestressing steel at nominal flexural resistance
k_{EC2}	size-effect coefficient
k_1	factor for the stress in prestressing steel
k_{cap}	factor for massive plates
l_{pt} , l_{pt2}	transmission length for prestressing force
n	amount of, as integer $\mathbb{Z}$
q_{DL}	distributed load due to dead load
q_{girder}	distributed load due to self-weight and dead load
r_u	non-dimensional relative strength
s	horizontal spacing
s_{theta}	diagonal crack spacing
s_x	crack spacing parameter
s_{xe}	crack spacing parameter influenced by the aggregate size
w	crack width
x	height of the concrete compression zone
x	considered cross-section or position of the external load from left support
y_t	distance from the centroidal axis to extreme fibers in tension
z	internal lever arm between the forces in the top- and bottom chord
z_{bottom}	distance from neutral axis to the extreme bottom fiber
z_{top}	distance from neutral axis to the extreme top fiber

Roman upper case

A	cross-sectional area
A_c	cross-sectional area of concrete
$A_{c,projected}$	projected cross-section for RBK
A_{ct}	cross-sectional area of concrete in the flexural tension side
A_D	cross-sectional area of the compressive strut
A_{equi}	equivalent cross-sectional area for transversal reinforcement
A_p , A_{ps}	area of a prestressing tendon or tendons
A_s , A_{sl}	area of the longitudinal tension reinforcement
A_{sc}	cross-sectional area of longitudinal reinforcement in the flexural compression chord
A_{st}	cross-sectional area of longitudinal reinforcement in the flexural tension chord
A'_s	area of the longitudinal compression reinforcement
A_{sw} , A_v	cross-sectional area of shear reinforcement within distance s
B	width of the HPZ girder
$C_{Rd,c}$	design value of factor for the shear resistance of concrete
$C_{Rk,c}$	5% lower bound value of factor for the shear resistance of concrete
$C_{Rm,c}$	mean value of factor for the shear resistance of concrete
D_{lower}	smallest value of the maximum diameter of the aggregates
D_{max}	maximum diameter of the aggregates
E_c	modulus of elasticity of concrete
E_p	design value of modulus of elasticity of prestressing steel
E_s	design value of modulus of elasticity of reinforcing steel
F_{cd}	design value for the force in the flexural compression chord
F_{exp}	value of the external load

$F_{sw,tot}$	total force from self-weight and dead load
F_T	value for the force in the flexural tension chord
$F_{T,max}$	maximum allowable value for the force in the flexural tension chord
F_{td}	design value for the force in the flexural tension chord
I_c	section modulus of the concrete member
L	length of a beam, girder or element
L_{span}	span length
M_0	decompression moment
M_{cr}	cracking moment, the moment that the stress exceeds the tensile strength
M_d	bending moment caused by dowel action
M_E	value for the internal bending moment with load- and resistance factors set to 1.0
M_{Ed}	design value for the applied internal bending moment
$M_{Ed,max}$	design value for the maximum internal bending moment
M_F	moment due to the external load
M_{fl}	flexural capacity for the applied internal bending moment
M_n , M_x	nominal flexural resistance at the considered cross-section
M_p	bending moment caused by an eccentric prestressing force
M_{Rd}	design value for the moment resistance
M_{sw}	moment due to self-weight
M_{sw+p}	moment due to self-weight and prestressing force
M_{tot}	total moment due to self-weight, prestressing force and external load
M_u	factored moment at cross-section
N_{avg}	average axial compressive force
N_E	value for the axial force with load- and resistance factors set to 1.0
N_{Ed}	design value for the axial force
N_{Edw}	design value for the web that can resist a portion of the axial compressive force
N_{Ew}	value for the web that can resist a portion of the axial compressive force
N_T	tensile force in the tensile tie
N_u	factored axial force at considered cross-section, negative for compression
N_V	value for the additional tensile force from the sectional shear force
N_{Vd}	design value for the additional tensile force from the sectional shear force
P_m , N_p	average prestressing force
R_{west}	support reaction for west support
R_n	contribution of the prestressing force to the shear resistance
R_{east}	support reaction for east support
S_c	section modulus of the concrete member
V_c	shear strength provided by the concrete
$V_{c,AI}$	contribution of the aggregate interlock of the cracked concrete
V_{cc}	contribution of the uncracked concrete
V_{ci}	shear strength provided by the concrete for flexural-shear-cracking
V_{cw}	shear strength provided by the concrete for web-shear-cracking
V_d	dowel shear force
$V_{d,max}$	maximum shear force dowel action can resist
V_E	value for the applied shear force with load- and resistance factors set to 1.0
V_{Ed}	design value for the applied shear force
V_F	shear force due to the external load
V_{flex}	shear strength provided by the concrete for flexural cracking
V_n , V_x	nominal shear resistance at the considered cross-section
V_p	vertical component of the prestressing force at section
V_R	mean value for the (total) shear resistance
V_{Rd}	design value for the shear resistance
$V_{Rd,c}$	design value for the shear resistance of concrete
$V_{Rd,STC}$	design value for the shear-tension capacity
$V_{Rd,FSC}$	design value for the flexural-shear capacity
$V_{Rd,max}$	design value for crushing of the concrete
$V_{Rd,s}$	design value for the strength of the shear reinforcement

$V_{Rd,shear}$	design value for the governing shear failure mode
$V_{Rk,c}$	characteristic value for the shear resistance of concrete
V_{Rm}	mean value for the shear resistance
$V_{Rm,c}$	mean value for the shear resistance of concrete
$V_{Rm,max}$	mean value for crushing of the concrete
$V_{Rm,s}$	mean value for the contribution of the stirrups to the shear resistance
V_s	shear strength provided by the shear reinforcement
V_{sw}	shear force due to self-weight
V_{sw+p}	shear force due to self-weight and prestressing force
V_{tot}	total shear force due to self-weight, prestressing force and external load
V_u	factored shear force at cross-section
W_c	moment of resistance of the concrete

Greek lower case

α_1	stress block factors
α	angle between the stirrups and the longitudinal axis
α_{cw}	factor to include the effect of the prestressing force
α_l	factor for transition length for prestressing steel
α_{photo}	measured angle of the shear crack from photographs taken during the experiments
β	factor to indicate if diagonally cracked concrete can transmit tension and shear
β_1	stress block factor
γ_c	material factor for concrete
γ_p	material factor for prestressing steel
γ_s	material factor for reinforcement steel
γ_{xy}	shear strain
ε	strain
ε_1	principal tensile strain
ε_2	principal compressive strain
ε_c	compressive strain in the concrete
ε_{c2}	compressive strain in the concrete at f_{ck} or f_{cd} for the parabola-rectangle diagram
ε_{cr}	strain in the concrete at the cracking moment
ε_p	strain of the prestressing steel
$\varepsilon_{p\infty}$	strain of the prestressing steel including prestressing losses
ε_s	net longitudinal tensile strain in the section at the centroid of the tension reinforcement
ε_x	average strain in longitudinal direction at mid depth of the girder or average strain between the top- and bottom chord
ε_{xc}	strain in the flexural compression chord
ε_{xt}	strain in the flexural tension chord
ε_z	average strain in transversal direction
ε_{uk}	characteristic strain of reinforcement or prestressing steel at maximum load
η	factor for the simplified rectangular stress distribution for concrete in compression
θ	inclination of the compression field
θ_{LVDT}	calculated inclination of the compression field from the LVDT measurements
θ_{min}	minimal inclination of the compression field
λ	factor for the simplified rectangular stress distribution for concrete in compression
ν	strength reduction factor for concrete cracked in shear
ν_1	strength reduction factor for concrete cracked in shear
ν_{cw}	shear stress in the concrete for web-shear-cracking
ξ	size-effect coefficient
ρ_x , ρ_l	longitudinal reinforcement ratio
ρ_z , ρ_w	transverse/shear reinforcement ratio
$\rho_{w,min}$	minimum transverse/shear reinforcement ratio
σ_1 , f_1	principle tensile stress in the concrete
σ_2 , f_2	principle compressive stress in the concrete

σ_c	stress in the concrete
$\sigma_{c,max}$	maximum allowable stress in the concrete compression field
σ_{cb}	stress in the concrete in the most outer fibre of the bottom flange
σ_{cd}	design value for the maximum compressive stress in the concrete compressive strut
σ_{cD}	stress in the concrete compressive strut
σ_{cp} , f_{pc}	compressive stress in concrete due to prestress forces only at the centroid of the cross-section
σ_{ct}	stress in the concrete in the most outer fibre of the top flange
$\sigma_{p\infty}$	stress in the prestressing steel including prestressing losses
σ_{pe} , f_{pe}	compressive stress in concrete due to prestress forces only at the extreme tensile fiber of section
σ_{pi}	maximum allowable initial prestressing stress
σ_{pm}	average ultimate strength of prestressing steel
σ_{sw}	stress in the transversal reinforcement
σ_{sx}, f_{sx}	average reinforcement steel stress in longitudinal direction
σ_{sz}, f_{sz}	average reinforcement steel stress in transversal direction
$\sigma_{sx,cr}, f_{sx,cr}$	reinforcement steel stress in the crack in longitudinal direction
$\sigma_{sz,cr}, f_{sz,cr}$	reinforcement steel stress in the crack transversal direction
σ_x , f_x	applied average stress in longitudinal direction
σ_z , f_z	applied average stress in transversal direction
τ	applied shear stress
τ_{ci}	concrete stress transferred by aggregate interlock
$\tau_{ci,max}$	maximum concrete stress transferred by aggregate interlock
τ_{Ed}	design value acting shear stress
$\tau_{Rd,c}$	design value for the shear stress resistance
$\tau_{Rdc,min}$	design value for the minimum shear stress resistance
$\tau_{Rm,c}$	mean value for the shear stress resistance
$\tau_{Rmc,min}$	mean value for the minimum shear stress resistance
τ_{xy} , ν_u	shear stress
ϕ	curvature
ϕ_s	diameter of the longitudinal reinforcement bar
ϕ_v	diameter of the transversal reinforcement bar
ϕ_{ACI}	strength reduction factor

Greek upper case

ΔN_p	additional horizontal prestressing force
ΔV_p	additional vertical prestressing force
$\Delta\varepsilon_p$	strain increase in the prestressing cables
$\Delta\sigma_p$	stress increase in the prestressing cables

Abbreviations

AASHTO	American Association of State Highway and Transportation Officials
ACI	American Concrete Institute
AE	Acoustic Emission
Brittle	no warning is given before failure
CEB-FIB	International Federation for Structural Concrete
CFT	Compression Field Theory
CHP	Combinatie Herepoort
c.o.g.	center of gravity
CSA	Canadian Standards Association
DC	diagonal cracking
DIC	Digital Image Correlation
DTC	diagonal tension cracking
Ductile	material that undergoes a (significant) plastic deformation before failure
E-B	Euler-Bernoulli beam theory
EC2 , NEN-EN 1992	National standard for concrete structures
EC2 draft 2018 / D18	National standard for concrete structures unpublished draft from 2018
EN	European Norm
FC	flexural cracking
FS	flexural-shear or flexure-shear
FSC	flexural-shear cracking
GBV	Gewapend-Betonvoorschriften (reinforced concrete guidelines)
girder	a horizontal main structural member of a bridge
HPZ	Helperzoom girder
HSC	high-strength concrete
KW	kunstwerk (infrastructure works)
LRFD	load and resistance factor design
LVDT	Lineair Variable Differential Transformer
`MatrixFrame`	professional software for structural analysis
MC	Model Code
MCFT	Modified Field Compression Theory
`MS Excel`	Microsoft Excel spreadsheet-program
NEN , NEN-EN	National standard
NSC	normal-strength concrete
`Response-2000`	cross-sectional program based on MCFT
QP170	prestressing steel quality used in the Helperzoom bridge
QR40	reinforcement steel quality used in the Helperzoom bridge
RBK	Richtlijnen Bestaande Kunstwerken (national standard for existing structures)
Rijkswaterstaat	Dutch Ministery of Infrastructure and Watermanagement
RSP	file type used by `Response-2000`
RVB	Richtlijnen voor Voorgespannen Beton (guidelines for prestressed concrete)
RW	rijksweg (national highway)
SAs	Smart Aggregates
Stevinlab II	Structures Laboratory of the Department of Structural Engineering at TU Delft
STF	shear-tension failure
TU Delft	Delft University of Technology
UK	United Kingdom
ULS	ultimate limit state
USA	United States of America
VB'74	Dutch concrete code of 1974
WS	web-shear

1

Introduction

Structural engineers have applied reinforced concrete in civil constructions since the 1800s. Concrete is a material that is strong under compression, but can hardly handle tension. Therefore reinforcement is added to resist the tensile stresses. Reinforced concrete has been used in places where steel or cast iron was not ideal to use, mostly due to environmental influences. In early stages, concrete structures were built with an arch construction to maintain structural integrity. This type of construction is very labor and material intensive. Another issue were the deflections at mid-span, which resulted in (very) limited span lengths [2].

After the Second World War the strength of concrete has shown an upward trend and became better specified in the design codes. With the use of higher strength concretes, structures can be built more slender and cost-efficiently. Reinforced concrete can be cast in-situ or precast and can be used in a lot of different structural applications, like a slab, wall, beam, foundation, etc. Also reinforced concrete requires little maintenance and is very durable. This is why reinforced concrete nowadays has grown to one of the most widely used building materials in modern construction.

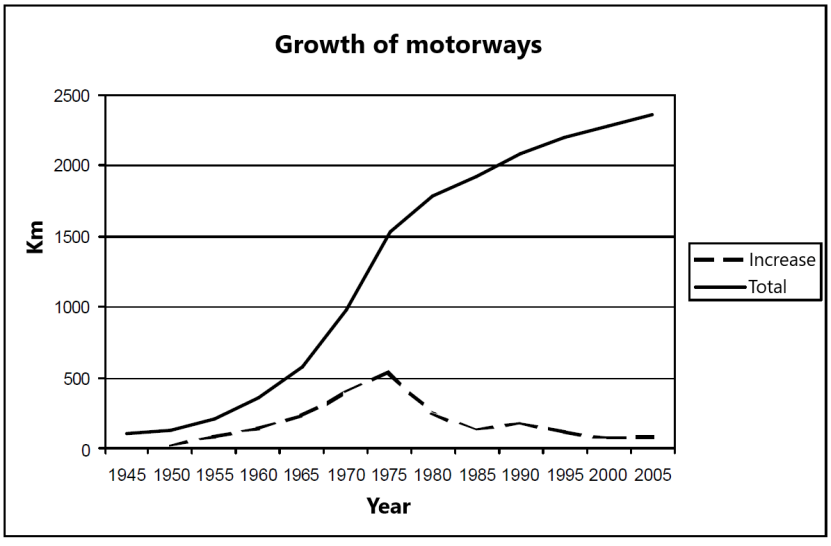

Figure 1.1: Increase of motor ways in the Netherlands between 1945-2007 [3]

In the fifties and sixties a real break-through took place for precast bridges. In these decades a lot of countries, among which the Netherlands, entered a period of economic expansion. The large growth of road traffic, increase of traffic loads and expansion of the motor way network urged a need for fast and economic solutions for under- and overpasses with as little as possible disturbance of the ongoing traffic, see Figure 1.1 [3].

Together with the introduction of prestressing and high-strength steel, which happened around the same time as the break-through of precast bridges, concrete structures can be built even more slender, longer, withstand larger service loads and become more durable [4]. The prestressing force fully or partially counteracts the stresses that occur during loading of a structure. There are several methods to apply a prestressing force in concrete, where pre- and post-tensioning are the most commonly used ones [5]. The application of prestressing in concrete means that the member is in a state of balance before it is put in place [6].

Looking back over the past 50 years, countries such as the Netherlands, Belgium, Germany, Italy, Spain, UK, USA and Canada are countries where precast and prestressed bridges are widely used and accepted as a classical solution. A constant growth of built bridges and increase of size and weight of bridge elements can be seen. In the early fifties, precast- and prestressed bridges were only used for short spans and constructed with rectangular beams (match-cast system) or small inverted T-beams. In the sixties a new solution was used, namely girder bridges with precast girders and a cast in-situ deck slab. In the Netherlands it was more common to place in-situ concrete in the space between the girders instead of an in-situ deck slab. The more recent developments are box girder bridges, composite bridges, through bridges (mostly for railways) and segmental bridges [4].

1.1. Background information

Figure 1.2 shows the number of concrete bridges built per period of five years over the past 70 years. A lot of bridges are built between 1960 and 1980 and around 70 percent, which are managed by the Dutch Ministry of Infrastructure and Watermanagement (Rijkswaterstaat in Dutch), are built before 1980. Most of these bridges are designed with a predicted service life of 50 years and are reaching the end of their working life. Also, as mentioned before, the traffic loads are a lot higher than originally designed for [7].

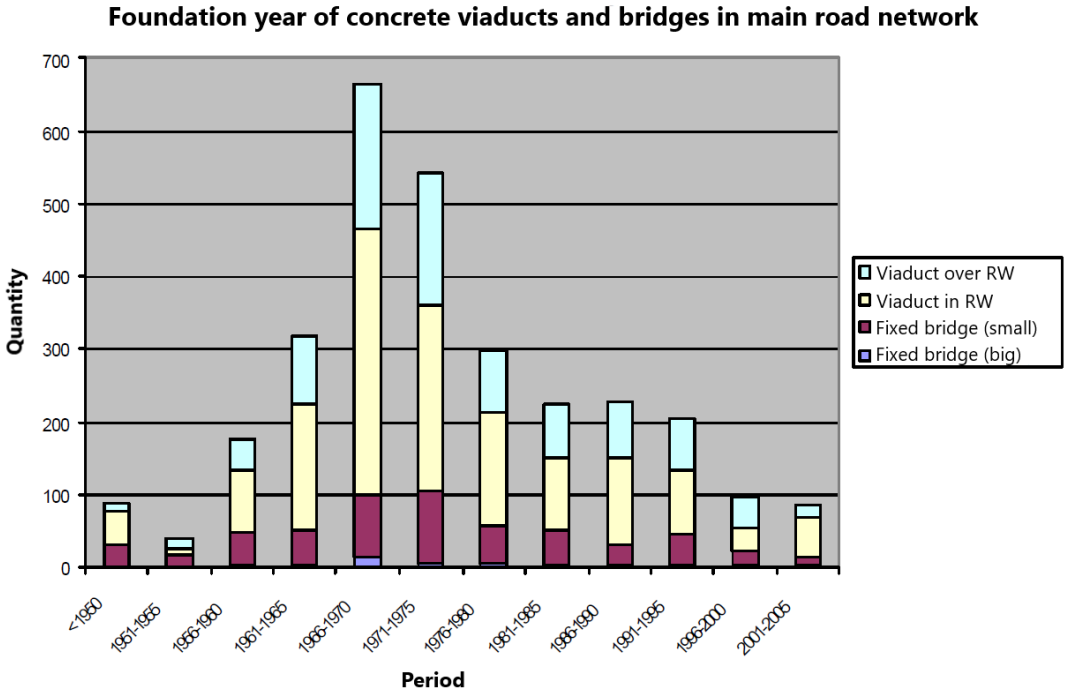

Figure 1.2: Number of concrete bridges built in the Netherlands between 1945-2007 [3]

Reaching the end of a designed life time, does not mean a bridge will collapse and needs to be replaced. Replacing all of the 3,700 bridges, currently managed by the Dutch Ministry, is estimated at 16 billion Euro. This is therefore a very expensive operation, which is why a lot of bridges are currently being assessed and repaired to prolong their service life [7].

One of the challenges is the ongoing discussion about the assessment of prestressed bridges, and in particular their structural safety. The reliability-based methods and perspectives to evaluate the integrity and safety of structures has increased significantly over the last decades [8]. Therefore the design codes of Eurocode (EC), Model Code (MC), American Concrete Institute (ACI) and American Association of State Highway and Transportation Officials (AASHTOO) have changed several times with regard to shear resistance of concrete structures, especially about the mechanics that enable the force flow through a concrete member and across cracks [9]. These changes mostly led to stricter requirements, which resulted in disapproval of existing structures with the current design codes [5].

It is of interest to know if these stricter requirements are valid for existing prestressed structures with thin/slender webs such as I-, T- and Box girder structures, since this influences about 25 percent of the 6000 concrete bridges in the Netherlands. If the EC, MC, ACI and AASHTO codes are overly conservative for these structures, a more accurate method should be considered for certain types of shear failure. Another point of interest are the bridges built prior to the Dutch concrete code of 1974 (VB'74). Until this design code minimum shear reinforcement was not prescribed, which raises the question if the current design codes are conservative or if the safety of the structure is too low [10].

The mode of shear failure depends on whether a girder is built with or without shear reinforcement. In case of girders with shear reinforcement several theories have been developed, like strut-and-tie models [11] [12] [13] and Compression Field Theories (CFT) [14] (Modified CFT) [15] (Simplified MCFT) [16]. The strut-and-tie models are also applicable for girders without shear reinforcement and for girders with low shear span-to-depth ratios with direct transfer of forces.

Models designed for girders with shear reinforcement usually do not work well for girders without shear reinforcement. Therefore experiments have been done by various researchers on beams without web reinforcement [17]. The intention of these experiments is to find out how accurate the judgment is of shear failures and to check whether the shear strength capacity of structures is predicted correctly with codes. Next to these codes, researchers have derived the most acceptable equations based on their experiments. Even with all the research that has been done on shear behavior of normal and high-strength concrete beams (NSC, HSC), no consensus is found regarding the dominating mechanism that generates shear failure [17].

The post-tensioned T-girders of the Helperzoom (HPZ) bridge, Groningen, Netherlands are an example of existing prestressed structures, which have been removed mid-February 2019. The HPZ edge girders have a UC of 1.69 and the middle girders of 1.05 according to the road layout provided in the RBK 1.1. Four of these girders are tested at TU Delft commissioned by Rijkswaterstaat for research purposes, with the first experiment taken place at the end of June 2019. The second experiment took place in September 2019. At the time of writing this thesis, the results of the last two experiments are still being analyzed. Therefore only the results of the first two experiments are used. The behavior of these concrete elements in shear is of most interest to this research, in particular the failure mechanism "shear-tension failure".

1.2. Research objective and questions

The research objective is to provide insight in the capacity and failure modes of the girders taken from the Helperzoom bridge in Groningen and in particular the shear-tension failure mode. A more precise capacity and failure mode should be determined, in order to assess existing bridges with similar type girders. The girders are designed with shear reinforcement that is not in line with current regulations and with a concrete design code that did not prescribe a minimum shear reinforcement ratio.

It is necessary to investigate which assessment method is the most feasible to predict shear-tension failure the most accurately. Alongside this research a destructive laboratory test is conducted at Stevinlab II at TU Delft, where results are compared and evaluated. With the gained insight of this experiment, a computer model will be calibrated to judge similar existing bridges. Based upon the project description and objective, the following main question is formed:

What is the predicted shear capacity and governing shear-failure mode of the post-tensioned T-beams taken from the Helperzoom Bridge (KW 17)?

The aim of this research is to answer this main question by providing an analytical- and numerical analysis, together with the results of the tests performed on the Helperzoom girders. In order to conduct these analyses, several things should be investigated first. As previously mentioned in Chapter 1.1 various **(inter)national** design standards and models can be used to evaluate the shear capacity of prestressed concrete members. With the help of these international and national standards a good impression can be made of how the shear capacity is calculated and how much this capacity is. This leads to the following questions:

- *Which codes can be used for (existing) structures?*
- *Which codes predict the critical shear capacity and associated failure mode the most accurately?*
- *What are the significant differences between the code provisions for the calculation of the shear resistance of prestressed concrete members?*

Next to the analytical analysis, a numerical model is made to check which shear failure mode is the most critical and what the ultimate shear capacity is of the girder. Since shear-tension failure is not the only failure mode, the capacity for other shear failures should also be checked. This results in the following questions:

- *What additional insights do the numerical calculations give to the contributions of the various components to the total shear resistance?*
- *What is the influence of the inclination of the compression field θ, how do the results change if θ changes?*

The numerical and analytical data are checked with experimental results:

- *How do the analytical and numerical calculations relate to the results of the test?*

Shear-tension failure is a hot topic nowadays. Several researches have been done on shear failure of beams, but not that many on shear-tension failure. Also there is no consensus found about the way shear-tension failure is predicted with current models. Therefore the topic of this research seems relevant enough to study further.

1.3. Outline of the study

The research methodology of this thesis is mostly following a quantitative (deductive) approach. The method consists of modeling and laboratory research. A specific case study, prestressed T-girders of the Helperzoom bridge, is modeled and experimented to simulate shear-tension failure. At first only analytical and numerical calculations were going to be done. However, since the window in which the T-girders are available for testing is known, laboratory tests are added to this thesis.

To answer the main- and sub-questions this report will be divided in seven chapters, namely:

Chapter 2 - Literature review

Chapter 3 - Overview of the Helperzoom girders

Chapter 4 - Experimental analysis

Chapter 5 - Analytical analysis

Chapter 6 - Numerical analysis with `Response-2010`

Chapter 7 - Discussion results analytical, numerical and experimental analyses

Chapter 8 - Conclusions and recommendations

Figure 1.3 gives an overview of the content and relations between Chapters 2 through 8. Several recent technical reports and theses contain valuable literature about shear-tension failure and the Helperzoom Bridge, like *shear-tension critical prestressed beams* [18], *quick check about the Helperzoom girders* [1], *literature review about shear-tension resistance of prestressed beams* [10] and `Response-2000` *and MCFT* [19]. This thesis will use the results of these documents together with other research that has been done on shear-tension failure. This is summarized in Chapter 2, e.g. different shear failures in reinforced and prestressed concrete beams, shear transfer mechanisms, concrete in cracked- and uncracked state, developed shear models, design codes, etc. and Chapter 6 for the Modified Compression Field Theory (MCFT).

All available data of the Helperzoom girders, mostly gathered from technical drawings and material tests, is evaluated in Chapter 3. The test set-up, span length and placement of the bearings that are used in the experiments are included. The cross-sectional properties and acting forces due to an external load and a prestressing force are calculated for several cross-sections.

Chapter 4 covers the results from the laboratory tests. Before the experiments took place, the concrete strength, concrete modulus of elasticity, steel strength of the prestressing cables and strength of the mild steel are tested to provide data that is as close as possible to reality (by means of the use of average material properties). Although four girders (HPZ1 - HPZ4) are tested in Stevinlab II at Delft University of Technology, only HPZ1 and HPZ2 are evaluated. For the laboratory tests relevant data regarding the failure mode, flexural-shear- or shear-tension failure, and capacity of the girders will be processed. Lastly the experimental results are evaluated.

Chapter 5 presents the results of the considered design codes and analytical calculations that are based on the Euler-Bernoulli beam theory. There are several models and design codes that are available to predict the shear capacity of the prestressed girders. Only a few commonly used design codes are studied, namely ACI, AASHTO, EC2, RBK 1.1 and EC2 draft 2018. These codes are presented in the form of mathematical equations and tables. The capacity is presented as a total shear resistance, but is also (if possible) divided in contribution of the steel and concrete together with the governing mechanism. Euler-Bernoulli theory is used to calculate multiple sections over the height and to check multiple shear spans of the beam. This requires a lot of input and generates a lot of output. Therefore, to evaluate and visualize this data `MS Excel` is used. The principal- and shear stresses for given cross-sections are presented in various figures. Also the shear capacity of the beam at different shear spans is presented in a table. At last all the results are summarized and compared with each other to note the differences between codes and the analytical model.

In Chapter 6 a numerical analysis is made to calculate the strength and ductility of the girders subjected to shear. `Response-2000` is an easy to use, cross-sectional program based on the MCFT (Modified Compression Field Theory) that is used and simplified in the Canadian Design Code (CSA) and American Bridge Code (AASHTO). This nonlinear finite element program quickly presents the results in graphs and raw data. This raw data can be copied and evaluated in `MS Excel` and is needed among other things to separate the total shear capacity into the contribution of reinforcement steel, prestressing steel, uncracked- and cracked concrete.

In Chapter 7 a global discussion of the results of the experimental- (Chapter 4), analytical- (Chapter 5) and numerical analysis (Chapter 6) is given. The conclusions and recommendations are presented at the end of the report in Chapter 8. Also answers are given to the main- and sub-questions given in Chapter 1.2. The approach of this thesis has been used by several researches and theses, either with experimental data from previously done experiments or with new experiments. It has been proven to be able to provide accurate statements and conclusions regarding shear failure in prestressed beams, either with or without shear reinforcement (stirrups). Although numerical calculations give a nice representation in the form of figures, one should always remain critical regarding the in- and output of these numerical models.

A disadvantage of this research approach is that a lot of experiments should be done on this subject in order to get accurate results. Since only four specimens are tested, the accuracy of this experiment could be questioned. Nevertheless, this method is useful for testing and validating current models and theories and the data could be used by other researchers that work on this subject.

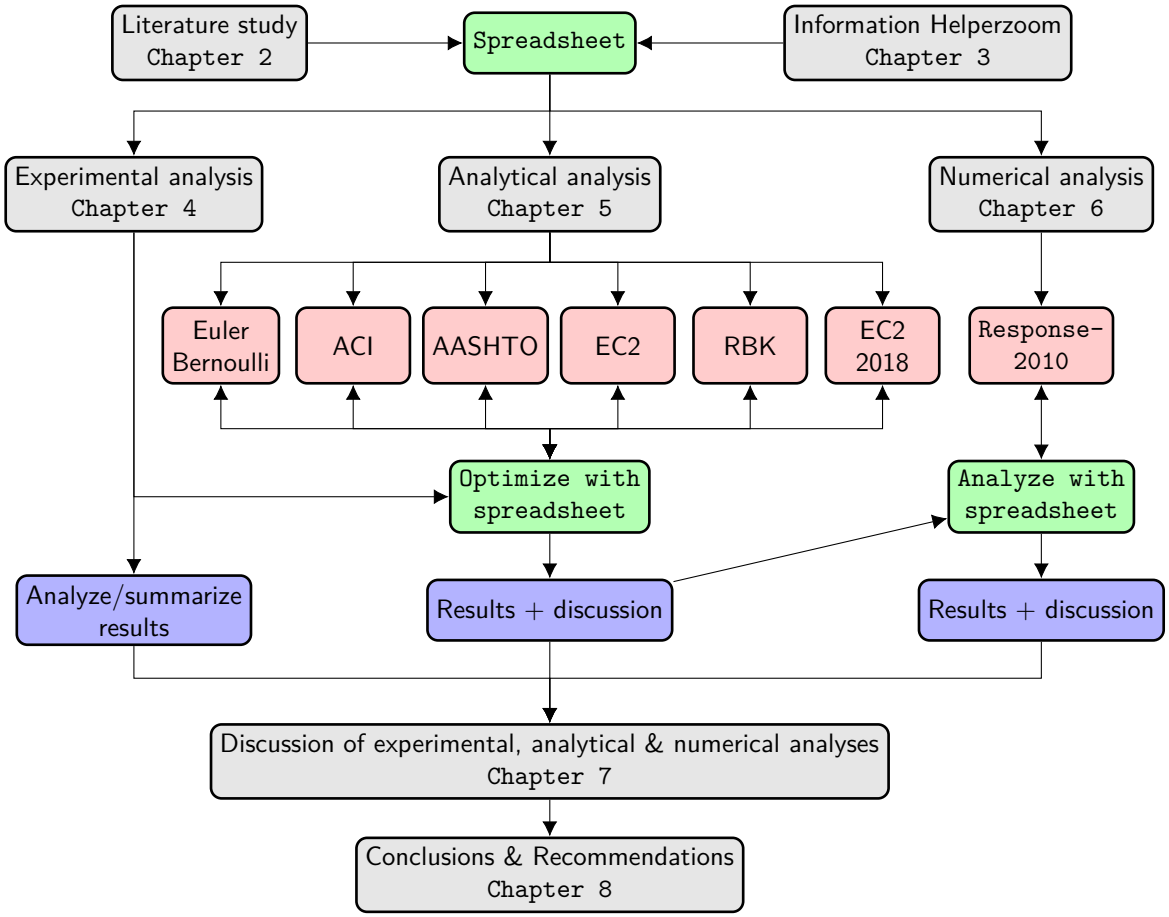

Figure 1.3: Flow chart representing the content and relations between chapters two through seven

1.4. Scope of the study

The intended result of this thesis is to prove which failure mode is governing in the post-tensioned T-girders of the Helperzoom bridge with non-code-compliant shear reinforcement and to provide clear data to calibrate the computer program to verify similar existing bridges in the Netherlands. The shear-failure mode and shear capacity of the girders are calculated with the following European and American design standards: ACI, AASHTO, EC2, RBK 1.1 and EC2 draft 2018. A lot of models exist to determine the shear capacity and if possible the failure mechanism of (prestressed) concrete members, but the used models and visions differ per code. The way these codes are derived differs for every code; some codes are derived analytically, empirically or a combination of both. To evaluate the different models, shear capacities, failure mechanisms and important differences between the codes these five code provisions are chosen. These codes give a good representation of the international standards, so that international practice is well covered. The numerical analysis is done with `Response-2010`. Different failure mechanisms can be given by `Response-2010`, the program gives a relative quick shear capacity, the results can be analyzed and divided in different components and according to previous studies `Response-2010` is an accurate tool for the calculation of the shear capacity and related failure mechanism.

The analytical and numerical models used in this research consist of data of a real T-girders, which are destructively tested at Stevinlab II. This type of girder does not get approved by arithmetic models in the current design codes. The results of the experimental, analytical and numerical analyses will give answers to the main- and sub-questions. In case the outcome is shear-tension failure, this subject can be addressed further. If not or if multiple failure modes are present, the view on prestressed T-girders of this type should be reconsidered where this thesis should give the start for further research on this topic. The various sub-questions are related to the research question and should give a basis to verify the governing failure mode and shear capacity of the Helperzoom girders.

2

Literature Review

As mentioned in the introduction, applying prestressing in concrete structures has its advantages. Unfortunately these slender prestressed structures also have disadvantages. For example in prestressed concrete beams, several failure mechanisms can occur such as flexural failure, shear-/diagonal failure and anchorage failure. Which type of failure is dominant depends on several factors such as shear-to-depth ratio, longitudinal reinforcement ratio, shear reinforcement, concrete compressive strength, etc.

For designing a reinforced or prestressed concrete member, all failure mechanisms should be checked in order to properly design a structure. There is a general agreement on designing of a concrete member subjected to bending; the required flexural strength and amount of transversal and longitudinal reinforcement of a concrete member to satisfy ductile flexural behavior. For the case when substantial shear is present, there is no general consensus found in literature and design codes, which is why every model and code provision has its own approach. However, every design code ensures that the element fails in flexure before it can fail in shear.

These models and code provisions can also differ in the way they are obtained, with analytical expressions, empirically determined through laboratory tests or a combination of both. All codes have some level of conservatism included to provide sufficient margin of safety. Existing structures often do not suffice to the current design codes. If design codes are used together with shear transfer mechanisms and influencing factors it is possible the existing structures meet the safety requirements.

To have a good understanding of shear behavior, mechanisms and failures this literature review provides general information about shear-failure mechanisms, shear transfer mechanisms, factors that influence the shear resistance, principal tensile stresses, concrete tensile strength and several design codes with corresponding models, approaches and expressions. Both flexural-shear- and shear-tension/web-shear failure will be addressed in this review, although shear-tension failure is of utmost importance for this thesis.

2.1. Failure mechanisms in reinforced concrete members

To understand the failure mechanisms for prestressed concrete, the failure mechanisms for reinforced concrete are first described as prestressing is an addition to reinforced concrete. There are specific areas in a concrete beam that are of interest:

1. Area with high moment and low shear
2. Area with high moment and high shear
3. Area with low moment and high shear

These areas have different governing types of cracking. An area with only a moment present, for single span members around mid-span, causes flexural cracks if the tensile strength of concrete is reached. Moving towards a support, the shear stress will increase and diagonal-tension cracks and flexural-shear cracks develop [20]. In Figure 2.1 two different areas with a combination of moment and shear are shown.

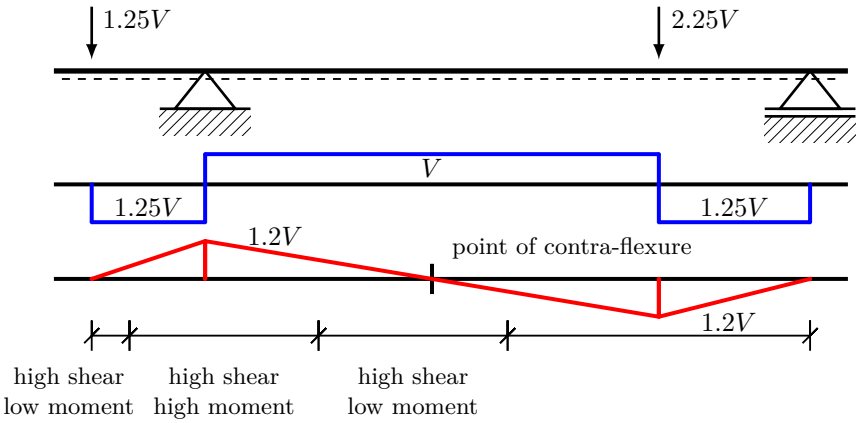

Figure 2.1: Moment and shear diagrams of an external loaded beam

In an area with a high moment and small shear, vertical cracks in the middle third of the beam and perpendicular to the lines of principal stress occur. The principal stresses are almost horizontal, see Figure 2.2. Very fine vertical cracks start to develop and as the external load increases additional cracks develop. The initial cracks grow wider and deeper towards and beyond the neutral axis, with noticeable deflection of the beam [21]. Ductile flexural failure (pure bending) occurs when the ultimate capacity of the concrete compression zone is reached. The concrete crushes after yielding of the steel. This type of failure is ductile in cracked state, because of yielding of the reinforcement. If the requirements for minimum reinforcement are not met, the crushing of the concrete happens suddenly without noticeable deformation, which results in brittle failure. For statically determinate structures the highest bending moments are at mid-span, which is where most likely flexural failure will occur [22].

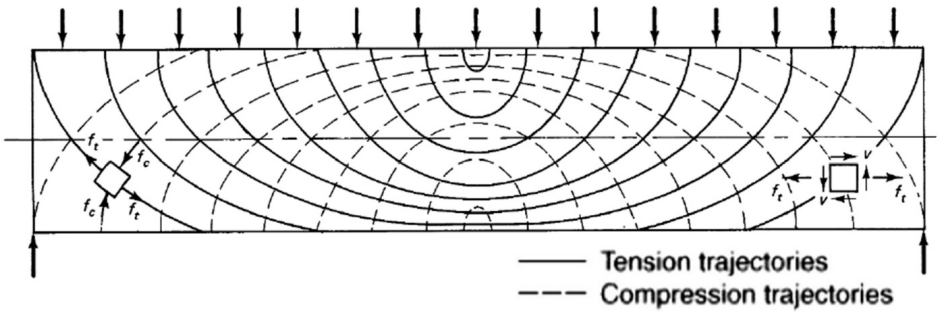

Figure 2.2: Trajectories of the principal stresses in a homogeneous isotropic beam [21]

Three types of shear failure can occur in reinforced concrete beams, see Figure 2.3; flexural-shear failure/diagonal-tension failure 2.3a, shear-compression failure 2.3b and shear-tension failure 2.3c, all of which fail in a brittle manner [22]. **Flexural-shear failure** occurs when the inclined (diagonal) cracks, propagating from vertical flexural cracks, reach a certain critical length. The shear transfer capacity reduces until no capacity is left, resulting in the collapse of a beam. **Shear-compression failure** occurs for beams with a short shear span. For external loads close to the support, arch action occurs. Arch action ensures direct transfer of forces to the support. The beam will fail in compression, due to high principal compressive stresses; between the shear cracks in the compressive strut, above the support or compression zone close to the load [23]. **Shear-tension failure** occurs when the principal tensile stresses exceed the tensile strength of the concrete. This type of failure appears in members with thin webs, where the shear force is large compared to the bending moment [18] [24].

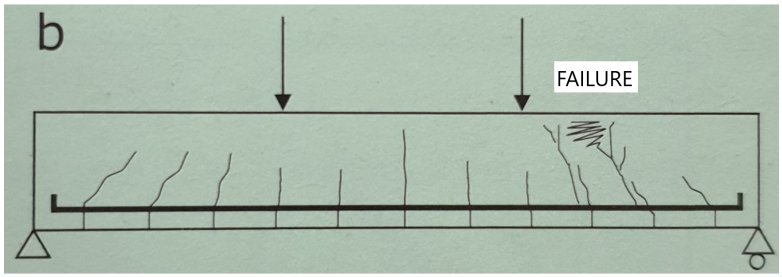

(a) Diagonal-tension failure at ULS

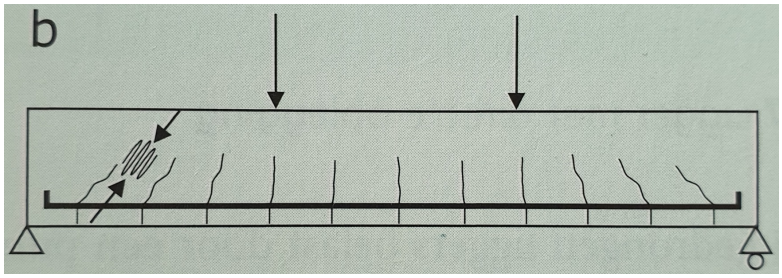

(b) Shear-compression failure at ULS

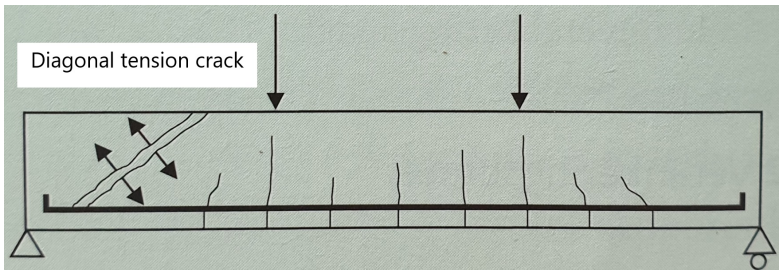

(c) Shear-tension failure at ULS

Figure 2.3: Modes of shear failure in concrete [22]

Another type of failure is anchorage failure. This failure mechanism is different than the previous described failures, because it depends on the bond between reinforcement steel and concrete, concrete cover and anchorage length. This type of failure can be avoided by sufficient detailing of reinforcement or concrete cover and will not be further discussed in this research [22].

Mentioned several times is that shear failures are brittle, thus happen without warning and can result in loss of human lives. The meaning of the national- and international structural design codes is to reduce, if not exclude this loss as much as possible. To avoid brittle behavior for flexural- and shear failures, a structural element should always be designed in a way that the cracking moment (M_{cr}) is smaller than the design bending moment (M_{Rd}). In other words, the reinforcement steel should first yield before crushing or splitting of the concrete. The amount of steel must be able to resist the cracking moment, which is taken into account with the minimum reinforcement requirement [5]. However for shear failures, brittle behavior can still occur if the cracking moment is smaller than the design bending moment. Therefore extra attention is needed when designing for shear.

For the assessment of existing structures, which is the goal for this thesis, the nominal shear resistance (and if possible the shear failure mode) can be calculated with the use of the structural design codes. Assessment of existing structures can be done with NEN8700 or can be compared with test results. A difference between designing new structures and assessing existing structures are the load- and resistance factors. For comparing an existing structure with test results, the factors are set to a value of 1.0. Instead of using design values for the material properties, as prescribed by the design codes, mean values from tests can be used. When concrete structures are destructively tested, the obtained results can be validated with the design codes to check if the calculated shear resistance is in line with the experimentally observed failure load and failure mode. If the results from the experiments are not in line with the calculated shear resistance and/or failure mode, an assessment report can be written for the shear resistance of similar existing structures.

2.2. Shear transfer mechanisms in reinforced concrete without transverse reinforcement

After cracks occur in a concrete beam, the shear redistributions are complex and difficult to calculate. This is why shear transfer mechanisms need special attention, because they are the fundamentals of the behavior of concrete under loading. They affect the shear resistance of prestressed beams with and without shear reinforcement in a positive way and therefore cannot be neglected. The ACI use findings from 1973 [25] and 1998 [26] on basic shear transfer mechanisms and are generally accepted [27].

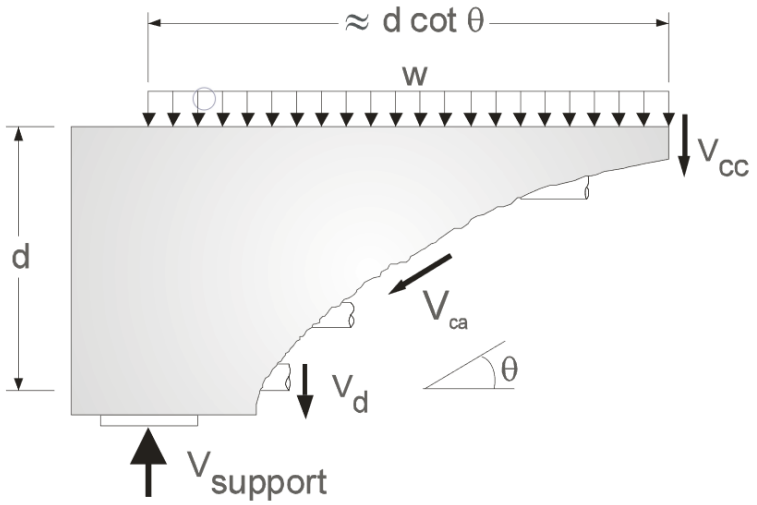

Figure 2.4: Shear transfer mechanisms in concrete without transverse reinforcement [27]

However, for the level of importance on the shear transfer mechanisms there is generally no consensus found. In this review the important shear mechanisms are described. The following three out of four mechanisms are shown in Figure 2.4. The fourth mechanism is arching action for short shear span-to-depth ratios (Chapter 2.2.4) [27].

V_{cc} – Shear in uncracked compression zone of the beam (Chapter 2.2.1);

V_d – Dowel action of the longitudinal reinforcement (Chapter 2.2.2);

V_{ca} – Interface shear transfer due to aggregate interlock (Chapter 2.2.3).

2.2.1. Shear in uncracked compression zone

A loaded concrete beam, after reaching the cracking moment, consists of a cracked- and uncracked part. The uncracked part is under both compressive- and shear stresses and contributes to the shear resistance, see Figure 2.4. The axial compressive force is due to the acting bending moment. The amount of contribution to the shear resistance depends on the height of the uncracked zone. The nominal shear stress exceeds the shear capacity of the beam when the concrete is cracked, although the shear transfer mechanism ensures that the uncracked zone can transfer shear force. The nominal shear stress is the mean stress of the compression zone of the cross-section. The shear force introduces local tensile stresses in the compression zone, which causes the concrete to be in a bi-axial stress state. Therefore a higher shear capacity is created in the compression zone than current code provisions suggest [28].

2.2.2. Dowel action

Dowel action can be of importance with beams with a low to zero transverse reinforcement ratio or with post-peak behavior. This post-peak resistance can be very high and therefore contribute to the shear ductility of concrete structures [29]. Baumann & Rüsch [30] were one of the first carrying out experimental tests on dowel action of longitudinal reinforcement with post-peak behavior [31]. They showed that after this post-peak behavior a large plastic deformation can be measured. Recent developments show that this phenomenon can be tested with Digital Image Correlation to obtain the displacements in transversal and longitudinal direction [32].

Dowel action occurs when concrete is in a cracked state. While the crack grows the shear transfer mechanism activates and cuts across the longitudinal reinforcement. This phenomenon increases the shear capacity of the beam and is usually 15-25% of the total shear capacity [33]. The crack transfers shear stresses from concrete to the reinforcement and as a result local bending and shear at the reinforcement can be observed, see Figure 2.5.

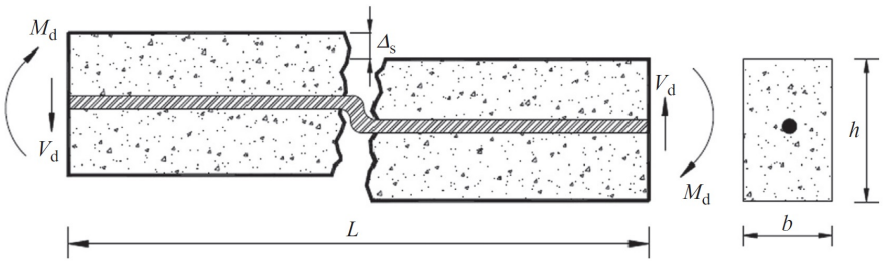

Figure 2.5: Dowel action of the longitudinal reinforcement in concrete [34]

Dowel action may be affected by the position of the reinforcement along the cross-section, thickness of the concrete cover, longitudinal and transversal reinforcement ratios and the tensile strength of concrete. The bending moment that is caused by the dowel action can be expressed as: $M_d = 0.25V_d \cdot L$, where V_d is the dowel shear force and L is the element length that is considered [34].

2.2.3. Aggregate interlock

Aggregate interlocking consists of a shear stress caused by friction or forces between the aggregates inside a crack [31]. The contribution of aggregate interlocking to the shear resistance depends on several factors; the width of the crack (the particles need to stay in contact to generate shear stresses) and mechanical properties of the aggregate particles used in the concrete. The transfer of the shear load also depends on the aggregate type and size, the ability of the crack to twist (tortuosity), strength and stiffness of the concrete, how much of the concrete is cracked, boundary conditions, magnitude of the load and amount of load cycles [29].

A relation of the aggregate interlock capacity to the depth of the beam is shown in Figure 2.6. It shows that aggregate interlocking depends on the maximum aggregate size. Aggregate sizes smaller than 32 mm are more effective in smaller beams than with the same aggregate size for deeper beams. If the aggregate size is kept equal, the shear strength drastically decreases for deeper beams [23] [35].

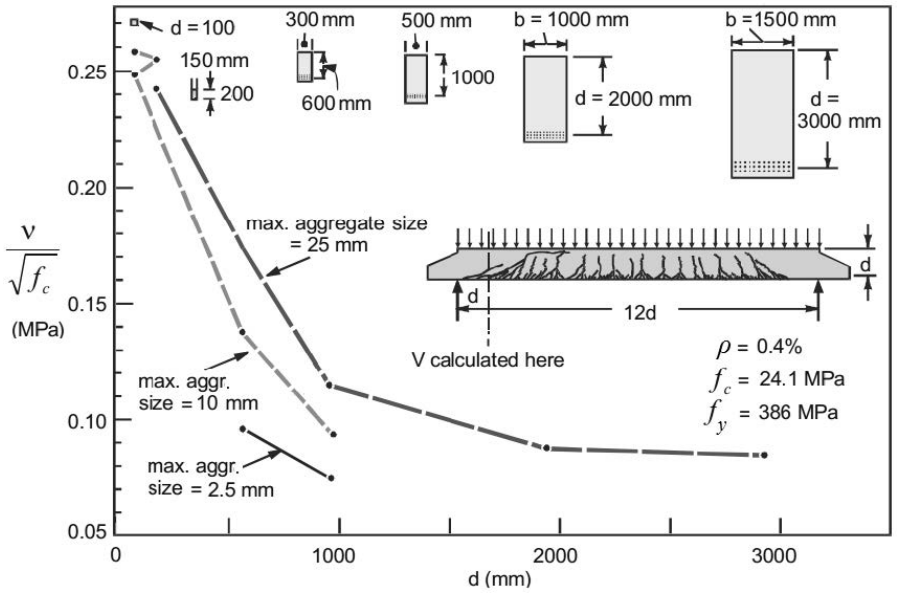

Figure 2.6: Influence of aggregate size for the absolute beam depth on the shear strength of beams without shear reinforcement according to Hawkings et al. [36] and Collins & Mitchell [37]

Late Seventies and early Eighties, Walraven [38] [39] experimentally researched four components that influence the aggregate interlocking in concrete members, which are shear stress, normal stress, tangential displacement and normal displacement. After the tests a model was proposed by Walraven [39] [40] shown in Figure 2.7. The experiments done by Walraven are the fundamentals of various models and formulas that were proposed after.

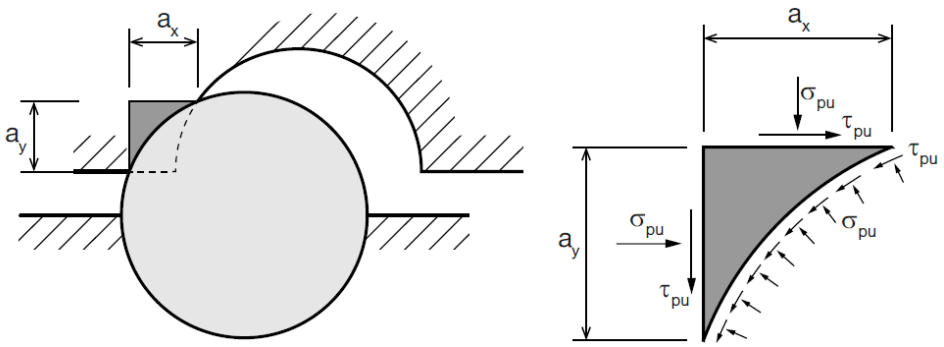

Figure 2.7: Proposed model for aggregate interlocking consisting of four components [40]

2.2.4. Arching action for short shear span-to-depth ratios

For concentrated loads close to the supports with shear span-to-depth ratios lower than 2.5, a large part of the load flows directly to the bearings of the member, see Figure 2.8. This is for visualized various researches, like Walraven & Lehwalter's strut and tie system [13].

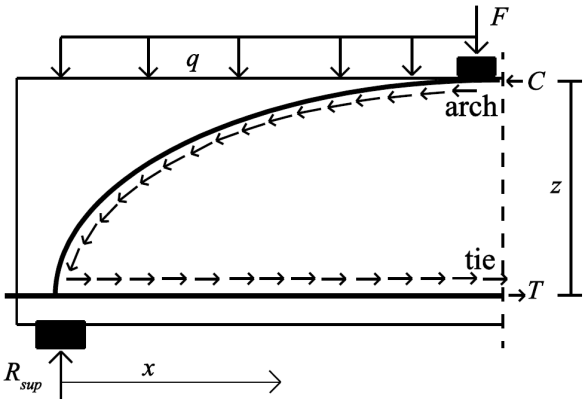

Figure 2.8: Arching action in a reinforced concrete member, showing the compression cord and tensile tie [41]

Where T is the tension force in the reinforcement, C is the compressive force in the concrete compression zone, z is the internal lever arm between the internal couple C and T, x is the location along the axis in the span direction, F, q and R_{sup} are the applied concentrated load, applied distributed load and the support reaction respectively.

Loads placed close to the supports result in higher shear capacity of the member due to [42] [43]

- arching action, with a constant z and changing T;
- beam action, with a constant T and changing z.

The shear capacity can be written as the sum of arching and beam action [44] [45]:

$$V = z \cdot \frac{dT}{dx} + T \cdot \frac{dz}{dx} \tag{2.1}$$

The shear capacity also increases with a lower shear span-to-depth ratio.

2.3. Influencing factors for shear resistance of reinforced concrete

Next to the shear transfer mechanisms there are factors influencing the shear resistance of a reinforced concrete member. The most important factors are [29]:

1. Concrete strength;
2. Longitudinal reinforcement ratio;
3. Shear span-to-depth ratio;
4. Size effect;
5. Axial force.

2.3.1. Concrete strength

According to experiments and design codes, except the ones from Angelakos et al. [46], the shear resistance of a concrete member increases with the use of higher concrete strength classes, see Figure 2.9. In many code provisions the shear strength of a concrete member is taken directly from the ultimate tensile strength of concrete, proportional to $\sqrt{f_c}$, $\sqrt[3]{f_c}$ or $\sqrt[3]{f_c^2}$. Moody et al. [47] related the shear strength of concrete members without stirrups to the concrete compressive strength with $\sqrt{f_c}$. Figure 2.9 shows the relation of concrete strength provided by several researchers and code provisions to the shear resistance of a concrete member [23]. The shear resistance remained constant for lightweight concretes and higher concrete strengths and can be explained by the occurrence of smoother shear cracks which reduce the aggregate interlocking mechanism [36].

The strength of concrete directly relates to the shear transfer mechanisms described in Chapter 2.2. The height of the compression zone depends on the concrete strength. The higher the concrete strength, the smaller the compression zone needs to be to create equilibrium provided that the tensile force remains constant. For dowel action, the concrete cover is stronger and stays in place with higher concrete strengths. Strut action can take up more compressive load, which decreases the aggregate interlocking capacity. For higher concrete strengths the aggregate interlock capacity decreases, because the matrix becomes stronger than the aggregates resulting in a straight crack through the aggregates instead of a inclined rough crack along the surface of the aggregates (fracture mechanics).

The ACI and AASHTO use a specified concrete compressive strength f'_c instead of f_{ck}, used by EC2 and RBK. The f'_c is slightly lower than f_{ck} and can be transformed by the following expression:

$$f'_c = \frac{f_{ck} + 8 - 4.28}{1.1} \quad \text{[MPa]} \tag{2.2}$$

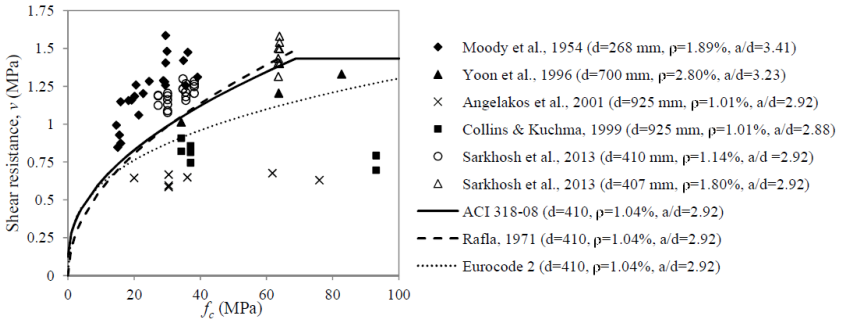

Figure 2.9: Relation compressive concrete strength f_c to the shear resistance of concrete V_c [23]

2.3.2. Longitudinal reinforcement ratio

The longitudinal reinforcement ratio ρ_l can have significant influence on the shear resistance. This ratio is related to aggregate interlocking and dowel action. If an externally loaded concrete member has a low longitudinal reinforcement ratio, the cracks will grow larger than in the case with a normal or high ratio. If the cracks grow large enough that aggregates cannot interact with each other, the contribution to aggregate interlocking is lost. The same happens with dowel action, the less reinforcement is placed in a member the less dowel action will occur, because the area of the reinforcement decreases [23].

2.3.3. Shear span-to-depth ratio

The shear span-to-depth is an important parameter for determining the shear strength of concrete members. For small simply supported beams subjected to concentrated loads the shear span-to-depth ratio a/d equals to the moment-shear ratio in relation to the depth of the beam $\frac{M_{Ed}}{V_{Ed} \cdot d}$. For concrete members subject to a concentrated load, shear span-to-depth ratios of $a/d = 2.0 - 5.0$ are of most interest. The bending moment in this region is usually the lowest and a relatively high shear force is active. This is shown in Kani's [48] [49] research called "valley of diagonal failure" and is presented in Figure 2.10a and 2.10b.

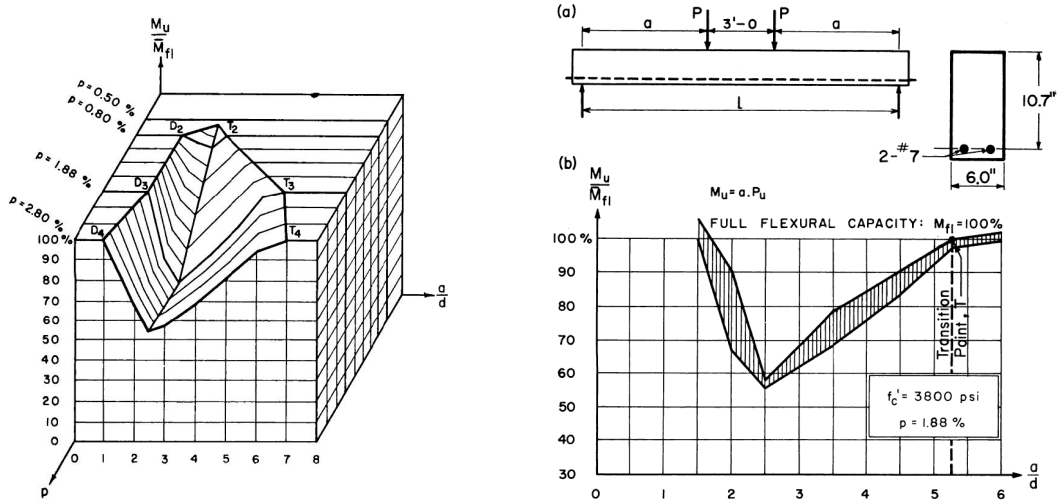

(a) Shear failure valley by Kani where the relative beam strength r_u depends on the shear span-to-depth- and lon- gitudinal reinforcement ratio ρ_l

(b) Influence of shear span-to-depth on the relative beam strength r_u for $\rho = 1.88\%$ and $f_c' = 26.2$ MPa

Figure 2.10: Influence of the shear span-to-depth ratio a/d on the non-dimensional relative strength r_u [48]

With the non-dimension relative strength of reinforced concrete $r_u = \frac{M_u}{M_{fl}} = \frac{M_{shear-failure}}{M_{flexural-capacity}}$.

Kani investigated different shear span-to-depth ratios with the longitudinal reinforcement ratios and found that the depth of the valley decreases with decreasing reinforcement ratios until the ratio is below $\rho_l = 0.60\%$. The shear span-to-depth ratio has been included in many code provisions, especially the ones that are empirically determined. For shear span-to-depth ratios below 2.5, a part of the shear force can be directly transferred to the support by inclined compressive struts as described in Chapter 2.2.4 [29].

2.3.4. Size effect

Kani [49] was one of the first researchers addressing size effect in concrete structures. He concluded that for reinforced concrete beams without transverse reinforcement, the nominal shear resistance decreases with increasing size of the member. Other researchers experimented or proposed models for the effect on sizes of concrete members, like Walraven [50], Bažant & Kim [42], Bažant & Xi [51] and Walraven & Lehwalter [52]. The best known law for size effect is Bažant's size effect law, that is later extended by Walraven & Lehwalter for shear span-to-depth ratios below 2.5. They concluded that for members below this ratio the size effect considerably influenced the shear resistance [23].

2.3.5. Axial force

Applying prestressing in a concrete member introduces an axial force. This axial compressive force will increase the height of the uncracked compressive zone and decrease the width of the shear cracks. This results in an increase of the shear capacity. However, for members subjected to high prestressing forces the shear capacity can decrease and can result in failure of the member in a brittle way. Design codes have added terms to accommodate for the effect of an axial force due to prestressing in the calculation for the shear capacity of concrete members.

2.4. Failure mechanisms in prestressed concrete members

Applying prestressing in a concrete structure is adding a compressive force to compensate for the tensile stresses in the tension zone. This eccentric compressive force causes the beam to resist a higher bending moment than ordinary reinforced concrete, which causes flexural cracks to occur at a higher external load. The compressive force can have impact on the presence of certain modes of cracking. For slender prestressed concrete girders without shear reinforcement and loaded perpendicular to its axis, typically four failure mechanisms are considered [21]:

- Flexural failure ($a/d \approx 5.5$)
- Flexural-shear failure ($a/d \approx 2.5 - 5.5$)
- Shear-tension failure ($a/d \approx 2.5$)
- Shear-compression failure ($a/d < 2.5$)

The a/d-ratios mentioned above are for concentrated loads. The failure mode of the beam is mostly determined by the slenderness of the beam, also called the span-to-depth- or shear span (a) to effective depth (d) ratio (a/d). Figure 2.11 shows the areas for the dominant failure mode. For a/d-ratios less than 2.4-2.5, direct load transfer mechanisms are considered as described in Chapter 2.2.4. For a higher a/d-ratio, thus the more slender the beam, the more flexural failure becomes dominant [53]. Flexural-shear failure occurs in a/d-ratios between flexural- and shear-tension failure, which are considered as intermediate slenderness beams [21]. Shear-tension failure is the failure mechanism that appears to be difficult to demonstrate and predict in terms of resistance.

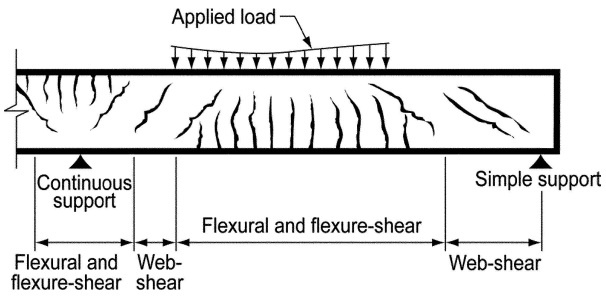

Figure 2.11: Areas in which modes of failure are dominant [54]

Prestressed girders are often slender structures with an I-shape or bulb-T-shape. These girders typically consist of a thin web with thick flanges and are constructed for both single and continuous span bridges. The method of prestressing can be with both pre- and post-tensioned tendons and the tendons can be either bonded or unbonded [5].

Prestressed members can be designed with and without shear reinforcement. In case shear-tension failure is the governing mechanism, beams without shear reinforcement can instantly fail after the formation of diagonal tension cracks in the web. This type of crack, independent of flexural cracks in the most tensioned flange, is typical for prestressed beams [55]. The behavior of such a failure is as follows: first a diagonal tension crack opens, secondly the stirrups will yield and lastly the stirrups will rupture without crushing of the concrete [24]. It is very difficult to predict what happens after the occurrence of a diagonal tension crack, which is why in general this is the point for the maximum resistance of a beam without shear reinforcement unless direct load transfer occurs [56].

For prestressed members without shear reinforcement, there are several models and design codes that describe the resistance to diagonal tension cracking. All of these models use Euler-Bernoulli beam theory to determine the principal tensile stresses and assume that diagonal cracking occurs if this stress exceeds the tensile strength of concrete. The models differ in the location (x, z-direction) where the principal stresses are considered and in the way the tensile strength of the concrete is determined from material tests as described in Chapters 2.5.1 and 2.5.2.

If girders contain a sufficient amount of shear reinforcement, the steel can resist additional load after the formation of diagonal tension cracks. The diagonal crack can propagate towards the top of the beam. Here the concrete crushes at the same time as yielding of the stirrups. There is an upper limit for

the shear resistance, this is when the concrete crushes in the compression zone (sometimes also called compression chord) without yielding of the stirrups. This shear failure mode is called shear-compression failure. For prestressed concrete members with thin webs the stresses in the web are much higher than in rectangular members. When the concrete compressive strength is reached in the web, the concrete member will fail in the web and is called web-crushing failure or failure of the compression field [23] [24] [57]. For prestressed members with shear reinforcement there is no general consensus about the ultimate shear capacity. For example the ACI code sums up the lowest resistance of the concrete failure mode and the resistance of the transverse reinforcement while the EC2 assumes a different approach for members with shear reinforcement.

Girders with insufficient shear reinforcement have a chance to fail in a brittle manner, in a same way as those without shear reinforcement. Bridges built before the Dutch concrete code of 1974 (VB'74) were designed using the principal stress criterion for shear and can have too low levels of shear reinforcement ($\rho_w < 0.3\%$) [53]. Another possibility is that these girders contain shear reinforcement that is not compliant with the current design code(s). This means that the transverse reinforcement is ineffective due to its shape, not anchored in the compression zone, welded stirrups, too large center-to-center distance or usage of plain steel [24].

Shear-tension and flexural-shear- failure are two different failure mechanisms and do not have the same mode of diagonal cracking in prestressed concrete structures. Table 2.1 shows failure mechanisms with corresponding cracking modes and areas. Diagonal tension cracks could lead to shear-tension failure. The two terms have two different meanings in the shear resistance of a (prestressed) concrete member. Xie [20] mentioned that shear-tension failure occurs in an area with diagonal tension cracks. In this area a low moment and a high shear force is active, which is typical around end supports of single span beams or if continuous, around a point of contra-flexure. If the principal tensile stresses exceed the concrete tensile strength of the web ($\sigma_1 > f_{ctm}$), diagonal tension cracks will occur. Flexural-shear failure occurs in an area with flexural shear cracks. This area contains a high moment and high shear force. Flexural cracks will occur if the flexural tensile strength is exceeded in the most tensioned flange. Flexural-shear cracks will develop from flexural cracks if enough shear stresses are present [24].

Table 2.1: Failure mechanisms with corresponding mode of diagonal cracking

Failure mechanism	**Mode of diagonal cracking**	**Area**
Shear-tension failure	Diagonal tension cracks	Low moment / High shear
Flexural-shear failure	Flexural shear cracks	High Moment / High shear

The level of prestressing can influence the occurrence of a certain diagonal cracking mode. Considering two identical beams shown in Figure 2.12, one with a high level and one with a low level of prestressing, both failing in shear-tension. In the beam with a high level of prestressing only diagonal tension cracks occur, without the presence of flexural- and flexural-shear cracks. The beam with a low level of prestressing all three types of cracks occur [20].

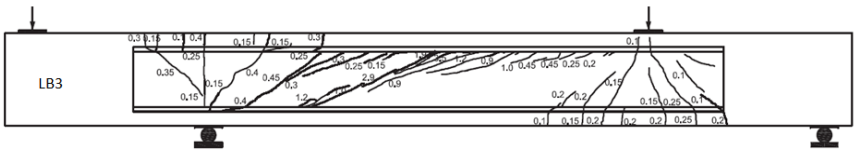

(a) Specimen LB3 with low prestressing force ($\sigma_{avg} = \dfrac{N_{avg} = -426{,}000\ \text{N}}{A_c = 86{,}980\ \text{mm}^2} = -4.90\ \text{MPa}$)

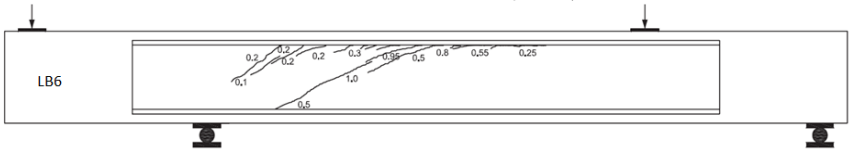

(b) Specimen LB6 with high prestressing force ($\sigma_{avg} = \dfrac{N_{avg} = -797{,}000\ \text{N}}{A_c = 73{,}230\ \text{mm}^2} = -10.88\ \text{MPa}$)

Figure 2.12: Specimen LB3 and LB6 with different types of cracking modes [20]

2.5. Diagonal tension cracking in the web

Concrete cracks when the principal stresses exceed the tensile strength of concrete. To calculate the principal stresses in a cross-section, the horizontal and vertical stresses need to be transformed as described in Chapter 2.5.1. The tensile strength of concrete can be obtained and calculated with different tests and approaches, which will be discussed in Chapter 2.5.2. With these two characteristics of concrete, diagonal tension cracking and flexural cracking can be determined in the web and the flange in tension.

2.5.1. Determining the principal tensile stresses

All analytical models use the Euler-Bernoulli beam theory to determine the shear stresses τ_{xy} and the stresses parallel to the beam axis σ_x. This theory uses a linear elastic stress-strain relationship and neglects the effect of shear deformation.

$$\tau_{xy} = \frac{V_E \cdot S_c}{b_w \cdot I_c} \quad \text{with} \quad S_c = \sum(\Delta h \cdot b_w) \cdot a \qquad \sigma_x = \frac{N_E}{A_c} + \frac{M_E \cdot z}{I_c} \tag{2.3}$$

To obtain the stresses in a cross section, the cross sectional properties (A_c, b_w, z), sectional forces (N_E, V_E, M_E) and resistances of the local cross-sections (I_c, S_c) should be determined. The stresses in Equation 2.3 should be related to the strength of concrete. Therefore it is necessary to transform the stresses (τ_{xy}, σ_x and σ_z) into principal stresses (σ_1, σ_2). This is done with the Mohr's Circle, see Figure 2.13. The corresponding transformation expression is shown in Equation 2.4. In this expression the tensile stresses are positive and compressive stresses negative.

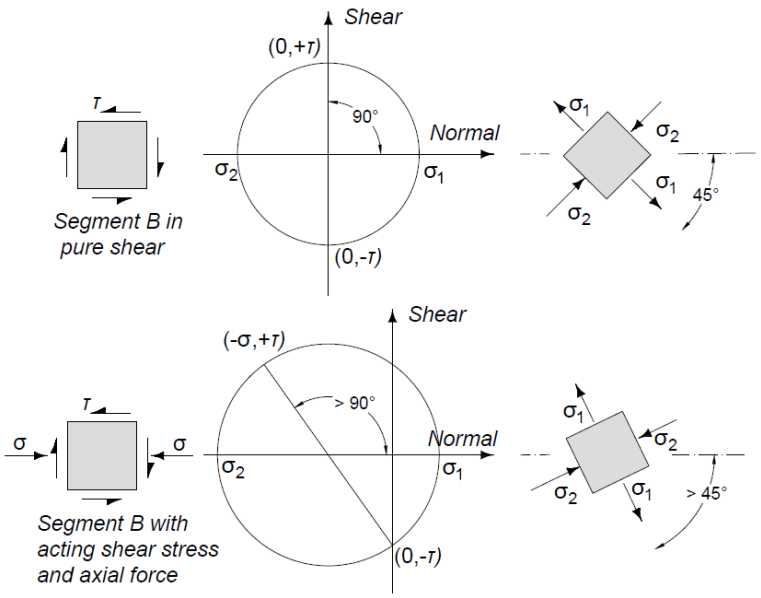

Figure 2.13: Mohr's circle to transform τ_{xy}, σ_x and σ_z into principal stresses [18]

$$\sigma_{1,2} = \frac{\sigma_x + \sigma_z}{2} \pm \sqrt{\left(\frac{\sigma_x - \sigma_z}{2}\right)^2 + {\tau_{xy}}^2} \tag{2.4}$$

Equation 2.4 is simplified in the existing analytical models, see Equation 2.5. By neglecting the stresses perpendicular to the longitudinal axis of the beam (σ_z) the highest principal stress is by definition a tensile stress, which is frequently described as the 'principal stress criterion' [24].

$$\sigma_1 = \frac{\sigma_x}{2} \pm \sqrt{\left(\frac{\sigma_x}{2}\right)^2 + {\tau_{xy}}^2} \tag{2.5}$$

It is recommended calculating the cross-sectional resistances together with the shear- and principal stresses with the use of data analyzing software like `MS Excel`, to get a good representation of the

stresses along the height of the beam. Since most cross-sections are not homogeneous, thus having varying widths along the height, a good method is dividing the cross sections in layers of 5 mm of height. The first moment of area (S_c) and second moment of area (I_c) can be calculated using the distance from the top of the layer to the center of gravity of the cross section.

2.5.2. Tensile strength of the concrete

If the principal stresses in the web exceed the tensile strength of the concrete, diagonal tension cracking occurs. Two different approaches are found in the literature to calculate the tensile strength of concrete, namely axial tensile strength f_{ct} and cracking strength f_{cr}. The Eurocode 2 and MC2010 use f_{ctm}, while the ACI (and CSA) use f_{cr}, see Figure 2.14 for the difference between the two approaches. The axial tensile strength of concrete is used in the EC2 and MC2010, which is a result of uniaxial tensile tests. The tensile strength is not derived directly from these tests, but is mostly acquired from split cylinder tests. From these tests the axial tensile strength is empirically determined from relations between the test results and uniaxial tensile strength. Diagonal tension cracking is assumed to occur when the principal stress is greater than the axial tensile strength, see Equation 2.6 [24].

$$f_{ctm} = \begin{cases} 0.3{f_{cm}}^{2/3}, & \text{for strength class} \leq C50/60 \\ 2.12ln\left[1 + \left(1 + \frac{f_{cm}}{10}\right)\right], & \text{for strength class} > C50/60 \end{cases} \tag{2.6}$$

For the relation between the cylinder compressive strength and cracking strength there are two commonly used expressions, namely the one used in ACI [58] and Bentz' expression [59]. Bentz's expression is an alternative expression that 'corrected' the cracking strength for higher concrete cylinder compressive strengths. He concluded that the expression used in the ACI was accurately predicting the cracking strength of lower concrete classes, but was overestimating for higher concrete classes [24]. In equations 2.7 and 2.8 the ACI and Bentz expression are given respectively.

$$f_{cr} = 0.332\sqrt{f_{cm}} \tag{2.7}$$

$$f_{cr} = 0.45{f_{cm}}^{0.4} \tag{2.8}$$

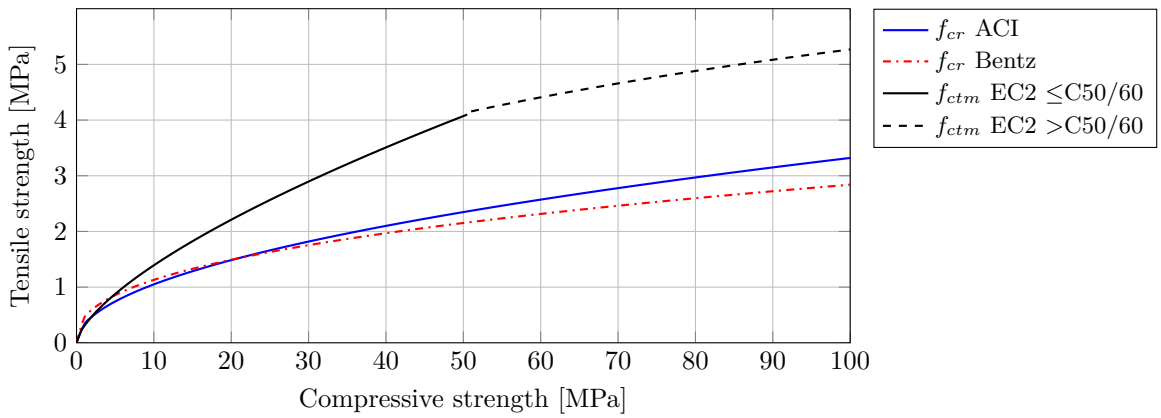

Figure 2.14: Different approaches obtaining the tensile strength of concrete

In literature different values for the diagonal tension strength are found, this is due to size effect and bi-axial stress state. The tensile strength of concrete is done on splitting tests, which is performed on small samples. Small samples tend to have the property that encountering the weakest link inside the concrete is less likely than with bigger samples, thus overestimating the tensile strength. The second argument is that the principal compressive stress cannot be neglected, as is done in ACI, EC2, MC2010 and CSA. Having a principal compressive stress next to a principal tensile stress reduces the concrete tensile strength. Various researchers have investigated this relation and confirmed that applying more compressive load reduces the tensile strength of concrete [24].

2.5.3. Calculating shear-tension capacity

To analytically calculate the shear-tension capacity of a girder with the use of Euler-Bernoulli beam theory, the principal stresses need to be calculated over the full height of the cross-section. Several cross-sections have to be checked, between the load and the thickened section of the girder for both the web and the most tensioned flange. Where the principal stresses exceeds the axial tensile strength (f_{ctm}) or cracking strength (f_{cr}) diagonal tension cracks occurs, which could lead to shear-tension failure. With the use of `MS Excel` and layers of the cross-section of 5 mm, an accurate result can be generated to see where the high principal stresses occur with a certain external load and shear span. For flexural cracks the measured average splitting tensile strength ($f_{ctm,sp}$) is used from tests, for diagonal tension cracks ($f_{ctm} = 0.9 f_{ctm,sp}$) is used. This means that the principal stresses in the tension flange are allowed to be higher than the principal stresses calculated in the web. Using the goal-seek function in `MS Excel` the maximum allowed external load can be calculated for shear-tension failure, if set to f_{ctm} or f_{cr} in the web provided that the principal stresses do not exceed $f_{ctm,sp}$ in the most tensioned flange of the girder. For determining the critical range of cross-sections for shear-tension failure, it is important to note that cross-sections closer than a 45° inclined line from the load to the neutral axis of the member are not of interest. This is due to the fact that diagonal-tension cracking will not occur for angles greater than 45°.

2.6. Code provisions for shear resistance of prestressed members

A lot of countries have different approaches on the failure mechanisms and determining the shear resistance of reinforced-/prestressed concrete members with and without transverse reinforcement. These approaches and models are adopted in the national codes of each country. Five design codes are evaluated in this literature review:

- Chapter 2.7: American Concrete Institute (ACI)
- Chapter 2.8: American Association of State Highway and Transportation Officials (AASHTO)
- Chapter 2.9: Eurocode 2 (EC2)
- Chapter 2.10: Richtlijnen Beoordeling Kunstwerken (RBK1.1)
- Chapter 2.11: Eurocode 2 DRAFT 2018 (EC2 2018)

Table 2.2 shows a summary of all considered design codes that distinguish between flexure-shear- and shear-tension failure. Only the ACI and EC2 (without stirrups) distinguish between flexure-shear- and shear-tension failure. Table 2.3 shows the models used by the five code provisions for members with and without transverse reinforcement.

Table 2.2: Summary of code provisions that distinguish between flexure-shear- and shear-tension failure

Code	Without stirrups		With stirrups	
	flexure-shear	shear-tension	flexure-shear	shear-tension
ACI	✓	✓	✓	✓
AASHTO				
EC2	✓	✓		
RBK1.1				
EC2 2018				

Table 2.3: Summary for the models used by the five code provisions

Code	Model for concrete	Model for stirrups
ACI	Experimentally derived	Truss Model
AASHTO	SMCFT[1]	Truss Model
EC2	Experimentally derived	Variable Angle Truss Model
RBK	Experimentally derived	Variable Angle Truss Model
EC2 2018	CSCT[2]	Variable Angle Truss Model

[1] Simplified Modified Compression Field Theory.
[2] Critical Shear Crack Theory.

2.7. American Concrete Institute (ACI)

The expressions used in ACI are based on experiments done by MacGregor [60] on prestressed single span girders with shear reinforcement. Therefore the ACI is based on a empirical model. When an external load is placed on a prestressed beam, for example a concentrated load, the principal stresses vary over the height of the beam. In case bending and shear are present, the maximum principal stress might be in another axis than the center of gravity. The ACI code considers the principal stresses only in the center of gravity, which could be seen as a simplification, although some researchers observed that diagonal tension cracks mostly initiate in this center [24]. The expressions used in this Chapter are based on SI metric system and Building Code Requirements for Structural Concrete (ACI 318-14) and commentary (ACI 318R-14).

2.7.1. ACI nominal shear resistance

The ACI makes the same distinction between the three modes of failure of beams without diagonal tension reinforcement derived from MacGregor's experiments [60]; flexural failure [F], flexural-shear failure [Flexure-Shear, FS] and web-shear failure/shear-tension failure [Web-Shear, WS]. Some simplifications were made, the resistances MacGregor has found for flexural-shear- and web-shear failure are changed to the same equation without shear reinforcement, provided in Equation 2.10 and 2.12. The concrete tensile strength is used as the specified concrete compressive strength f'_c instead of the modulus of rupture f_r. Finally, the factor of the contribution of the shear reinforcement is set to 1.0 [24].

When designing for shear, it is necessary to determine which mode of failure is dominant. The lowest resistance to flexure-shear (V_{ci}) and web-shear (V_{cw}) is used to calculate the shear strength of concrete V_c. This method is also called the lowest resistance approach and is the same as MacGregor's expression [21] [58]. The nominal shear resistance V_n is given in Equation 2.9. For a prestressed member without shear reinforcement the nominal shear resistance is equal to the inclined cracking load V_c. For prestressed members with shear reinforcement the resistance of the transverse reinforcement V_s is added. The concrete contribution (V_c) is the lowest of flexural-shear- (V_{ci}) and web-shear-cracking (V_{cw}).

$$V_n = V_c + V_s \quad \text{with} \quad V_c = \min(V_{ci}, V_{cw}) \tag{2.9}$$

The ACI makes no distinction in the concrete shear strength V_c between members with and without transverse reinforcement. The shear strength of concrete is taken as the shear causing inclined cracking. After cracking the concrete shear strength takes into account the shear transfer mechanisms: aggregate interlock, dowel action and the shear transmitted across the concrete compression zone [58]. The equations provided in this paragraph are converted to the metric system (N and mm) [20]. According to the ACI, the first critical cross-section for shear is considered at a distance of h/2 from the face of the support.

2.7.2. Resistance to flexure-shear cracking

The flexure-shear resistance is given in Equation 2.10. The first part ($0.0498\sqrt{f'_c} \cdot b_w \cdot d_p$) is the result of experimental tests. This additional shear force is needed to fully develop an inclined crack that originates from a flexural crack. This means that the ACI code only allows diagonal tension cracks (flexural-shear cracks) with the presence of flexural cracks. The second part contains the cracking moment M_{cr} (Equation 2.11), which is the moment causing flexural cracks due to an external load [21].

$$V_{ci} = 0.0498\sqrt{f'_c} \cdot b_w \cdot d_p + \frac{V_u}{M_u} \cdot M_{cr} \tag{2.10}$$

$$\text{with} \quad M_{cr} = \frac{I_c}{y_t} \cdot \left(0.498\sqrt{f'_c} + f_{pe} - f_d\right) \quad \text{with} \quad f_{pe} = \frac{M_p \cdot z_{bottom}}{I_c} - \frac{N_p}{A_c} \tag{2.11}$$

Where d_p is the effective depth to the centroid of the prestressing steel and need to be taken greater than $0.80h$, b_w is the width of the web, f_{pe} is the concrete compressive stress due to effective prestress at extreme fibers of the cross section where tensile stress is caused by external load and f_d is the stress due to the dead load. V_u/M_u is the factored shear force at the calculated cross section due to an externally applied load occurring simultaneously with the moment. Multiplying this factor with the cracking moment reflects the resistance to flexural cracking.

2.7.3. Resistance to web-shear cracking

The ACI provides a simplified method to calculate the web-shear cracks in a prestressed beam, which is experimentally tested by Elzanaty [61]. An external load will cause indeterminate stresses and are calculated by evaluating the principal tensile stresses at the critical plane, based on Equation 2.5. Extensive testing shows that the web shear stress $\nu_{cw} = 0.291\sqrt{f'_c} + 0.3f_{pc}$ (in MPa) is maximum near the center of gravity of the cross section where the diagonal crack develops. The principal tensile stress is assumed to be equal to the concrete tensile strength ($\sigma_1 = f'_t$). The stress in the concrete due to prestressing f_{pc} is calculated at the centroid of the section when the center of gravity is in the web. By multiplying the web-shear stress by $b_w \cdot d_p$, the resistance to web-shear-/shear-tension failure results in:

$$V_{cw} = \left(0.291\sqrt{f'_c} + 0.3f_{pc}\right) \cdot b_w \cdot d_p + V_p \quad \text{with} \quad f_{pc} = \frac{N_p}{A_c} \tag{2.12}$$

With $d_p > 0.80h$ and V_p as the vertical component of the prestressing force. For V_{cw} it holds that when the centroidal axis is located in the web of the prestressed cross-section, the principal tensile stresses are calculated at the centroidal axis. Elzanaty [61] found that using this simplified expression for higher prestressed girders, the shear resistance decreased. He assumed that this is because of neglecting the bi-axial stress state. This means that using a higher concrete strength class with the same level of prestressing would increase the shear resistance [24] [58].

2.7.4. Contribution of the shear reinforcement

The resistance of the transverse reinforcement is added with the term V_s, which holds for both non- and prestressed concrete members. The design of transverse reinforcement in the ACI is based on a modified truss analogy. This means the vertical ties in the truss need to be resisted by the shear reinforcement, but only the shear exceeding that causes inclined cracking. In other words, the concrete resists shear until inclined cracking occurs, where after the transverse reinforcement takes over the remaining shear force [21]. The transverse reinforcement also functions for:

- Restriction of the diagonal crack growth;
- Holds longitudinal bars in place to provide for dowel action;
- Providing some restraint in the compressive zone of the concrete if the stirrups are in the form of closed ties.

The ACI provides an expression to calculate the strength of the transverse reinforcement and assumes that the diagonal truss is inclined at $\theta = 45°$. The stirrups can be designed with an angle α, with $\alpha = 90°$ for vertical stirrups. The concrete is assumed to contribute to the shear capacity with shear transfer mechanisms described in Chapter 2.2; concrete compressive zone, aggregate interlocking and dowel action.

$$\begin{aligned} \text{General expression ACI: } V_s &= \frac{A_v \cdot f_{yt} \cdot (\sin\alpha + \cot\alpha) \cdot d}{s} \\ \text{For } \alpha = 90° \quad &\Rightarrow \quad V_s = \frac{A_v \cdot f_{yt} \cdot d}{s} \\ \text{With } \frac{A_v}{s} = \frac{V_u - \phi_{ACI} \cdot V_c}{\phi_{ACI} \cdot f_{yt} \cdot d} \quad &\Rightarrow \quad A_{v,req} = \frac{(V_u - \phi_{ACI} \cdot V_c) \cdot s}{\phi_{ACI} \cdot f_{yt} \cdot d} \end{aligned} \tag{2.13}$$

Where α is the angle between the inclined stirrups and the longitudinal axis of the member, θ is the angle between the diagonal compressive strut and the longitudinal axis of the member, s is the spacing between stirrups and is measured along the longitudinal axis, f_{yt} is the design yield strength of the transverse reinforcement between spacing s, A_v is the effective area of all stirrups within spacing s, d is the effective depth of the longitudinal tension reinforcement and ϕ_{ACI} is a strength reduction factor and is taken as 0.75 [58].

2.8. American Association of State Highway and Transportation Officials (AASHTO)

The AASHTO is a design code for calculating bridges, while the ACI is intended for the calculation of buildings. Section 5 of the AASHTO provides calculations for reinforced- and prestressed concrete structures with- and without transverse reinforcement. This Chapter is based on the SI-metric system [54] and on the AASHTO - 8th Edition released in 2017 [62]. The expressions provided by the AASHTO are derived from the Modified Compression Field Theory (MCFT) [15], which is explained in Chapter 6.1.

The AASHTO is divided into three methods to calculate the nominal shear resistance of a prestressed beam. If the member is provided with transverse reinforcement it is necessary to check if the requirements of the minimum transverse reinforcement are fulfilled to determine which method is applicable [54].

2.8.1. Critical cross-section for shear near the end support

The critical cross-section according to the AASHTO is located at:

> Where the reaction force in the direction of the applied shear introduces compression into the end region of a member, the location of the critical section for shear is taken as the larger of $0.5 d_v \cot\theta$ or d_v from the internal face of the support [62].

The values for d_v and θ are measured at the critical section for shear. This requires to first estimate the location of the critical section and calculate d_v and θ. After determining the shear resistance at that section, a more accurate location must be determined.

2.8.2. Minimum transverse reinforcement

The AASHTO requires the use of transverse reinforcement, usually stirrups, in all regions that have a high chance of occurrence for diagonal cracking. It is to restrain the growth of the diagonal cracking and to increase the ductility of the member. The area of the transverse reinforcement that is required must satisfy:

$$A_v \geq 0.083\sqrt{f'_c} \cdot \frac{b_v \cdot s}{f_y} \tag{2.14}$$

The area of the transverse reinforcement A_v is calculated for all stirrups within distance s, where b_v is the width of the web adjusted for the presence of ducts as specified in Figure 2.15a, s is the spacing of the transverse reinforcement and f_y is the yield strength of the transverse reinforcement.

Flexural failures occur over a vertical plane, while shear failures have an incline plane. This means a shear crack typically intersects a number of stirrups. The length of this crack along the longitudinal axis of the member is taken as $d_v \cot\theta$, see Figure 2.15b [54].

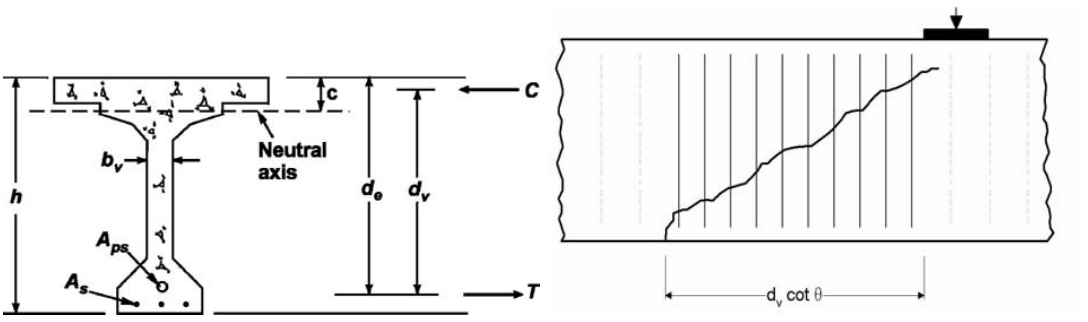

(a) Determining the terms b_v and d_v

(b) Theoretical effective zone of the stirrups and shear design section location

Figure 2.15: Determining the minimum transverse reinforcement according to AASHTO [54]

2.8.3. AASHTO Nominal shear resistance

The nominal shear resistance V_n is the minimum value of the two expressions given in Equation 2.15. The first formula separates the shear resistance of a concrete member in three components; V_c depends on the tensile stresses in the concrete, V_s depends on the tensile stresses in the shear reinforcement and V_p as the vertical component of the prestressing force. The second formula is the upper limit of V_n and ensures that the concrete compressive struts will not crush before yielding of the stirrups [54].

$$V_n = \min \begin{cases} V_c + V_s + V_p \\ 0.25 f'_c \cdot b_v \cdot d_v + V_p \end{cases} \tag{2.15}$$

The effective shear depth of the longitudinal reinforcement and the prestressing steel d_v must be taken greater than the maximum of $0.72h$ or $0.9d_e$:

$$d_e = \frac{A_{ps} f_{ps} d_p + A_s f_y d_s}{A_{ps} f_{ps} + A_s f_y} \text{ [mm]} \quad \text{and} \quad d_v = \frac{M_n}{A_s f_y + A_{ps} f_{ps}} \text{ [mm]}$$

$$M_n = A_{ps} f_{ps} \left(d_p - \frac{a}{2}\right) + A_s f_s \left(d_s - \frac{a}{2}\right) - A'_s f'_s \left(d'_s - \frac{a}{2}\right) + \alpha_1 \cdot f'_c \cdot (b_{cf} - b_v) \cdot h_f \left(\frac{a}{2} - \frac{h_f}{2}\right)$$

$$f_{ps} = f_{pu}\left(1 - k\frac{c}{d_p}\right) \text{ [MPa]} \quad \text{with} \quad k = 2\left(1.04 - \frac{f_{py}}{f_{pu}}\right) \quad \text{(for bonded tendons only)} \tag{2.16}$$

$$c = \begin{cases} c_T = \dfrac{A_{ps} f_{pu} + A_s f_s - A'_s f'_s - \alpha_1 \cdot f'_c \cdot (b_{cf} - b_v) \cdot h_f}{\alpha_1 \cdot f'_c \cdot \beta_1 \cdot b_v + k \cdot A_{ps} \cdot \dfrac{f_{pu}}{d_p}} \text{ [mm]}, & \text{(for T-section behavior)} \\ c_{rect} = \dfrac{A_{ps} f_{pu} + A_s f_s - A'_s f'_s}{\alpha_1 \cdot f'_c \cdot \beta_1 \cdot b_{cf} + k \cdot A_{ps} \cdot \dfrac{f_{pu}}{d_p}} \text{ [mm]}, & \text{(for rectangular behavior)} \end{cases}$$

Where M_n is the nominal flexural resistance, A_{ps}, A_s, A'_s and f_{ps}, f_s, f'_s are the areas and average stresses of the prestressing steel, non-prestressed tension reinforcement and compression reinforcement respectively, f_y is the yield strength of the transverse reinforcement (< 690 MPa), f_{pu} is the specified tensile strength of the prestressing steel, f_{py} is the yield strength of the prestressing steel, b_{cf} and b_v are the widths of the compression flange and web respectively, h_f is the depth of the compression flange, d_e is the distance from the extreme compression fiber to the centroid of the prestressing and longitudinal tension reinforcement, d_p, d_s and d'_s are the distances from the extreme compression fiber to the centroid of the prestressing tendons, longitudinal tension reinforcement and longitudinal compression reinforcement respectively, c is the distance between the neutral axis and the extreme compression fiber (depending on the behavior $c = c_T$ or $c = c_{rect}$), k is a factor for the stress in the prestressing steel at nominal flexural resistance, $a = c \cdot \beta_1$ is the depth of the equivalent stress block and α_1 and β_1 are stress block factors specified as:

$$\alpha_1 = \begin{cases} 0.85, & \text{for } f'_c < 69 \text{ MPa} \\ 0.85 - 0.02 \text{ for each 7 MPa exceeding 69 MPa} > 0.75, & \text{for } f'_c > 69 \text{ MPa} \end{cases}$$

$$\beta_1 = \begin{cases} 0.85, & \text{for } f'_c < 28 \text{ MPa} \\ 0.85 - 0.02 \text{ for each 7 MPa exceeding 28 MPa} > 0.65, & \text{for } f'_c > 28 \text{ MPa} \end{cases}$$

The contribution of the transverse reinforcement is in general:

$$V_s = \frac{A_v \cdot f_y \cdot d_v \cdot (\cot\theta + \cot\alpha) \cdot \sin\alpha}{s}$$

$$\text{if } \alpha = 90° \quad \Rightarrow \quad V_s = \frac{A_v \cdot f_y \cdot d_v \cdot \cot\theta}{s} \tag{2.17}$$

$$\text{if } \alpha = 90° \text{ and } \theta = 45° \quad \Rightarrow \quad V_s = \frac{A_v \cdot f_y \cdot d_v}{s}$$

Where α is the inclination between the transverse reinforcement and the longitudinal axis of the member and θ is the inclination between the compressive strut and the longitudinal axis of the member.

The procedure for determining the shear resistance of the concrete V_c is divided in two methods. The second method is derived from the MCFT [15]. These equations are equivalent to the equations used in the CSA design code [62]:

Method 1: only applicable for nonprestressed sections;

Method 2: applicable for all prestressed and nonprestressed members, with and without shear reinforcement, with and without axial load.

Method 1 is of no interest in this research, since it is not applicable for prestressed members. The general procedure for Method 2 can be calculated with two different approaches, one with algebraic equations and one with iterative use of tables (Appendix B5 in AASHTO). According to AASHTO both approaches lead to the same results. The difference between the two approaches is that with algebraic equations the strain at the tension reinforcement ε_s is calculated see Figure 2.16, while with the use of tables the longitudinal strain is calculated at mid depth of the girder ε_x see Figure 2.17.

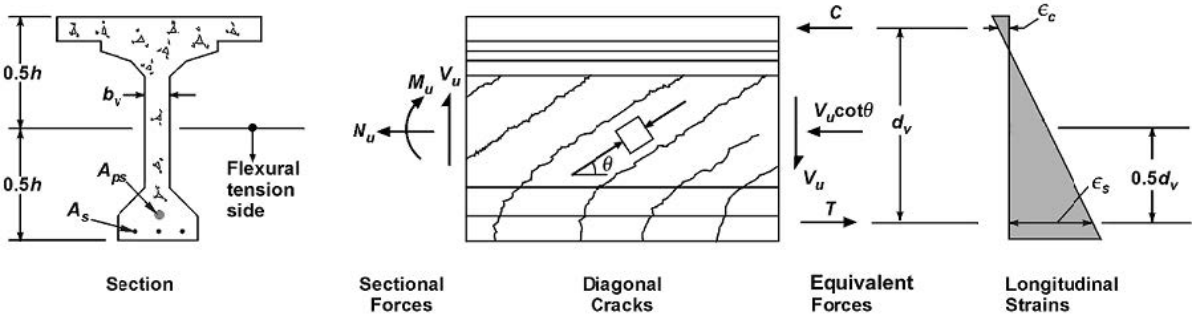

Figure 2.16: Illustration to determine the longitudinal strain at the tension reinforcement with sufficient transverse reinforcement (approach with algebraic equations) [62]

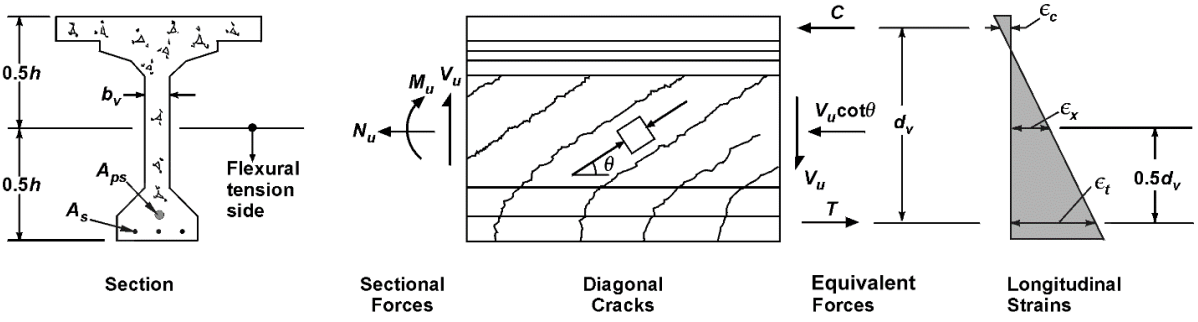

Figure 2.17: Illustration to determine the longitudinal strain at the mid depth of the member with sufficient transverse reinforcement (approach with tables) [62]

For Method 2, which is applicable for members with and without transverse reinforcement, the shear resistance of the concrete is calculated with:

$$V_c = 0.083\beta\sqrt{f'_c} \cdot b_v \cdot d_v \tag{2.18}$$

Where β is a factor indicating ability of diagonally cracked concrete to transmit tension (aggregate interlock component). This factor depends on the longitudinal (tensile) strain and in case of insufficient transverse reinforcement, also on the crack spacing parameters s_{xe} and s_x. These factors are derived from the MCFT [15] and are calculated as follows (valid for both approaches for Method 2):

$$s_{xe} = s_x \cdot \frac{35}{a_g + 16} \leq 2000 \text{ [mm]} \tag{2.19}$$

Where s_x is the minimum value of d_v or the maximum distance between layers of the longitudinal reinforcement ($A_s \geq 0.003 b_v \cdot s_x$), see Figure 2.18. The crack spacing parameter s_{xe} depends on the maximum aggregate size a_g in mm.

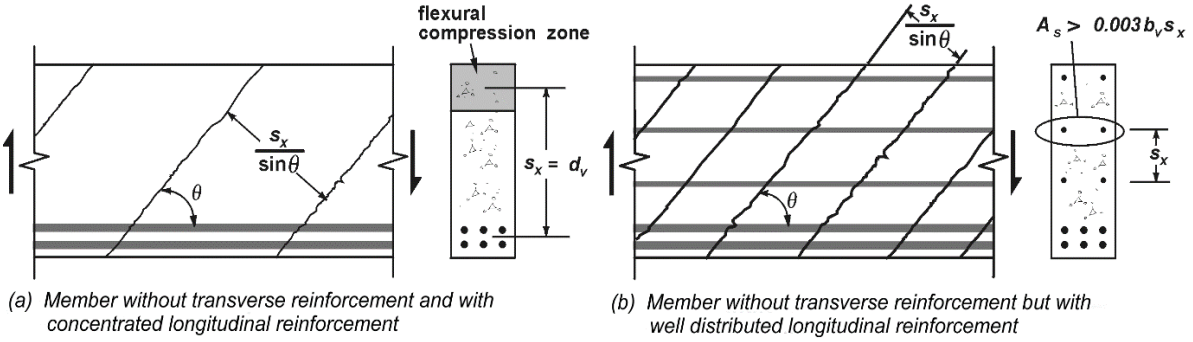

Figure 2.18: Determining the crack spacing parameter s_x for girders with insufficient transverse reinforcement [62]

2.8.4. Inclined cracking load with the use of algebraic equations

The aggregate interlock factor β and angle for the compression chord θ are calculated as follows:

$$\beta = \begin{cases} \dfrac{4.8}{1 + 750\varepsilon_s}, & \text{for fullfilling Equation 2.14} \\ \dfrac{4.8}{1 + 750\varepsilon_s} \cdot \dfrac{1300}{1000 + s_{xe}}, & \text{for not fullfilling Equation 2.14} \end{cases} \tag{2.20}$$

$$\theta = 29 + 3500\varepsilon_s \tag{2.21}$$

The values of $\theta = 45°$ and $\beta = 2.0$ correspond to reinforced concrete with a compressive strut under 45°. This equals Equation 2.18 to the equation traditionally used for evaluating shear resistance $V_c = 0.166\sqrt{f'_c} \cdot b_v \cdot d_v$. This may lead to very unconservative values for the inclined cracking load and is not valid for prestressed members, because the angle of the compression strut is usually lower and neglects the size effect in shear.

The AASHTO code provides an expression to calculate the net longitudinal strain in the section at the centroid of the tension reinforcement, see Figure 2.16. This expression can be used regardless of the requirements for the minimum transverse reinforcement as specified in Equation 2.14:

- General expression:

$$\varepsilon_s = \frac{\left(\dfrac{|M_u|}{d_v} + 0.5N_u + 0.5|V_u - V_p| \cdot \cot\theta - A_{ps} f_{po}\right)}{E_s A_s + E_p A_{ps}} < 6.0 \cdot 10^{-3}$$

- If the longitudinal strain ε_s is negative the following expression should be used:

$$\varepsilon_s = \frac{\left(\dfrac{|M_u|}{d_v} + 0.5N_u + 0.5|V_u - V_p| \cdot \cot\theta - A_{ps} f_{po}\right)}{E_c A_{ct} + E_s A_s + E_p A_{ps}} > -0.40 \cdot 10^{-3}$$

The area of concrete on the flexural tension side A_{ct} is calculated for the bottom $0.5h$ as shown in Figure 2.16. A_{ps} is the area of the prestressing steel on the flexural tension side. A_s is the area of the longitudinal reinforcement on the flexural tension side. f_{po} is usually taken as $0.7 f_{pu}$ for both pre- and post-tensioned members. N_u is the factored axial force and is taken negative for compression. $|M_u|$ is the absolute value of the factored moment which must be bigger than $|V_u - V_p| \cdot d_v$. V_u is the factored shear force on the member.

2.8.5. Inclined cracking load with the use of tables

The AASHTO code provides an expressions to calculate the net longitudinal strain at mid depth of the girder, see Figure 2.17. This expression depend on the fulfillment of the requirement for the minimum transverse reinforcement as specified in Equation 2.14:

- General expression with sufficient transverse reinforcement:

$$\varepsilon_x = \frac{\left(\frac{|M_u|}{d_v} + 0.5N_u + 0.5|V_u - V_p| \cdot \cot\theta - A_{ps}f_{po}\right)}{2(E_sA_s + E_pA_{ps})} < 0.001$$

- General expression with insufficient transverse reinforcement:

$$\varepsilon_x = \frac{\left(\frac{|M_u|}{d_v} + 0.5N_u + 0.5|V_u - V_p| \cdot \cot\theta - A_{ps}f_{po}\right)}{E_sA_s + E_pA_{ps}} < 0.002$$

- If the longitudinal strain ε_s is negative the following expression should be used:

$$\varepsilon_x = \frac{\left(\frac{|M_u|}{d_v} + 0.5N_u + 0.5|V_u - V_p| \cdot \cot\theta - A_{ps}f_{po}\right)}{2(E_cA_{ct} + E_sA_s + E_pA_{ps})} > -0.40 \times 10^{-3}$$

These expressions are based on:

$$\varepsilon_x = \frac{\varepsilon_c + \varepsilon_t}{2} \tag{2.22}$$

With ε_c as the strains in the compression chord "C" and ε_t as the strains in the tension chord "T", see Figure 2.17. The first equation conservatively takes $\varepsilon_x = 0.5\varepsilon_t$ and the second equation conservatively takes $\varepsilon_x = \varepsilon_t$. Notice that for both the first and second equation, the strain in the concrete is conservatively set to $\varepsilon_c = 0$. The longitudinal strain ε_x may also be calculated with a more detailed analysis for ε_c and ε_t with the use of Equation 2.22 and Figure 2.19.

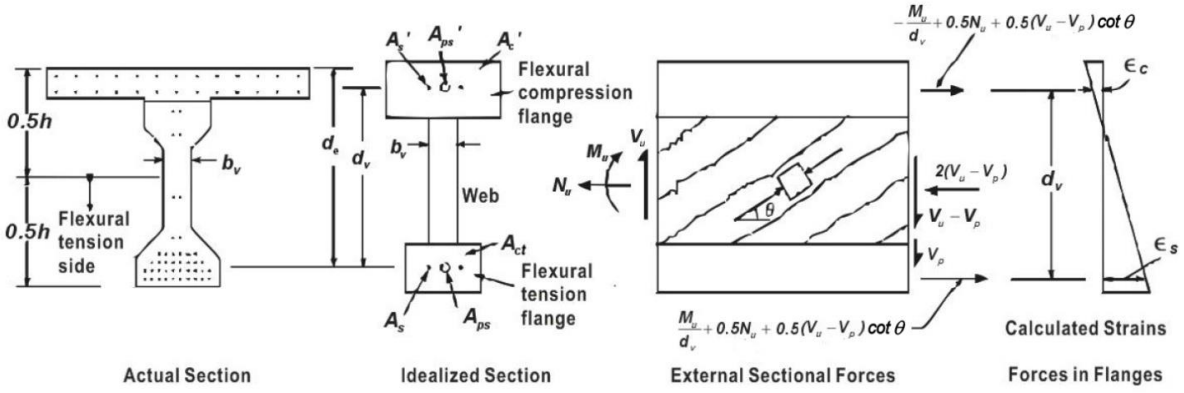

Figure 2.19: Illustration for a more detailed calculation for the strains at mid depth of the girder ε_x [54]

With the calculated longitudinal strain at mid depth of the girder, the values for β and θ can be found with the use of tables shown in Tables 2.4 or 2.5. For members with sufficient transverse reinforcement the ratio between the shear stress in the concrete ν_u and the concrete compressive strength f'_c must be known. The stress in the concrete equals:

$$\nu_u = \frac{V_u - \phi \cdot V_p}{d_v \cdot b_v} \text{ [MPa]} \tag{2.23}$$

With ϕ as the resistance factor for shear.

To determine the values for β and θ with the use of tables, the following actions are allowed:

- Linear interpolation between the rows of the table is permitted to account for the value of ν_u/f'_c (Table 2.4) or s_{xe} (Table 2.5) at the considered cross-section;
- Linear interpolation between the columns of the table is allowed to account for the calculated value of ε_x;
- Apart from linear interpolating between the cells, the values of θ and β from a cell that correspond to the values of ν_u/f'_c (Table 2.4) or s_{xe} (Table 2.5) with ε_x greater than the calculated value is allowed. For hand calculations this is faster and easier, but will lead to a more conservative result.

$\frac{v_u}{f'_c}$	$\varepsilon_x \times 1{,}000$								
	≤−0.20	≤−0.10	≤−0.05	≤0	≤0.125	≤0.25	≤0.50	≤0.75	≤1.00
≤0.075	22.3 6.32	20.4 4.75	21.0 4.10	21.8 3.75	24.3 3.24	26.6 2.94	30.5 2.59	33.7 2.38	36.4 2.23
≤0.100	18.1 3.79	20.4 3.38	21.4 3.24	22.5 3.14	24.9 2.91	27.1 2.75	30.8 2.50	34.0 2.32	36.7 2.18
≤0.125	19.9 3.18	21.9 2.99	22.8 2.94	23.7 2.87	25.9 2.74	27.9 2.62	31.4 2.42	34.4 2.26	37.0 2.13
≤0.150	21.6 2.88	23.3 2.79	24.2 2.78	25.0 2.72	26.9 2.60	28.8 2.52	32.1 2.36	34.9 2.21	37.3 2.08
≤0.175	23.2 2.73	24.7 2.66	25.5 2.65	26.2 2.60	28.0 2.52	29.7 2.44	32.7 2.28	35.2 2.14	36.8 1.96
≤0.200	24.7 2.63	26.1 2.59	26.7 2.52	27.4 2.51	29.0 2.43	30.6 2.37	32.8 2.14	34.5 1.94	36.1 1.79
≤0.225	26.1 2.53	27.3 2.45	27.9 2.42	28.5 2.40	30.0 2.34	30.8 2.14	32.3 1.86	34.0 1.73	35.7 1.64
≤0.250	27.5 2.39	28.6 2.39	29.1 2.33	29.7 2.33	30.6 2.12	31.3 1.93	32.8 1.70	34.3 1.58	35.8 1.50

Table 2.4: Table to determine the values θ and β with sufficient transverse reinforcement [62]

s_{xe} (mm)	$\varepsilon_x \times 1000$										
	≤–0.20	≤–0.10	≤–0.05	≤0	≤0.125	≤0.25	≤0.50	≤0.75	≤1.00	≤1.50	≤2.00
≤130	25.4 6.36	25.5 6.06	25.9 5.56	26.4 5.15	27.7 4.41	28.9 3.91	30.9 3.26	32.4 2.86	33.7 2.58	35.6 2.21	37.2 1.96
≤250	27.6 5.78	27.6 5.78	28.3 5.38	29.3 4.89	31.6 4.05	33.5 3.52	36.3 2.88	38.4 2.50	40.1 2.23	42.7 1.88	44.7 1.65
≤380	29.5 5.34	29.5 5.34	29.7 5.27	31.1 4.73	34.1 3.82	36.5 3.28	39.9 2.64	42.4 2.26	44.4 2.01	47.4 1.68	49.7 1.46
≤500	31.2 4.99	31.2 4.99	31.2 4.99	32.3 4.61	36.0 3.65	38.8 3.09	42.7 2.46	45.5 2.09	47.6 1.85	50.9 1.52	53.4 1.31
≤750	34.1 4.46	34.1 4.46	34.1 4.46	34.2 4.43	38.9 3.39	42.3 2.82	46.9 2.19	50.1 1.84	52.6 1.60	56.3 1.30	59.0 1.10
≤1000	36.6 4.06	36.6 4.06	36.6 4.06	36.6 4.06	41.2 3.20	45.0 2.62	50.2 2.00	53.7 1.66	56.3 1.43	60.2 1.14	63.0 0.95
≤1500	40.8 3.50	40.8 3.50	40.8 3.50	40.8 3.50	44.5 2.92	49.2 2.32	55.1 1.72	58.9 1.40	61.8 1.18	65.8 0.92	68.6 0.75
≤2000	44.3 3.10	44.3 3.10	44.3 3.10	44.33 3.10	47.1 2.71	52.3 2.11	58.7 1.52	62.8 1.21	65.7 1.01	69.7 0.76	72.4 0.62

Table 2.5: Table to determine the values θ and β with insufficient transverse reinforcement [62]

2.9. Eurocode 2 (EC2)

The NEN-EN 1992-1-1 or Eurocode 2 (EC2) uses a distributed stress model to predict failure for prestressed members. This implies that this model takes into account the stress distribution over the height of the beam and not only in the center of gravity axis of the beam. The axial tensile strength of concrete is used to determine diagonal tension cracking [24]. For determining the shear resistance, prestressed members are divided into members with and without transverse reinforcement [63]. First the method for members without stirrups is explained, which uses the cracked and uncracked in bending approach. Secondly the method for members with stirrups is described, which uses the variable angle truss method to determine the shear capacity. It is important to note that the EC2 distinguishes flexural-shear failure and shear-tension failure for members without shear reinforcement, but does not account for the two failure types for members with shear reinforcement.

2.9.1. EC2 without transverse reinforcement

Chapter 2.1 mentioned three areas in a concrete beam that are of interest. The EC2 provides a method in which the prestressed element without shear reinforcement should be divided in two areas, an area with low moment and high shear (Area A) and an area with high moment and high shear (Area B). These two areas are shown in Figure 2.20 and are called uncracked and cracked in bending [5]. The EC2 also implies that it is not necessary to calculate shear resistances for cross-sections that are in range of an inclined line of 45 degrees from the support to the elastic centroidal axis [63].

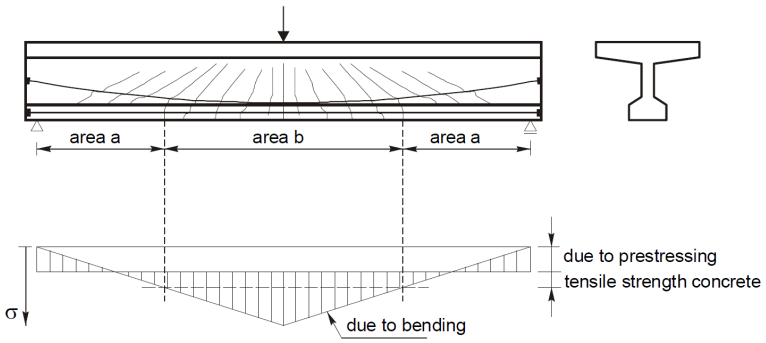

Figure 2.20: Regions in a prestressed beam with corresponding stresses [5]

Minimum shear reinforcement

The EC2 uses a lower bound value for the transverse reinforcement of members that do not require transverse reinforcement, with f_{yk} as the characteristic yield strength of the transverse reinforcement and f_{ck} as the characteristic compressive cylinder strength of concrete:

$$\rho_w = \frac{A_{sw}}{s \cdot b_w \cdot \sin\alpha} > \rho_{w,min} = 0.08\frac{\sqrt{f_{ck}}}{f_{yk}} \tag{2.24}$$

Where ρ_w is the shear reinforcement ratio, A_{sw} is the area of the shear reinforcement within length s, s is the spacing of the shear reinforcement measured along the longitudinal axis of the member, b_w is the width of the web of the member and α is the angle of the shear reinforcement and can be chosen between 45° and 90° with respect to the longitudinal axis of the beam.

Area A (Region uncracked in bending)

The first area A is close to the supports (for single-span beams) and shows no flexural cracks in the ultimate limit state. The cracks originate in the web at the position where the principal tensile stresses exceed the concrete tensile strength. The shear capacity of the beam is determined with the principal tensile stresses caused by the stresses from prestressing, external load and the bending moment. The principal stresses are determined from the linear elastic branch of the $\sigma - \varepsilon$-diagram, before reaching the cracking moment M_{cr}, see Equation 2.25. Members externally loaded without shear reinforcement will fail in this area when inclined cracks develop [5] [24].

$$\sigma_1 = \frac{\sigma_x}{2} \pm \sqrt{\left(\frac{{\sigma_x}^2}{4}\right)^2 + {\tau_{xy}}^2} = f_{ctd} \text{ [MPa]}$$
$$\text{with} \quad \tau_{xy} = \frac{V_{Rd,c} \cdot S_c}{b_w \cdot I_c} \quad \text{and} \quad \sigma_x = \alpha_l \cdot \sigma_{cp} \quad \text{and} \quad \sigma_{cp} = \frac{N_{Ed}}{A_c} < 0.2 f_{cd} \tag{2.25}$$

With f_{ctd} as the design axial tensile strength of concrete and σ_{cp} and N_{Ed} as the stresses and axial force caused by loading or prestressing (positive for compression). The factor for the transition length α_l is added for prestressed members and is used for (bonded) pre-tensioned tendons where the compressive prestressing force is transmitted to the concrete by bond. Equation 2.26 is for regions uncracked in bending and calculates the **shear-tension capacity** of a member. Concrete is uncracked in bending if the flexure tensile stresses in the extreme fiber is less than $\frac{f_{ctk,0.05}}{\gamma_c} = \frac{0.7 f_{ctm}}{\gamma_c}$ [18] [63].

$$V_{Rd,c} = \frac{I_c \cdot b_w}{S_c} \sqrt{{f_{ctd}}^2 + \alpha_l \cdot \sigma_{cp} \cdot f_{ctd}} \tag{2.26}$$

Area B (Region cracked in bending)
The shear capacity of a beam without shear reinforcement depends on several factors, such as the development of flexural cracks, as they can grow into flexural-shear cracks. Due to a compressive prestressing force in the outer tensile fiber σ_{cb}, flexural cracks start to develop at a higher external force. Hedman & Losberg [64] proposed a method which takes into account the influence of the prestressing force. By applying a concentrated load (introducing a bending moment) and $\sigma_{cb} = 0$, a compensating moment M_0 is obtained see Equation 2.27. R_n is the support reaction due to prestressing and a is the shear span, see Figure 2.21 [5].

$$M_0 = \sigma_{cb} \cdot W_{cb} = P_m \left(\frac{W_{cb}}{A_c} \cdot e_p\right) = P_m \left(\frac{1}{6}h + e_p\right) = R_n \cdot a \tag{2.27}$$

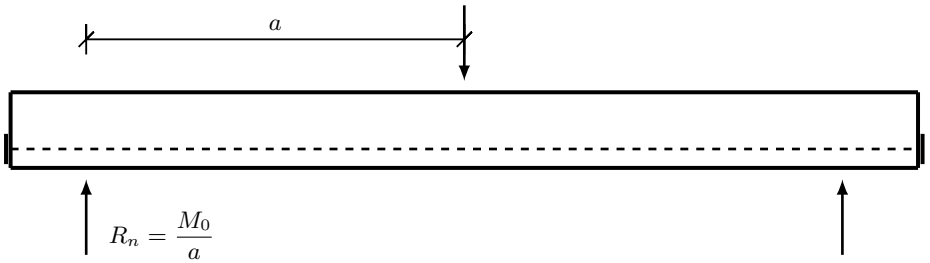

Figure 2.21: Shear resistance influenced by introducing a prestressing force R_n [5]

For beams with rectangular cross-sections, the following values are found through experiments for shear critical beams: $d = 0.85h$ and $e_p = 0.35h$. This results in a shear force increase of [5] [29]:

$$R_n = \begin{cases} 0.24 P_m, & \text{for } a/d = 2.5 \\ 0.15 P_m, & \text{for } a/d = 4.0 \end{cases} \tag{2.28}$$

The lowest contribution is when $a/d = 4.0$ with $R_n = 0.15 P_m = \sigma_{cp} \cdot b_w \cdot d$ and is used in the EC2 to calculate the **flexural-shear capacity** of beams without reinforcement, see Equation 2.29. It was originally implemented in the CEB-FIP Model Code of 1990 (MC90) [65], is empirically derived and is based on a 5% lower limit of the shear capacity of beams without shear reinforcement and prestressing. The EC2 states that an axial compressive force σ_{cp} increases the shear capacity of that element, because the crack width and growth is reduced [5].

$$V_{Rd,c} = \left[C_{Rd,c} \cdot k \cdot (100 \rho_l \cdot f_{ck})^{1/3} + k_1 \cdot \sigma_{cp}\right] \cdot b_w \cdot d$$
$$\text{with} \quad k = 1 + \sqrt{\frac{200}{d}} \leq 2.0 \quad \text{and} \quad \rho_l = \frac{A_{sl}}{b_w \cdot d} \leq 0.02 \tag{2.29}$$

The recommended values according to EC2 are $C_{Rd,c} = 0.18/\gamma_c$ with $\gamma_c = 1.5$, k is the size-effect coefficient with d as the effective depth in mm, ρ_l is the longitudinal reinforcement ratio, $k_1 = 0.15$ (see Equation 2.28 for $a/d = 4.0$) and b_w is the smallest width of the cross section in the tensile area.

Equation 2.29 shows that if the reinforcement ratio ρ_l goes to zero, the contribution of the concrete to the shear resistance goes to zero. Solving ρ_l for $a/d = 2.5$ (most unfavourable) results in a minimum contribution of the concrete:

$$\begin{aligned} \nu_{min} &= 0.035 k^{3/2} \sqrt{f_{ck}} \quad [\text{MPa}] \\ V_{Rd,c} &> \Big[\nu_{min} + k_1 \cdot \sigma_{cp}\Big] \cdot b_w \cdot d \end{aligned} \tag{2.30}$$

For concentrated loads closer than $a < 2.5d$, the shear capacity is increased due to arching action. EC2 takes this into account with a factor β. If a concentrated load is closer to the support than $a_v < 2d$, with a_v as the clear shear span, the shear resistance $V_{Rd,c}$ may be multiplied by $\beta = a_v/2d$ provided that the longitudinal reinforcement is fully anchored at the support. The minimum value is $a_v \geq 0.5d$. However, the shear force without the factor β should always be less than $0.5 b_w \cdot d \cdot \nu \cdot f_{cd}$, where ν is a reduction factor for cracked concrete due to shear [63].

$$V_{Rd,c} \cdot \beta_{EC2} = \Big[C_{Rd,c} \cdot k \cdot (100 \rho_l \cdot f_{ck})^{1/3} + 0.15 \sigma_{cp}\Big] b_w d \quad \text{with} \quad \beta_{EC2} = \max\left(\frac{a_v}{1.2d}\right) \leq 4 \tag{2.31}$$

$$V_{Ed} \leq 0.5 b_w \cdot d \cdot \nu \cdot f_{cd} \quad \text{with} \quad \nu = 0.6 \left[1 - \frac{f_{ck}}{250}\right] \quad (f_{ck} \text{ in MPa}) \tag{2.32}$$

2.9.2. EC2 with transverse reinforcement

The approach of the Eurocode to determine the shear resistance of members with shear reinforcement differs from members without shear reinforcement: a truss model is used and it is assumed that cracked concrete does not contribute to the shear resistance. The truss model is named variable angle truss model and is based on the 45° model.

Variable angle truss model

The earlier model for trusses, the 45 degree truss model developed by Ritter [11] and Mörsch [12]), explained the flow of forces in cracked concrete beams. An angle of 45° is assumed for the diagonal compressive strut and the truss consists of a transverse tension tie, top compression chord and a bottom tension chord [18] [24]. Three assumptions were made for this model:

- Neglecting the tensile stresses in cracked concrete;
- Diagonal compressive stress is related to the cracking angle and stays 45° after cracking;
- The top and bottom chord do not contribute to the shear resistance and shear stresses are uniformly distributed over an effective shear area ($b_w \cdot d$).

Research showed that prestressed/reinforced concrete beams with shear reinforcement, shear cracks form at a smaller angle than 45°. The 45° model overestimated the stresses in the stirrups, which means the girder has (substantial) more resistance than originally thought. This additional resistance consists of: aggregate interlock; dowel action; arch action and additional truss action (connections are not perfect hinges). This discovery led to the variable angle truss model [24].

Walraven et al. [66] [67] have done experiments to check the behavior of the rotating struts, by measuring the deformation of the web in shear-loaded I-beams. For non-prestressed beams the angle of principal strain is 45°, before any diagonal cracks occur. The rotation of the strut, thus a decrease of the angle θ, depends on the amount of shear reinforcement. If a large amount of shear reinforcement is present in the beam, the concrete will crush before yielding of the stirrups. On the other hand if the shear reinforcement ratio is low the stirrups will yield, which causes the compressive struts to rotate. The lower the angle, the more stirrups will be activated, the more load can be resisted. However, the rotation of the struts is limited by crushing of the concrete [18] [24].

For members with shear reinforcement, the variable angle truss model is the basis for the Eurocode. In this model the angle of the compressive strut can be variable ($2.5 \leq \cot\theta \leq 1.0$ or $21.8° \leq \theta \leq 45°$), which results in more shear capacity if the angle of the truss is assumed lower than 45°. It is a

lower bound approach of the theory of plasticity and is based on equilibrium. It assumes that a truss is present in the member, where the concrete and reinforcement are different elements. The shear reinforcement (stirrups) represents the vertical component of this truss, the concrete the diagonal component (compression) and the longitudinal reinforcement (tension) the tension chords, see Figure 2.22. The variable angle truss model implemented in the Eurocode is adjusted for prestressed members with shear reinforcement. The derivation of the variable angle truss model does not distinguish between the two shear failure modes: shear-tension failure and flexural-shear failure [24] [53] [63].

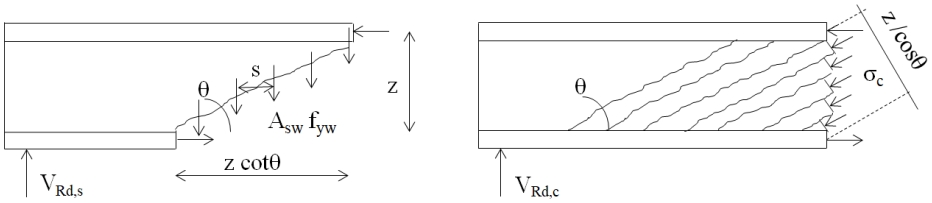

Figure 2.22: Variable angle truss model with stirrups, longitudinal reinforcement and an inclined compression field [24]

Calculation of members that require shear reinforcement

If the acting shear force is higher than the shear resistance of the member, transverse reinforcement should be provided. As explained in the previous paragraph the behavior of a beam with stirrups significantly changes, because the formation of a diagonal crack does not lead to instant failure. The amount of shear reinforcement required is calculated with the variable angle truss model, which covers a new load transfer mechanism after formation of diagonal cracks. The transfer of loads is divided in a tensile tie and a compressive strut [5].

The Eurocode explicitly separates the cross-section of a member in uncracked and cracked state. Before the EC2, in the Dutch concrete design code NEN 6720, it was assumed that the shear resistance of a member with transverse reinforcement was the contribution of the concrete and steel resistances, as is used in ACI and AASHTO code provisions. This approach assumed that the concrete resistance was equal to the resistance calculated with Equation 2.29. In Eurocode another approach is followed [5] [18].

Tensile struts

The tensile tie of the truss model has to carry the shear force V_{Ed} after inclined cracking. The tensile tie is a representation of the transverse reinforcement in the beam over a distance $z \cdot (\cot\theta + \cot\alpha)$, see Figure 2.23. The factor z is the distance from the tensile longitudinal reinforcement to the resulting force in the compressive zone. To calculate the amount of transverse reinforcement in a tensile tie, an equivalent steel cross-sectional area A_{equi} is used. The tensile force N_T (ULS) in the tensile tie is based on equilibrium, provided that the model is a full truss. To find the ultimate capacity of the shear reinforcement, the stress in the transverse reinforcement σ_{sw} is replaced by the design yield stress f_{ywd} [5]:

$$\begin{aligned} A_{equi} = \frac{A_{sw}}{s} \cdot z \cdot (\cot\theta + \cot\alpha) \quad \text{with} \quad N_T = A_{equi} \cdot \sigma_{sw} = \frac{V_{Rd,s}}{\sin\alpha} \\ \Rightarrow \quad \frac{A_{sw}}{s} \cdot z \cdot (\cot\theta + \cot\alpha) \cdot f_{ywd} = \frac{V_{Rd,s}}{\sin\alpha} \end{aligned} \tag{2.33}$$

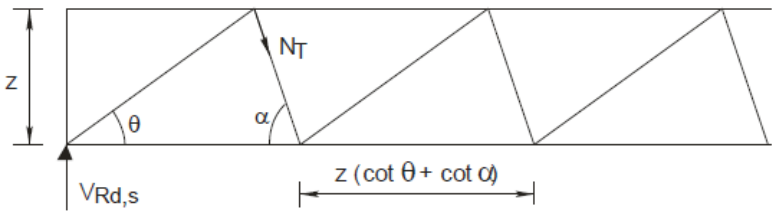

Figure 2.23: Geometry of the truss model for the tensile tie [5]

The contribution of the shear reinforcement to the shear resistance $V_{Rd,s}$ in Figure 2.22 is given for vertical transverse reinforcement ($\alpha = 90°$):

$$V_{Rd,s} = \frac{A_{sw}}{s} \cdot z \cdot f_{ywd} \cdot \cot\theta \tag{2.34}$$

$$\text{if } \theta = 45° \quad \Rightarrow \quad V_{Rd,s} = \frac{A_{sw}}{s} \cdot z \cdot f_{ywd} \tag{2.35}$$

A_{sw} is the cross-sectional area of the shear reinforcement, s is the spacing of the stirrups, f_{ywd} is the design yield strength of the shear reinforcement, $z \approx 0.9d$ is the internal lever arm (which is assumed to be equal to the compressive and tension chords parallel to the beam axis) and θ is angle between the concrete compressive strut and the beam axis perpendicular to the shear force [63]. According to Walraven & Braam [5] this angle θ can be reduced to 18.4°. The EC2 uses the following range for θ:

$$21.8° \leq \theta \leq 45° \tag{2.36}$$

Compressive struts

The compressive strut of the truss model must be designed in a way that it can withstand a certain design force V_{Ed}. The compressive strut has a certain width b_D and a cross-sectional area A_D. With the force in the compressive strut N_D divided by the area A_D the concrete compressive stress σ_{cD} is obtained. The concrete has a maximum allowable concrete compressive stress σ_{cd}. When this maximum allowable stress is used the shear force resistance of the concrete compressive strut is calculated $V_{Rd,max}$:

$$b_D = z \cdot (\cot\theta + \cot\alpha) \cdot \sin\theta \text{ [mm]}$$

$$A_D = b_w \cdot b_D = b_w \cdot z \cdot (\cot\theta + \cot\alpha) \cdot \sin\theta \text{ [mm}^2\text{]}$$

$$\sigma_{cD} = \frac{V_{Ed}}{b_w \cdot z} \cdot \frac{1}{(\cot\theta + \cot\alpha) \cdot \sin^2\theta} = \frac{V_{Ed}}{b_w \cdot z} \cdot \frac{1 + \cot^2\theta}{(\cot\theta + \cot\alpha)} \text{ [MPa]} \quad \text{with} \quad V_{Ed} = N_D \cdot \sin\theta \tag{2.37}$$

$$V_{Rd,max} = b_w \cdot z \cdot (\cot\theta + \cot\alpha) \cdot sin^2\theta \cdot \sigma_{cd} = b_w \cdot z \cdot \sigma_{cd} \cdot \frac{\cot\theta + \cot\alpha}{1 + \cot^2\theta}$$

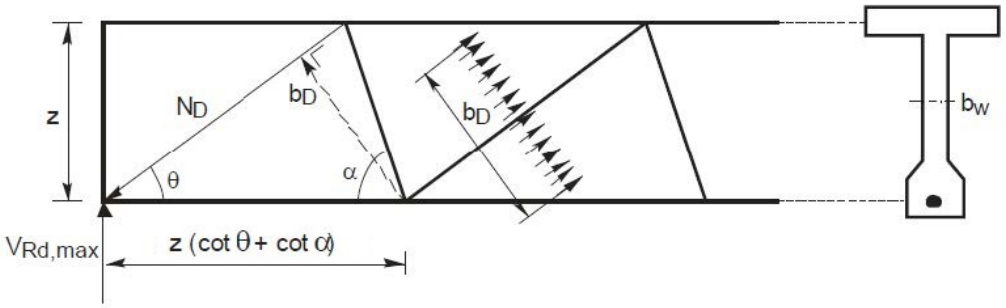

Figure 2.24: Geometry of the truss model for the compressive strut [5]

The maximum allowable stress in the compressive strut is lower than the uni-axial compressive strength of concrete, therefore $\sigma_{cd} \neq f_{cd}$. The concrete is in a bi-axial stress state, because of the tension in the transverse reinforcement. The tensile forces perpendicular to direction of the struts are transferred by bond, see Figure 2.25. The stirrups cross the inclined compressive strut and results in a reduced maximum compressive stress. This phenomena is included in the factor α_{cw}, where a stress below $0.6f_{cd}$ has a positive effect on the resistance of the compressive struts and a stress higher than $0.6f_{cd}$ has a negative effect. The concrete strength class is included with a factor ν_1, as a higher concrete class does not linearly increase with the maximum compressive stress [5].

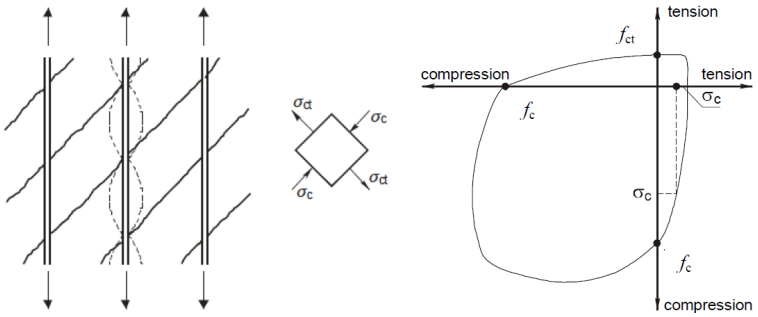

Figure 2.25: Bi-axial stress state reduces concrete compressive strength [5]

Crushing of concrete

$V_{Rd,max}$ shown in Figure 2.24 limits the shear resistance of a member by crushing of the concrete. The concrete is assumed to crush when the compressive stress in the diagonal strut is equal to $\alpha_{cw} \cdot \nu_1 \cdot f_{cm}$, as shown in Equation 2.38. If crushing of concrete is governing, the design shear force is given with Equation 2.39.

$$\sigma_{cd} = \alpha_{cw} \cdot \nu_1 \cdot f_{cd} \text{ [MPa]} \tag{2.38}$$

$$\text{If } \sigma_{sw} \leq 0.8 f_{yk}: \quad \nu_1 = \begin{Bmatrix} 0.6, & (f_{ck} \leq 60 \text{ MPa}) \\ 0.9 - \dfrac{f_{ck}}{200} > 0.5, & (f_{ck} > 60 \text{ MPa}) \end{Bmatrix} \quad \text{Else:} \quad \nu_1 = 0.6 \left(1 - \frac{f_{ck}}{250}\right)$$

$$\alpha_{cw} = \begin{cases} 1.0, & \text{for non-prestressed structures} \\ 1.0 + \dfrac{\sigma_{cp}}{f_{cd}}, & \text{for } 0 < \sigma_{cp} \leq 0.25 f_{cd} \\ 1.25, & \text{for } 0.25 f_{cd} < \sigma_{cp} \leq 0.50 f_{cd} \\ 2.5 \left(1.0 - \dfrac{\sigma_{cp}}{f_{cd}}\right), & \text{for } 0.50 f_{cd} < \sigma_{cp} < 1.0 f_{cd} \end{cases}$$

$$V_{Rd,max} = \frac{\alpha_{cw} \cdot b_w \cdot z \cdot \nu_1 \cdot f_{cd}}{\cot\theta + \tan\theta} \tag{2.39}$$

The strength reduction factor ν_1 is for cracked concrete in shear. The effect of an axial force is adapted in the factor α_{cw} (for reinforced concrete $\alpha_{cw} = 1$). The concrete compressive strength in the web is assumed to be less than the axial compressive strength of a cylinder (f_{cm}/f_{ck}) and is due to a bi-axial stress state in the concrete as previously described [63].

Summary EC2 with transverse reinforcement

The EC2 calculates two limits for girders with transverse reinforcement, yielding of the stirrups $V_{Rd,s}$ and crushing of the concrete $V_{Rd,max}$. The minimum shear resistance is the governing failure mode:

$$V_{Rd,shear} = \min(V_{Rd,s}, V_{Rd,max}) \tag{2.40}$$

The range of the rotating strut (angle θ) can be derived from the theory of plasticity. The maximum shear resistance for a member is when the two expressions 2.34 and 2.39 are set equal. This means that yielding of the stirrups occurs simultaneously with crushing of the concrete. The inclination will start at 45° and starts to decrease when externally loaded. For lower angles more stirrups are activated until the concrete crushes. The model predicts two limits:

- 21.8° : yielding of shear reinforcement occurs without crushing of the concrete (low ratio stirrups)
- 45.0° : crushing of the concrete without yielding of the shear reinforcement (high ratio stirrups)

The EC2 lets the user freely choose the cracking angle θ between 21.8° and 45°. In practice the angle of the rotation strut for prestressed concrete members with transverse reinforcement is taken as $\theta = 30°$. It is also possible to assume $\theta = 21.8°$ and increase the value if crushing of concrete is the governing failure mechanism [5].

2.10. Richtlijnen Beoordeling Kunstwerken (RBK1.1)

The Dutch Ministry of Infrastructure and Watermanagement (Rijkswaterstaat) made its own guidelines for the assessment of existing structures, which contains instructions for the assessment of the structural safety of existing structures that are maintained by Rijkswaterstaat. This document is an addition to the design codes provided by the Eurocode [68]. The shear resistance provided by the RBK1.1 distinguishes the contribution of the concrete and reinforcement steel separately. It is important to note that the RBK does not define shear-tension- nor flexural-shear failure, just the shear capacity of a prestressed/reinforced concrete member. The shear resistance of members without shear reinforcement only consists of the concrete part $V_{Rd,c}$. The shear capacity of the shear reinforcement is $V_{Rd,s}$. The design value for the shear resistance of a prestressed girder is defined as:

$$V_{Rd} = V_{Rd,s} + V_{Rd,c}$$

$$V_{Rd,c} = \left[0.12 k_{cap} \cdot k \sqrt[3]{100 \rho_l \cdot f_{ck}} + 0.15 \sigma_{cp}\right] \cdot b_{w,gem} \cdot d \quad \geq \quad \left[\nu_{min} + 0.15 \sigma_{cp}\right] \cdot b_{w,gem} \cdot d \tag{2.41}$$

$$V_{Rd,s} = \frac{A_{sw} \cdot z \cdot f_{ywd} \cdot \cot\theta}{s}$$

The shear resistance of a prestressed concrete member with shear reinforcement is the sum of the contribution of concrete and steel. This is different from EC2, where members with shear reinforcement are calculated with the variable angle truss model. The $V_{Rd,c}$ in RBK is the same formula as for regions cracked in bending in EC2, except for the factor k_{cap} and $b_{w,gem}$. The factor k_{cap} is added for massive plates, but is 1.0 for everything else. The factor $b_{w,gem}$ considers a projected cross-section instead of a vertical cross-section, see Figure 2.26. The mean width takes into account the contribution of the concrete and is limited to $1.25 b_w$:

$$b_{w,gem} = \frac{A_{c,projected}}{d_{mean}} < 1.25 b_w \text{ [mm]} \tag{2.42}$$

The influence of the prestressing ducts do not have to be taken into account. The expression for the contribution of the concrete $V_{Rd,c}$ given in Equation 2.41 is only valid if the angle θ for the compressive strut is taken 30°.

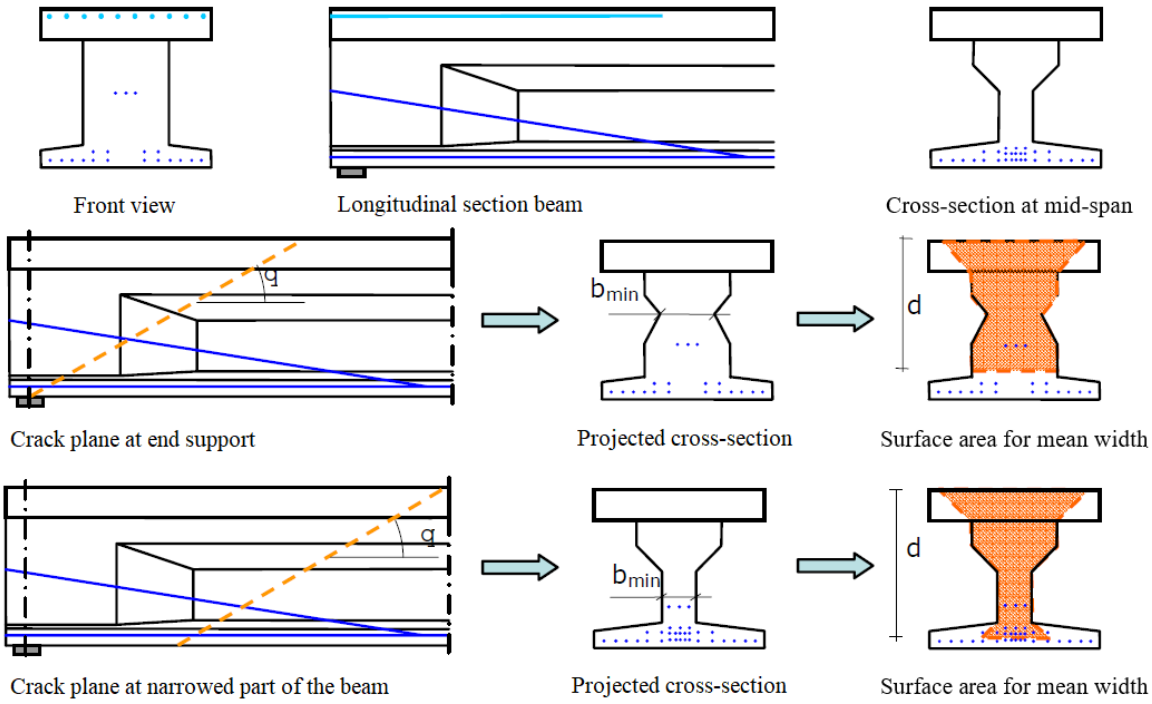

Figure 2.26: Projected cross-section of a prestressed member [68]

2.11. Eurocode 2 DRAFT 2018 (EC2 2018)

The first generation of the Eurocodes is available since 2005 and replaced the old dutch concrete design code NEN 6720 in April 2012. The second generation is still in development and is to be released after 2020. In this thesis a draft version will be used: "Final Version of PT1-draft prEN 1992-1-1 2018 D3", internally released 2018-06-12 [69]. This version is not publicly released and no commentary is available. The most important goal of the new Eurocodes is to make the codes easier and more transparent to use, in other words the ease of use. The size of the new codes is reduced and unnecessary rules and repetitions are avoided as much as possible [70].

The procedure for designing a (prestressed) concrete member for shear is as follows:

1. General verification procedure as preliminary check;
2. Detailed calculation without shear reinforcement if the general procedure is not fulfilled;
3. Calculation for shear reinforcement if the detailed calculation is not fulfilled.

This procedure means that first a global and easy check is made for the shear resistance of a concrete member without using the internal forces (M_{Ed}, V_{Ed}, M_{Ed}) and longitudinal reinforcement. If this check is not satisfied, a more detailed calculation is made for the design value of the shear stress resistance. Lastly, the required shear reinforcement and resistance is calculated when required.

2.11.1. General verification procedure

In the draft version, the general verification procedure for shear is given in Chapter 8.2.1 [69]. First an easy verification is made to check if the member requires a calculation for the resistance to shear. If the acting design shear stress τ_{Ed} is lower than the minimum design shear resistance $\tau_{Rdc,min}$, a detailed verification is not required:

$$\begin{aligned} \tau_{Ed} &\leq \tau_{Rdc,min} \\ \tau_{Ed} &= \frac{V_{Ed}}{b_w \cdot d} \text{ [MPa]} \\ \tau_{Rdc,min} &= \frac{10}{\gamma_c} \cdot \sqrt{\frac{f_{ck}}{f_{yd}} \cdot \frac{d_{dg}}{d}} \text{ [MPa]} \end{aligned} \tag{2.43}$$

Where f_{yd} is the design yield strength of the flexural reinforcement in MPa, f_{ck} is the characteristic compressive strength of concrete in MPa, b_w is the width of the cross-section in mm and γ_c is the material factor for concrete. For cross-sections with variable widths, b_w is defined in Figure 2.27. The effective depth d depends on the presence of prestressed tendons. For bonded tendons the effective depth is calculated with Equation 2.44. The factor d_{dg} takes into account the failure zone roughness and aggregate properties of the concrete type and is calculated with Equation 2.45.

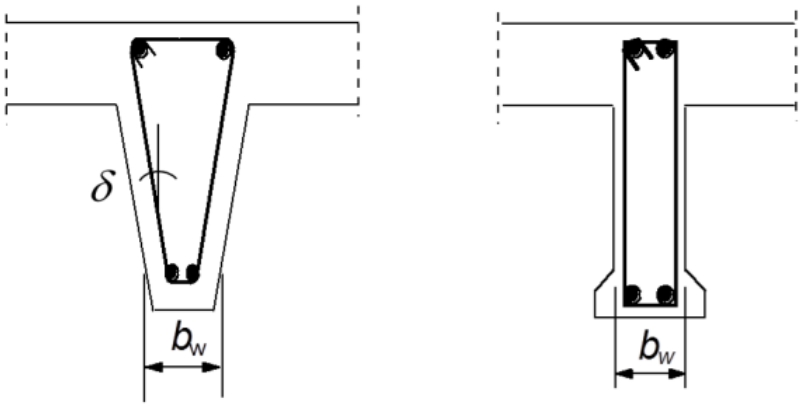

Figure 2.27: Illustration for the web width b_w of a cross-section with a variable width [69]

$$d = \frac{d_s^2 \cdot A_s + d_p^2 \cdot A_p}{d_s \cdot A_s + d_p \cdot A_p} \text{ [mm]} \tag{2.44}$$

$$d_{dg} = \begin{cases} 16 + D_{lower} \text{ [mm]}, & (f_{ck} \leq 60 \text{ MPa}) \\ 16 + D_{lower} \cdot \left(\frac{60}{f_{ck}}\right)^2 \leq 40 \text{ [mm]}, & (f_{ck} > 60 \text{ MPa}) \end{cases} \tag{2.45}$$

With d_p and d_s as the distances from the extreme compression fiber to the centroid of the prestressing tendons and longitudinal tension reinforcement respectively, A_p and A_s as the areas of the prestressing tendons and longitudinal tension reinforcement respectively and D_{lower} as the smallest value of the maximum diameter of the aggregates D_{max} in mm. If the influence of the prestressed tendons is unfavorable for the shear resistance, the area of the prestressed reinforcement A_p may be neglected for the calculation of the effective depth.

For a more detailed calculation a distinction is made between members with and without shear reinforcement, which are addressed in the following two paragraphs. For the design of a structure it is clearly stated that the more detailed calculations are not necessary when Equation 2.43 is fulfilled.

2.11.2. Detailed verification without shear reinforcement

In the EC2 it is given that regions closer than a 45 degree line from the support to the elastic centroidal axis do not have to be checked for the shear resistance. The EC2 draft 2018 has extended these regions for significant concentrated loads. Next to regions within length d to the support, regions within length d to the concentrated load are also considered as shown in Figure 2.28.

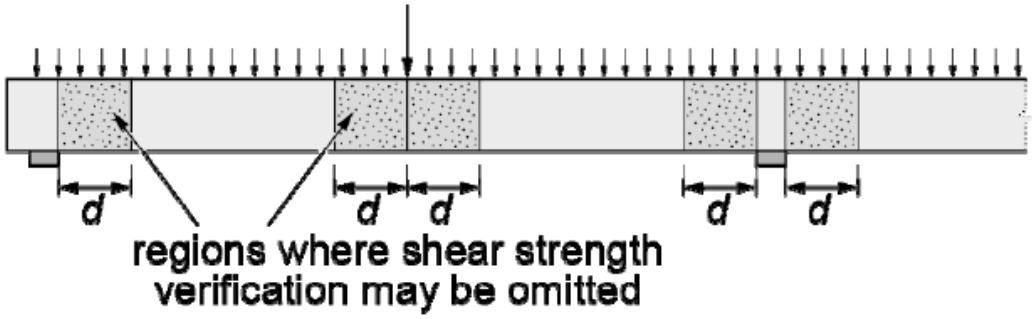

Figure 2.28: Regions that do not have to checked for the shear resistance [69]

Outside the regions shown in Figure 2.28, the design value of the shear stress resistance is calculated as given in Equation 2.46. The reinforcement ratio ρ_l depends on the presence of prestressed (bonded) tendons. If an axial force N_{Ed} is present, like a compressive force from prestressing, the value of d for $\tau_{Rd,c}$ needs to be replaced by the mechanical shear span a_v.

$$\tau_{Rd,c} = \frac{0.6}{\gamma_c} \cdot \left(100\rho_l \cdot f_{ck} \cdot \frac{d_{dg}}{d}\right)^{1/3} \geq \tau_{Rdc,min} \text{ [MPa]} \tag{2.46}$$

$$\text{with} \quad \rho_l = \begin{cases} \frac{A_{sl}}{b_w \cdot d}, & \text{for non-prestressed members} \\ \frac{d_s \cdot A_s + d_p \cdot A_p}{b_w \cdot d^2}, & \text{for prestressed members} \end{cases} \tag{2.47}$$

$$a_v = \sqrt{\frac{a_{cs}}{4} \cdot d} \text{ [mm]} \quad \text{and} \quad a_{cs} = \left|\frac{M_{Ed}}{V_{Ed}}\right| + \frac{N_{Ed}}{|V_{Ed}|} \cdot \frac{d}{3} \geq d \text{ [mm]}$$

Where a_{cs} is the effective shear span with respect to the control section and M_{Ed}, V_{Ed} and N_{Ed} as the forces acting on the member at the considered cross-section. A negative value of the axial force N_{Ed} refers to a compressive force.

2.11.3. Shear resistance with shear reinforcement

If shear reinforcement is required, the design procedure is based on a compression field. This model is shown in Figure 2.29. The procedure for the shear resistance with shear reinforcement is almost the same as the current EC2 provisions. The most important difference is the inclination of the compression field θ in the web, which is now changed to the following range:

$$1 \leq \cot\theta \leq \cot\theta_{min} \tag{2.48}$$

with a minimal inclination of the compression field θ_{min}:

$$\cot\theta_{min} = \begin{cases} 2.5, & \text{for oridinary reinforced members without axial force} \\ 3.0, & \text{for prestressed members with a height of the compression chord} x < 0.25d \\ 2.5 - 0.1 \cdot N_{Ed}/V_{Ed} \geq 1.0, & \text{for members subjected to axial tension} \end{cases}$$

The height for the compression zone height x follows from a sectional analysis. For prestressed members with a compression zone height less than $0.25d$, the following range of θ applies:

$$19.08° \leq \theta \leq 45° \tag{2.49}$$

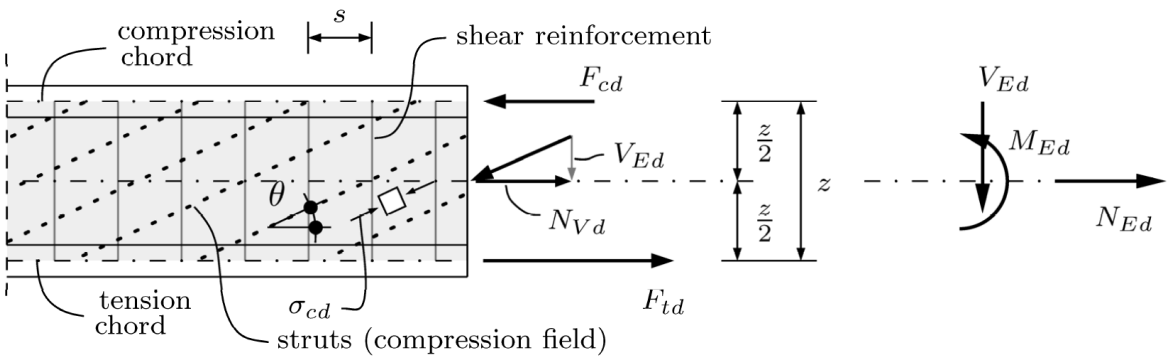

Figure 2.29: Compression field model for members with shear reinforcement [69]

The shear resistance for members with shear reinforcement is calculated in case of yielding of the shear reinforcement. This resistance is limited by crushing of the concrete:

$$V_{Rd} = \frac{A_{sw} \cdot z \cdot f_{ywd} \cdot \cot\theta}{s} \leq b_w \cdot z \cdot \frac{\nu \cdot f_{cd}}{2} \tag{2.50}$$

The stress in the compression field σ_{cd} needs to be lower than $\nu \cdot f_{cd}$:

$$\sigma_{cd} = \frac{V_{Ed}}{b_w \cdot z} \cdot (\cot\theta + \tan\theta) \leq \nu \cdot f_{cd} \text{ [MPa]} \tag{2.51}$$

With ν as a strength reduction factor for concrete in cracked state due to shear or other actions and the internal lever arm assumed as $z = 0.9d$. For values of θ in range according to Equation 2.48, the value for $\nu = 0.5$ can be chosen. For values lower than θ_{min} the strength reduction factor must be calculated according to the state of strains of the member:

$$\nu = \frac{1}{1.2 + 80 \cdot (\varepsilon_x + (\varepsilon_x + 0.001) \cdot \cot^2\theta)} \leq 1.0 \tag{2.52}$$

$$\text{with} \qquad \varepsilon_x = \frac{\varepsilon_{xt} + \varepsilon_{xc}}{2} \geq 0$$

$$\varepsilon_{xt} = \frac{F_{td}}{A_{st} \cdot E_s}$$

$$\varepsilon_{xc} = \begin{cases} 0, & \text{for } F_{cd} > 0 \\ \dfrac{-F_{cd}}{A_{ct} \cdot E_s}, & \text{for } F_{cd} < 0 \end{cases}$$

With ε_{xt} as the strain in the flexural tension (bottom) chord, ε_{xc} as the strain in the flexural compression (top) chord, ε_x as the average strain between the top- and bottom chord and A_{st}, A_{sc} as the areas for the longitudinal reinforcement in the flexural tension and compression chords respectively. If prestressing is present with bonded tendons, the areas of the longitudinal reinforcement in both chords may be increased by a part of the area of the prestressing tendons:

$$\begin{aligned} A_{st} &= A_s + A_p \left(0.5 + \frac{e_p}{z}\right) \ [\text{mm}^2] \\ A_{sc} &= A_s + A_p \left(0.5 - \frac{e_p}{z}\right) \ [\text{mm}^2] \end{aligned} \tag{2.53}$$

The forces to calculate the strains are shown in Figure 2.29. The additional tensile axial force N_{Vd} due to the acting shear force on the member can be calculated with Equation 2.54. When the member is subjected to a design axial compression force N_{Ed}, a portion of this force N_{Edw} can be resisted by the web and N_{Vd} can be calculated with Equation 2.55 provided that $-N_{Edw} \leq |V_{Ed}| \cdot \cot\theta$.

$$N_{Vd} = |V_{Ed}| \cdot \cot\theta \tag{2.54}$$

$$N_{Vd} = |V_{Ed}| \cdot \cot\theta + N_{Edw} \tag{2.55}$$

The forces in both chords then become:

$$\begin{aligned} F_{td} &= \frac{M_{Ed}}{z} + \frac{N_{Vd} + N_{Ed}}{2} \leq \frac{M_{Ed,max}}{z} + \frac{N_{Ed}}{2} \\ F_{cd} &= \frac{M_{Ed}}{z} - \frac{N_{Vd} + N_{Ed}}{2} \end{aligned} \tag{2.56}$$

With $M_{Ed,max}$ as the maximum moment occuring in the member.

3

Overview of available information of Helperzoom girders

Combinatie Herepoort (CHP) is a collaboration project in which several Dutch parties participate to the project "Aanpak Ringweg Zuid in Groningen". The demolition work of the Helperzoom bridge (KW17) is part of this project, which took place in week 7 and 8 of 2019. In these two weeks the southern part of the bridge is demolished and consists of four parts, field one to four (veld 1 - 4 in Dutch) see Figure 3.1. Four girders from field three (highlighted with blue) are carefully removed and cut in half for research purposes at TU Delft, which is commissioned by Rijkswaterstaat [71]. With $L_{girder} = 11.75$ m the weight of the girder is approximately 19 tons [1]. In this thesis only the first two girders, HPZ1 and HPZ2 are considered.

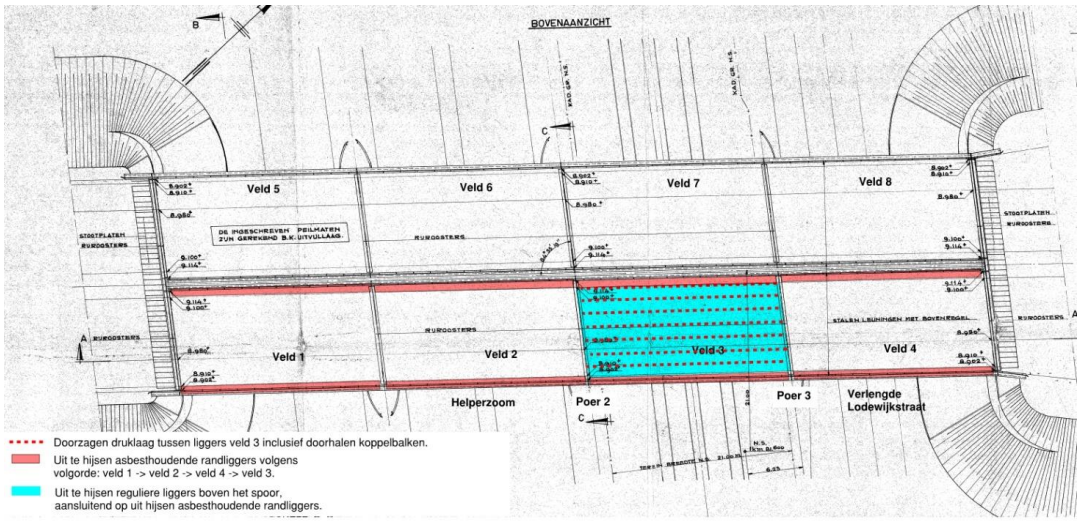

Figure 3.1: Overview of the Helperzoom Bridge KW17. Girders from field three (blue) are destructively tested at TU Delft [71]

The technical drawings of the Helperzoom bridge date from 1965 to 1967 and are shown in Chapter 3.1. The material properties of the concrete, prestressing steel and mild steel are tested and documented in a measuring and analysis report by Lantsoght et al. [72] [73] and given in Chapter 3.2. Roosen [1] made a preliminary report of the Helperzoom bridge with data used according to the RBK, as most of the data from tests were not available yet. It contains assumptions made for the dimensions and cross-sectional properties, location of the supports and external load, location of the prestressing cables and internal and external loads on the girder. These are addressed in Chapters 3.3 through 3.6. The parts considered from the Helperzoom bridge are supplemented and changed where necessary.

3.1. Technical drawings

Figure 3.2 shows drawings of the Helperzoom bridge, Figure 3.2a shows the cross-section with the positions of the saw cuts, Figure 3.2b shows a sawn girder with a length of 11.7m and Figure 3.2c shows three different cross-sections.

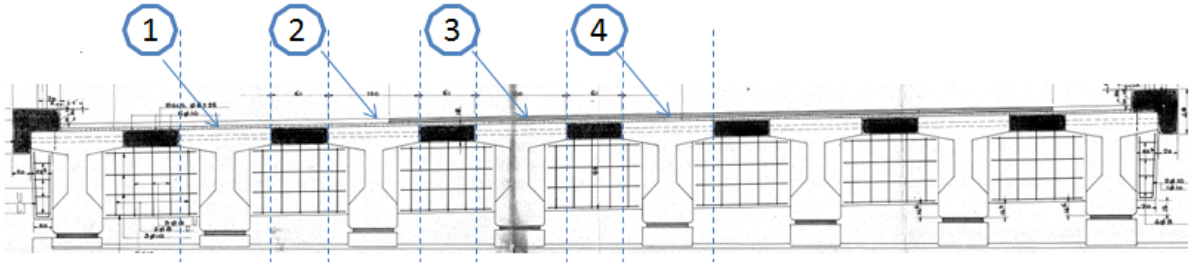

(a) Cross-section of Helperzoom bridge

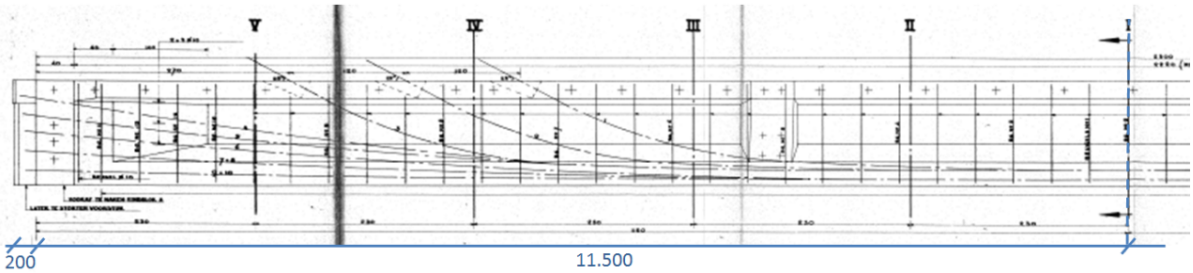

(b) Detailed side-view from Helperzoom

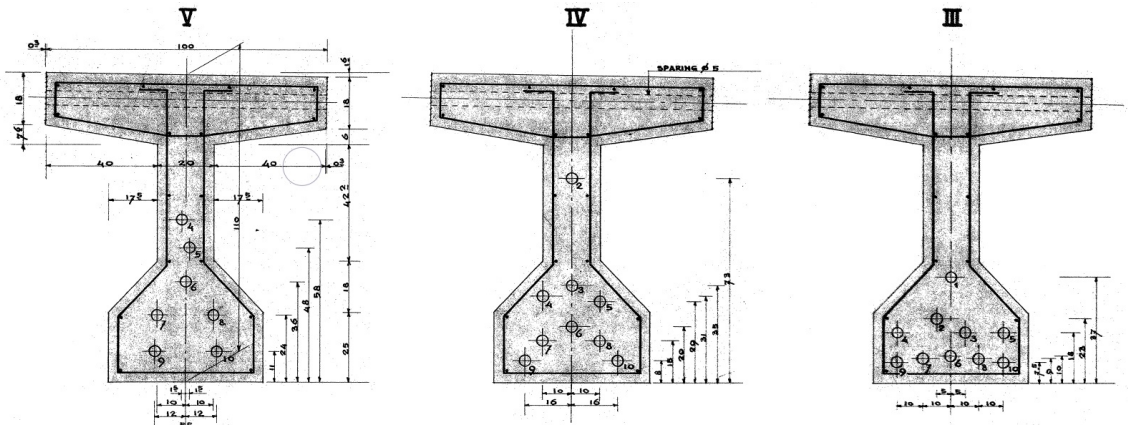

(c) Cross-sections at various sections of a Helperzoom girder (dimensions in cm)

Figure 3.2: Technical drawings of the Helperzoom bridge with the considered part highlighted [1]

3.2. Material properties

3.2.1. Concrete

Back in 2009 tests were performed on twelve cores of the Helperzoom bridge, six were used for measuring the compressive strength and six for measuring the tensile strengths of the concrete. The measured compressive strengths are: 37.0, 77.0, 77.0, 78.5, 92.0 and 96.0 MPa. The average concrete compressive strength is $f_{cm,cube} = 76.3$ MPa, with a characteristic compressive strength of $f_{ck,cube} = 62.7$ MPa. This corresponds to a concrete class C55/67. The measured tensile strengths from splitting tensile tests are: 3.7, 4.9, 5.4, 5.8, 6.2 and 6.3 MPa. The average tensile splitting strength is $f_{ctm,sp} = 5.4$ MPa, with an average tensile strength of $f_{ctm} = 0.9 f_{ctm,sp} = 0.9 \cdot 5.4 = 4.86$ MPa [1] [74].

Tests were also performed during the experiments of the Helperzoom girders to determine the elastic modulus of the concrete. In total six cores were drilled, but only the last three cores are analyzed. The average result from the cores 4, 5 and 6 is $E_c = 39{,}548$ MPa [72].

3.2.2. Prestressing steel

The technical drawings of Helperzoom bridge from 1965 shows that 40 tons prestressing cables are used of the Freyssinet system. RBK 1.1 table B4-1 [68] states that "Freyssinet 40 tons cables" are used since 1966 with 12⌀7, $A_p = 462$ mm^2 and a prestressing steel quality of QP170. Roosen [1] determined the prestressing level in the girder according to the RBK. Next to the information from the drawings and RBK, tests have been performed to obtain the ultimate tensile strength together with a bilinear stress-strain diagram. Also the prestressing level in the girder is tested.

In March 2019 twelve samples of prestressing steel were tested. Three samples showed slip or failed during testing and are excluded from the average ultimate strength of the prestressing steel. The successful tests give an average ultimate strength of $f_{pm} = 1824$ MPa, with a failure strain of 0.0535. The average stress at $\varepsilon = 0.01$ is $f_{p0.01m} = 1433$ MPa. Lantsoght [72] derived a bilinear curve based on the tests of the prestressing steel with the following assumptions based on EC2 [63]: the modulus of elasticity of the prestressing steel E_p is assumed 185,000 MPa, the transition between the two linear branches is assumed at $0.9f_{pu}$ and failure of the prestressing steel is based on the average tensile strength with corresponding strain. The second branch of the bilinear stress-strain diagram is calculated with:

$$\sigma = 4086.8\varepsilon + 1605.6 \text{ [MPa]} \tag{3.1}$$

3.2.3. Mild steel reinforcement

According to the data provided by the technical drawings, the steel quality used is QR40 for the longitudinal and transverse reinforcement. Both consist of ⌀10 ribbed bars and the vertical stirrups have 400 mm spacing in longitudinal direction of the girder. RBK 1.1 Table 2.6 provides data for QR40 (GBV 1962) and gives a characteristic yield strength of $f_{yk,RBK} = 400$ MPa. Langtsoght [72] assumed an average yield strength of the stirrups of $f_{ym,RBK} = 400 + 40 = 440$ MPa.

Nine samples are tested in the laboratory, four stirrups and five longitudinal bars, where both the yield- and ultimate stress are tested. Two tests failed (sample 2 and 4) at the top, which are excluded for calculating the average stresses. The remaining seven tests result in an average yield stress $f_{ym} = 454$ MPa and average tensile strength $f_{um} = 655$ MPa [72].

3.3. Dimensions and cross-sectional properties of the girders

The cross-sectional properties of the Helperzoom girders are taken from the technical drawings, see Figure 3.2c. The girders have a horizontal slope of 1.6% at the top flange, but is neglected in the calculations. The total area of the cross-section is $A_{c,original} = 507{,}000$ mm^2 and is only used for the calculation of the self-weight. For calculations of the first moment of area S_c and the moment of inertia I_c the cross-section is simplified, see Figure 3.3. The simplified cross-section has an area of $A_{c,simplified} = 517{,}000$ mm^2, hereafter A_c. The total height of the simplified girder is $h = 1110$ mm, the neutral axis is at $z_{top} = 492$ mm from the top and $z_{bottom} = 618$ mm from the bottom [1].

Table 3.1: Cross-sectional properties of a Helperzoom girder [1]

A_i	$A_{c,i}$ [mm^2]	b_i [mm]	h_i [mm]	z_i [mm]	$z_{top} - z_i$ (a_i) [mm]	$I_{c,i}$ [$\times 10^{10}$ mm^4]
A_1	180,000	1000	180	90	402	2.96
A_2	136,000	200	680	520	-28	0.53
A_3	137,500	550	250	985	-493	3.42
A_4	32,000	400	80	207	285	0.26
A_5	31,500	175	180	800	-308	0.30
$\sum =$	517,000					7.47

The first and second moment of area are calculated as follows:

$$\begin{aligned} I_c &= \sum_{i=1}^{5} A_{c,i} \cdot a_i^2 + \frac{b_i \cdot h_i^3}{12} = 7.47 \cdot 10^{10} \text{ mm}^4 \\ S_c &= A_1 \cdot a_1 + A_4 \cdot a_4 + 312 \cdot 200 \cdot (z_{top} - 336) = 9.12 \cdot 10^7 \text{ mm}^3 \quad \text{(with respect to c.o.g.)} \\ S_c &= A_1 \cdot a_1 + A_4 \cdot a_4 + 500 \cdot 200 \cdot (z_{top} - 430) = 8.77 \cdot 10^7 \text{ mm}^3 \quad \text{(with respect to bottom web)} \end{aligned} \tag{3.2}$$

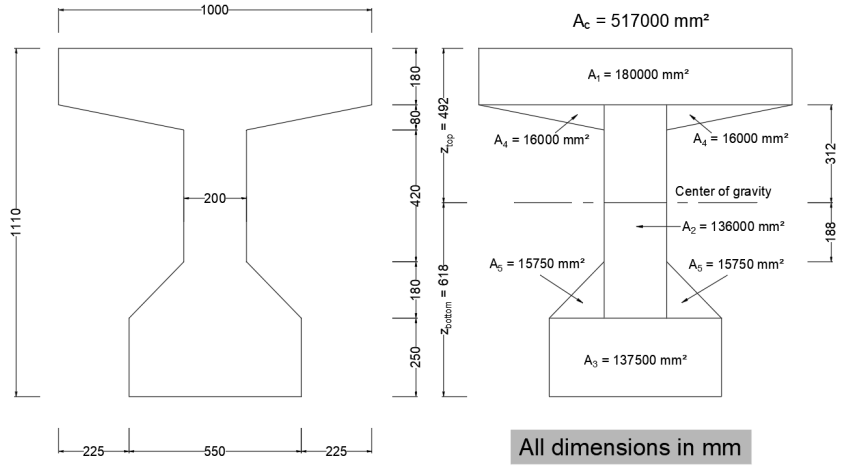

Figure 3.3: Simplified cross-sectional properties of a Helperzoom girder [1]

The lengths of the first two girders, HPZ1 and HPZ2, are shown in Table 3.2 [72].

Table 3.2: Dimensions of the Helperzoom girders used for destructive testing [72]

girder [no.]	**L** [m]	B_{east} [m]	B_{west} [m]	B_{mid} [m]	B_{mean} [m]	**H** [m]
HPZ1	10.51	0.965	0.94	0.96	0.96	1.11
HPZ2	11.1	1.06	0.96	1.043	1.02	1.11

3.4. Position of external load and supports

At Stevinlab II the bearings can be placed with increments of 600 mm. As the shortest girder is of length $L_{HPZ1} = 10.51$ m, the span length for all experiments is chosen as $L_{span} = 9.6$ m, see also Figure 4.2 in Chapter 4.2.2. The left support is assumed at 275 mm from the most western edge and the right support at 9.6 m from the left support. In the rest of the report the position of the left support will be set as $x = 0$ m.

In the calculations the position of the external load is placed at $x = 2.903$ m. This position is assumed to be the most critical position for shear-tension failure. The crack is assumed to be inclined at 30°, which is plausible and commonly used for prestressed girders. With the load placed at $x = 2.903$ m this crack will be the first crack away from the hammerhead and the anchorage region. Three prestressing cables are anchored in the top flange at positions $x = 2.625, 3.825$ and 5.025 m. It is assumed that the anchorages have no influence on the resistance to shear cracks [1].

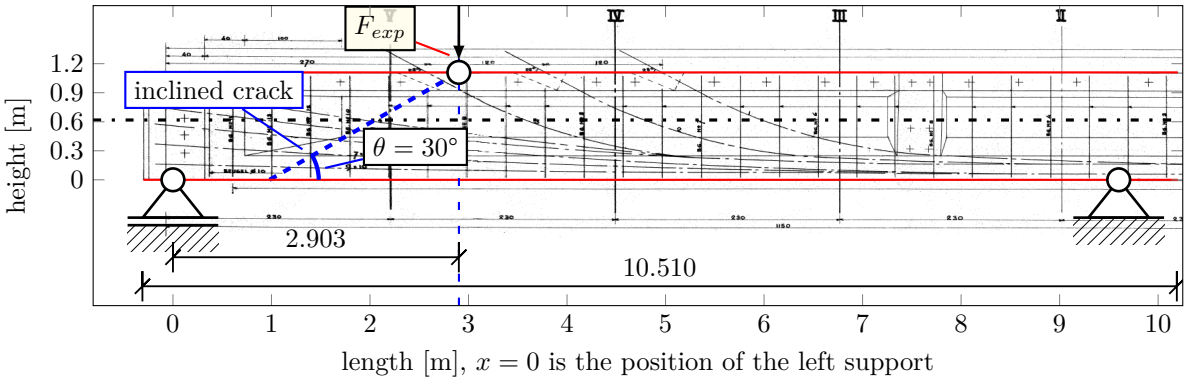

Figure 3.4: Position of the external load with location of the supports and span length for HPZ1 [1]

3.5. Location of the prestressing cables and considered cross-sections

To calculate the cross-sectional forces of the girders HPZ1 and HPZ2, the z-coordinate of all prestressing cables must be known. The cross-sections **E** and **V** through **I** (only **V** through **II** are shown in Figure 3.4) are used to determine the position of the cables at locations x = -0.075 [**E**], 2.300 [**V**], 4.600 [**IV**], 6.825 [**III**], 9.125 [**II**], 11.425 [**I**] m. `MS Excel` is used to determine the locations for all ten cables by linear interpolation shown in Table 3.3 [1].

Table 3.3: Z-coordinates of the prestressing cables for various cross-sections of a Helperzoom girder for $x = -75,..,4600$ mm [1][1]

Cable	**-75**	**1725**	**1800**	**1850**	**1900**	**1950**	**2000**	**2051**	**2300**	**2453**	**2903**	**4600**
1 [mm]												
2 [mm]												730
3 [mm]												350
4 [mm]	910	660	649	643	636	629	622	615	580	562	509	310
5 [mm]	730	541	533	527	522	517	512	506	480	467	430	290
6 [mm]	550	406	400	396	392	388	384	380	360	349	318	200
7 & 8 [mm]	350	267	263	261	259	256	254	252	240	234	216	150
9 & 10 [mm]	150	120	118	118	117	116	115	114	110	108	102	80
N_p = [kN]	3067								3067			3944

With an external load at x = 2.903 m and an inclined crack of 30°, several important cross-sections are considered [1]. Figure 3.5 shows these cross-sections together with the inclined crack and center of gravity of the girder.

- x = 1.725 m ⇒ position where the crack crosses the intersection of the bottom flange and the web
- x = 2.051 m ⇒ position where the crack crosses the center of gravity of the girder
- x = 2.453 m ⇒ position where the crack crosses the intersection of the web and the top flange
- x = 2.903 m ⇒ position of the load

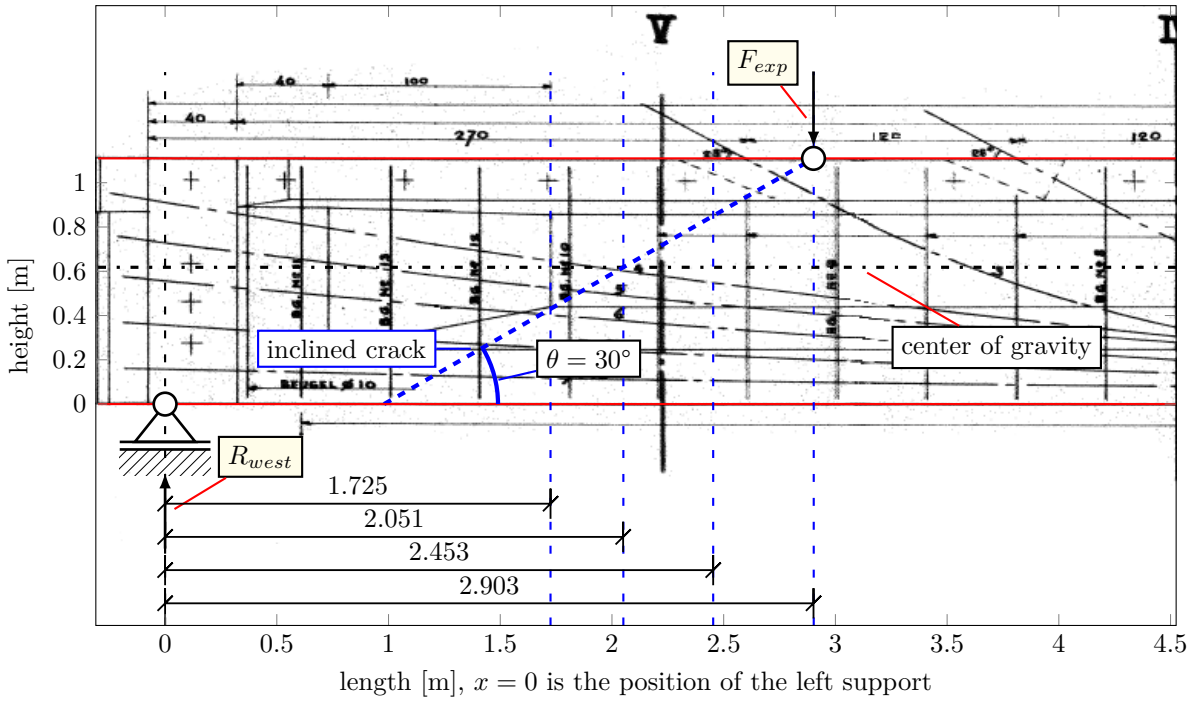

Figure 3.5: Important cross-sections with an inclined shear crack of 30° [1]

[1]Based on M. Roosen's preliminary report, but made more extensive by considering more cross-sections

3.6. Loads on the Helperzoom girders

Four loads are considered acting on the girder; dead load, self weight, axial force due to prestressing and an external load positioned at $x = 2.903$ m. Assumptions and calculations are taken from Roosen's report [1].

3.6.1. Dead load

The dead load only consists of a concrete wearing surface of 35 mm, see Figure 3.6. The asphalt layer of 50 mm thickness is removed before the experiment. The dead load is 0.84 kN/m^2 and is further included in the calculations for self weight:

$$q_{DL} = 0.035 \cdot 24 = 0.84 \text{ kN/m}^2 \tag{3.3}$$

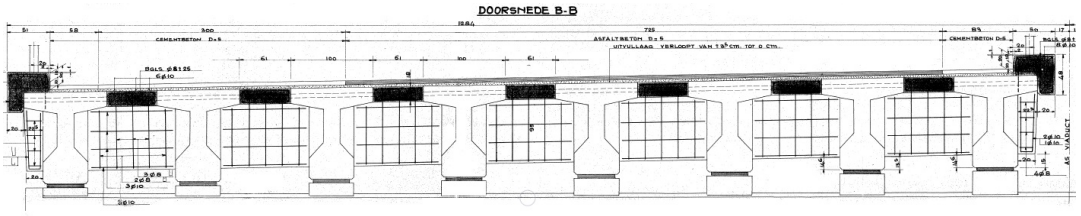

Figure 3.6: Dead loads acting on the girder

3.6.2. Self-weight

The girder is divided in four different cross-sections for calculation of the self weight; girder (1), full section (2-1), narrowing part (2-2) and hammerhead (3). The girder cross-section (A_1 is taken as a distributed load over the whole length of the girder), the rest of the cross-sections (A_2 and A_3 are taken as point load with a certain lever arm). The areas for the cross-sections 1, 2 and 3 with corresponding regions and point loads are;

- $A_1 = 0.507$ m^2 in $x = 1.725$,..,$7.425, 7.875$,..,11.425 m $\Rightarrow$ distributed load;
- $A_{2-1} = 0.700$ m^2 in region $x = -0.275$,..,0.725 m $\Rightarrow$ load at $x = 0.100$ and 7.650 m.
- $A_{2-2} = 0.507$,..,0.700 m^2 in region $x = 0.725$,..,1.725 m $\Rightarrow$ load at $x = 0.100$ m;
- $A_3 = 1.041$ m^2 in regions $x = -0.125$,..,$0.325, 7.425$,..,7.875 m $\Rightarrow$ load at $x = 0.100$ and 7.650 m;

The destructively tested girders are not of equal length, see Table 3.2. In principle the calculations for the girders are the same, except for the values for self-weight, support reactions and cross-sectional forces. Therefore only the girder HPZ1 will be discussed further.

Total force from self-weight

In this section the measured length of girder HPZ1 will be used, $L_{HPZ1} = 10.51$ m. The widths of the top flange vary along the longitudinal axis of the girder. For simplicity the width of the top flange (B) will be set constant to $B_{mean,HPZ1} = 0.96$ m. The specific weight of concrete is taken as $\gamma_c = 24.5$ kN/m^3. The cross-section of the 'girder' ($A_1 = 0.507$ m^2) is taken as distributed load over the whole length and the thicker cross-sections (A_{2-1}, A_{2-2} and A_3) are calculated with the difference with (A_1).

$$\begin{aligned}
q_{girder} = A_1 \cdot \gamma_c + q_{DL} \cdot B_{mean,HPZ1} &= 0.507 \cdot 24.5 + 0.84 \cdot 0.96 &&= 13.23 \text{ kN/m} \\
F_{girder} = L_{HPZ1} \cdot q_{girder} &= 10.51 \cdot 13.22 &&= 139.05 \text{ kN} \\
F_{2-1} = (A_{2-1} - A_1) \cdot \gamma_c \cdot L_{2-1} &= (0.700 - 0.507) \cdot 24.5 \cdot 1.0 &&= 4.7 \text{ kN} \\
F_{2-2} = 0.5(A_{2-1} - A_1) \cdot \gamma_c \cdot L_{2-2} &= 0.5(0.700 - 0.507) \cdot 24.5 \cdot 1.0 &&= 2.4 \text{ kN} \\
F_{3-1} = (A_3 - A_{2-1}) \cdot \gamma_c \cdot L_{3-1} &= (1.041 - 0.700) \cdot 24.5 \cdot 0.45 &&= 3.8 \text{ kN} \\
F_{3-2} = (A_3 - A_{2-2}) \cdot \gamma_c \cdot L_{3-2} &= (1.041 - 0.507) \cdot 24.5 \cdot 0.45 &&= 5.9 \text{ kN}
\end{aligned}$$

The total force $F_{sw,tot}$ from self-weight:

$$F_{sw,tot} = F_{girder} + F_{2-1} + F_{2-2} + F_{3-1} + F_{3-2} = 139.05 + 4.7 + 2.4 + 3.8 + 5.9 = 155.8\text{kN}$$

Support reactions R_{east} and R_{west} from self-weight

The two supports of the girder create two overhangs, one at the west side of $L_{west} = 0.275$ m and one at the east side of $L_{east} = 0.625$ m. The support reactions from self-weight R_{west} and R_{east} are:

$$R_{west} = \frac{0.5q_{girder}\left[(L_{HPZ1} - L_{east})^2 - L_{east}^2\right] + F_{2-1}\cdot a_{2-1} + F_{2-2}\cdot a_{2-2} + F_{3-1}\cdot a_{3-1} + F_{3-2}\cdot a_{3-2}}{L_{span}}$$

$$= \frac{0.5\cdot 13.23\cdot\left[(10.51 - 0.625)^2 - 0.625^2\right] + 4.7\cdot 9.375 + 2.4\cdot 8.542 + 3.8\cdot 9.5 + 5.9\cdot 1.95}{9.6}$$

$$= 78.69 \text{ kN}$$

$$R_{east} = F_{sw,tot} - R_{west} = 155.8 - 78.69 = 77.08 \text{ kN}$$

Cross-sectional forces V_{sw} and M_{sw} from self-weight

The shear- and moment forces at various cross-sections are calculated with `MS Excel` and checked with `MatrixFrame`, see Table 3.4 and Figure 3.7. The following equations are valid for $x = 1.725,..,7.650$ m:

$$V_{sw} = R_{west} - F_{2-1} - F_{2-2} - F_{3-1} - q_{girder}\cdot(x + 0.275)$$
$$= 67.84 - 13.23\cdot(x + 0.275) \text{ [kN]}$$

$$M_{sw} = R_{west}\cdot x - 0.5q_{girder}\cdot(x + 0.275)^2 - F_{2-1}\cdot(x - 0.225) - F_{2-2}\cdot(x - 1.058) - F_{3-1}\cdot(x - 0.1)$$
$$= 78.69x - 6.61\cdot(x + 0.275)^2 - 4.7\cdot(x - 0.225) - 2.4\cdot(x - 1.058) - 3.8\cdot(x - 0.1) \text{ [kNm]}$$

Table 3.4: Cross-sectional moments M_{sw} and shear forces V_{sw} for HPZ1 for $x = 0,..,9.600$ m [1][1]

x [m]	**0**	**1.725**	**1.8**	**1.85**	**1.9**	**1.95**	**2**	**2.051**	**2.453**	**2.903**	**5.575**	**9.6**
V_{sw} [kN]	75.05	41.38	40.39	39.73	39.07	38.40	37.74	37.07	31.75	25.80	−9.55	−68.68
M_{sw} [kNm]	−0.50	94.50	97.57	99.57	101.54	103.48	105.38	107.29	121.12	134.07	155.78	−2.58

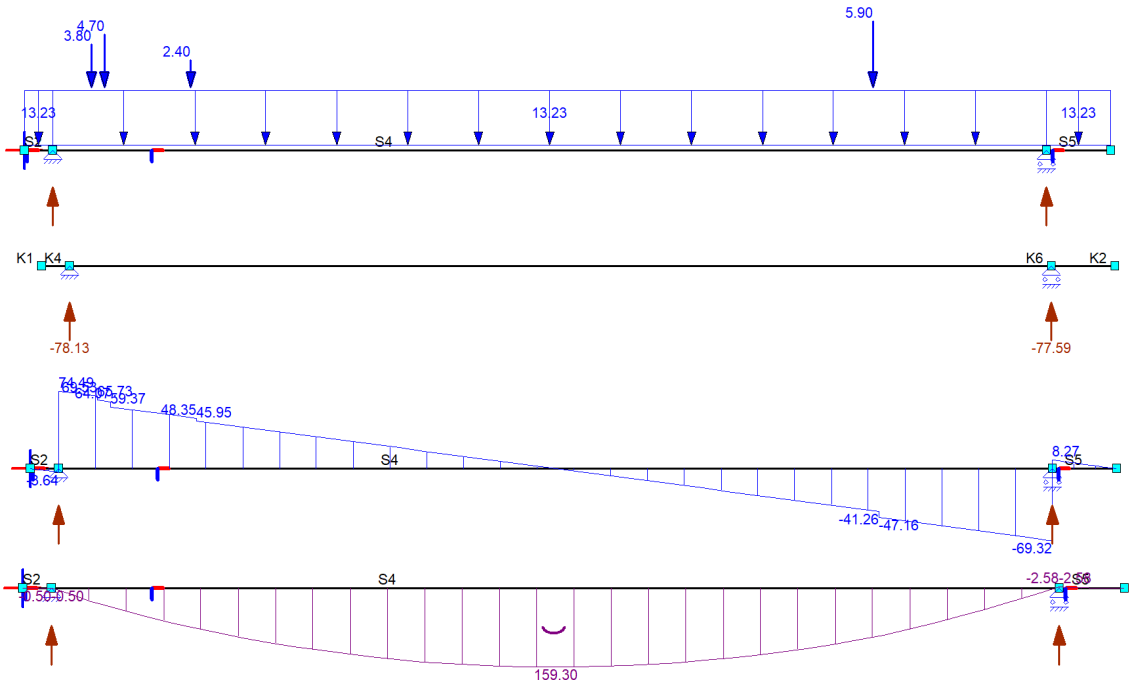

Figure 3.7: `MatrixFrame` results for the moment and shear forces for self-weight for HPZ1

[1]Based on M. Roosen's preliminary report, but made more extensive by considering more cross-sections

3.6.3. Prestressing

The moment and shear forces are calculated with Ritter's method of sections [11]. With the position of the cables shown in Table 3.3 the mean concrete cover with respect to the prestressing cables c, mean effective depth $d_p = h - c$ and eccentricity $e_p = d - z_{top}$ can be calculated. The moment due to the eccentric prestressing force can be easily calculated with $M_p = N_p \cdot e_p$, see Table 3.5. The total prestressing force N_p depends on the amount of cables in a cross-section and needs a certain length before the full force is transmitted into the concrete. This is called the transmission length of the prestressing element, in EC2 l_{pt} with $l_{pt2} = 1.2 l_{pt}$ for ultimate limit states. A quick calculation shows that $l_{pt} \approx 1$ m, which means that the considered cross-sections are out of the transmission zone. The remaining prestressing force from Equation 4.3 is used and results in a force per strand:

$$N_{p,strand} = 0.57 \cdot 401.2 = 228.7 \text{ kN} \tag{3.4}$$

Cables 1 to 3 are anchored at the top flange along the longitudinal axis of the girder. Cable 3 is anchored at $x = 2.700 - 0.075 = 2.625$ m, cable 2 is anchored at $x = 2.700 - 0.075 + 1200 = 3.825$ m and cable one is anchored at $x = 2.700 - 0.075 + 1200 + 1200 = 5.025$ m. This results in a total prestressing force of:

- From $x = 1.725$,..,3.625 m cables 4 to 10 are present with a total of $N_p = 1598$ kN;
- From $x = 3.625$,..,4.825 m cables 3 to 10 are present with a total of $N_p = 1827$ kN;
- From $x = 4.825$,..,6.025 m cables 2 to 10 are present with a total of $N_p = 2054$ kN;
- From $x = 6.025$,..,10.510 m cables 1 to 10 are present with a total of $N_p = 2282$ kN.

Table 3.5: Cross-sectional moment M_p from prestressing for $x = 1725$,..,4600 mm [1][1]

x [mm]	**1725**	**1800**	**1850**	**1900**	**1950**	**2000**	**2051**	**2300**	**2453**	**2903**	**4600**
c [mm]	340	335	332	329	325	322	319	303	295	271	180
d_p [mm]	770	775	778	781	785	788	791	807	815	839	930
e_p [mm]	278	283	286	289	293	296	299	315	323	347	438
M_p [kNm]	444	452	457	462	467	473	478	503	517	555	700

A point of attention is that cables 7 & 8 and 9 & 10 have the same location. This is taken into account in the calculation for c. To calculate the shear forces V_p the angle of the cables α is required. Also here the cables 7 & 8 and 9 & 10 count double ($2 \cdot N_{p,strand}$) for V_p. The cross-sectional forces from prestressing are calculated as follows and are also shown in Tables 3.5 through 3.7 [1]:

$$V_p = \Sigma V_{p,i} = \Sigma N_{p,strand} \cdot \sin \alpha_i \text{ [kN]} \tag{3.5}$$

Table 3.6: Slope of the cables α in degrees for $x = 1725$,..,4600 mm [1][1]

x [mm]	**1725**	**1800**	**1850**	**1900**	**1950**	**2000**	**2051**	**2300**	**2453**	**2903**	**4600**
1 [°]											
2 [°]											4.32
3 [°]											1.49
4 [°]	7.62	7.58	7.55	7.53	7.50	7.47	7.45	7.31	7.23	6.99	5.55
5 [°]	5.70	5.66	5.63	5.60	5.58	5.55	5.52	5.38	5.29	5.03	4.08
6 [°]	4.43	4.41	4.40	4.39	4.37	4.36	4.35	4.28	4.24	4.12	3.50
7 & 8 [°]	2.55	2.54	2.53	2.52	2.51	2.50	2.49	2.45	2.42	2.34	2.00
9 & 10 [°]	0.91	0.91	0.90	0.90	0.89	0.89	0.88	0.86	0.84	0.80	0.54

[1]Based on M. Roosen's preliminary report, but made more extensive by considering more cross-sections

Table 3.7: Cross-sectional shear force V_p from prestressing for $x = 1725,..,4600$ mm [1][1]

x [mm]	**1725**	**1800**	**1850**	**1900**	**1950**	**2000**	**2051**	**2300**	**2453**	**2903**	**4600**
1 [kN]											
2 [kN]											17
3 [kN]											6
4 [kN]	30	30	30	30	30	30	30	29	29	28	22
5 [kN]	23	23	22	22	22	22	22	21	21	20	16
6 [kN]	18	18	18	17	17	17	17	17	17	16	14
7 & 8 [kN]	20	20	20	20	20	20	20	20	19	19	16
9 & 10 [kN]	7	7	7	7	7	7	7	7	7	6	4
V_p [kN]	98	98	97	97	96	96	96	94	93	89	72

3.6.4. External load

Table 3.8 shows the cross-sectional forces due to the external load. The internal shear and -moment V_F and M_F are ratios and need to be multiplied by the external load F_{exp}. The moment and shear forces are calculated as follows, with $a = 2.903$ m as the position of the external load:

$$V_F(x) = \begin{cases} R_{left} = F_{exp} \cdot \dfrac{L_{span} - a}{L_{span}} = 0.70F_{exp}, & \text{for } x = 0,..,2.903 \text{ m} \\ R_{right} = F_{exp} \cdot -\dfrac{a}{L_{span}} = -0.30F_{exp}, & \text{for } x = 2.903,..,9.600 \text{ m} \end{cases}$$

$$M_F(x) = \begin{cases} R_{left} \cdot a = 0.70a \cdot F_{exp}, & \text{for } x = 0,..,2.903 \text{ m} \\ R_{right} \cdot (a - L_{span}) = -0.30 \cdot (a - L_{span}) \cdot F_{exp}, & \text{for } x = 2.903,..,9.600 \text{ m} \end{cases}$$

Table 3.8: Cross-sectional moment and shear force from the external load M_F and V_F for HPZ1 for $x = 0,..,9.600$ m [1][1]

x [m]	**0**	**1.725**	**1.8**	**1.85**	**1.9**	**1.95**	**2**	**2.051**	**2.453**	**2.903**	**9.6**
$V_F[\times F_{exp}]$	0.70	0.70	0.70	0.70	0.70	0.70	0.70	0.70	0.70	0.70	−0.30
$M_F[\times F_{exp}]$	0.00	1.20	1.26	1.29	1.33	1.36	1.40	1.43	1.71	2.03	0.00

3.7. Summary of loads

A summary for the loads due to self-weight and the prestressing force are shown in Table 3.9 for HPZ1. The loads for HPZ1 and HPZ2 are assumed to be identical, although the length of HPZ2 is a bit longer resulting in a higher self-weight.

Table 3.9: Summary of loads for HPZ1 for $x = 0,..,9.600$ m [1][1]

x [m]	**0**	**1.725**	**1.8**	**1.85**	**1.9**	**1.95**	**2**	**2.051**	**2.453**	**2.903**	**9.6**
$V_F[\times F_{exp}]$	0.70	0.70	0.70	0.70	0.70	0.70	0.70	0.70	0.70	0.70	−0.30
$M_F[\times F_{exp}]$	0.00	1.20	1.26	1.29	1.33	1.36	1.40	1.43	1.71	2.03	0.00
V_p [kN]	−111	−98	−98	−97	−97	−96	−96	−96	−93	−89	−7
V_{sw} [kN]	75	41	40	40	39	38	38	37	32	26	−69
V_{sw+p} [kN]	−36	−57	−57	−58	−58	−58	−58	−59	−61	−63	−75
M_p [kNm]	−259	−444	−452	−457	−462	−467	−473	−478	−517	−555	−1124
M_{sw} [kNm]	−1	95	98	100	102	103	105	107	121	134	−3
M_{sw+p} [kNm]	−260	−350	−354	−358	−361	−364	−367	−371	−395	−421	−1126

[1]Based on M. Roosen's preliminary report, but made more extensive by considering more cross-sections

4

Experimental analysis

Four girders from the Helperzoom bridge, HPZ1 through HPZ4, are sawn to a length so they can be moved, lifted and tested in Stevenlab II at TU Delft. These girders are destructively tested under a concentrated load with an hydraulic jack with a maximum capacity of 2000 kN. In this chapter the goal of the experiments, how the girders are tested and the results from the tests are discussed for HPZ1 and HPZ2. The material properties of the girders from tests are already discussed in Chapter 3.

4.1. Goal of the experiments

The goal of the four experiments is to determine the failure mode, shear-tension failure or flexural-shear failure, and to check which design codes are best for calculating the shear capacity of these types of girders. Next to the failure mode, the tests are used to calibrate for nonlinear finite element models. These models will be used in the revision of existing structures with similar girders that do not comply with the current codes. Lastly, the goal of the experiments is to check if the non-code-compliant stirrups contribute to the shear capacity. Examples of these types of stirrups is given in Chapter 2.2. For the Helperzoom girder the following apply [73]:

- the stirrups are not anchored in the compression zone;
- the stirrups follow the shape of the girder and therefore have a kink at the intersections of both the bottom and top flange with the web. The possibility exists that the stirrups can burst out;
- the stirrups have a spacing of 400 mm.

4.2. Preparation of the experiments

The experiments are done on behalf of Rijkswaterstaat. First two beams are tested with the original setup, where after the results are evaluated to determine the method of testing for the remaining girders. The occurring failure mechanism also plays a role for the latter experiments.

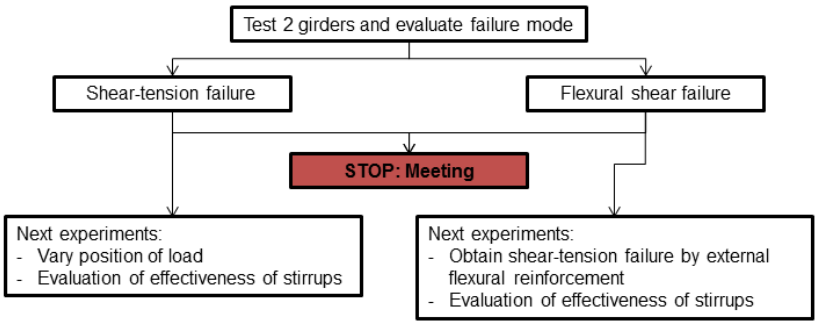

Figure 4.1: Flowchart for the experiments for girders HPZ1 through HPZ4 [72]

4.2.1. Position of the load

The preliminary analysis of Roosen [1] assumed a critical position for the load at $x = 2.903$ m from the east support with an inclined shear crack of 30°. This critical position is at $x = 1.725$ m with a web width of 200 mm. With an inclined crack of 30° it is the first position where a crack can form in a thin-webbed cross-section, away from the hammerhead and anchorage region, see Figure 3.5. The position for the external load at $x = 2.903$ m is used for both the experiments of HPZ1 and HPZ2.

4.2.2. Test setup

At Stevinlab II the supports can be placed with increments of 600 mm. The span length for HPZ1 and HPZ2 is taken as $L_{span} = 9.6$ m, to have enough overhang at both supports for the shortest girder. At the time of writing, only the test setups for HPZ1 and HPZ2 are known. Figure 4.2 shows a schematization of HPZ1 and HPZ2 at north side with span length, length of overhang and location of the bearings used in the tests. Figure 4.3 shows a side- and front-view of the stiffened steel gantry with hydraulic jack that is used for the experiments.

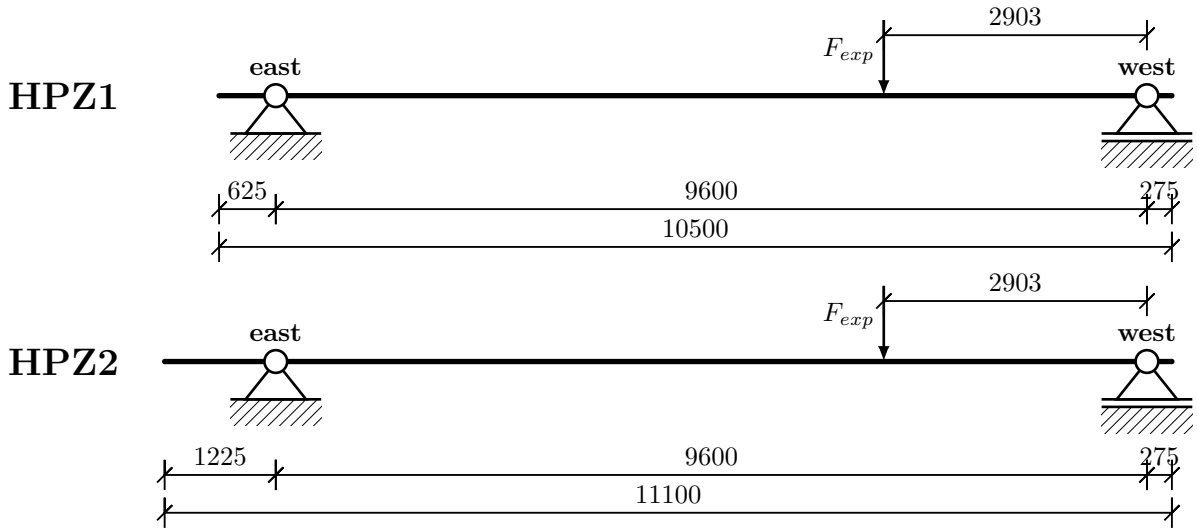

Figure 4.2: Span length, overhang and position of the external load in mm for HPZ1 and HPZ2 (north side)

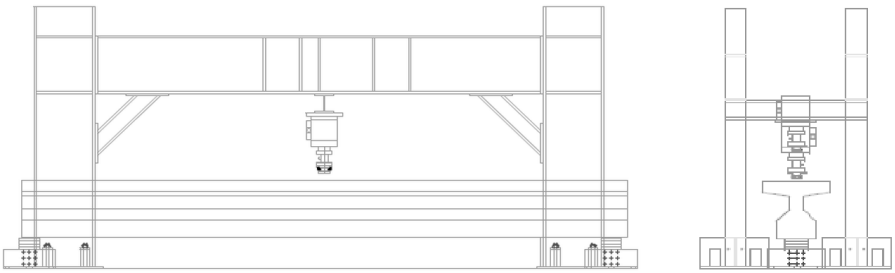

Figure 4.3: Side- and front view of the steel gantry with hydraulic jack [72]

4.3. Prestressing level

The prestressing level in the Helperzoom girders is determined in three ways. The first is based on the values given in the RBK 1.1. The second and third method is based on measurements done for HPZ2.

4.3.1. Prestressing level according to RBK

According to the RBK 1.1, the maximum allowable initial prestressing stress σ_{pi} is 65% of the ultimate strength. The time-dependent losses; shrinkage, creep and relaxation, can be assumed 20% for systems used before 1975. This results in a working prestressing stress of $0.65 f_{pk} \cdot 0.8 = 0.52 f_{pk}$ in MPa. The RBK states that the working prestressing stress σ_{pw} for systems used up to and including the RVB

1967 can be calculated with $0.52 f_{pk}$ in MPa. This is the same result as the maximum allowable initial prestressing stress with time dependent losses. RBK gives additional information to NEN-EN 1992-1-1 art. 3.3.2 [63] for prestressing steel used in the past like QP170. This data is shown in Table 4.1 [68].

Table 4.1: Properties of QP170 from RBK 1.1 [68] and QP170 from tests [72]

Steel quality	f_{pk} [MPa]	f_{pk}/γ_s [MPa]	$f_{p0.1k}$ [MPa]	f_{pd} [MPa]	ε_{uk} [%]	σ_{pi} [MPa]	σ_{pw} [MPa]
RBK1.1 : QP170	1670	1516	1422	1293	3.5	1084	868

Preliminary calculations performed by Roosen [1] are based on the data from RBK 1.1. According to the data provided in Table 4.1 the prestressing force of one cable results in:

$$N_{p,RBK} = 0.52 f_{pk} \cdot A_p = 0.52 \cdot 1670 \cdot 462 = 401{,}200 \text{ N} \tag{4.1}$$

4.3.2. Prestressing level according to tests on HPZ2

Two different measurements have been performed on HPZ2 to obtain the prestressing level in the girder. The first measurement is done with core samples to obtain the change in strains in the cores. This measured strain is converted to a stress in the cross-section and compared to the calculated stress distribution to obtain amount of prestressing. The result from this measurement is 48.3% of the assumed prestressing level, see Equation 4.2.

The second type of test measures the remaining stress in the strands in a more direct way. First the concrete and ducts surrounding the strands are removed. Next the prestressing strands are cut to measure the change in strain. Only results from the first cut are used as the cross-section will undergo elastic elongation after each cut. The measured average strain is $\mu\varepsilon = 2670.525$ and multiplying this with a Young's modulus of 185 GPa results in a stress $\sigma_{p,cut} = 494$ MPa. This results in 57% of the assumed prestressing level, see Equation 4.3 [73].

$$N_{p,cores} = 0.483 \cdot N_{p,RBK} \tag{4.2}$$

$$N_{p,cut} = 0.570 \cdot N_{p,RBK} \tag{4.3}$$

In this report $N_{p,cut} = 228.7$ kN (per cable) will be used for further calculations.

4.4. Sensor plan

Prior to the experiments sensors are installed to measure the horizontal and vertical deflections of the girder during the experiments. These sensors are placed in the web of the girder between the load and the bearings, near the supports and under the load. Next to the LVDTs and lasers, Acoustic Emission (AE) sensors are used to detect internal cracking from wave signals. Also photographs are taken to analyze the cracking process with Digital Image Correlation (DIC).

- 13 LVDTs are used to measure the x- and z-displacements in the web;
- 2 LVDTs are used to measure the deflection at the bearings;
- 2 laser distance finders, one 25 mm laser and one 100 mm laser, to measure the deflection at the position of the load;
- DIC and AE are used for monitoring the cracking process and estimating the origin of the cracks.

For HPZ2 four additional LVDTs were added. Also another type of sensor was used, smart aggregates (SAs). The SAs consists of two marble layers with a PZT layer in between and have similar mechanical properties as normal aggregates.

4.5. Results of HPZ1 and HPZ2

In this section the results for the experiment of HPZ1 and HPZ2 are given. First an overview of the results of the experiments are shown. Secondly the results of the laser distance finders are illustrated. Lastly the results of the AE and DIC measurements of the measurement report [72] are summarized and analyzed.

4.5.1. Overview of the test

Table 4.2 gives an overview of the results for HPZ1 and HPZ2.

Table 4.2: Overview of HPZ1 and HPZ2 results and parameters [72]

Name of girder	**HPZ1**	**HPZ2**
Date of experiment	27-06-2019	12-09-2019
Shear span-to-depth ratio (a/d)	3	3
Loading speed	0.01 mm/s & 0.02 mm/s	0.02 mm/s
Load at first flexural crack	965 kN	1001 kN
Load at inclined crack in the web	1344 kN	1299 kN
Load at failure	1892.7 kN	1849 kN
Deflection at failure	51.5 mm	39.66 mm
Failure mode	Shear-compression / flexural-shear	Shear-compression / flexural-shear

4.5.2. Results from sensors

The sensors that are of interest are the sensors that measure the deflection under the load, which are Laser01 and Laser02. Laser01 (red) stopped measuring after a deflection of 22 mm due to its limited range, so only Laser02 is shown. The force-displacement diagram for both HPZ1 and HPZ2 is shown in Figure 4.4.

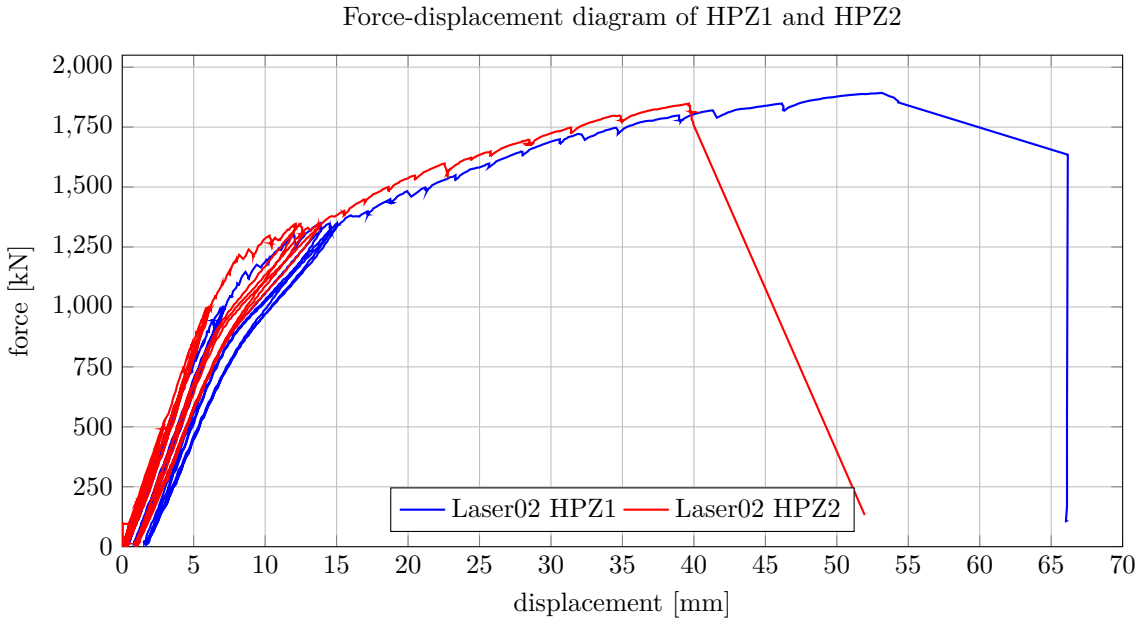

Figure 4.4: Load-deflection diagram measured by Laser01 and Laser02 for HPZ1 and HPZ2

Apart from the cyclic loading, the concrete behaves linear elastic until the first flexural crack occurs: $F_{crack} = 965$ kN for HPZ1 and $F_{crack} = 950$ kN for HPZ2. Beyond these loads the concrete starts to show non-linear behavior. The three cycles to 1350 kN show a different (lower) stiffness than the first two set of cycles for both experiments. Also the non-linear behavior starts at an lower load ≈ 750 kN. The load at failure is: $F_{exp} = 1892.7$ kN for HPZ1 and $F_{exp} = 1849$ kN for HPZ2.

Figure 4.5 shows the loading schemes of the first two experiment together with the deflections of the girders. The scheme for HPZ1 consists of 34 loading steps and 9 unloading steps and the scheme for HPZ2 consists of 34 loading steps and 11 unloading steps. The loading scheme for HPZ1 and HPZ2 was as follows:

- Three cycles to 500 kN;
- Three cycles to 1000 kN with a pause every 50 kN for first cycle;
- Three cycles to 1350 kN with a pause every 50 kN for first cycle;
- Load until failure and pause every 50 kN.

The cycles to 500, 1000 and 1350 kN were performed to gather data for the AE sensors. For HPZ1 the loading and unloading speed at first was 0.01 mm/s. After the last cycle to 500 kN, the loading and unloading speed was increased to 0.02 mm/s until failure occurred. For HPZ2 the loading and unloading speed was 0.02 mm/s for the whole duration of the experiment.

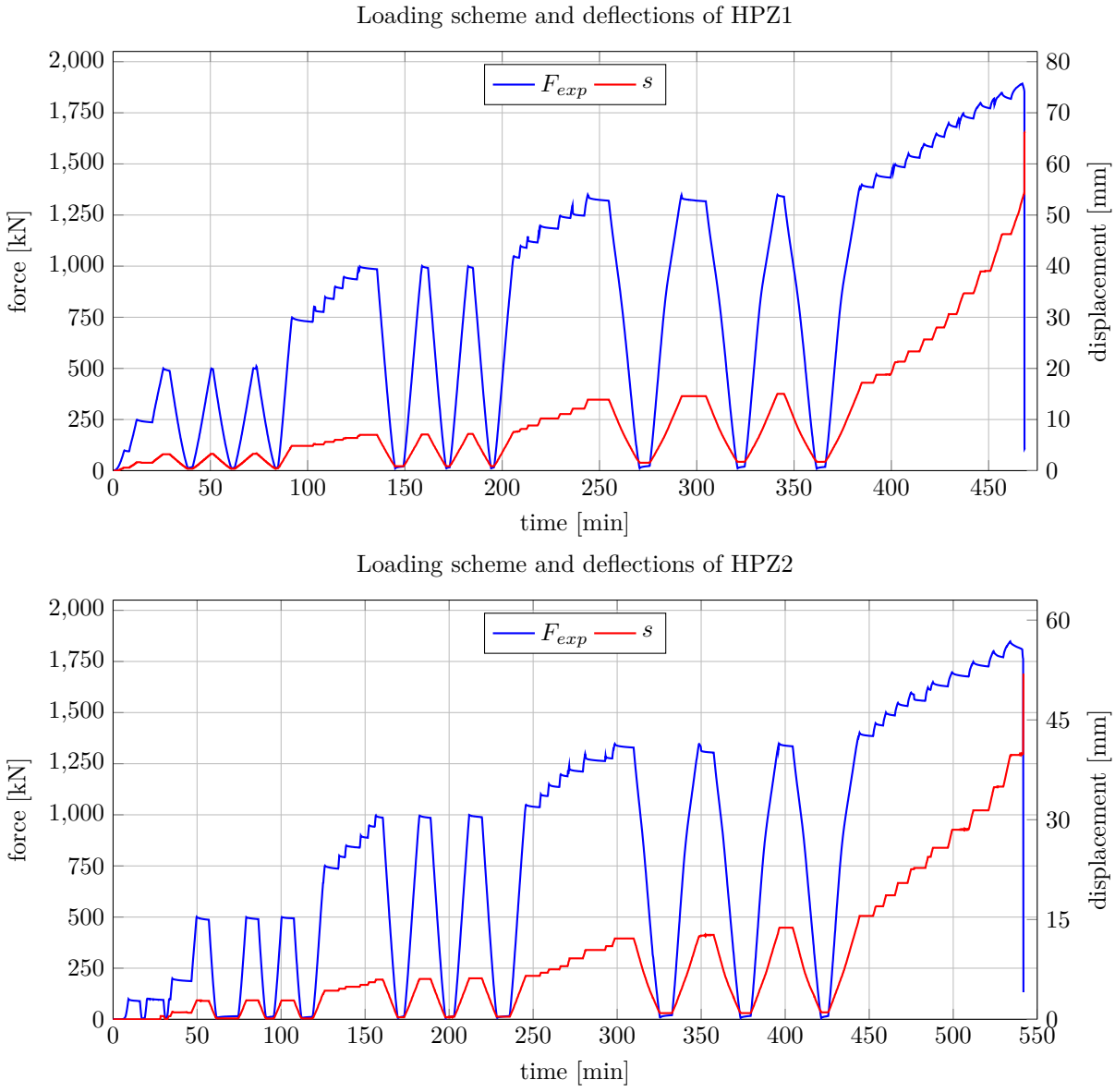

Figure 4.5: Loading scheme with corresponding displacement from Laser02 for HPZ1 and HPZ2

4.6. Analysis of experimental results

In this section the results from AE, DIC, photographs and LVDTs measurements are analyzed. With these results the crack angles and patterns are visualized (photographs) or calculated (LVDTs) and are used to determine the contribution of the stirrups and the contribution of the prestressing force. Next to the results from the experiments, the contribution of the prestressing force is analytically checked with a sectional analysis.

4.6.1. Analysis of AE and DIC results

The results from AE monitoring can be used to detect internal cracking. With the data from the AE sensors, the location of the cracks can be estimated by a localization technique. Next to AE monitoring a series of photographs are taken, to identify the crack development in the girder during loading. First a reference photograph is taken from the unloaded and undeformed girder. Subsequently at the end of every load step and every fully unloaded step, three photographs were taken from the deformed girder. After the last cycle of 1350 kN photographs were taken roughly every 10 seconds. The photographs that were taken during loading can be compared to the reference photograph with the DIC technique. The output of this method is a displacement field. The displacements are converted into strains where after the crack patterns can be identified [32]. Figure 4.6 shows a few DIC results at three different load steps: 1350 kN, at maximum capacity (HPZ1: 1892 kN, HPZ2: 1850 kN) and after failure [72].

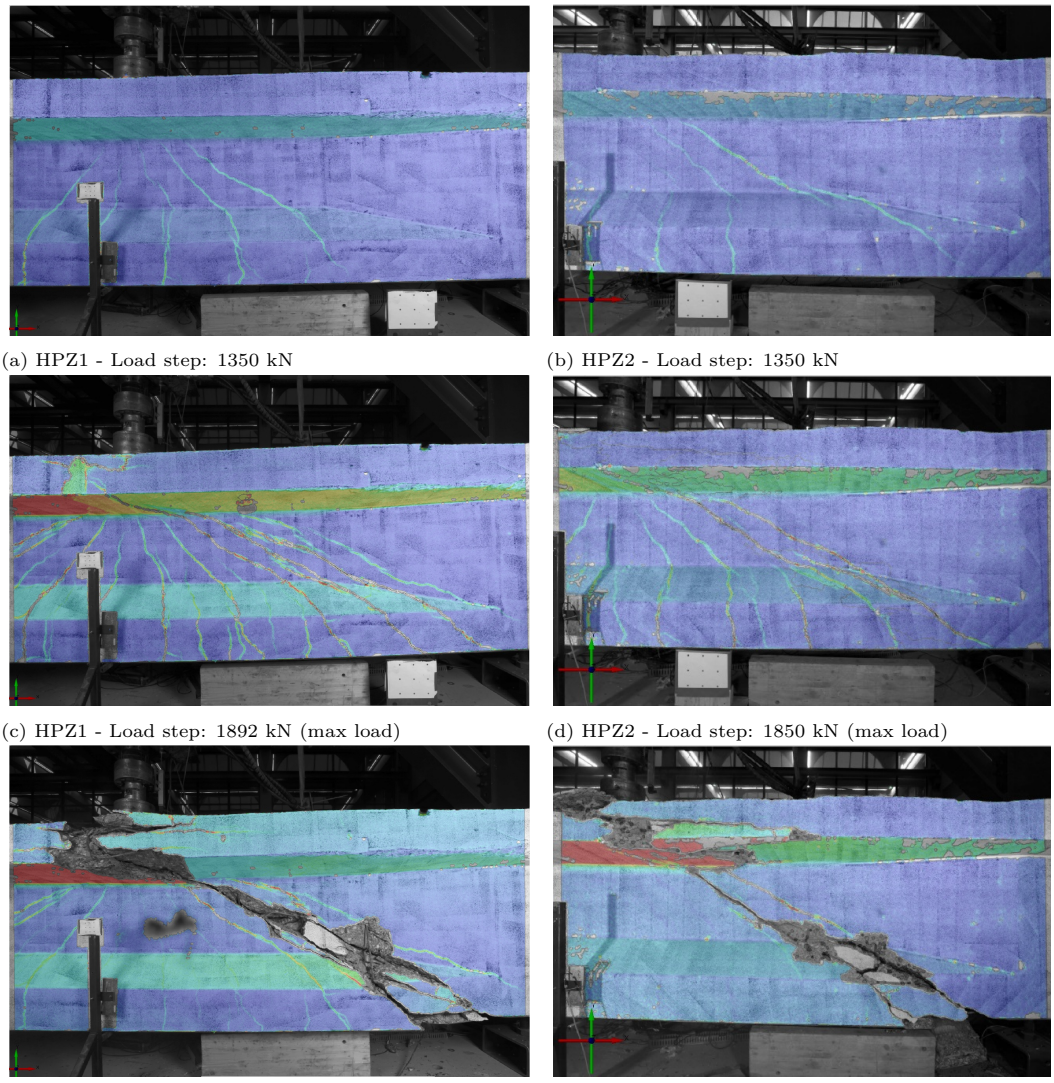

(a) HPZ1 - Load step: 1350 kN

(b) HPZ2 - Load step: 1350 kN

(c) HPZ1 - Load step: 1892 kN (max load)

(d) HPZ2 - Load step: 1850 kN (max load)

(e) HPZ1 - Load step: failure

(f) HPZ2 - Load step: failure

Figure 4.6: DIC results at three different load steps for HPZ1 and HPZ2 [72]

– **HPZ1:** At 1150 kN only a few flexural cracks are visible. As the load increases the number of flexural cracks and shear cracks increases. At load step 1775 kN, strains at the top flange are visible. At 1892 kN, just before failure, the compression strains in the top flange are clearly visible over the full height of the flange. The last figure shows the shear crack after failure of the girder, which crosses the intersection of the web with the bottom flange at $x = 1.725$ m.

– **HPZ2:** At 1000 kN no flexural cracks are visible. As the load increases the number of flexural cracks and shear cracks increases. At load step 1850 kN (peak load), strains at the top flange are visible (few lines). At 1790 kN, just before failure, the compression strains in the top flange are more visible below the external load. The last figure shows the shear crack after failure of the girder, with a steeper crack angle than HPZ1.

Five major cracks were observed during the first and second experiment, CR1 through CR5 (CR5 closest to the support). A summary for the AE and DIC results is given in Table 4.3. AE is able to detect micro cracks, while DIC can only detect crack openings greater than 0.1 mm. For this reason, in both experiments, AE detects cracks and crack openings at a lower external load than DIC [73].

Table 4.3: Summary of the analysis of the AE results for HPZ1 (values in kN)

No.		**Load at crack formation in kN (CR1 closest to load)**					**Failure load**
		CR1	CR2	CR3	CR4	CR5	
HPZ1	AE	950*	1100	1300	1350	1300	**1893**
	DIC	1050	1150	1300	1350	1300	
HPZ2	AE	1000	1200*	1300	1300	1300	**1850**
	DIC	1050	1245	1350	1350	1350	

* micro cracks, major crack opening was at a slightly higher load

The crack patterns and -angles (α_{photo}) are measured from the photographs taken just before failure of HPZ1 and HPZ2, see Figure 4.7 [73]. The crack angles for the girders range from:

Table 4.4: Crack angles for HPZ1 and HPZ2 according to the DIC results

No.	**Crack angles α_{photo}**				**Total range**	**Critical crack(s)**
	CR5	CR4	CR3	CR2		
HPZ1	15° to 33°	22° to 37°	28° to 32°	26° to 41°	15° to 41°	22° to 37°
HPZ2	18° to 34°	29° to 36°	37° to 43°		18° to 43°	29° to 36°

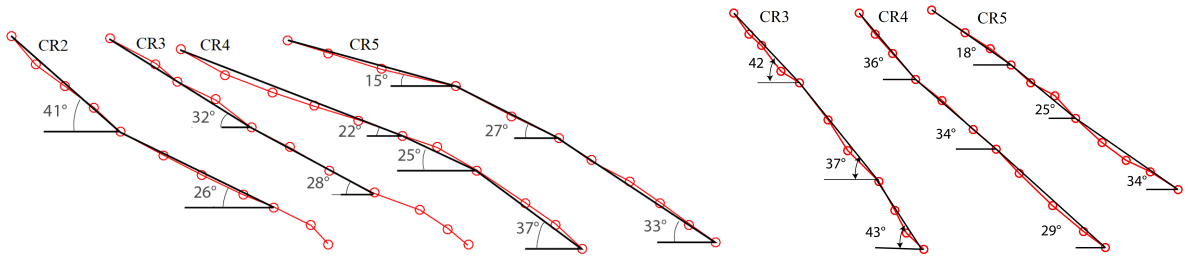

(a) HPZ1 (b) HPZ2

Figure 4.7: Vizualization of the crack angles and -profiles for HPZ1 and HPZ2 [72]

Critical cracks and critical positions

Based on the DIC results the critical cracks for HPZ01 are CR3 and CR4 (these cracks are branches propagating of one crack at the top of the web) and the critical crack for HPZ02 is CR4. Based on the location of these critical cracks, the critical position is assumed. The critical position is based on the location of tendon 6 for both girders, for HPZ01 at $x = 2.903 - 1.075 = 1.828$ m and for HPZ02 at $x = 2.903 - 1.030 = 1.873$ m [73].

4.6.2. Inclination of the compression field from LVDTs results

The inclination of the compression field θ is calculated from the x- and y-displacement measured by the LVDTs. The sensor plan for HPZ02, including the LVDTs, is given in Figure 4.8. The sensor plan for HPZ01 is identical, except no diagonal LVDTs (LVDT 14 and 15) were present during the experiment. The horizontal length of a grid is $L_{hor} = 500$ mm and the vertical length is $L_{vert} = 320$ mm. This results in a diagonal length of LVDT14 and LVDT15 of $L_{diag} = 593$ mm. The strains are calculated by dividing the measured displacements from the LVDTs by the lengths of the related (horizontal, vertical or diagonal) LVDTs. The inclination θ is calculated with two methods, namely the "XY" method and the "Rosette" method.

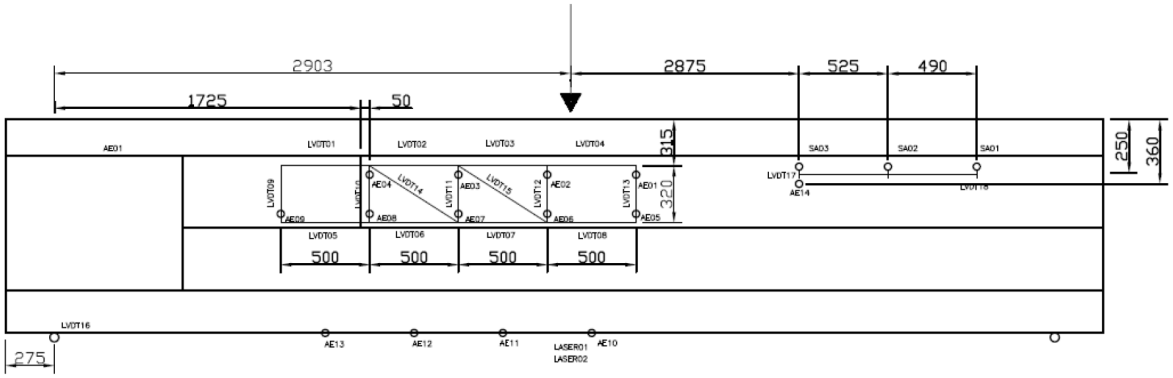

Figure 4.8: Sensor plan for HPZ02 [72]

The XY-method calculates γ_{xy} according to the shortening or elongation of a 2D element subjected to shear, see Figure 4.9 and Equation 4.4. The differences in displacements (or strains) are very small, which means the small-angle approximation ($\tan\Psi \approx \Psi$) holds. Note that Ψ_1 and Ψ_2 are presented as angles, but are dimensionless quantities [75].

$$\gamma_{xy} = \Psi_1 + \Psi_2 = \frac{\frac{\Delta x}{500}}{\frac{320}{320} + \frac{\Delta y}{320}} + \frac{\frac{\Delta y}{320}}{\frac{500}{500} + \frac{\Delta x}{500}} = \frac{\varepsilon_{xx}}{1+\varepsilon_{yy}} + \frac{\varepsilon_{yy}}{1+\varepsilon_{xx}} \tag{4.4}$$

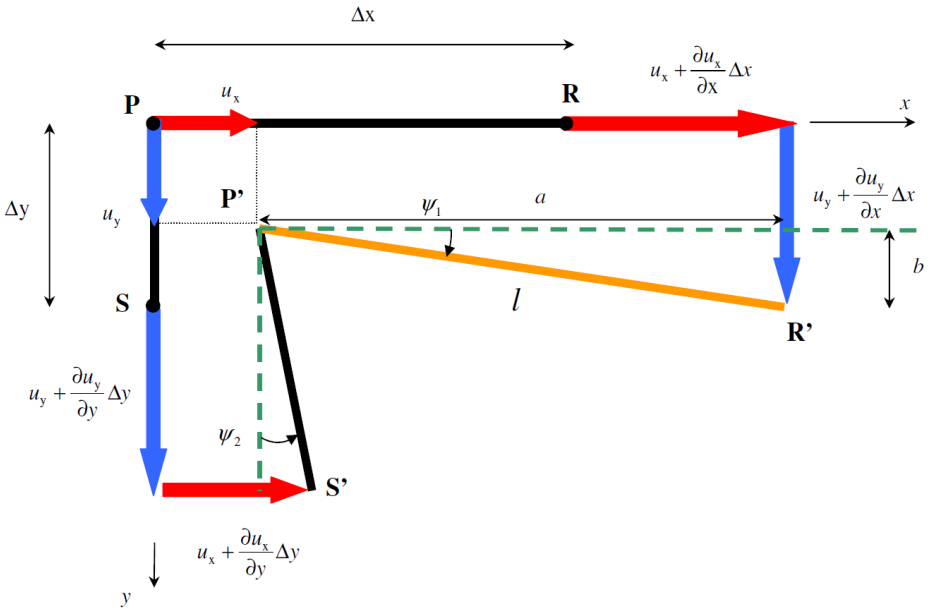

Figure 4.9: Calculating the inclination θ with the XY-method [75]

The Rosette-method is based on three strain gauges, see Figure 4.10. The strains, ε_{xx}, ε_{yy} and γ_{xy} are calculated according to three strain equations, see Equation 4.5. The inclinations θ_A ($= 0°$), θ_B ($= \theta_{AB}$) and θ_C ($= \theta_{AB} + \theta_{BC} = 90°$) are calculated as the inclinations between the horizontal x-axis and the strain gauge. The strains ε_A, ε_B and ε_C are the measured displacements from the LVDTs divided by the lengths of the LVDTs: L_{hor}, L_{vert} and L_{diag}.

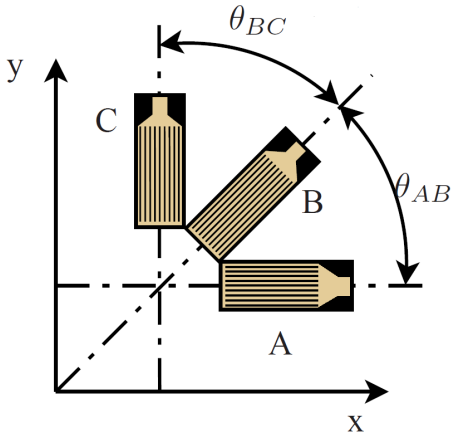

Figure 4.10: Calculating the inclination θ with the Rosette-method [76]

$$\begin{aligned}
\varepsilon_A &= \varepsilon_{xx}\cos^2\theta_A + \varepsilon_{yy}\sin^2\theta_A + \gamma_{xy}\sin\theta_A\cos\theta_A \\
\varepsilon_B &= \varepsilon_{xx}\cos^2\theta_B + \varepsilon_{yy}\sin^2\theta_B + \gamma_{xy}\sin\theta_B\cos\theta_B \\
\varepsilon_C &= \varepsilon_{xx}\cos^2\theta_C + \varepsilon_{yy}\sin^2\theta_C + \gamma_{xy}\sin\theta_C\cos\theta_C
\end{aligned} \tag{4.5}$$

With the grid for the LVDTs given in Figure 4.8 the angles are:

$$\theta_{AB} = 32.62° \text{ and } \theta_{BC} = 57.38°$$

This results in the following set of equations:

$$\begin{bmatrix} \varepsilon_A \\ \varepsilon_B \\ \varepsilon_C \end{bmatrix} = \begin{bmatrix} 1 & 0 & 0 \\ 0.7094 & 0.2906 & 0.454 \\ 0 & 1 & 0 \end{bmatrix} \begin{bmatrix} \varepsilon_{xx} \\ \varepsilon_{yy} \\ \gamma_{xy} \end{bmatrix} \tag{4.6}$$

The normal- ($\varepsilon_{xx}, \varepsilon_{yy}$) and shear strains ($\gamma_{xy}$) result in:

$$\begin{bmatrix} \varepsilon_{xx} \\ \varepsilon_{yy} \\ \gamma_{xy} \end{bmatrix} = \begin{bmatrix} \varepsilon_A \\ \varepsilon_C \\ \dfrac{\varepsilon_B - 0.7094\varepsilon_{xx} - 0.2906\varepsilon_{yy}}{0.454} \end{bmatrix} \tag{4.7}$$

The XY-method is used for HPZ01, because no diagonal LVDTs were present during the experiment, and for HPZ02 both methods are used. Mohr's Circle is used to determine the inclination of the compression field θ from the calculated γ_{xy} from both methods together with ε_{xx} and ε_{yy}. Several combinations of LVDTs are made to calculate θ, based on the position of the critical crack of HPZ01 and HPZ02. Combinations that have multiple horizontal or vertical LVDTs the strains are averaged, for example if LVDT1 and LVDT2 (both horizontal) are used the measurements are summed and divided by two. Not all calculated combinations are presented in this report, because the results were unrealistic (due to averaging multiple LVDTs).

Figure 4.11 shows the combinations that are used for both girders (the abbreviation "XY" relates to the XY-method). For the Rosette-method (HPZ2 only) the combinations shown in Figure 4.12 are used.

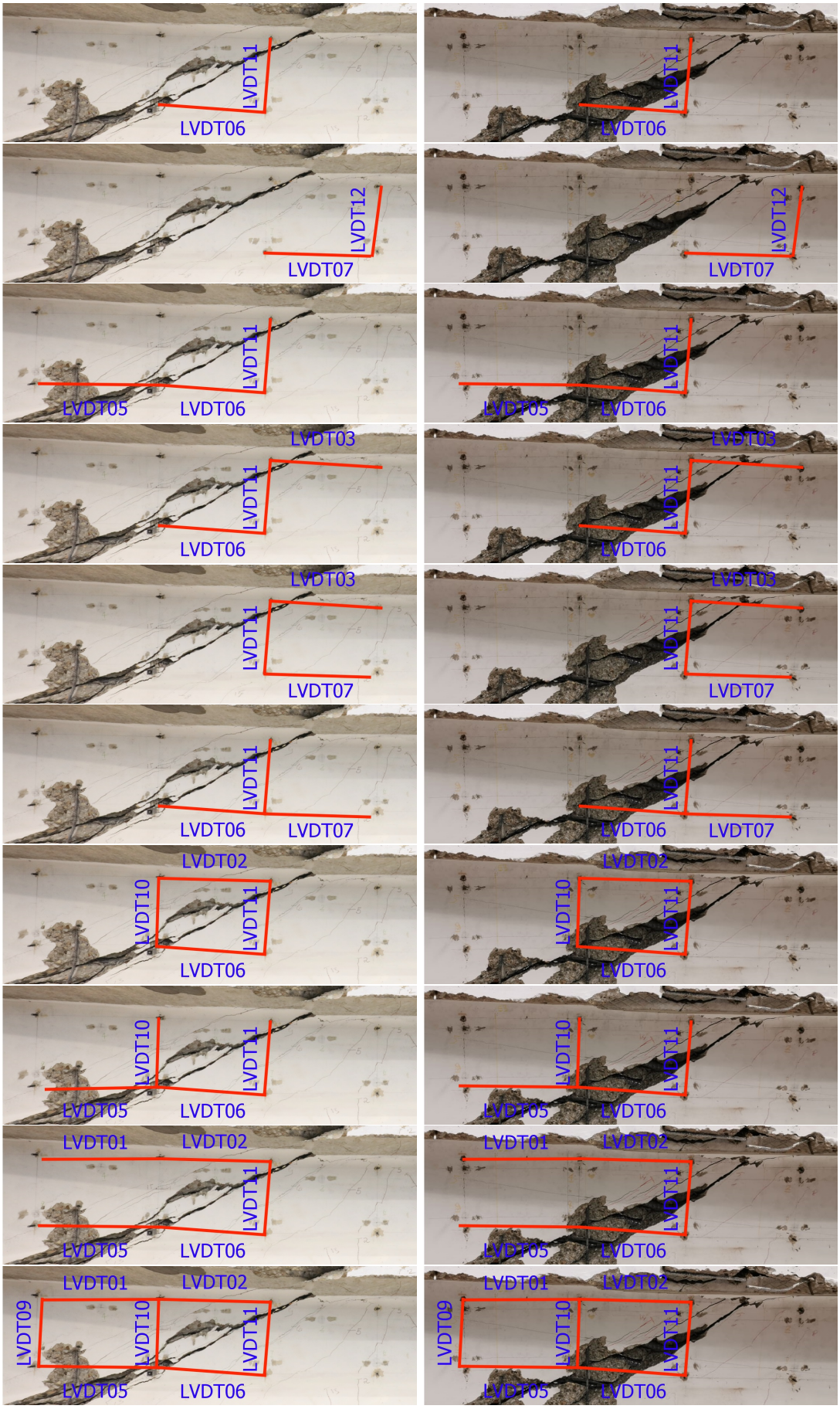

Figure 4.11: Combinations of LVDTs used for HPZ1 (left) and HPZ2 (right) for the XY-method

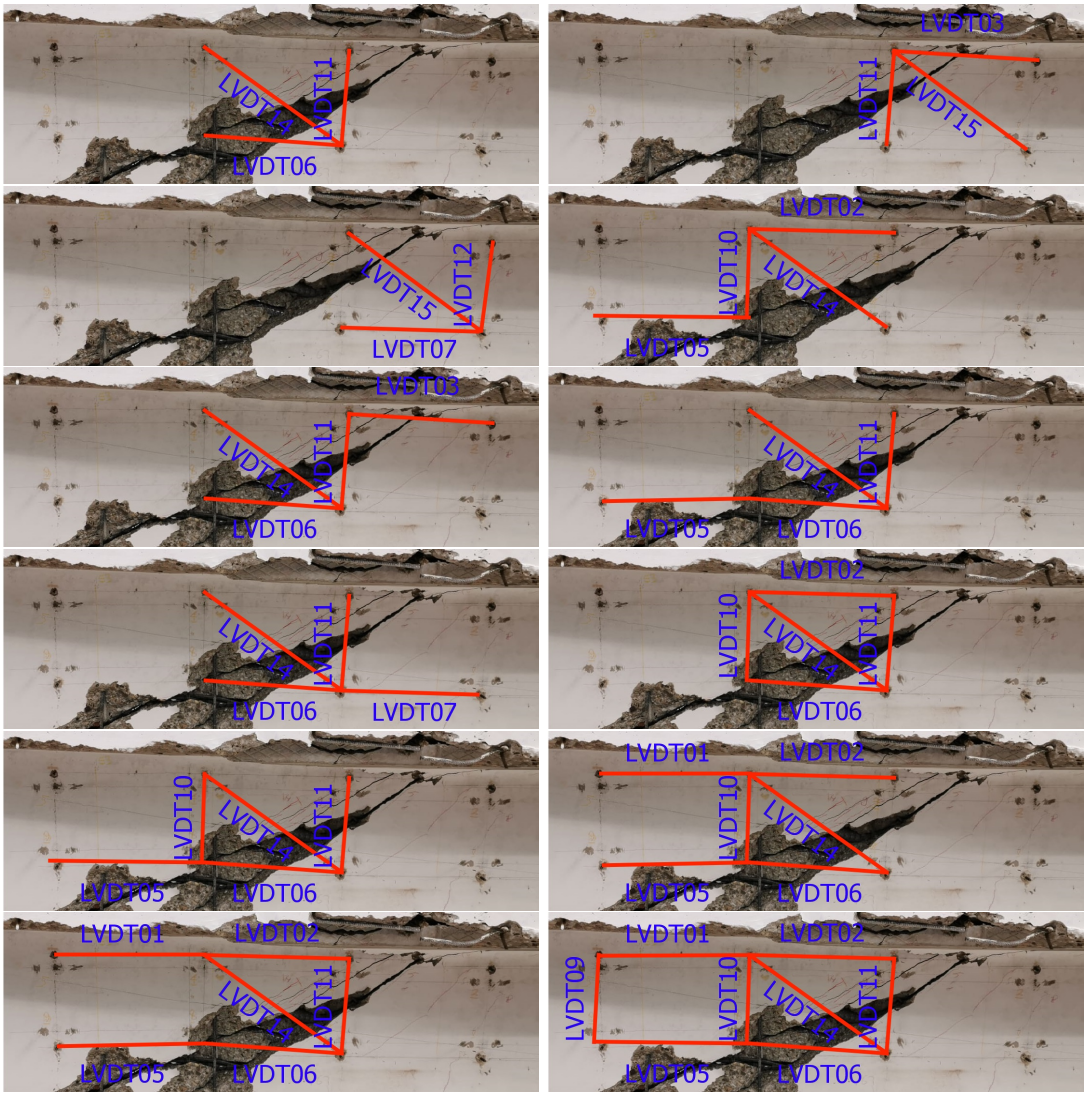

Figure 4.12: Combinations of LVDTs used for HPZ2 for the Rosette-method

The measured displacements from the LVDTs are taken from an initial point. This initial point (or starting point) for HPZ01 is index number $i = 21962$ and for HPZ02 index number $i = 25542$ and have been chosen as the starting point for the last loading cycle, from an almost fully unloaded girder to the maximum load. The calculated inclinations θ for the combinations above are given in figures 4.13 through 4.15. The first plot in each figure gives the results for the full (last) cycle and the second plot in each figure gives the results from 1500 kN to maximum load.

Note 1: this section presents two methods to calculate θ, namely XY-method and Rosette-method. HPZ1 did not have diagonal LVDTs 14 and 15, which means a degree of freedom is missing. These methods do not lead to the same results as can be observed for HPZ2 (Figures 4.14 and 4.15).

Note 2: the grids of the LVDTs are big (500x320 mm) and the strains are calculated at an infinitesimal plane element that represents average strains around an area of that element. Locally at or around the crack, the values for θ can be lower than the results obtained from the LVDTs.

Note 3: some combinations use averaged displacements from a top and bottom LVDT. This can lead to (very) unrealistic average values for ε_{xx} and ε_{yy} (and indirectly for γ_{xy}). These unrealistic results have been omitted from the plots. The results of the combinations that are plotted should be treated carefully, especially when combining LVDTs under compression and tension.

Note 4: the LVDTs of HPZ1 which are (mostly) in compression are: 01, 02 and 09 and for HPZ2: 01, 02, 05 and 09.

Note 5: absolute values are plotted for θ obtained from Mohr's Circle. For example, LVDTs combination 1-2-5-6-9-10-11-XY from HPZ1 touches the x-axis, meaning that θ reaches zero. If the normal values are plotted, this combination starts at $\theta = +5°$ and shifts to a negative θ above 850 kN. The end value is $\theta = -25°$ at 1893 kN.

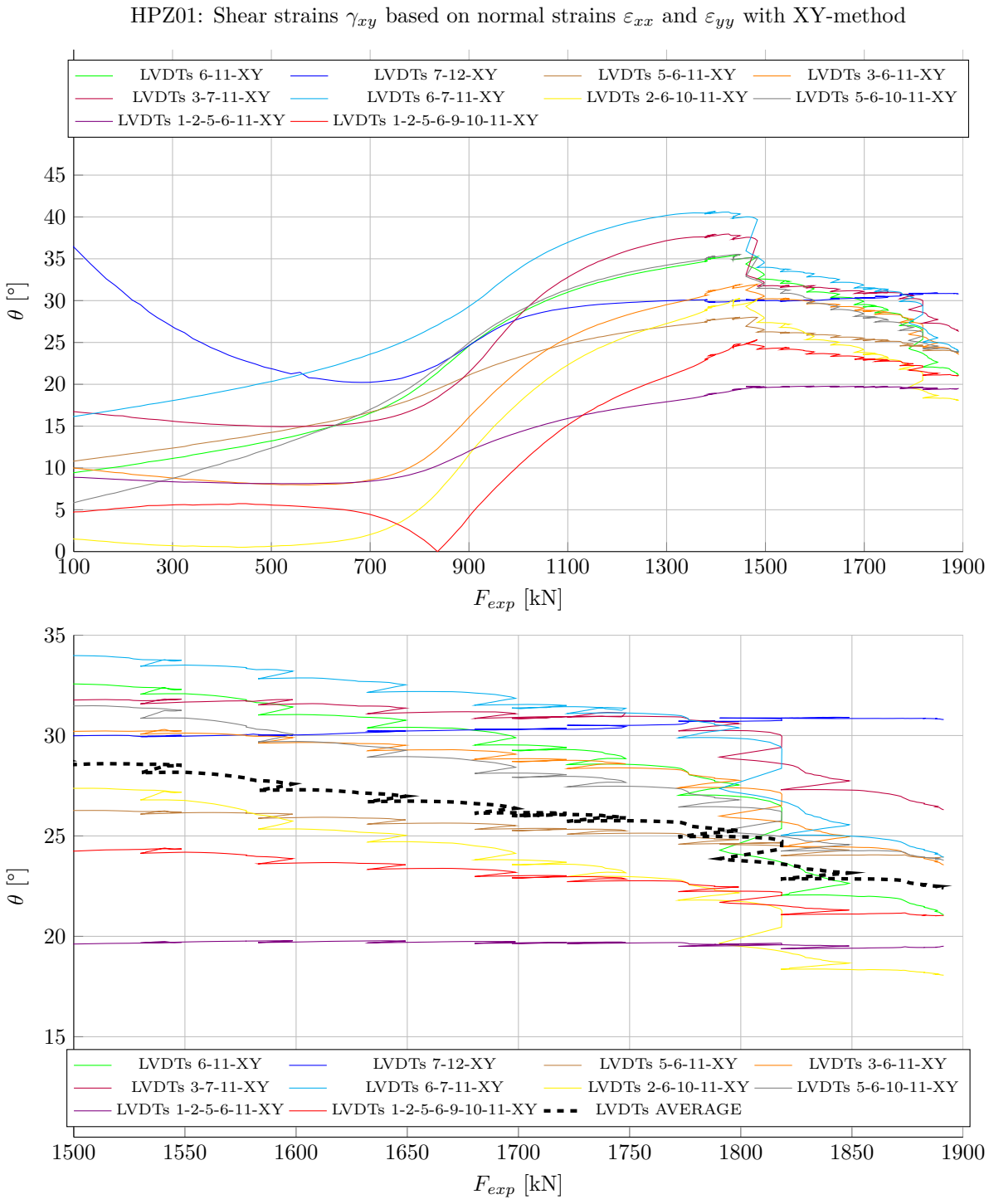

Figure 4.13: Calculated inclinations of the compression field θ with different combinations of LVDTs for HPZ01 with "XY" method

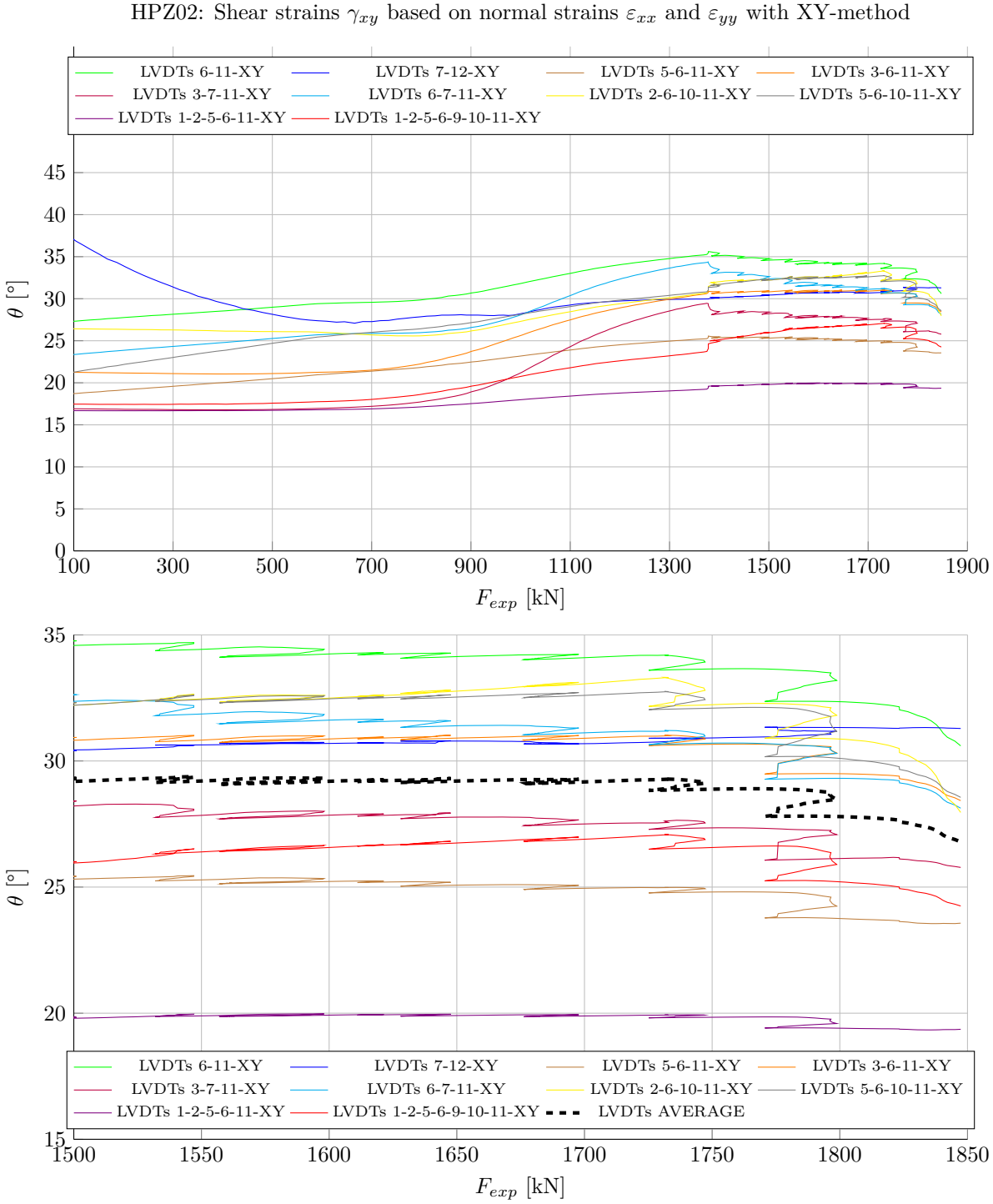

Figure 4.14: Calculated inclinations of the compression field θ with different combinations of LVDTs for HPZ02 with "XY" method

The calculated values with the XY-method give results that are in line with the measured cracking angles from the photographs, given in the previous paragraph. The inclination θ ranges from 18 - 26° (average: 23°) at maximum load for HPZ01 ($F_{exp} = 1893$ kN) and ranges from 20 - 30° (average: 27°) at maximum load for HPZ02 ($F_{exp} = 1848$ kN). The combinations that include (vertical) LVDT10 have been mostly omitted from the plots, as the results were not representative with respect to the combinations with (vertical) LVDT11.

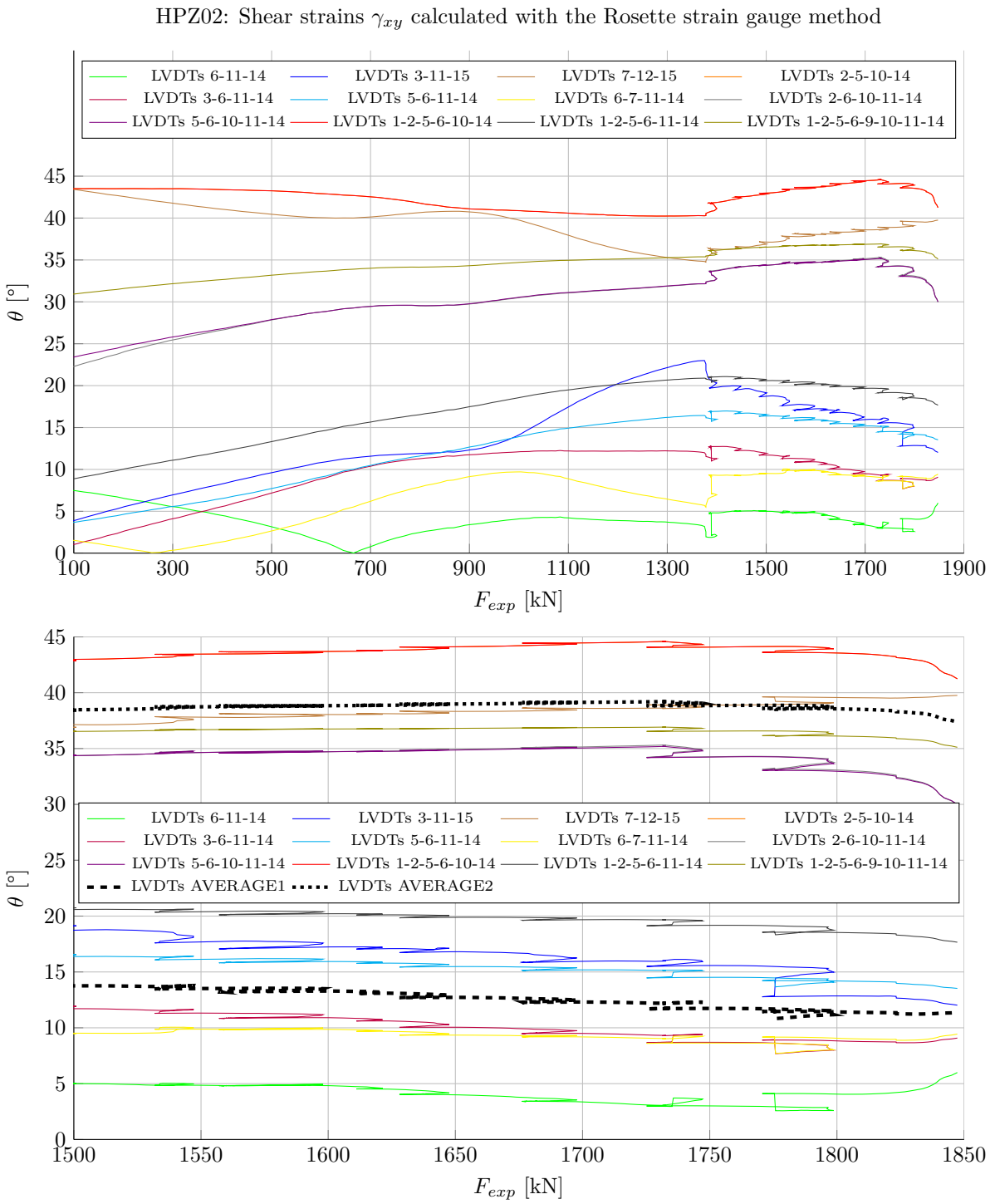

Figure 4.15: Calculated inclinations of the compression field θ with different combinations of LVDTs for HPZ02 with "Rosette" method

The calculated values with the Rosette-method either give a (very) low value (average1: 11°) or a high value (average2: 38°) for the inclinations θ. The results vary widely compared to the XY-method for HPZ2, therefore two averages are presented in the graph. All combinations with (vertical) LVDT10 and LVDT12 (2-5-10-14, 2-6-10-11-14, 5-6-10-11-14, 1-2-5-6-10-14, 1-2-5-6-9-10-11-14 and 7-12-15) result in $42° > \theta > 30°$, while the combinations without this LVDT result in $20° > \theta > 7°$. A direct strut from the external load to the support is $\theta = 20.93°$, which is why the (very) low angles $< 10°$ could be questioned. Comparing combinations "LVDTs 3-11-15" ($\theta = 12°$ at 1848 kN), "LVDTs 5-6-11-14" ($\theta = 13.51°$ at 1848 kN) and "LVDTs 1-2-5-6-11-14" ($\theta = 17.62°$ at 1848 kN) with the measured angle

for the shear crack from the photographs for CR5 (top of the web) $\alpha_{photo} = 18°$, these combinations are considered as the only valuable/reasonable result from this method.

4.6.3. Contribution of the transverse reinforcement

The observations from photographs and DIC results at failure are used to determine the contribution of the stirrups to the load-carrying capacity of the girder. The location of the stirrups are determined from the photographs as well as the shear crack after failure. The contribution of a single stirrup to the shear resistance depends on whether the stirrup is still intact after failure and if the stirrup is activated, in other words crosses the shear crack:

$$V_{stirrup} = n_{stirrup} \cdot A_v \cdot f_{ym} \tag{4.8}$$

With $n_{stirrup}$ as the number of stirrups that contribute, $A_v = 0.25\pi\phi^2 = 157$ mm^2 as the area of the stirrups (two legs per stirrup) and $f_{ym} = 454$ MPa as the measured yield strength of the stirrups. Table 4.5 gives an overview of the contribution of the stirrups to the shear resistance according to DIC results [72].

Table 4.5: Stirrup contribution for HPZ1 and HPZ2 according to the DIC results [72]

No.	# of intact stirrups	Contribution
HPZ1	3	214 kN
HPZ2	5	357 kN

4.6.4. Contribution prestressing cable to the shear reinforcement (LVDT)

During loading of the girder the prestressing steel elongates. This elongation gives an additional vertical prestressing force ΔV_p. When the prestressing cables cross the measured shear crack and are subjected to tension, ΔV_p can be considered as additional shear reinforcement. The results from the LVDTs are shown in Tables 4.6 and 4.7. These tables are based on the following procedure [73]:

- Derive position of the shear crack from DIC results, see Chapter 4.6.1;
- Determine the prestressing cables that cross the shear crack;
- Determine the x- and y-coordinates of the considered prestressing cables at the shear crack;
- Determine the nearest/adjacent LVDTs that can be used to calculate the strains;
- Linear interpolate the strains just before failure $F_{exp,HPZ1}$ over the height and use the strains at the y-coordinates that match the prestressing cables;
- Calculate the stress increase in the cables: $\Delta\sigma_p = \Delta\varepsilon_p \cdot E_p$ provided that $\sigma_{p\infty} + \Delta\sigma_p \leq f_{p0.1m}$;
- Calculate the force increase: $\Delta N_p = \Delta\sigma_p \cdot A_p$;
- Calculate the vertical component of ΔN_p that acts as shear reinforcement: $\Delta V_p = \Delta N_p \cdot \sin\alpha$, with the angles α given in Table 3.6.

According to the results of DIC and the LVDTs the prestressing cables that cross the shear crack are cables 4, 5 and 6. For HPZ1 all three cables show tensile strains at the positions of the shear crack, which means that all three can be considered as additional shear reinforcement. The total contribution for cables 4 through 6 for HPZ1 is $\Delta V_p = 36$ kN, see Table 4.6. For HPZ2 compression strains were observed for cable 6. This cable is excluded from the contribution to the shear reinforcement. The total contribution for cables 4 and 5 for HPZ2 is $\Delta V_p = 52$ kN.

Table 4.6: Results of the contribution to the shear reinforcement for HPZ1 [73]

Cable [No.]	x [mm]	y [mm]	**LVDTs** [No.]	ε [$\mu\varepsilon$]	$\Delta\sigma_p$ [MPa]	N_p [kN]	α [°]	V_p [kN]
4	2144	521	2 & 6	859	159	73	7.3	9.28
5	1892	605	2 & 6	1353	205	116	7.5	15.14
6	1658	706	1 & 5	1796	332	153	4.5	12.00
							$\sum =$	36

Table 4.7: Results of the contribution to the shear reinforcement for HPZ2 [73]

Cable [No.]	x [mm]	y [mm]	**LVDTs** [No.]	ε [$\mu\varepsilon$]	$\Delta\sigma_p$ [MPa]	N_p [kN]	α [°]	V_p [kN]
4	1983	495	2 & 6	2218	410	185	7.5	25
5	1873	570	2 & 6	3285	608	281	5.6	27
6	1753	675	1 & 5	-147	-	-	-	-
							$\sum =$	52

4.6.5. Contribution prestressing cable to the shear reinforcement (analytical)

The additional prestressing force ΔV_p is also analytically checked for HPZ1. The calculation procedure is given below and is based on the stress-strain relations according to the EC2 [63]. At cross-section $x = 1.725$ m the concrete strain at the top fiber will not reach ε_{cu} at failure $F_{exp,HPZ1} = 1890$ kN. This means ε_c is unknown and is a variable in the calculation of the concrete compressive stress σ_c. This stress σ_c is calculated according to the parabola-rectangle diagram for concrete in compression, see Figure 4.16 and Equation 4.9. Also the concrete compression zone height x is an unknown variable.

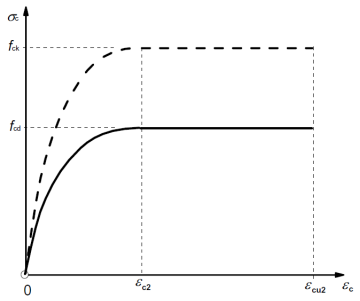

Figure 4.16: Parabola-rectangle diagram for concrete under compression [63]

$$\sigma_c = f_{cm} \cdot \left[1 - \left(1 - \frac{\varepsilon_c}{\varepsilon_{c2}}\right)^n\right] \quad \text{for} \quad 0 \le \varepsilon_c \le \varepsilon_{c2} \tag{4.9}$$

with
$$n = 1.4 + 23.4\left(\frac{90 - f_{cm}}{100}\right)^4 = 1.533 \qquad \text{(for } f_{cm} = 62.6 \text{ MPa)}$$
$$\varepsilon_{c2} = 2.0 + 0.085 \cdot (f_{cm} - 50)^{0.53} = 2.33‰ = 0.00233$$

The increase of the strain in the prestressing steel $\Delta\varepsilon_p$ and the strain in the reinforcement steel ε_s can be expressed with the strain in the concrete ε_c:

$$\varepsilon_s = \varepsilon_c\left(\frac{d_s}{x} - 1\right) \quad \text{and} \quad \Delta\varepsilon_p = \varepsilon_c\left(\frac{d_p}{x} - 1\right) \tag{4.10}$$

The total strain in the prestressing steel is:

$$\varepsilon_p = \varepsilon_{p\infty} + \Delta\varepsilon_p = \frac{\sigma_{p\infty}}{E_p} + \Delta\varepsilon_p \quad \text{with} \quad \sigma_{p\infty} = \frac{N_p}{A_p} = \frac{1598 \cdot 10^3}{3234} = 494 \text{ MPa} \tag{4.11}$$

The forces in the concrete N_c, reinforcement steel N_s and increase in force in the prestressing steel ΔN_p can be calculated with the concrete stress from Equation 4.9 and strains from Equations 4.10 and 4.11. The concrete compressive force N_c is calculated with the simplified rectangular stress distribution, see Figure 4.17 with:

$$\begin{aligned} \eta &= 0.8 - \frac{f_{cm} - 50}{400} = 0.7685 \\ \lambda &= 1.0 - \frac{f_{cm} - 50}{200} = 0.937 \end{aligned} \qquad \text{(for } f_{cm} = 62.6 \text{ MPa)} \tag{4.12}$$

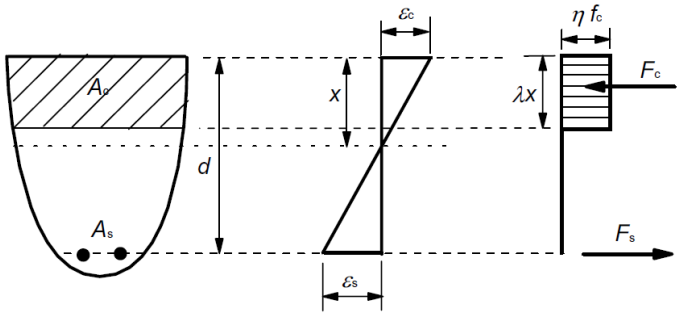

Figure 4.17: Rectangular stress distribution for the concrete compression zone [63]

The width of the girder is taken as the mean width of the top flange $b = b_{tfl} = 960$ mm, see Chapter 3.3. The concrete compressive force is given in equation 4.13 and is only valid if the concrete compression zone is smaller than the height of the top flange $x \leq h_{tfl}$ with $h_{tfl} = 180$ mm.

$$N_c = \lambda x \cdot \eta \sigma_c \cdot b_{tfl} \qquad \text{(for } x \leq h_{tfl} = 180 \text{ mm)} \tag{4.13}$$

The force in the reinforcement steel is given in Equation 4.14. The steel stress can not exceed $f_{ym} = 454$ MPa, so it needs to be checked if $\sigma_s = E_s \cdot \varepsilon_s \leq f_{ym}$ with ε_s calculated in Equation 4.10. Otherwise the steel stress is taken as $\sigma_s = f_{ym}$. The Young's modulus for the reinforcement steel is taken as $E_s = 200{,}000$ MPa.

$$\begin{aligned} N_s &= A_s \cdot \sigma_s \\ \text{with} \qquad \sigma_s &= \min(E_s \cdot \varepsilon_s, f_{ym}) \end{aligned} \tag{4.14}$$

The increase of the force in the prestressing steel is calculated as follows, with $E_p = 185{,}000$ MPa and provided that the total prestressing stress is still in the first linear branch:

$$\begin{aligned} \Delta N_p &= A_p \cdot \Delta\sigma_p \\ \text{with} \qquad \Delta\sigma_p &= \frac{\Delta\varepsilon_p}{\varepsilon_{p0.1m}} \cdot f_{p0.1m} \qquad \text{(for } \sigma_{p\infty} + \Delta\sigma_p \leq f_{p0.1m}) \\ \varepsilon_{p0.1m} &= \frac{f_{p0.1m}}{E_p} = 0.0077 \end{aligned} \tag{4.15}$$

Two equilibrium checks have to be made, horizontal equilibrium and moment equilibrium (around the centroidal axis). N_p follows from Equation 4.3 and M_{Ed} follows from the cross-sectional analysis given in Table 3.9 with $F_{exp} = 1890$ kN and $M_{Ed} = M_{tot} = M_{sw+p} + M_F$. The expression for M_{Rd} is only valid if $x \leq h_{tfl}$.

$$\text{CHECK:} \qquad N_s + \Delta N_p + N_p = N_c \tag{4.16}$$

$$\begin{aligned} &\text{CHECK:} && M_{Rd} = M_{Ed} \\ &\text{with} && M_{Rd} = N_c \cdot (z_{top} - 0.5 \cdot \lambda x) + N_s \cdot (d_s - z_{top}) + \Delta N_p \cdot (d_p - z_{top}) \end{aligned} \tag{4.17}$$

This procedure requires iterations as two unknown variables x and ε_c need to be solved provided that the two equilibrium conditions are met. When these conditions are met, the contribution of the increase

of the prestressing force to the shear capacity can be calculated. The total ΔV_p is a summation of all prestressing cables in the cross-section, as all cables have different angles α:

$$\begin{aligned} \Delta V_p &= \Sigma \Delta N_p \cdot \sin \alpha_i \\ \text{with} \qquad \Delta N_p &= \Delta \sigma_p \cdot A_{p,cable} \end{aligned} \tag{4.18}$$

The end result for cross-section $x = 1.725$ m with $F_{exp,HPZ1} = 1890$ kN is given below. Table 4.8 gives the values used in the calculations for ΔV_p. The prestressing cables present in the cross-section are cables 4 through 10, each with a different effective depth d_p. One cable has an area of $A_p = 462$ mm^2. For the sectional analysis the bottom two layers of the longitudinal reinforcement are considered, with each layer $A_s = 157$ mm^2.

Table 4.8: Values used for ΔV_p for HPZ1 at $x = 1.725$ m

	Value	**Units**	**Commentary**
A_p	462	mm^2	for one prestressing cable
A_s	157	mm^2	$0.25\pi\phi_s^2 * 2$ = per layer
b_{tfl}	960	mm	mean width of the top flange for HPZ1
d_{p4}	450	mm	calculated in `MS Excel`
d_{p5}	569	mm	calculated in `MS Excel`
d_{p6}	704	mm	calculated in `MS Excel`
$d_{p7,8}$	843	mm	calculated in `MS Excel`
$d_{p9,10}$	990	mm	calculated in `MS Excel`
d_{s1}	1065	mm	effective depth bottom layer reinforcement
d_{s2}	870	mm	effective depth second bottom layer reinforcement
E_p	185,000	MPa	see Chapter 3.2.2
E_s	200,000	MPa	see Chapter 3.2.3
f_{cm}	62.6	MPa	see Chapter 3.2.1
$f_{p0.1m}$	1433	MPa	see Chapter 3.2.2
f_{ym}	454	MPa	see Chapter 3.2.3
$F_{exp,HPZ1}$	1890	kN	external load at failure HPZ1
h_{tfl}	180	mm	height of the top flange
M_{Ed}	1926	kNm	from sectional analysis with $F_{exp,HPZ1} = 1890$ kN
n	1.533	-	see Equation 4.9
N_p	1598	kN	$= \sigma_{p\infty} \cdot A_p$
ε_{c2}	0.00233	-	see Equation 4.9
$\varepsilon_{p0.1m}$	0.00775	-	see Equation 4.15
η	0.937	-	see Equation 4.12
λ	0.7685	-	see Equation 4.12
$\sigma_{p\infty}$	494	MPa	see Equation 4.3

With the values given in Table 4.8 and with a concrete strain $\varepsilon_c = 0.000731$ and a concrete compression zone height $x = 171.82$ (CHECK: $x \leq h_{tfl}$ **OK**), the stress in the concrete at top fiber results in:

$$\sigma_c = 62.6 \cdot \left[1 - \left(1 - \frac{0.000731}{0.00233}\right)^{1.533}\right] = 27.46 \text{ MPa} \tag{4.19}$$

With σ_c known, the concrete compressive force can be calculated:

$$N_c = 0.7685 \cdot 171.82 \cdot 0.937 \cdot 27.46 \cdot 960 = 3262 \text{ kN} \tag{4.20}$$

The strains in the reinforcement steel and increase in strains in the prestressing steel:

$$\begin{aligned}
1^{\text{st}} \text{ bottom layer:} \quad & \varepsilon_{s1} = 0.000731 \cdot \left(\frac{1065}{171.82} - 1\right) = 0.00380 \\
2^{\text{nd}} \text{ bottom layer:} \quad & \varepsilon_{s2} = 0.000731 \cdot \left(\frac{870}{171.82} - 1\right) = 0.00297 \\
\text{Cable 4:} \quad & \Delta\varepsilon_{p4} = 0.000731 \cdot \left(\frac{450}{171.82} - 1\right) = 0.00118 \\
\text{Cable 5:} \quad & \Delta\varepsilon_{p5} = 0.000731 \cdot \left(\frac{569}{171.82} - 1\right) = 0.00169 \\
\text{Cable 6:} \quad & \Delta\varepsilon_{p6} = 0.000731 \cdot \left(\frac{704}{171.82} - 1\right) = 0.00226 \\
\text{Cable 7 \& 8:} \quad & \Delta\varepsilon_{p7-8} = 0.000731 \cdot \left(\frac{843}{171.82} - 1\right) = 0.00286 \\
\text{Cable 9 \& 10:} \quad & \Delta\varepsilon_{p9-10} = 0.000731 \cdot \left(\frac{990}{171.82} - 1\right) = 0.00348
\end{aligned} \tag{4.21}$$

The forces in the reinforcement steel:

$$\begin{aligned}
&\text{CHECK:} \quad \sigma_{s1} = \min(200{,}000 \cdot 0.00380, 454) = \min(759, 454) = 454 \text{ MPa} \\
&\text{CHECK:} \quad \sigma_{s2} = \min(200{,}000 \cdot 0.00297, 454) = \min(594, 454) = 454 \text{ MPa}
\end{aligned}$$

$$\begin{aligned}
N_{s1} &= 157 \cdot 454 = 71.3 \text{ kN} \\
N_{s2} &= 157 \cdot 454 = 71.3 \text{ kN}
\end{aligned} \tag{4.22}$$

$$N_{s,tot} = 142.6 \text{ kN}$$

The increase of the stresses in the prestressing steel:

$$\begin{aligned}
\Delta\sigma_{p4} &= \frac{0.00118}{0.00775} \cdot 1433 = 219 \text{ MPa} \\
\Delta\sigma_{p5} &= \frac{0.00169}{0.00775} \cdot 1433 = 313 \text{ MPa} \\
\Delta\sigma_{p6} &= \frac{0.00226}{0.00775} \cdot 1433 = 419 \text{ MPa} \\
\Delta\sigma_{p7-8} &= \frac{0.00286}{0.00775} \cdot 1433 = 528 \text{ MPa} \\
\Delta\sigma_{p9-10} &= \frac{0.00348}{0.00775} \cdot 1433 = 644 \text{ MPa}
\end{aligned} \tag{4.23}$$

$$\text{CHECK:} \quad 644 + 494 \leq 1433 \qquad \textbf{OK}$$

The increase of the force in the prestressing steel (cables 7 & 8 and 9 & 10 have the same effective depth d_p and are taken together):

$$\begin{aligned}
\Delta N_{p4} &= 219 \cdot 462 = 101.1 \text{ kN} \\
\Delta N_{p5} &= 313 \cdot 462 = 144.5 \text{ kN} \\
\Delta N_{p6} &= 419 \cdot 462 = 193.4 \text{ kN} \\
\Delta N_{p7-8} &= 528 \cdot 924 = 488.1 \text{ kN} \\
\Delta N_{p9-10} &= 644 \cdot 924 = 594.9 \text{ kN}
\end{aligned} \tag{4.24}$$

$$\Delta N_{p,tot} = 1521.9 \text{ kN}$$

The following equilibrium conditions must be satisfied:

$$\textbf{Horizontal equilibrium}: \quad \Delta N_{p,tot} + N_s + N_p = N_c$$
$$1521.9 + 142.6 + 1598 = 3262 \text{ kN} \tag{4.25}$$
$$\text{CHECK:} \quad 3262 = 3262 \text{ kN} \quad \textbf{OK}$$

$$\textbf{Momentum equilibrium}: \quad M_{Rd} = M_{Ed}$$
$$\begin{aligned} &3262 \cdot 10^3 \cdot (492 - 0.5 \cdot 0.7685 \cdot 171.82) + 71.3 \cdot 10^3 \cdot (1065 - 492) + 71.3 \cdot 10^3 \cdot (870 - 492) \\ &+101.1 \cdot 10^3 \cdot (450 - 492) + 144.5 \cdot 10^3 \cdot (569 - 492) + 193.4 \cdot 10^3 \cdot (704 - 492) \\ &+488.1 \cdot 10^3 \cdot (843 - 492) + 594.9 \cdot 10^3 \cdot (990 - 492) = 1926 \cdot 10^6 \end{aligned} \tag{4.26}$$
$$\text{CHECK:} \quad 1926 = 1926 \text{ kNm} \quad \textbf{OK}$$

In Chapter 4.6.4 the contribution of the prestressing cables to the shear reinforcement was analyzed from the results of the LVDTs. For HPZ1 only prestressing cables 4 through 6 passed through the shear crack in the web. Therefore only these three cables are considered in ΔV_p. Given the angles of the prestressing cables in Table 3.6, the increase in contribution of cables 4 through 6 to the shear resistance becomes:

$$\begin{aligned} &\text{Cable 4:} \quad \Delta V_p = 101.1 \cdot \sin(7.62) = 13.4 \text{ kN} \\ &\text{Cable 5:} \quad \Delta V_p = 144.5 \cdot \sin(5.70) = 14.4 \text{ kN} \\ &\text{Cable 6:} \quad \Delta V_p = 193.4 \cdot \sin(4.43) = 14.9 \text{ kN} \\ &\text{Total:} \quad \Delta V_p = 42.7 \text{ kN} \end{aligned} \tag{4.27}$$

5

Analytical analysis

In Chapters 2.7 through 2.11 of the literature review, five code provisions are discussed. Except for RBK (Chapter 2.10), the expressions given in these chapters are for the design of new (prestressed) concrete structures. In this chapter the shear capacity is calculated according to the design codes for comparison with the test results. Therefore mean values are used for the material properties and the load- and resistance factors are set to a value of 1.0. These changes result in a *mean* shear resistance of a member (denoted as V_{Rm} in EC2 for example), instead of a *design* shear resistance (denoted as V_{Rd} in EC2).

The analytical analysis is done with five code provisions, ACI, AASHTO, EC2, RBK and EC2 draft 2018. These codes are used to calculate the shear resistance of the Helperzoom girders and if possible the corresponding failure mode. The ACI, EC2 (flexure-shear resistance) and RBK are based on experimental results. The EC2 (shear-tension capacity) is based on Euler-Bernoulli beam theory to determine the principal (tensile) stresses. The AASHTO is based on the MCFT, which is addressed in Chapter 6.1, and uses this model to determine the stresses and strains in a cross-section. The EC2 draft 2018 is based on the Critical Shear Crack Theory (CSCT).

First the background of the Euler-Bernoulli beam theory with calculations for the Helperzoom girders are described. Secondly, the five considered codes are used to calculate the shear resistance and are given in Chapters 5.2 through 5.6. Lastly, the results are discussed in Chapter 5.7.

5.1. Euler-Bernoulli beam theory

The Euler-Bernoulli beam theory is a widely used theory to determine the deflections and internal forces and moments for a beam under bending and is considered the basis for structural engineering. This theory has two primary assumptions:

- plane sections remain plane;
- deflections and angles are small.

The first assumption means that sections remain perpendicular to the longitudinal axis of the beam after deforming. The longitudinal axis of the beam is parallel to the neutral axis. The second assumption is that the angles φ of the deformed beam are small. Due to this second assumption the calculations, the derivatives of the deflection δ, for the internal forces and angles are simplified by the use of valid mathematical approximations [77].

5.1.1. Calculating the principal stresses with Euler-Bernoulli beam theory

Bending moments and shear forces causes stresses in a beam. These stresses can be transformed into principal stresses as described in Chapter 2.5.1. Chapter 2.5.3 mentioned that the principal stresses need to be calculated along the full depth of the beam, meaning that the location of the maximum principal stress is not known beforehand. The loads on the girder with self-weight, dead load, prestressing and the position of the external load with supports are given in Chapters 3.4 and 3.6 respectively.

A summary of the loads is given in Table 3.9. To determine the stresses, this table is made more extensive with a variable external load.

> As a **reference point**, the value of the external force is set to 1283 kN, as this is the load where the principal stresses exceed the f_{ctm} in the web at $x = 1.725$ m, see Figure 5.1.

The internal total shear force V_{tot} and total moment M_{tot} that are acting on the girder are shown in Table 5.1. Only the cross-sections between $x = 1.725$,..,2.453 m are of interest, as only shear-tension failure can be predicted with this theory. It can not be concluded that exceeding $f_{ctm,sp}$ in the most-tensioned flange will lead to flexural- and/or flexural-shear failure.

For the calculations presented in this chapter, the HPZ1 girder with length $L_{HPZ1} = 10.51$ m and span length $L_{span} = 9.60$ m is considered. The differences in the loads between HPZ1 and HPZ2 are assumed negligible small. The external load is positioned at $x = 2.903$ m, resulting in a shear span $a = 2.903$ m. The calculation for the sectional shear forces and moments for cross-sections between $x = 0..2.903$ m are as follows:

$$\begin{aligned} V_{tot} &= V_{sw} + V_p + V_F \qquad \text{with} \quad V_F = \frac{L_{span} - a}{L_{span}} \cdot F_{exp} \\ M_{tot} &= M_{sw} + M_p + M_F \quad \text{with} \quad M_F = \frac{L_{span} - a}{L_{span}} \cdot a \cdot F_{exp} \end{aligned} \tag{5.1}$$

Table 5.1: Summary of loads for $x = 1.725$,..,2.903 m with $F_{exp} = 1283$ kN

x [m]	**1.725**	**1.8**	**1.85**	**1.9**	**1.95**	**2**	**2.051**	**2.453**	**2.903**
V_p [kN]	−98.21	−97.63	−97.25	−96.87	−96.49	−96.11	−95.72	−92.65	−89.22
V_{sw} [kN]	41.38	40.39	39.73	39.07	38.40	37.74	37.07	31.75	25.80
V_F [kN]	895	895	895	895	895	895	895	895	895
V_{tot} [kN]	839	838	838	838	837	837	837	835	832
M_p [kNm]	−444	−452	−457	−462	−467	−473	−478	−517	−555
M_{sw} [kNm]	95	98	100	102	103	105	107	121	134
M_F [kNm]	1545	1612	1657	1701	1746	1791	1837	2197	2600
M_{tot} [kNm]	1195	1257	1299	1341	1382	1424	1466	1801	2179

The stresses are calculated with the cross-sectional and material properties of the Helperzoom girders, described in Chapter 3.2 and 3.3. A spreadsheet is made to determine the shear stresses τ, stresses in longitudinal direction σ_{xx}, the principal tensile stresses σ_1 and the principal compressive stresses σ_2 along the full depth of the girder with layers of 5 mm of height. This means that the cross-section is divided in 222 layers ($222 \cdot 5 = 1110$ mm). The section modulus for every layer $S_{c,i}$ follows from:

$$S_{c,i} = S_{c,i-1} + A_i \cdot a_i \quad \text{with} \quad S_{c,0}, S_{c,222} = 0 \text{ mm}^3 \tag{5.2}$$

With $A_i = h_i \cdot b_i$, h_i as the cumulative total height: $h_0 = 0$ mm and $h_{222} = 1110$ mm, b_i as the mean width of the layer and a_i as the internal arm between the center of the layer in z-direction and the center of gravity axis of the girder $a_i = -z_{top} + 0.5(h_{i-1} + h_i)$. The mean width is calculated with the simplified cross-section of the girder, shown in Figure 3.3.

The stresses in MPa are calculated as follows, with the values for the internal forces (axial force $N_p = 1598$ kN, bending moment M_{tot}, shear force V_{tot}) varying per cross-section:

$$\begin{aligned} \tau_i &= \frac{V_{tot} \cdot S_{c,i}}{b_i \cdot I_c} & \sigma_{xx,i} &= -\frac{N_p}{A_c} + \frac{M_{tot} \cdot a_i}{I_c} \\ \sigma_{1,i} &= \frac{\sigma_{xx,i}}{2} + \sqrt{\frac{\sigma_{xx,i}}{2}^2 + \tau_i^2} & \sigma_{2,i} &= \frac{\sigma_{xx,i}}{2} - \sqrt{\frac{\sigma_{xx,i}}{2}^2 + \tau_i^2} \end{aligned} \tag{5.3}$$

5.1.2. Diagonal tension cracking in the web

As previously mentioned, diagonal tension cracking will occur when the principal tensile stress σ_1 exceeds the tensile strength of concrete. Two different approaches for determining the tensile strength of concrete are given in Chapter 2.5.2, with the mean value of the axial tensile strength f_{ctm} and the cracking strength f_{cr}. The mean value of the axial tensile strength can be calculated from tensile splitting tests or can be calculated from the mean values of the compressive strength with Equation 2.6. The cylinder compressive strength f_{cm} is assumed as $0.82 f_{cm,cube}$ [78]:

$$f_{cm} = 0.82 f_{cm,cube} = 0.82 \cdot 76.3 = 62.6 \text{ N/mm}^2 \tag{5.4}$$

In Chapter 3.2.1 it is given that the mean value of the concrete compressive strength of the Helperzoom girders is $f_{cm,cube} = 76.3$ MPa and a mean value of the tensile splitting strength of $f_{ctm,sp} = 5.4$ MPa. For the tensile strength, two different values are used, the mean value of the splitting tensile strength $f_{ctm,sp}$ and the mean value of the axial tensile strength $f_{ctm} = 0.9 f_{ctm,sp} = 4.86$ MPa. The mean value of the axial tensile strength calculated with Equations 2.6 and 5.4 results in a lower value:

$$f_{ctm} = 2.12 \ln\left(1 + \frac{f_{cm}}{10}\right) = 2.12 \ln\left(1 + \frac{62.6}{10}\right) = 4.2 \text{ N/mm}^2 \tag{5.5}$$

For the onset of diagonal tension cracking $f_{ctm} = 4.86$ MPa is used. With the `Goal-Seek`-function in `MS Excel` and the location in the web where the highest principal tensile stress σ_1 occurs, the maximum external load can be calculated. The location where the highest principal tensile stress occur is set to $f_{ctm} = 4.86$ MPa. Also the tensile strength at the most tensioned flange is checked and is set to $f_{ctm,sp} = 5.4$ MPa. Figure 5.1 shows four plots at $x = 1.725, 1.900, 2.051$ and 2.453 m. These are the important cross-sections given in Chapter 3.5 considering an inclined shear crack of 30°. Figure 5.2 shows the stresses along the inclined shear crack for $F_{exp} = 1283$ kN.

Cross-section x = 1.725 m

It can be concluded from the plots that the maximum principal stress in the web occurs at the bottom, at the intersection with the bottom flange at $y = 680$ mm (y calculated from the top of the girder). With an inclined shear crack of 30°, the critical cross-section for shear-tension failure is $x = 1.725$ m. The value for the principal tensile at $h = 680$ mm of this cross-section is set to $f_{ctm} = 4.86$ MPa. This results in $F_{exp} = 1283$ kN for diagonal tension cracking. Flexural cracks will occur in this cross-section, as the principal tensile stresses in the most-tensioned flange at $y = 1110$ mm exceed $f_{ctm,sp}$.

Cross-sections x = 1.900, 2.051 and 2.453 m

With an external load of $F_{exp} = 1283$ kN the cross-sections closer to the external load, $x = 1.900, 2.051$ and 2.453 m, exceed both f_{ctm} in the web and $f_{ctm,sp}$ in the most-tensioned flange. As the critical cross-section is assumed $x = 1.725$ m with $\theta = 30°$ for diagonal tension cracking, shear-tension failure will not occur at the other cross-sections at$y = 680$ mm. This requires a higher angle θ of the inclined shear crack. On the other hand, flexural cracks occur at the bottom of the girder as the principal tensile stresses considerably exceed $f_{ctm,sp}$.

Cross-sections x = 1.725,..,2.903 m

Table 5.2 shows a summary of the principal stresses $\sigma_{1,web}$ at $h = 680$ mm and $\sigma_{1,bottom}$ at $h = 1110$ mm for calculated cross-sections between $x = 1.725$,..,2.903 m with an external load $F_{exp} = 1283$ kN. All cross-sections and especially at the external load, the principal tensile stresses at the most-tensioned flange considerably exceed $f_{ctm,sp}$. Exceeding this tensile stress does not mean the beam will fail in flexural failure, as longitudinal reinforcement is present in the bottom of the girder.

Table 5.2: Principal stresses $\sigma_{1,web}$ at $h = 680$ mm and $\sigma_{1,bottom}$ at $h = 1110$ mm with $F_{exp} = 1283$ kN

x = [m]	**1.725**	**1.800**	**1.850**	**1.900**	**1.950**	**2.000**	**2.051**	**2.453**	**2.903**
$\sigma_{1,web}$ [MPa]	4.86	4.94	4.99	5.04	5.09	5.14	5.20	5.65	6.18
$\sigma_{1,bottom}$ [MPa]	6.79	7.31	7.65	7.99	8.34	8.67	9.04	11.81	14.93

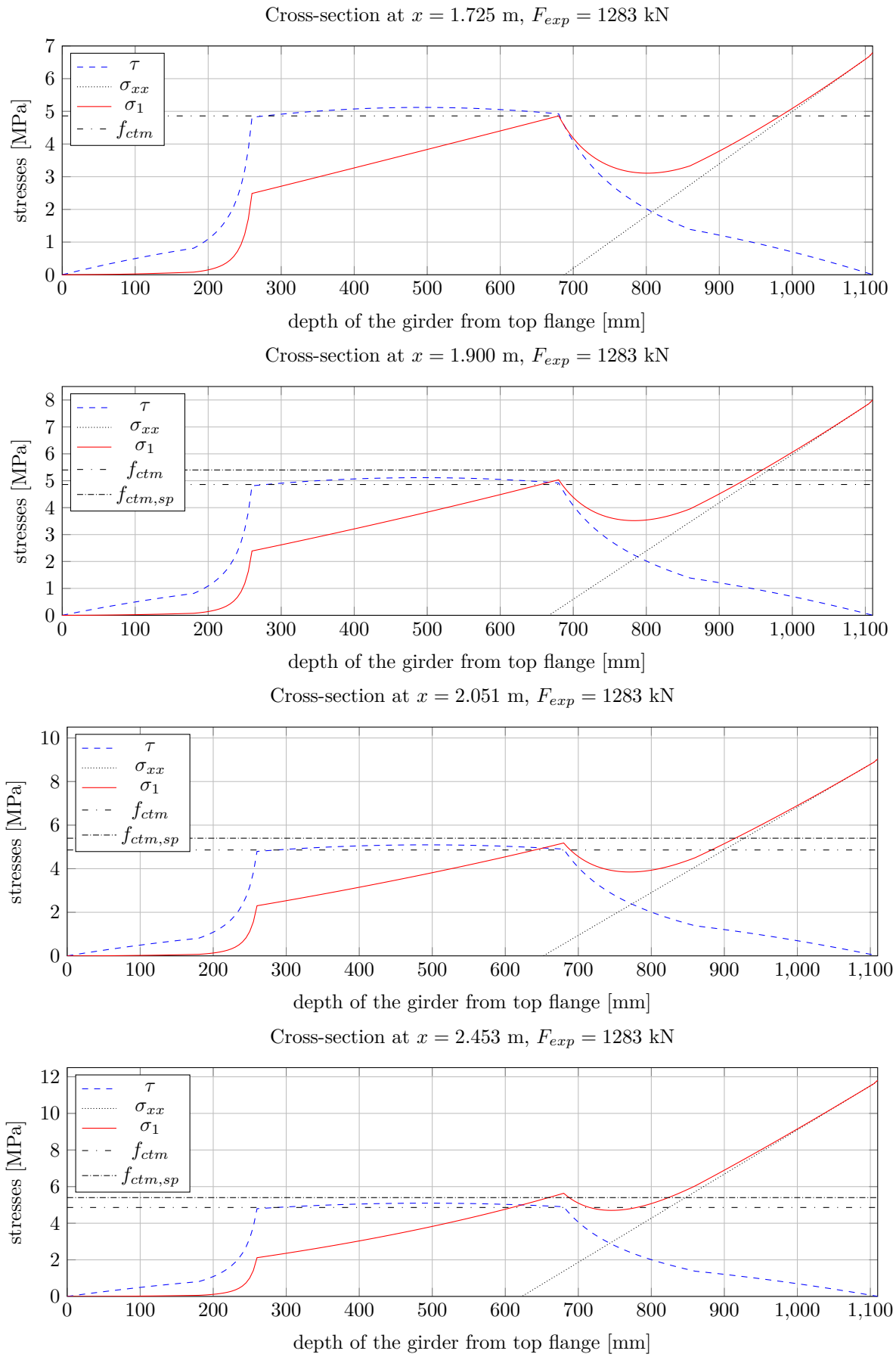

Figure 5.1: Stress distribution at x =1.725, 1.900, 2.051 and 2.453 m with $F_{exp} = 1283$ kN

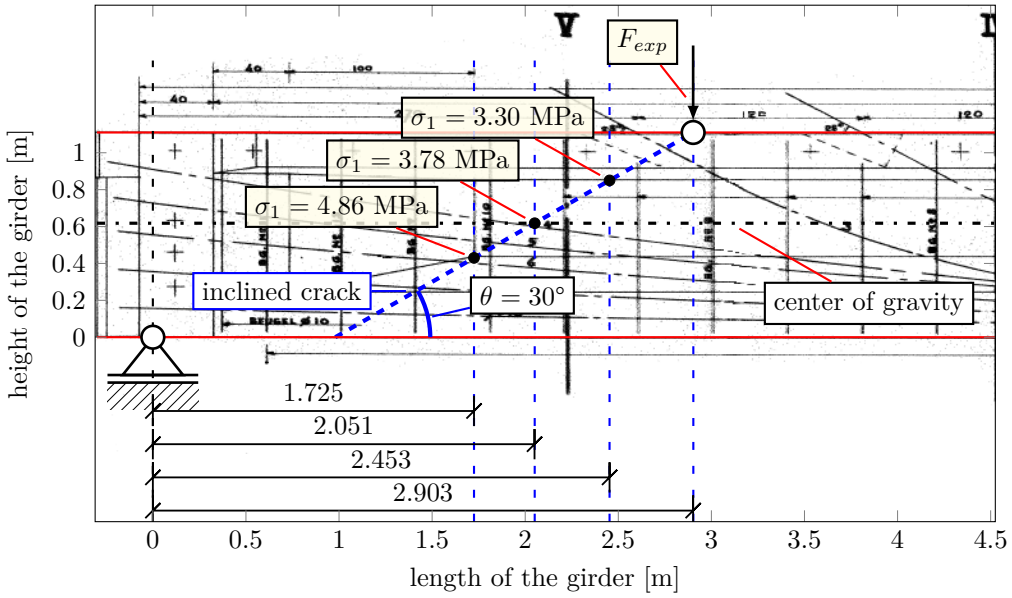

Figure 5.2: Principal tensile stresses along the inclined shear crack with $F_{exp} = 1283$ kN [1]

5.1.3. Flexural cracking load

The cross-section under the external load has the highest bending moment and is the cross-section where flexural cracking will first occur. Table 5.2 already showed that the principal tensile stresses at $x = 2.903$ m are the highest among the cross-sections. The value for the external load when flexural cracks occur (cracking load) in the most tensioned flange is $F_{exp} = 714$ kN, see Figure 5.3. Equation 5.6 shows a hand calculation and confirms the stress at the most tensioned flange for $F_{exp} = 714$ kN.

$$M_{tot} = M_F + M_{sw+p} = 2.03 \cdot 714 - 421 = 1026 \text{ kNm}$$
$$\sigma_{bottom} = \frac{M_{tot} \cdot z_{bottom}}{I_c} - \frac{N_p}{A_c} = \frac{605 \cdot 10^6 \cdot 618}{7.47 \cdot 10^{10}} - \frac{1598 \cdot 10^3}{517 \cdot 10^3} = 8.49 - 3.09 = 5.40 \text{ MPa} \tag{5.6}$$

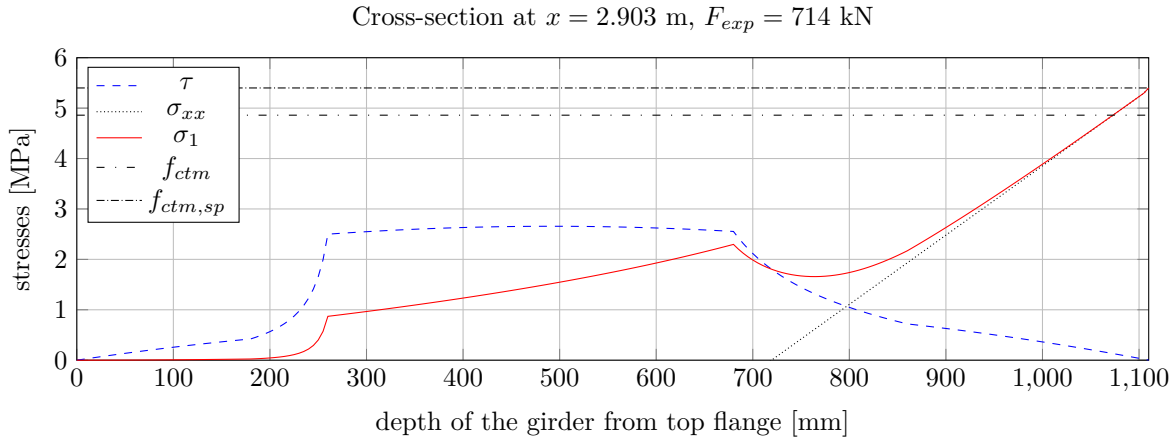

Figure 5.3: Stress distribution at $x = 2.903$ m with $N_p = 1598$ kN

5.1.4. Flexural cracking load from first crack (CR1) in experiment

According to the test results given in Chapter 4.6.1 the first flexural crack opening occurred at $F_{exp} \approx 1000$ kN under the external load. This is a higher value for the external load calculated in the previous paragraph. A backward calculation is done to calculate the prestressing force N_p that is required to exceed $f_{ctm,sp}$ in the most-tensioned flange at $x = 2.903$ m. For $N_p = 2593$ kN ($\sigma_p = 801.8$ MPa) the extreme tensile fiber exceeds $f_{ctm,sp} = 5.4$ MPa, see Figure 5.4. When considering that the flexural

tensile strength is exceeded at the occurrence of micro cracks at $F_{exp} = 950$ kN, the value for becomes $N_p = 2419$ kN with $\sigma_p = 748$ MPa.

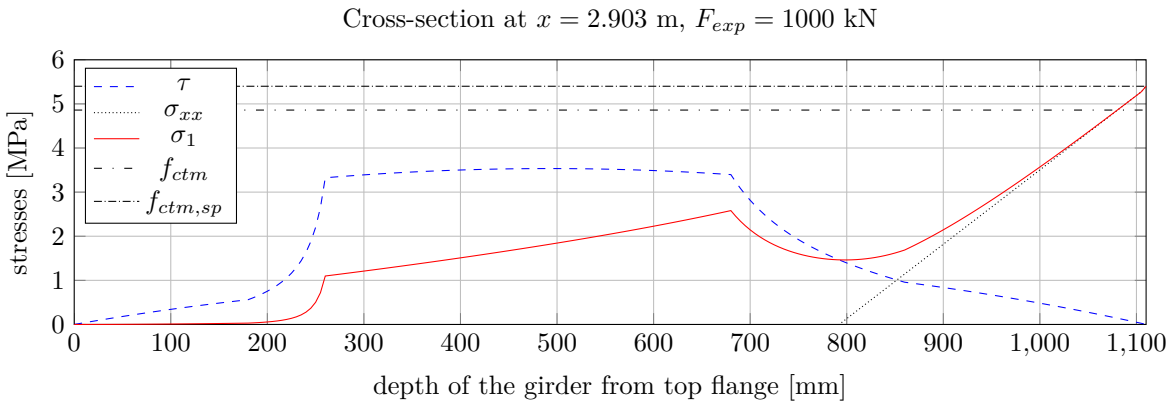

Figure 5.4: Stress distribution at $x = 2.903$ m with $N_p = 2593$ kN

5.2. ACI

The ACI expressions for calculating the shear resistance of a prestressed concrete member with- and without shear reinforcement are given in Chapter 2.7. This code provision divides the shear failure modes of concrete in two, regardless of the presence of stirrups; flexural-shear failure and shear-tension failure. If present, the contribution of the shear reinforcement is added to the inclined cracking load. In the first sub-paragraph, the values used for determining the shear resistance are given. In the second sub-paragraph a detailed calculation is done for the shear resistance of the Helperzoom girder. In the last sub-paragraph, a summary for the shear resistances of the other cross-sections is given.

5.2.1. Values used for ACI

The contribution of the concrete to the shear resistance, the inclined cracking load V_c, is calculated for both flexural-shear- and web-shear cracking. This resistance is the minimum of the two cracking modes, given in Equations 2.10 and 2.12. Table 5.3 provides the values used for the shear resistance at $x = 1.725$ m.

Table 5.3: Values used for $x = 1.725$ m and $a = 2.903$ m

	Value	Units	Commentary
A_v	157.08	mm^2	$0.25\pi\phi_v^2 * 2 = 2$ legs per 400 mm
b_w	200	mm	width of the web
d	1065	mm	$h - cover - \phi_v - 0.5\phi_b = 1110 - 30 - 10 - 5$
d_p	770	mm	see Table 3.5
f'_c	60.3	MPa	$= \frac{f_{cm} + 8 - 4.28}{1.1}$
$\sqrt{f'_c}$	7.76	MPa	
f_d	0.78	MPa	$= \frac{M_{sw} \cdot z_{bottom}}{I_c} = \frac{94.50 \cdot 10^6 \cdot 618}{7.47 \cdot 10^{10}}$
f_{pc}	3.09	MPa	$= \frac{N_p}{A_c}$ (positive for compression)
f_{pe}	6.77	MPa	$= \frac{M_p \cdot z_{bottom}}{I_c} + \frac{N_p}{A_c} = \frac{853 \cdot 10^6 \cdot 618}{7.47 \cdot 10^{10}} + \frac{1598 \cdot 10^3}{517 \cdot 10^3}$
f_{yt}	454	MPa	f_{ym} used, see Chapter 3.2.3
I_c	$7.47 \cdot 10^{10}$	mm^4	see Equation 3.2
N_p	1598	kN	see Chapter 3.6.3
M_{sw}	94.50	kNm	see Table 3.4
s	400	mm	spacing transverse reinforcement
$\frac{V_u}{M_u}$	0.00058	mm^{-1}	$\frac{V_F}{M_F} = \frac{0.7 \cdot 10^3}{1.2 \cdot 10^6}$
V_p	98.21	kN	see Table 3.7

Note that the ratio V_u/M_u used in this chapter is only calculated from the shear force/moment from the external load. According to the ACI this ratio is calculated as the shear force/moment from the external load plus the shear force/moment due to self weight denoted as:

$$\frac{V_u}{M_u} = \frac{V_F + V_{sw}}{M_F + M_{sw}} \tag{5.7}$$

This procedure takes iterations. It has been concluded that this difference is minimal and therefore neglected in the calculations:

$$\begin{aligned} F_{exp} = 800 \text{ kN: } \frac{V_u}{M_u} &= 0.000567 \text{ mm}^{-1} \\ F_{exp} = 1900 \text{ kN: } \frac{V_u}{M_u} &= 0.000574 \text{ mm}^{-1} \end{aligned} \tag{5.8}$$

5.2.2. ACI shear resistance detailed calculation

The procedure according to the ACI, to calculate the inclined cracking load plus the contribution of the stirrups, is quick and straight forward. Equations 5.9 through 5.12 show the detailed calculation for the shear resistance according to the ACI for cross-section $x = 1.725$ m. The cracking moment M_{cr}, which takes into account the concrete compressive strength f'_c, stress at the bottom fiber due to the prestressing force f_{pe} and self weight f_d, equals:

$$\begin{aligned} M_{cr} &= \frac{I_c}{y_t}\left(0.498\sqrt{f'_c} + f_{pe} - f_d\right) = 1191 \text{ kNm} \\ &= \frac{7.47 \cdot 10^{10}}{618} \cdot (0.498 \cdot 7.76 + 6.77 - 0.78) \end{aligned} \tag{5.9}$$

Check if the internal lever arm d_p fulfills the requirement for the minimum value for $d_{p,ACI} > 0.8h$:

$$\begin{aligned} d_p > 0.8h &= 0.8 \cdot 1110 = 888 \text{ mm} \\ \text{CHECK:} \qquad 770 &> 888 \qquad \textbf{NOT OK} \\ d_{p,ACI} &= 888 \text{ mm} \end{aligned} \tag{5.10}$$

The inclined cracking load V_c becomes the smaller of V_{ci} and V_{cw}:

$$\begin{aligned} V_{c,ACI} &= \min(V_{ci}, V_{cw}) \\ V_{ci} &= 0.0498\sqrt{f'_c} \cdot b_w d_{p,ACI} + \frac{V_u}{M_u} M_{cr} \\ &= 0.0498 \cdot 7.76 \cdot 200 \cdot 888 + 0.00058 \cdot 1191 \cdot 10^6 = 759 \text{ kN} \\ V_{cw} &= \left(0.291\sqrt{f'_c} + 0.3 f_{pc}\right) b_w d_{p,ACI} + V_p \\ &= (0.291 \cdot 7.76 + 0.3 \cdot 3.09) \cdot 200 \cdot 888 + 98.21 \cdot 10^3 = 664 \text{ kN} \\ V_{c,ACI} &= 664 \text{ kN} \end{aligned} \tag{5.11}$$

The contribution of the transverse reinforcement (note that ACI uses internal lever arm d of the longitudinal reinforcement instead of $d_{p,ACI}$):

$$V_{s,ACI} = \frac{A_v \cdot f_{yt} \cdot d}{s} = \frac{157 \cdot 454 \cdot 1065}{400} = 190 \text{ kN} \tag{5.12}$$

The nominal shear resistance (web-shear cracking) at $x = 1.725$ m results in:

$$V_{n,ACI} = V_{c,ACI} + V_{s,ACI} = V_{cw} + V_{s,ACI} = 664 + 190 = 854 \text{ kN} \tag{5.13}$$

5.2.3. ACI shear resistance summary

The flexure-shear- and web-shear resistance of the cross-sections between $x = 1.725,..,2.903$ m are calculated and the values used in the detailed calculations are shown in Table 5.4. The effective depth $d_{p,ACI}$ is 888 mm for every cross section, because $d_{p,calc}$ does not fulfill the requirement for $d_p > 0.8h$.

Table 5.4: Values used for calculating the nominal shear resistance for $x = 1.725,..,2.903$ m and $a = 2.903$ m

x [m]	**1.725**	**1.8**	**1.85**	**1.9**	**1.95**	**2**	**2.051**	**2.453**	**2.903**
V_u/M_u [mm^{-1}]	0.00058	0.00056	0.00054	0.00053	0.00051	0.0005	0.00049	0.00041	0.00034
f_{pe} [MPa]	−6.77	−6.83	−6.87	−6.91	−6.96	−7	−7.04	−7.36	−7.68
f_d [MPa]	0.78	0.81	0.82	0.84	0.86	0.87	0.89	1	1.11
$d_{p,calc} > d_{p,min}$	FALSE	FALSE	FALSE	FALSE	FALSE	FALSE	FALSE	FALSE	FALSE
$d_{p,ACI}$ [mm]	888	888	888	888	888	888	888	888	888

The resistance for web-shear failure V_{cw} is almost the same for every cross-section although it is decreasing for $x > 1.725$ m, because the shear contribution of the vertical prestressing force V_p slightly decreases. The resistance to web-shear is dominating from $x = 1.725,..,2.000$ m, while the resistance to flexural-shear is dominating from $x = 2.051,..,2.903$ m. Considering full contribution of the stirrups for the shear resistance, the inclined cracking load is increased by $V_{s,ACI} = 190$ kN. According to the ACI, the cross-section at $x = 2.903$ m is the most critical cross-section for shear failure, see Table 5.5 and Figure 5.5. The dominating shear failure mode is flexural-shear failure with a resistance of $V_{n,ACI} = 693$ kN, taking into account full contribution of the stirrups. Note that the ACI does not allow to calculate the angle of the compression chord. This means that a conservative calculation is done for the shear contribution of the stirrups, as $\theta = 45°$ is mostly true for ordinary reinforced concrete but not for prestressed concrete (see also results from the experiment in Chapter 4.6.1 and AASHTO in Chapter 5.3). This results in a lower value of $V_{s,ACI}$. Another point of interest is that for the calculation of flexural-shear failure, the vertical component of the prestressing force V_p is not added in the expression.

Table 5.5: Nominal shear resistance for $x = 1.725,..,2.903$ m and $a = 2.903$ m

x [m]	**1.725**	**1.8**	**1.85**	**1.9**	**1.95**	**2**	**2.051**	**2.453**	**2.903**
M_{cr} [kNm]	1191	1195	1199	1202	1205	1208	1212	1236	1262
V_{ci} [kN]	759	733	717	701	687	673	659	573	503
V_{cw} [kN]	664	663	663	663	662	662	662	658	655
$V_{s,ACI}$ [kN]	190	190	190	190	190	190	190	190	190
$V_{n,ACI}$ [kN]	854	853	853	853	852	852	849	763	693

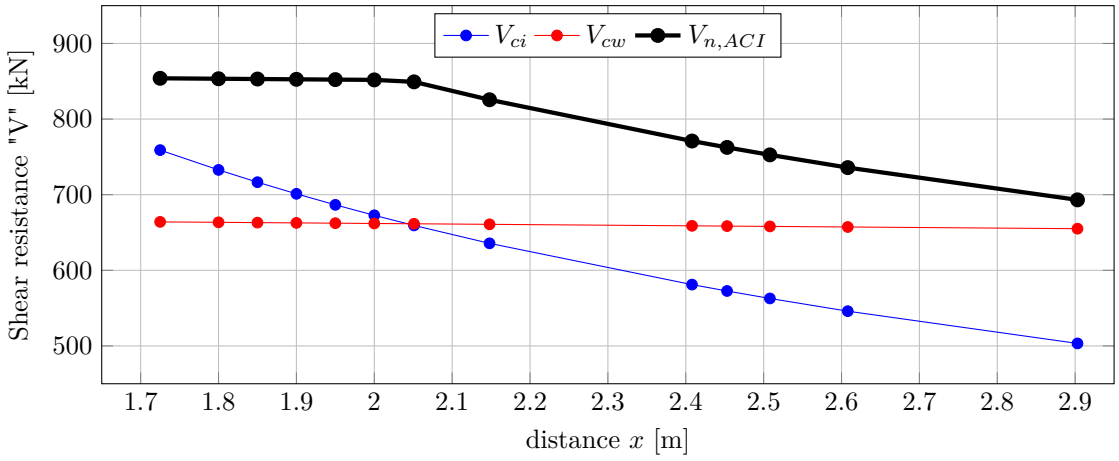

Figure 5.5: Shear resistance for $x = 1.725,..,2.903$ m and $a = 2.903$ m

5.3. AASHTO

The AASHTO expressions for calculating the shear resistance of a prestressed concrete member with- and without shear reinforcement are given in Chapter 2.8. This code provision uses the MCFT to calculate the inclined cracking load. No distinction between flexural-shear failure and shear-tension failure is made. The contribution of the shear reinforcement and the vertical prestressing force is added to the nominal shear resistance, which is the same procedure as the ACI code. In the first sub-paragraph, the values used for determining the shear resistance are given. In the second sub-paragraph a detailed calculation is done for the shear resistance of the Helperzoom girder. In the last sub-paragraph, a summary for the shear resistances of the other cross-sections is given.

5.3.1. Values used for AASHTO

Table 5.6 provides the values used for the shear resistance at $x = 1.725$ m.

Table 5.6: Values used for $x = 1.725$ m and $a = 2.903$ m

	Value	Units	Commentary
A_{ct}	230,000	mm^2	$= A_3 + A_5 + \left(\frac{h}{2} - 250\right) \cdot 200$
A_{ps}	3234	mm^2	$= 7 \cdot 462$
A_s	314	mm^2	$0.25\pi\phi_s^2 * 4$ = two bottom layers on tensioned side
A'_s	314	mm^2	$0.25\pi\phi_s^2 * 4$ = top layer on compression side
A_v	157.08	mm^2	$0.25\pi\phi_v^2 * 2 = 2$ legs per 400 mm
b	960	mm	width of the compression flange
b_v	200	mm	width of the web
d_e	777	mm	$= \frac{A_{ps}f_{ps}d_p + A_sf_yd_s}{A_{ps}f_{ps} + A_sf_y} = \frac{3234 \cdot 1725 \cdot 770 + 314 \cdot 454 \cdot 1065}{3234 \cdot 1725 + 314 \cdot 454}$
d_p	770	mm	calculated in `MS Excel`
d_s	1065	mm	$= h - cover - \phi_v - 0.5\phi_s = 1110 - 30 - 10 - 5$
d'_s	45	mm	$= cover + \phi_v + 0.5\phi_s = 1110 - 30 - 10 - 5$
E_c	36590	MPa	$= 4800\sqrt{f'_c}$
E_p	185,000	MPa	see Chapter 3.2.2
E_s	200,000	MPa	according to AASHTO
f'_c	60.3	MPa	$= \frac{f_{cm} + 8 - 4.28}{1.1}$
$\sqrt{f'_c}$	7.76	MPa	
f_{ps}	1725	MPa	$= f_{pu}\left(1 - k\frac{c}{d_p}\right)$
f_{pu}	1824	MPa	see Chapter 3.2.2
f_{py}	1642	MPa	$0.9f_{pu}$ used
f_{py}/f_{pu}	0.9	-	
f_y	454	MPa	f_{ym} used, see Chapter 3.2.3
h_f	180	mm	height of the top flange (compression flange)
I_c	$7.47 \cdot 10^{10}$	mm^4	calculated in `MS Excel`
k	0.28	-	$= 2 \cdot (1.04 - f_{py}/f_{pu})$
N_u	0	kN	see explanation below
s	400	mm	spacing transverse reinforcement
s_x	240	mm	spacing longitudinal reinforcement
s_{xe}	175	mm	$s_x\frac{35}{a_g + 16} \leq 2000$ mm
V_p	98.21	kN	calculated in `MS Excel`
α_1	0.85	-	$f'_c < 69$ MPa
β_1	0.77	-	$= 0.85 - 0.02 \cdot$ ROUNDUP $\left[\frac{f'_c - 28}{7}\right]$

5.3.2. AASHTO shear resistance detailed calculation

The procedure to calculate the shear resistance according to the AASHTO requires extensive calculations and iterations. First a sectional analysis is performed to calculate the flexural resistance of the member. From this analysis the internal lever arm (in AASHTO named effective shear depth) is determined. This effective shear depth must meet the requirements for the minimum effective shear depth. Next the longitudinal strains are calculated to determine the values for β and θ and to calculate the inclined cracking load. The nominal shear resistance of the member is the sum of the inclined cracking load, the contribution of the stirrups and the vertical component of the prestressing force. Equations 5.14 through 5.31 show the detailed calculation for the shear resistance for cross-section $x = 1.725$ m.

To calculate the inclined cracking load, the effective shear depth must be known. According to AASHTO this can be calculated with equations for the flexural resistance of a member. First it must be checked if the girder behaves like a T-section or a rectangle:

$$\begin{aligned} c_T &= \frac{A_{ps}f_{pu} + A_s f_s - A'_s f'_s - \alpha_1 f'_c(b - b_v)h_f}{\alpha_1 f'_c \beta_1 b_v + kA_{ps}\dfrac{f_{pu}}{d_p}} \\ &= \frac{3234 \cdot 1824 + 314 \cdot 454 - 314 \cdot 454 - 0.85 \cdot 60.3 \cdot (960 - 200) \cdot 180}{0.85 \cdot 60.3 \cdot 0.77 \cdot 200 + 0.28 \cdot 3234 \cdot \dfrac{1824}{770}} = -113 \text{ mm} \end{aligned} \tag{5.14}$$

$$\begin{aligned} c_{rect} &= \frac{A_{ps}f_{pu} + A_s f_s - A'_s f'_s}{\alpha_1 f'_c \beta_1 b + kA_{ps}\dfrac{f_{pu}}{d_p}} \\ &= \frac{3234 \cdot 1824 + 314 \cdot 454 - 314 \cdot 454}{0.85 \cdot 60.3 \cdot 0.77 \cdot 1000 + 0.28 \cdot 3234 \cdot \dfrac{1824}{770}} = 151 \text{ mm} \end{aligned} \tag{5.15}$$

According to Equations 5.14 and 5.15 the girder has rectangular behavior, as the result for c_T is negative. Therefore the distance from the neutral axis to the extreme compression fiber c and the height of the equivalent stress block a become:

$$\begin{aligned} c &= 151 \text{ mm} \qquad \text{(rectangular behavior)} \\ a &= c\beta_1 = 151 \cdot 0.77 = 113 \text{ mm} \end{aligned} \tag{5.16}$$

The stress in the prestressing steel at nominal flexural resistance f_{ps} for bonded tendons is calculated as follows:

$$\begin{aligned} k &= 2\left(1.04 - \frac{f_{py}}{f_{pu}}\right) = 2(1.04 - 0.9) = 0.28 \\ f_{ps} &= f_{pu}\left(1 - k\frac{c}{d_p}\right) = 1824\left(1 - 0.28 \cdot \frac{151}{770}\right) = 1724 \text{ MPa} \end{aligned} \tag{5.17}$$

With the results of Equations 5.16 and 5.17, the nominal flexural resistance becomes:

$$\begin{aligned} M_n &= A_{ps}f_{ps}\left(d_p - \frac{a}{2}\right) + A_s f_s\left(d_s - \frac{a}{2}\right) - A'_s f'_s\left(d'_s - \frac{a}{2}\right) + \alpha_1 f'_c(b - b_v)h_f\left(\frac{a}{2} - \frac{h_f}{2}\right) \\ &= 3234 \cdot 1724\left(770 - \frac{113}{2}\right) + 314 \cdot 454\left(1065 - \frac{113}{2}\right) - 314 \cdot 454\left(45 - \frac{113}{2}\right) \\ &+ 0.85 \cdot 60.3 \cdot (960 - 200) \cdot 180\left(\frac{114}{2} - \frac{180}{2}\right) = 3880 \text{ kNm} \end{aligned} \tag{5.18}$$

With the nominal flexural resistance known, the effective shear depth can be calculated:

$$d_{v,calc} = \frac{M_n}{A_s f_y + A_{ps}f_{ps}} = \frac{3880 \cdot 10^6}{314 \cdot 454 + 3234 \cdot 1724} = 679 \text{ mm} \tag{5.19}$$

Check if the calculated effective shear depth is greater than the minimal effective shear depth:

$$\begin{gathered} d_{v,calc} \geq \max(0.72h, 0.9d_e) = \max(799, 700) = 799 \text{ mm} \\ \text{CHECK:} \qquad 679 > 799 \qquad \textbf{NOT OK} \\ d_v = 799 \text{ mm} \end{gathered} \tag{5.20}$$

The parameter β is determined by the requirement of the minimum amount of shear reinforcement in the girder:

$$\begin{gathered} A_{v,min} \leq A_{v,provided} \\ 0.083 \cdot 7.76 \cdot \frac{200 \cdot 400}{454} \leq 157 \\ \text{CHECK:} \qquad 114 \leq 157 \text{ mm}^2 \qquad \textbf{OK} \end{gathered} \tag{5.21}$$

Procedure with algebraic equations

Satisfying Equation 5.21 results in an expression for β that only depends on the longitudinal strain in the tension reinforcement ε_s (reinforcement bars and prestressing steel). The angle of the compression chord also depends on ε_s:

$$\begin{gathered} \beta = \frac{4.8}{1 + 750\varepsilon_s} \\ \theta = 29 + 3500\varepsilon_s \end{gathered} \tag{5.22}$$

To calculate the longitudinal strain in the tension reinforcement, the sectional forces M_u and V_u and the angle θ must be known. The sectional forces follow from the sectional analysis done in `MS Excel` and are shown in Table 3.9. The following procedure is followed to calculate ε_s and the nominal shear resistance of the girder and is according to Method 2 in AASHTO (algebraic equations):

- Assume a value for $\theta_{assumed}$;
- Assume a value for $F_{exp,assumed}$;
- The values for M_u and V_u follow from the spreadsheet calculations with:

$$M_u = M_{F,exp} + M_{sw}$$

$$V_u = V_{F,exp} + V_{sw}$$

- The minimum value for M_u:

$$M_u > |V_u - V_p| d_v$$

- The value for f_{po} is taken as the stress in the prestressing steel $f_{po} = 0.27 f_{pu} = 470.6$ MPa.
- Check if ε_s is positive, if negative replace denominator of ε_s with $E_s A_s + E_p A_{ps} + E_c A_{ct}$ and must be greater than $\varepsilon_s > -0.0004$;
- Calculate β and θ with the value found for ε_s;
- Calculate the inclined cracking load V_c and contribution of the stirrups $V_{s,AASHTO}$ with the calculated values for β and θ_{calc};
- Calculate the external load $F_{exp,AASHTO}$ that the girder can resist:

$$V_{n,AASHTO} = V_{c,AASHTO} + V_{s,AASHTO} + V_p$$

$$F_{exp,AASHTO} = (V_{n,AASHTO} - V_{sw}) \cdot \frac{L_{span}}{L_{span} - a}$$

- Check if the assumed value for $F_{exp,assumed}$ equals $F_{exp,AASHTO}$ and $\theta_{assumed}$ equals θ_{calc}. If not assume a new value for both θ and F_{exp} and restart the procedure until the following holds:

$$\theta_{assumed} = \theta_{calc}$$

$$F_{exp,assumed} = F_{exp,AASHTO}$$

This procedure requires iterative calculations, therefore only the end result is given. The iterations are done with the `MS Excel Solver package`. The following values are used to calculate ε_s:

$$\begin{aligned} F_{exp,assumed} &= 914{,}877 \text{ N} = 915 \text{ kN} \\ V_u = \frac{L_{span} - a}{L_{span}} \cdot F_{exp,assumed} + V_{sw} &= 0.70 \cdot 915 + 41.38 = 680 \\ M_u = \frac{L_{span} - a}{L_{span}} \cdot F_{exp,assumed} \cdot a + M_{sw} &= 1.20 \cdot 915 + 94.50 = 1196 \text{ kNm} \\ \theta_{assumed} &= 31.02° \end{aligned} \tag{5.23}$$

Check if M_u is greater than the allowed minimum (note that $V_u - V_p$ equals $V_{tot} = V_F + V_{sw} - V_p$):

$$\begin{aligned} M_u &> |V_u - V_p| d_v \\ 1196 \cdot 10^6 &> |680 \cdot 10^3 - 98.21 \cdot 10^3| \cdot 799 = 465 \text{ kNm} \\ \text{CHECK:} \qquad 1196 &\leq 465 \text{ kNm} \qquad \textbf{OK} \end{aligned} \tag{5.24}$$

To calculate the longitudinal strain in the tension reinforcement, the strain in the prestressing steel after completion of the post-tensioning f_{po} must be known. AASHTO gives a value of $f_{po} = 0.7 f_{pu} = 1277$ MPa for both pre- and post-tensioned members. However, for the assessment of the Helperzoom girders this value might be too high. According to RBK the stress in the prestressing steel is 52% of the ultimate strength (= 948 MPa) including prestressing losses. The results from the tests given in Chapter 3.6.3 give a value of 27% of the ultimate strength $f_{po} = 0.27 f_{pu} = 494$ MPa. This results in a value of ε_s:

$$\begin{aligned} \varepsilon_s &= \frac{\left(\frac{|M_u|}{d_v} + 0.5 N_u + 0.5 |V_u - V_p| \cot\theta - A_{ps} f_{po} \right)}{E_s A_s + E_p A_{ps}} = 0.000578 \\ &= \frac{\left(\frac{1196 \cdot 10^6}{799} + 0 + 0.5 \cdot |(680 - 98.21) \cdot 10^3| \cdot \cot(31.02) - 3234 \cdot 494 \right)}{200{,}000 \cdot 314 + 185{,}000 \cdot 3234} \end{aligned} \tag{5.25}$$

Note: the AASHTO does not follow the principle of prestressing is preloading, therefore $N_u = 0$.

Note 2: the AASHTO simplifies the axial tensile force in the flanges caused by the acting shear force in the member to $0.5 \cot\theta = 1.0$, which corresponds to a value of $\theta = 26.565°$. This makes the calculation less iterative, but more conservative as lower values for θ result in a higher force.

This results in a value for θ and β of:

$$\begin{aligned} \beta &= \frac{4.8}{1 + 750\varepsilon_s} = \frac{4.8}{1 + 750 \cdot 0.000578} = 3.35 \\ \theta_{calc} &= 29 + 3500 \cdot 0.000578 = 31.02° \end{aligned} \tag{5.26}$$

The inclined cracking load and contribution of the stirrups follow from the results of Equations 5.25 and 5.26:

$$\begin{aligned} V_{c,AASHTO} &= 0.083 \beta \sqrt{f'_c} b_v d_v = 0.083 \cdot 3.35 \cdot 7.76 \cdot 200 \cdot 799 = 345 \text{ kN} \\ V_{s,AASHTO} &= \frac{A_v f_y d_v \cot\theta}{s} = \frac{157 \cdot 454 \cdot 799 \cot(31.02)}{400} = 237 \text{ kN} \end{aligned} \tag{5.27}$$

The external load that the girder can resist equals:

$$F_{exp,AASHTO} = (V_{n,AASHTO} - V_{sw}) \cdot \frac{L_{span}}{L_{span} - a} = \frac{345 + 237 + 98 - 41.38}{0.7} = 915 \text{ kN} \tag{5.28}$$

Check if the constraints are met:

$$\begin{aligned} \theta_{assumed} &= \theta_{calc} \\ \text{CHECK:} \qquad 31.02° &= 31.02° \qquad \textbf{OK} \\ F_{exp,assumed} &= F_{exp,AASHTO} \\ \text{CHECK:} \qquad 915 &= 915 \text{ kN} \qquad \textbf{OK} \end{aligned} \tag{5.29}$$

The nominal shear resistance according to the AASHTO for $x = 1.725$ m equals:

$$V_{n,AASHTO} = V_{c,AASHTO} + V_{s,AASHTO} + V_p = 345 + 237 + 98 = 680 \text{ kN} \tag{5.30}$$

The calculated nominal shear resistance $V_{n,AASHTO}$ must be smaller than the shear force required for the crushing of concrete in the web. When the nominal shear resistance calculated in Equation 5.3.2 is smaller, the stirrups will yield before crushing of the web:

$$\begin{aligned} V_{n,AASHTO} &< 0.25 f'_c b_v d_v + V_p \\ 680 &< 0.25 \cdot 60.3 \cdot 200 \cdot 799 + 98.21 \\ \text{CHECK:} \qquad 680 &\leq 2506 \text{ kN} \qquad \textbf{OK} \end{aligned} \tag{5.31}$$

Procedure with tables

The same procedure is followed as with the algebraic equations, except that the longitudinal strains are calculated at mid depth of the girder and used in the table given in Table 2.4 to obtain θ and β. First θ and F_{exp} are assumed to calculate the longitudinal strains at mid depth. Again, only the end result is given with $\theta = 27.57°$ and $F_{exp,assumed} = 894$ kN:

$$\begin{aligned} \varepsilon_x &= \frac{\left(\frac{|M_u|}{d_v} + 0.5N_u + 0.5|V_u - V_p| \cot\theta - A_{ps} f_{po}\right)}{2(E_s A_s + E_p A_{ps})} = 0.000310 \\ &= \frac{\left(\frac{1268 \cdot 10^6}{799} + 0 + 0.5 \cdot |(665.3 - 56.8) \cdot 10^3| \cdot \cot(27.57) - 3234 \cdot 494\right)}{200{,}000 \cdot 314 + 185{,}000 \cdot 3234} \end{aligned} \tag{5.32}$$

The ratio between the shear stress in the concrete equals:

$$\frac{\nu_u}{f'_c} = \frac{\left(\frac{V_u - V_p}{d_v b_v}\right)}{f'_c} = \frac{\left(\frac{567}{799 \cdot 200}\right)}{60.3} = 0.059 \tag{5.33}$$

According to the table given in Table 2.4 with $\varepsilon_x < 0.00050$ and $\nu_u / f'_c < 0.075$, the values are $\theta = 30.5°$ and $\beta = 2.59$. For $\varepsilon_x < 0.00025$ and $\nu_u / f'_c < 0.075$, the values are $\theta = 26.6°$ and $\beta = 2.94$. Interpolating for $\varepsilon_x = 0.000310$ results in:

$$\begin{aligned} \theta &= 26.6 + \frac{30.5 - 26.6}{0.00050 - 0.00025} \cdot (0.00031 - 0.00025) = 27.57° \\ \beta &= 2.94 - \frac{2.94 - 2.59}{0.00050 - 0.00025} \cdot (0.00031 - 0.00025) = 2.86 \end{aligned} \tag{5.34}$$

The inclined cracking load and contribution of the stirrups equals to:

$$\begin{aligned} V_{c,AASHTO} &= 0.083 \cdot 2.86 \cdot 7.76 \cdot 200 \cdot 799 = 294 \text{ kN} \\ V_{s,AASHTO} &= \frac{157 \cdot 454 \cdot 799 \cot(27.57)}{400} = 273 \text{ kN} \end{aligned} \tag{5.35}$$

Check if the external load that the girder can resist equals to the applied external load:

$$F_{exp,AASTHO} = \frac{V_{c,AASHTO} + V_{s,AASHTO} + V_p + V_{sw+p}}{0.7} = \frac{294 + 273 + 98 - 41.38}{0.7} = 893.9 \text{ kN}$$
$$\text{CHECK:} \qquad 893.9 \approx 894 \text{ kN} \qquad \textbf{OK} \tag{5.36}$$

The nominal shear resistance becomes:

$$V_{n,AASHTO} = 294 + 273 + 98 = 665 \text{ kN} \tag{5.37}$$

The result for the nominal shear resistance is almost the same for both approaches:

$$V_{n,algebraic} = 680 \approx V_{n,tables} = 665 \text{ kN} \tag{5.38}$$

This might implicate that the two approaches for Method 2 may be considered equivalent. As shown in the detailed calculations, this statement is not true for the calculations performed in this paragraph. The β and θ values are not the same $\theta = 31.02°$ vs. $27.57°$ and $\beta = 3.35$ vs. 2.86. This means that the inclined cracking loads for both methods are not equal $V_{c,AASHTO} = 345$ kN vs. 294 kN and the same holds for the contribution of the stirrups $V_{s,AASHTO} = 237$ kN vs. 273 kN. Subsequently, the value of the applied external load found from the procedure with tables is lower than the procedure with algebraic equations $F_{exp} = 914$ kN vs. 894 kN.

Taking a closer look at the tables, the values for θ and β range from:

$$\begin{aligned} 18.1° \leq \theta \leq 37.3° \\ 1.50 \leq \beta \leq 6.32 \end{aligned} \tag{5.39}$$

With a maximum for the nominal shear resistance with values:

$$\begin{aligned} &\text{Max:} \quad \theta = 22.3°,\ \beta = 6.32 \quad \varepsilon_x \leq -0.2 \cdot 10^{-3},\ \nu_u/f'_c \leq 0.075) \\ &\text{Min:} \quad \theta = 35.8°,\ \beta = 1.50 \quad \varepsilon_x \leq 1.0 \cdot 10^{-3},\ \nu_u/f'_c \leq 0.250) \end{aligned} \tag{5.40}$$

While according to the algebraic equations θ and β range from:

$$\begin{aligned} &(= 29 + 3500 \cdot -0.0004) \quad 27.6° \leq \theta \leq 50° \quad (= 29 + 3500 \cdot 0.006) \\ &\left(= \frac{4.8}{1 + 750 \cdot 0.006}\right) \quad 0.87 \leq \beta \leq 6.86 \quad \left(= \frac{4.8}{1 + 750 \cdot -0.0004}\right) \end{aligned} \tag{5.41}$$

Figure 5.6 shows the linear equation for θ according to the CSA design code. The linear equation fits between the upper and lower limit for yielding of the stirrups and crushing of the concrete respectively. The longitudinal strains in the CSA code provision are calculated at a different position than the AASHTO (algebraic) and therefore results in a different equation $\theta = 29 + 7000\varepsilon_x$ (CSA) instead of $\theta = 29 + 3500\varepsilon_s$ (AASHTO). The x-axis will also be different for AASHTO, but the concept is the same. Note that the algebraic equation is based on $\nu/f'_c = 0.25$ and the table approach gives values for θ and β for different ν/f'_c-ratios.

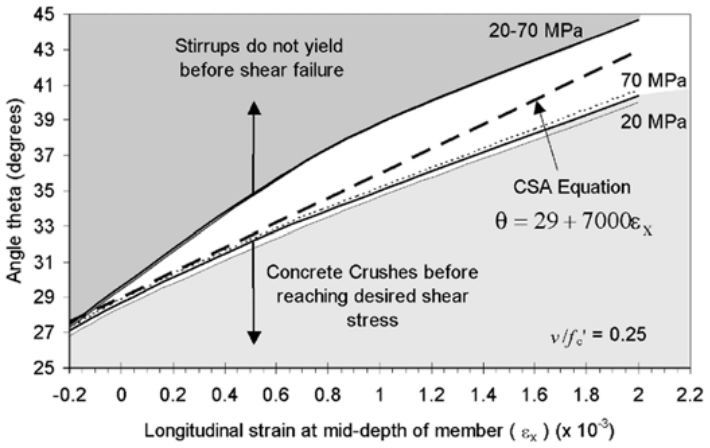

Figure 5.6: Illustration of the CSA Equation for the calculation of θ [79]

5.3.3. AASHTO shear resistance summary

The nominal shear resistances of the cross-sections between $x = 1.725$,..,2.903 m are calculated with the **algebraic equations only** and $f_{po} = 0.27 f_{pu}$ in MPa. The values used in the detailed calculations are shown in Table 5.7. The effective shear depth d_v is 799 mm for every cross section, because $d_{v,calc}$ does not fulfill the requirement: $d_{v,calc} > 0.72h$. All cross-sections have rectangular behavior in the sectional analysis for the flexural resistance of the member. In this procedure the height of the concrete compression zone (stress block in AASHTO) is simplified with an equivalent height of the stress block $a = \beta_1 \cdot c$. Before calculations are done for the longitudinal strains in the tension reinforcement, a check is done that the factored moment at the considered cross-section is not less than the minimum value ($|V_u - V_p| \cdot d_v$). This check is true for all considered cross-sections.

The procedure according to Method 2 (algebraic equations), as shown in detail in the previous paragraph, is done for all cross-sections. The angles for the compression chord range between 31.02° and 33.5° and the longitudinal strains in the tension chord range from $0.58 \cdot 10^{-3}$ to $1.29 \cdot 10^{-3}$. This means that the strains in cross-section $x = 2.903$ m are more than 2 times larger than $x = 1.725$ m. For cross-sections closer to the applied external load, the value for β decreases, which is a result from the larger longitudinal tension strains.

Table 5.7: Values used for calculating the nominal shear resistance for $x = 1.725$,..,2.903 m and $a = 2.903$ m with $0.27 f_{pu}$

x [m]	**1.725**	**1.8**	**1.85**	**1.9**	**1.95**	**2**	**2.051**	**2.453**	**2.903**
$F_{assumed}$ [kN]	915	901	893	884	876	868	861	807	760
c_T [mm]	−113	−113	−113	−113	−113	−113	−113	−114	−114
c_{rect} [mm]	151	151	151	151	151	151	151	152	152
c [mm]	151	151	151	151	151	151	151	152	152
a [mm]	113	113	113	113	113	114	114	114	114
$f_{ps,AASHTO}$ [MPa]	1724	1724	1725	1725	1726	1726	1726	1729	1730
d_e [mm]	777	782	785	788	792	795	798	819	830
M_n [kNm]	3880	3909	3928	3946	3965	3984	4003	4131	4194
$d_{v,calc}$ [mm]	679	683	687	690	693	696	699	721	731
$0.9d_e$ [mm]	700	704	707	710	712	715	718	737	747
d_v [mm]	799	799	799	799	799	799	799	799	799
$M_u > \lvert V_u - V_p \rvert d_v$	TRUE	TRUE	TRUE	TRUE	TRUE	TRUE	TRUE	TRUE	TRUE
M_u [kNm]	1196	1230	1252	1274	1296	1318	1339	1503	1674
$\theta_{assumed}$ [°]	31.02	31.19	31.3	31.41	31.52	31.62	31.73	32.58	33.5
ε_s [-]	0.00058	0.00063	0.00066	0.00069	0.00072	0.00075	0.00078	0.00102	0.00129
$\varepsilon_s > 0$	TRUE	TRUE	TRUE	TRUE	TRUE	TRUE	TRUE	TRUE	TRUE
β [-]	3.35	3.27	3.22	3.17	3.12	3.07	3.03	2.72	2.44
θ_{calc} [°]	31.02	31.19	31.3	31.41	31.52	31.62	31.73	32.58	33.5

The calculation procedure for the inclined cracking load, derived from the Modified Compression Field Theory [15], makes no distinction in the different shear-failure modes. Both the inclined cracking load and the contribution of the stirrups depend on the inclination of the compression chord. The inclined cracking load indirectly: $\theta \rightarrow \varepsilon_s \rightarrow \beta \rightarrow V_{c,AASHTO}$, the shear contribution of the stirrups directly: $\theta \rightarrow V_{s,AASHTO}$. The value for θ remains almost constant, while the value for β decreases for cross-sections closer to the applied external load. Therefore the inclined cracking load V_c decreases more rapidly towards the load than the contribution of the stirrups $V_{s,AASHTO}$ does.

The cross-section at $x = 2.903$ m is the most critical cross-section for shear failure, see Table 5.8 and Figure 5.7. The nominal shear resistance is $V_{n,AASHTO} = 556$ kN, taking into account full contribution of the stirrups. Crushing of the compression field occurs at $V_{max} = 2497$ kN and is almost the same for every cross-section, as the inclination of the compression field θ is not included in the simplified expression derived from the MCFT.

Table 5.8: Nominal shear resistance for $x = 1.725$,..,2.903 m and $a = 2.903$ m with $f_{po} = 0.27 f_{pu}$

x [m]	**1.725**	**1.8**	**1.85**	**1.9**	**1.95**	**2**	**2.051**	**2.453**	**2.903**
$V_{c,AASHTO}$ [kN]	345	336	331	326	321	316	312	280	252
$V_{s,AASHTO}$ [kN]	237	235	234	233	232	231	230	223	215
V_p [kN]	98	98	97	97	96	96	96	93	89
$0.25 f'_c b_v d_v + V_p$ [kN]	2506	2506	2505	2505	2504	2504	2504	2501	2497
$V_{n,AASHTO}$ [kN]	680	669	663	656	650	644	638	595	556

The maximum calculated external load $F_{exp,AASHTO} = (V_{n,AASHTO} - V_{sw})/0.7$ needs to be the same as the maximum assumed external load $F_{exp,assumed}$, given in Table 5.7:

Table 5.9: Failure load for $x = 1.725$,..,2.903 m and $a = 2.903$ m with $f_{po} = 0.27 f_{pu}$

x [m]	**1.725**	**1.8**	**1.85**	**1.9**	**1.95**	**2**	**2.051**	**2.453**	**2.903**
$F_{exp,AASHTO}$ [kN]	915	901	893	884	876	868	861	807	760

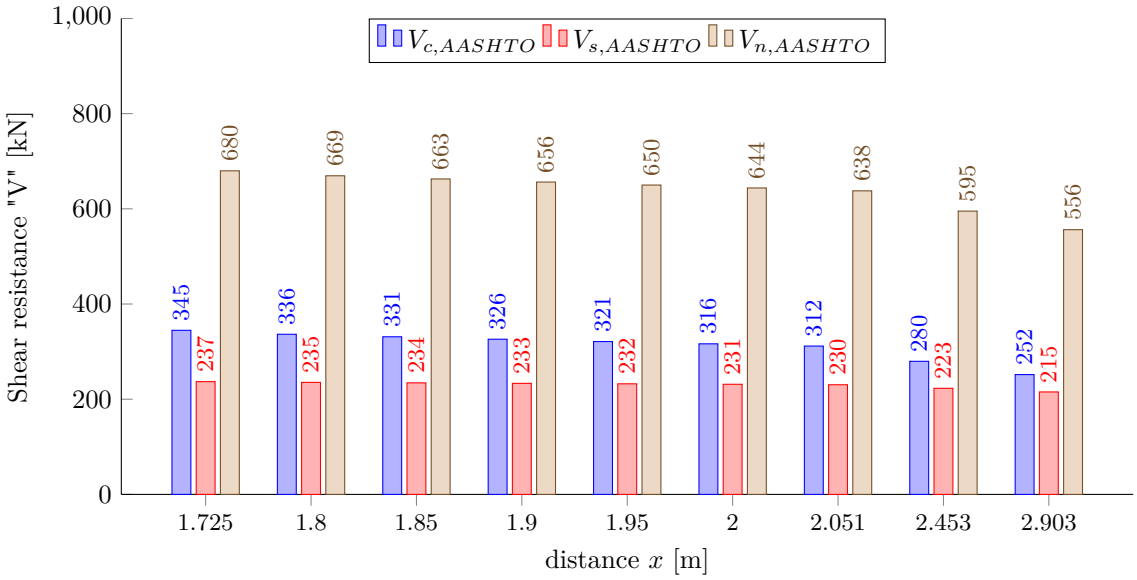

Figure 5.7: Shear resistance for $x = 1.725$,..,2.903 m and $a = 2.903$ m with $f_{po} = 0.27 f_{pu}$

5.3.4. AASHTO shear resistance summary with different f_{po}

In the previous paragraph the stress in the prestressing steel is taken as $f_{po} = 0.27f_{pu} = 494$ MPa. According to the AASHTO this value should be taken as $f_{po} = 0.7f_{pu}$. In this paragraph the nominal shear resistance is calculated for different values: $f_{po} = 0.342f_{pu}$, $0.52f_{pu}$ and $0.7f_{pu}$. The detailed results are given in Appendix A. The following conclusions are drawn from Tables A.1, A.2 and A.3:

- For higher values of f_{po} the longitudinal strain ε_s decreases and even becomes negative. Note that negative values for the longitudinal strain (greater than $\varepsilon_s > -0.0004$) do not result in negative diagonal crack widths. If the calculated longitudinal strains from Equation 2.22 are negative, the denominator is replaced with $E_cA_{ct} + E_sA_s + E_pA_{ps}$;
- For lower longitudinal strains the value of θ decreases and β increases;
- A decrease for the angle of the compression field results in a higher contribution of the stirrups, as more stirrups are crossing the inclined field;
- An increase of the aggregate interlock factor β is the result of a lower diagonal crack width, thus an increase of the friction in between the crack. This results in a higher inclined cracking load;
- The resistance for crushing of the concrete is not affected, as the angle of the compression field is not included in the expression.

Finally, a comparison is made between the results of the calculations with $f_{po} = 0.27f_{pu}, 0.342f_{pu}, 0.52f_{pu}$ and $0.70f_{pu}$ for cross-section $x = 1.725$ m:

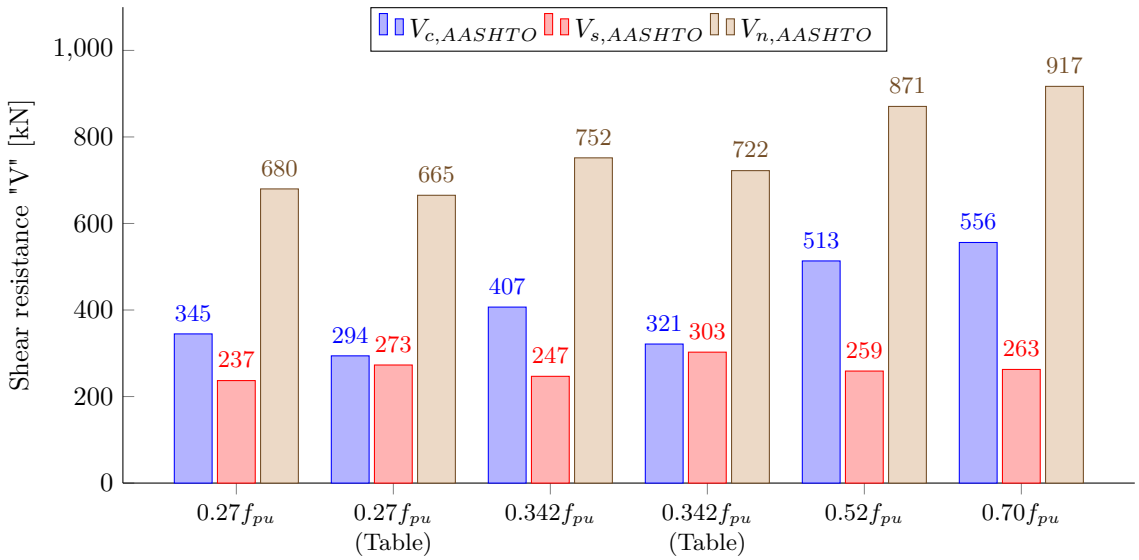

Figure 5.8: Shear resistance for $x = 1.725$ m and $a = 2.903$ m with different values of f_{po}

5.4. EC2

The EC2 expressions for calculating the shear resistance of a concrete member with- and without shear reinforcement are given in Chapter 2.9. This code provision uses two different approaches depending on the presence of shear reinforcement. For members without shear reinforcement distinction is made between flexural-shear failure and shear-tension failure. The strut-and-tie method used for members with shear reinforcement makes no distinction between the two failure modes, because after the concrete is cracked the shear reinforcement should take over shear force. This is different from the approaches according to the ACI and the AASHTO, where the nominal shear resistance is a sum of the inclined cracking load plus the contribution of the stirrups. Another important difference is that EC2 follows the principle of prestressing is preloading. In the first sub-paragraph, the values used for determining the shear resistance are given. In the second sub-paragraph a detailed calculation is done for the shear resistance of the Helperzoom girder. In the last sub-paragraph, a summary for the shear resistances of the other cross-sections is given.

5.4.1. Values used for EC2

Table 5.10 provides the values used for the shear resistance at $x = 1.725$ m.

Table 5.10: Values used for $x = 1.725$ m and $a = 2.903$ m

	Value	Units	Commentary
A_{sl}	3234	mm^2	A_p used
A_{sw}	157	mm^2	$0.25\pi\phi_v^2 * 2 = 2$ legs per 400 mm
b_w	200	mm	width of the web
d	770	mm	d_p used
f_{cm}	62.6	MPa	see Chapter 3.2.1
f_{ctm}	4.85	MPa	see Chapter 3.2.1
f_{ywm}	454	MPa	f_{ym} used, see Chapter 3.2.3
I_c	$7.47 \cdot 10^{10}$	mm^4	calculated in `MS Excel`, see Chapter 3.3
k_{EC2}	0.151	-	$= 1 + \sqrt{200/d}$
s	400	mm	spacing transverse reinforcement
S_c	$9.12 \cdot 10^7$	mm^3	see Chapter 3.3, with respect to c.o.g.
α	0.71	-	for C55/67
α_{cw}	1.05	-	$= 1 + \sigma_{cp}/f_{cm}$
α_l	1	-	transition length for bonded pre-tensioned tendons
β	0.37	-	for C55/67
γ_c	1.0	-	material factor
ν_1	0.6	-	
ν_{min}	0.04	MPa	$= 0.035\sqrt[3]{k}\sqrt{f_{cm}}$
ρ_l	0.02	-	$= A_{sl}/(b_w \cdot d_p) \leq 0.02$ with $A_{sl} = A_p$
σ_{cp}	3.09	MPa	$= N_E/A_c$

5.4.2. EC2 flexural analysis for the internal lever arm

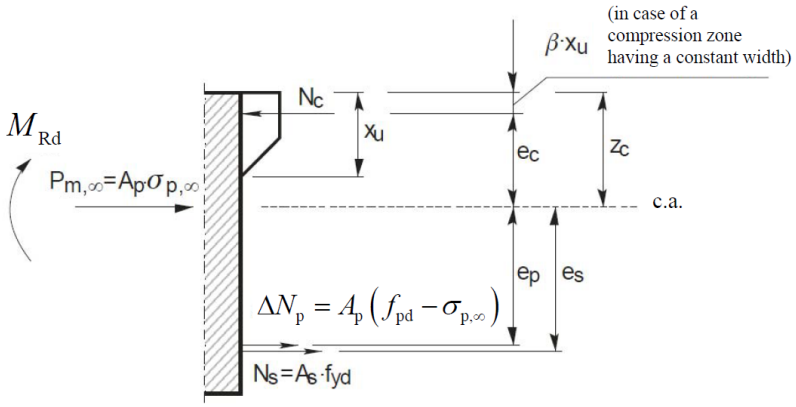

Figure 5.9: Equilibrium between external and internal forces [5]

The internal lever arm z is calculated with the equilibrium method. In this method the internal and external forces need to make equilibrium as shown in Figure 5.9. In this flexural analysis a bi-linear stress-strain relationship is considered and it is assumed that the concrete compressive strain ε_c exceeds ε_{c3}. This means the concrete compressive stress σ_c reaches f_{cm} in the compression zone. To calculate z the height of the compression zone x_u needs to be known. To obtain x_u, first an approximation is made from equilibrium of horizontal forces [5]:

$$x_u = \frac{A_s f_{ym} + A_p(f_{pd} - \sigma_{p,\infty}) + P_{m,\infty}}{\alpha \cdot b \cdot f_{cm}} = \frac{A_s f_{ym} + A_p f_{pd}}{\alpha \cdot b \cdot f_{cm}} \tag{5.42}$$

With $\alpha = 0.71$ for C55/67, the width of the girder as the mean width of the top flange $b = b_{tfl} = 960$ mm (see Chapter 3.3) and $f_{pd} = f_{pu} = 1824$ MPa for the first approximation. Equation 5.42 can only be used in case of a rectangular compression zone cross-section, which means x_u needs to be smaller than the height of the top flange $h_{tfl} = 180$ mm.

$$x_u \leq h_{tfl}$$
$$\frac{157 \cdot 454 + 3234 \cdot 1824}{0.71 \cdot 960 \cdot 62.6} \leq 180 \tag{5.43}$$
$$141.7 \leq 180 \text{ [mm]} \Rightarrow \textbf{OK}$$

Next the increase of the strain in the prestressing steel $\Delta\varepsilon_p$ is determined, provided that $\varepsilon_{cu} = 0.035$:

$$\Delta\varepsilon_p = \varepsilon_{cu}\left(\frac{d_p}{x_u} - 1\right) = 0.035\left(\frac{770}{141.7} - 1\right) = 0.0155 \tag{5.44}$$

The total strain in the prestressing steel is:

$$\varepsilon_p = \varepsilon_{p,\infty} + \Delta\varepsilon_p = \frac{\sigma_{pm,\infty}}{E_p} + \Delta\varepsilon_p \quad \text{with} \quad \sigma_{pm,\infty} = \frac{N_p}{A_p} = \frac{1598 \cdot 10^3}{3234} = 494 \text{ MPa}$$
$$\varepsilon_p = \frac{494}{185{,}000} + 0.0155 = 0.0182 \tag{5.45}$$

The stress in the prestressing steel can be calculated with the equation of the second branch of the bilinear stress-strain diagram, given in Equation 3.1:

$$\sigma_{pd} = 4086.8\varepsilon_p + 1605.6 = 4086.8 \cdot 0.0182 + 1605.6 = 1680 \text{ MPa} \tag{5.46}$$

Comparing the result for σ_{pd} with the used f_{pd} for the first approximation of x_u, a new iteration is required:

$$\sigma_{pd} = f_{pd} \Rightarrow 1680 \neq 1824 \tag{5.47}$$

After several iterations to satisfy $\sigma_{pd} = f_{pd}$, $x_u = 131.2$ mm is obtained with $\sigma_{pd} = 1686.2$ MPa. The internal lever arm follows with $\beta = 0.37$ for C55/67:

$$z = d_p - \beta \cdot x_u = 770 - 0.37 \cdot 131.2 = 721 \text{ mm } (\approx 0.94d) \tag{5.48}$$

5.4.3. EC2 shear resistance detailed calculation

In comparison to the ACI and AASHTO, the EC2 does not account for the acting moment and shear forces in the girder in the calculation for the shear resistance of the member. Only the acting axial compressive force from prestressing is accounted for as $k_1 \cdot \sigma_{cp}$. First calculations are made for the inclined cracking load (without shear reinforcement), where after calculations are made for the shear resistance of the shear reinforcement.

Without transverse reinforcement:

For the calculation of members without shear reinforcement there are two regions to be considered, regions uncracked in bending for the shear-tension capacity (STC) and regions cracked in bending for the flexure-shear capacity (FSC). To know whether a region is cracked in bending, Table 5.2 is checked for the stresses at the bottom of the girder. The positions at which $\sigma_{1,bottom}$ exceeds $f_{ctm,sp} = 5.4$ MPa holds for all considered cross-sections between $x = 1.725$,..,2.903 m, meaning that all cross-sections are cracked in bending. Nevertheless, for the calculations in this paragraph, both STC and FSC are calculated for $x = 1.725$ m. For regions uncracked in bending, the resistance to shear-tension failure is calculated at two different heights of the cross-section. According to Figure 5.1 the highest principal stress is at the bottom of the web. The resistances to shear-tension failure for both at the center of gravity and at the bottom of the web equal to (see Equation 3.2 for values of S_c):

$$\begin{aligned} V_{Rm,STC,cog} &= \frac{I_c \cdot b_w}{S_{c,cog}}\sqrt{{f_{ctm}}^2 + \alpha_l \cdot \sigma_{cp} \cdot f_{ctm}} \\ &= \frac{7.47 \cdot 10^{10} \cdot 200}{9.12 \cdot 10^7}\sqrt{4.85^2 + 1 \cdot 3.09 \cdot 4.85} = 1016 \text{ kN} \\ V_{Rm,STC,bottomweb} &= \frac{I_c \cdot b_w}{S_{c,bottomweb}}\sqrt{{f_{ctm}}^2 + \alpha_l \cdot \sigma_{cp} \cdot f_{ctm}} \\ &= \frac{7.47 \cdot 10^{10} \cdot 200}{8.77 \cdot 10^7}\sqrt{4.85^2 + 1 \cdot 3.09 \cdot 4.85} = 1056 \text{ kN} \end{aligned} \tag{5.49}$$

For regions that are cracked in bending the resistance to flexural-shear failure equals to:

$$\begin{aligned} V_{Rm,FSC} &= \left(C_{Rm,c} \cdot k_{EC2} \sqrt[3]{100\rho_l \cdot f_{cm}} + k_1\sigma_{cp}\right) b_w \cdot d_p \\ &= \left(0.15 \cdot 0.151 \sqrt[3]{100 \cdot 0.02 \cdot 62.6} + 0.225 \cdot 3.09\right) \cdot 200 \cdot 770 = 246 \text{ kN} \\ V_{Rm,FSC,min} &= (\nu_{min} + k_1 \cdot \sigma_{cp})\, b_w \cdot d_p = (0.041 + 0.225 \cdot 3.09) \cdot 200 \cdot 770 = 78 \text{ kN} \end{aligned} \tag{5.50}$$

- *Note 1: for the longitudinal reinforcement ratio ρ_l the area of the prestressing steel is used instead of the area of the ordinary reinforcement steel*;
- *Note 2: in the EC2 there is no expression to calculate the value for d. In figures d is drawn to the tension reinforcement bars and not to the prestressing steel. For the calculations in this paragraph the value for the effective depth is taken as $d = d_p$ (this is also done for the flexural analysis of the internal lever arm z)*;
- *Note 3: $C_{Rd,c}$ and k_1 include resistance factors in the EC2, which is for the design of new structures. For assessment these values are taken as $C_{Rm,c} = 0.15$ (Regan [33]) and $k_1 = 0.225$ (by multiplying $0.15 \cdot \gamma_c$).*

With transverse reinforcement:
For the calculation with shear reinforcement two failure modes have to be calculated, yielding of the stirrups and crushing of the concrete. The lowest value of the two failure modes represents the shear capacity of the member. For this detailed calculation, only $\theta = 30°$ is considered. The result of the internal lever arm in the previous paragraph for $x = 1.725$ m is $z \approx 0.94d = 721$ mm. This result is higher than the (conservative) expression of the EC2, which states that the internal lever arm may be assumed $z = 0.9d$ for all calculations.

Yielding transverse reinforcement and crushing of the concrete:

$$\begin{aligned} V_{Rm,s,EC2} &= \frac{A_{sw}}{s} \cdot z \cdot f_{ywm} \cot\theta = \frac{157}{400} \cdot 721 \cdot 454 \cdot \cot(30) = 223 \text{ kN} \\ V_{Rm,max,EC2} &= \frac{\alpha_{cw} \cdot b_w \cdot z \cdot \nu_1 \cdot f_{cm}}{\cot\theta + \tan\theta} = \frac{1.05 \cdot 200 \cdot 721 \cdot 0.6 \cdot 62.6}{\cot(30) + \tan(30)} = 2409 \text{ kN} \end{aligned} \tag{5.51}$$

Note that the inclined cracking load is higher than the resistance of the shear reinforcement when an inclination of the compression chord $\theta = 30°$ is chosen. The resistance of the shear reinforcement is lower than the maximum resistance $V_{Rm,max}$, crushing of the concrete.

5.4.4. EC2 shear resistance summary

For the calculations of the inclined cracking load, the acting axial compressive force from prestressing is the same for each cross-section. The only changing variables are the effective depth d_p, factor for size effect k and ratio for the (prestressing) steel ρ_l. The internal lever arm is assumed to be $z = 0.94d_p$ for all cross-sections, see Table 5.11.

Table 5.11: Values used for calculating the shear resistance for $x = 1.725$,..,2.903 m and $a = 2.903$ m

x [m]	**1.725**	**1.8**	**1.85**	**1.9**	**1.95**	**2**	**2.051**	**2.453**	**2.903**
$z = 0.94d$ [mm]	722	726	730	733	736	739	743	764	775
k [-]	1.51	1.51	1.51	1.51	1.50	1.50	1.50	1.50	1.49
ρ_l [-]	0.0200	0.0200	0.0200	0.0200	0.0200	0.0200	0.0200	0.0199	0.0196

Shear-tension failure is neglected in this summary, as the value is the same for every cross-section and all considered cross-sections are cracked in bending. For the shear resistance of the stirrups, the designer is free to choose the value θ according to Equation 2.36. As a reference the calculated inclinations of the compression field θ, according to the experimental results, are used for the shear resistance (see Chapters 4.6.1 and 4.6.2.

The cross-section at $x = 1.725$ m is the most critical cross-section for shear failure, see Table 5.12 and Figure 5.10. The dominating shear failure mode is flexural-shear failure with a resistance of $V_{Rm,c} = 246$ kN, considering no shear reinforcement. Taking into account full contribution of the stirrups with $\theta = 21.8°$ results in a resistance of $V_{Rm,s,\theta=21.8°} = 322$ kN. Crushing of the compression field occurs for $V_{Rm,max,\theta=21.8°} = 1918$ kN.

Table 5.12: Shear resistance for $x = 1.725$,..,2.903 m and $a = 2.903$ m with variable θ

x [m]	**1.725**	**1.8**	**1.85**	**1.9**	**1.95**	**2**	**2.051**	**2.453**	**2.903**
$\sigma_1 > f_{ctm,sp}$	TRUE	TRUE	TRUE	TRUE	TRUE	TRUE	TRUE	TRUE	TRUE
$V_{Rm,c}$ [kN]	282	283	284	285	286	287	288	295	298
$V_{Rmc,min}$ [kN]	113	114	115	115	116	116	116	120	121
$V_{Rm,s,\theta=15°}$ [kN]	480	483	485	488	490	492	494	509	516
$V_{Rm,s,\theta=21.8°}$ [kN]	322	324	325	327	328	330	331	341	345
$V_{Rm,s,\theta=30°}$ [kN]	223	224	225	226	227	228	229	236	239
$V_{Rm,s,\theta=41°}$ [kN]	148	149	150	150	151	152	152	157	159
$V_{Rm,max,\theta=15°}$ [kN]	1391	1400	1406	1413	1419	1425	1431	1473	1494
$V_{Rm,max,\theta=21.8°}$ [kN]	1918	1931	1940	1948	1957	1965	1974	2032	2061
$V_{Rm,max,\theta=30°}$ [kN]	2409	2425	2436	2447	2457	2468	2479	2552	2588
$V_{Rm,max,\theta=41°}$ [kN]	2755	2773	2785	2798	2810	2822	2835	2918	2959

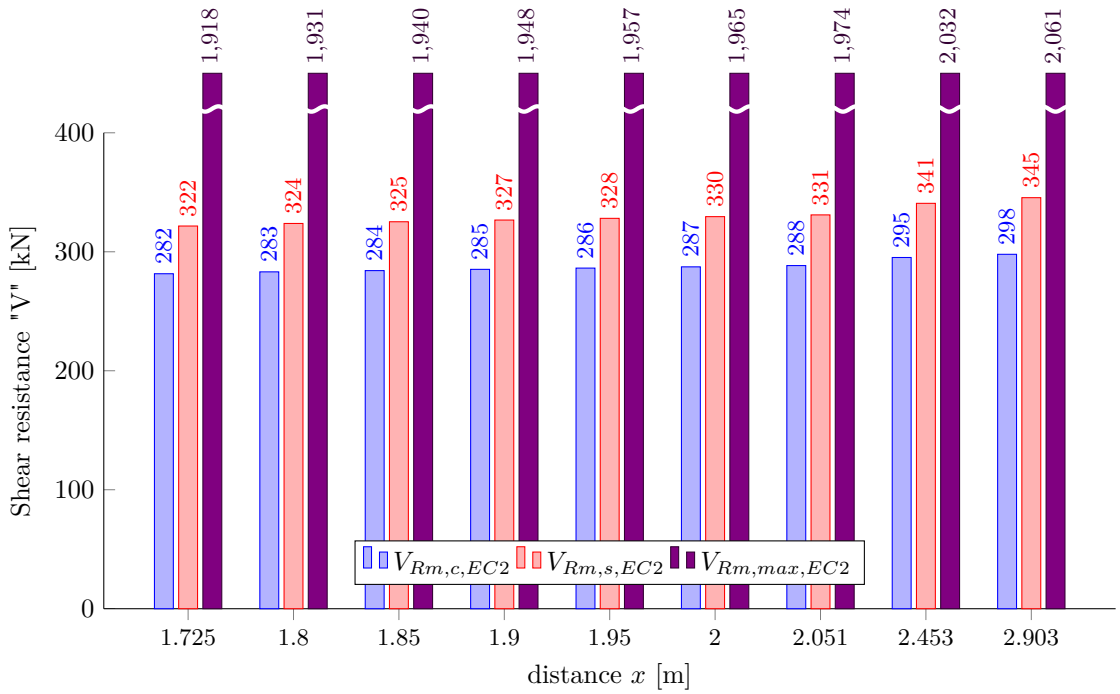

Figure 5.10: Shear resistance for $x = 1.725$,..,2.903 m and $a = 2.903$ m with $\theta = 21.8°$

Chapter 2.9.2 mentioned that the maximum shear resistance is obtained when yielding of the stirrups occurs simultaneously with failure of the compression field. With the EC2 the limit for the rotating strut is 21.8°. Ignoring this limit and solving the inclination of the rotating strut for which $V_{Rm,s} = V_{Rm,max}$ and $F_{exp,asssumed} = F_{exp,calc}$ holds, results in $\theta = 8.67°$ and $V_{Rm,s} = V_{Rm,max} = 838$ kN. This corresponds to $F_{exp} = 1282$ kN.

5.5. RBK1.1

The RBK expressions for calculating the shear resistance of a concrete member with- and without shear reinforcement are given in Chapter 2.10. This code provision is an addition to the EC2 with adjustment for existing structures. This code only uses one expression to calculate the shear resistance for a (prestressed) concrete member, without making a distinction between the shear failure modes. The total shear resistance is the sum of the inclined cracking load plus the contribution of the stirrups, which is the same approach according to the ACI and the AASHTO. The values used for determining the shear resistance are the same as in Table 5.10, except for the width of the web.

In the RBK the width b_w is denoted as the mean width calculated over a projected area as shown in Figure 2.26. The mean width of the web b_{wgem} is calculated as follows:

$$\begin{aligned} b_{w,gem} &= \frac{A_{c,projected}}{d_p} = \frac{339{,}850}{770} > 1.25 b_w \\ b_{w,gem} &= 1.25 \cdot 200 = 250 \text{ mm} \end{aligned} \tag{5.52}$$

The inclined cracking load equals:

$$\begin{aligned} V_{Rm,c,RBK} &= \left(0.15 k \sqrt[3]{100 \rho_l \cdot f_{cm}} + 0.225 \sigma_{cp}\right) \cdot b_{w,gem} \cdot d_p = 352 \text{ kN} \\ &= \left(0.15 \cdot 1.51 \sqrt[3]{100 \cdot 0.02 \cdot 62.6} + 0.225 \cdot 3.09\right) \cdot 250 \cdot 781 \end{aligned} \tag{5.53}$$

The value for the angle of the compression chord for prestressed structures is set to $\theta = 30°$ in the RBK. The contribution of the shear reinforcement equals:

$$\begin{aligned} V_{Rm,s,RBK} &= \frac{A_{sw}}{s} \cdot z \cdot f_{ywm} \cdot \cot\theta \\ &= \frac{157}{400} \cdot 722 \cdot 454 \cdot \cot(30) = 223 \text{ kN} \end{aligned} \tag{5.54}$$

The sum of the inclined cracking load and the contribution of the stirrups results in:

$$V_{Rm,RBK} = V_{Rm,c,RBK} + V_{Rm,s,RBK} = 352 + 223 = 575 \text{ kN} \tag{5.55}$$

The cross-section at $x = 1.725$ m is the most critical cross-section for shear failure, see Table 5.13 and Figure 5.11. The inclined cracking load is $V_{Rm,c} = 352$ kN. Taking into account full contribution of the stirrups with $\theta = 30°$ results in a resistance of $V_{Rm,s,\theta=30°} = 223$ kN (same as EC2). Crushing of the compression field occurs for $V_{Rm,max,\theta=30°} = 2409$ kN (same as EC2). The total shear resistance results in $V_{Rm,RBK} = V_{Rm,c,RBK} + V_{Rm,s,RBK} = 352 + 223 = 575$ kN.

Table 5.13: Shear resistance for $x = 1.725$,..,2.903 m and $a = 2.903$ m

x [m]	**1.725**	**1.8**	**1.85**	**1.9**	**1.95**	**2**	**2.051**	**2.453**	**2.903**
$V_{Rm,c,RBK}$ [kN]	352	354	355	357	358	359	361	369	372
$V_{Rm,s,RBK}$ [kN]	223	224	225	226	227	228	229	236	239
$V_{Rm,RBK}$ [kN]	575	578	581	583	585	587	590	605	612

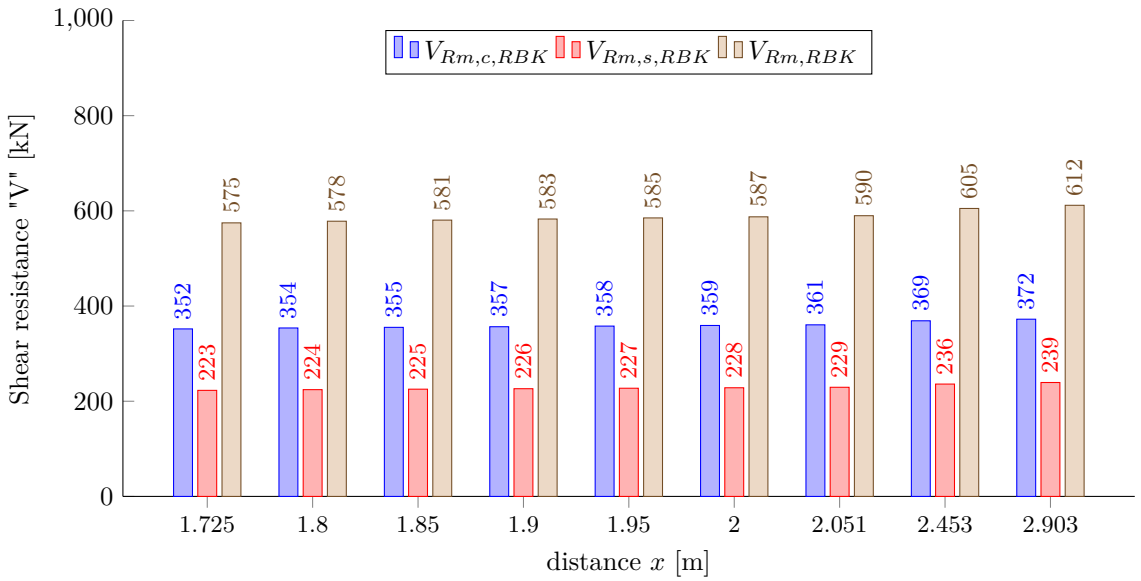

Figure 5.11: Shear resistance for $x = 1.725,..,2.903$ m and $a = 2.903$ m with $\theta = 30°$

Changing the angle of the compression chord to $\theta = 21.8°$ (lower limit for θ in EC2) results in a total shear resistance of $V_{Rm,RBK} = V_{Rm,c,RBK} + V_{Rm,s,RBK} = 352 + 322 = 674$ kN for $x = 1.725$ m. Note that the expression given in Equation 5.55 is only valid for $\theta = 30°$, so changing θ is not allowed according to the RBK.

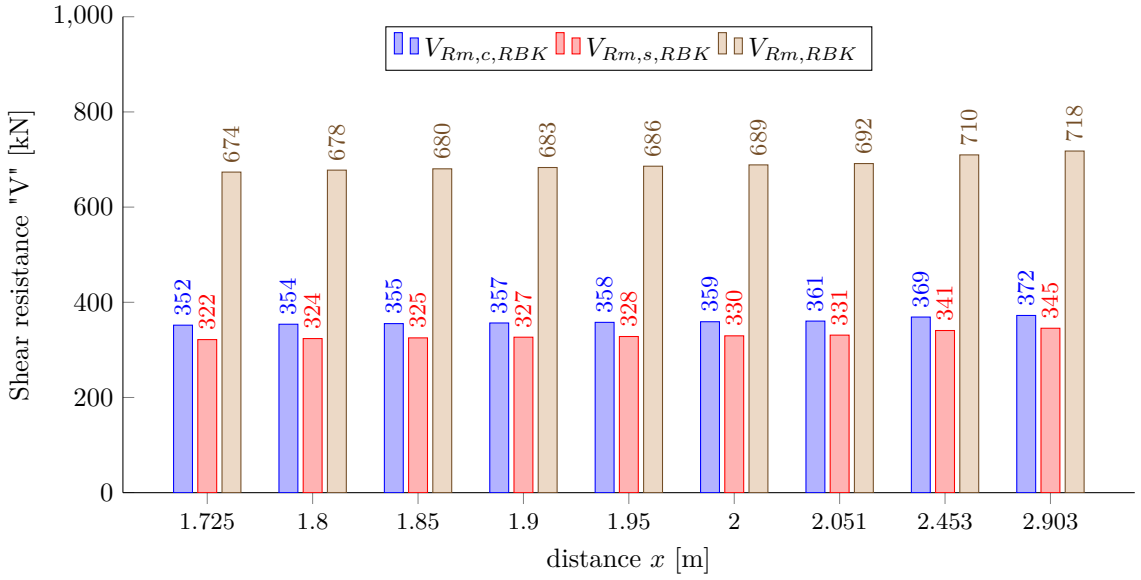

Figure 5.12: Shear resistance for $x = 1.725,..,2.903$ m and $a = 2.903$ m with $\theta = 21.8°$

5.6. EC2 DRAFT 2018

The EC2 draft 2018 expressions for calculating the shear resistance of a concrete member with- and without shear reinforcement are given in Chapter 2.11. This code provision uses a different procedure for determining the shear resistance of a (prestressed) concrete member. two different approaches depending on the presence of shear reinforcement. For members without shear reinforcement distinction is made between flexural-shear failure and shear-tension failure. The strut-and-tie method used for members with shear reinforcement makes no distinction between the two failure modes, because after the concrete is cracked the shear reinforcement should take over shear force. This is different from the approaches according to the ACI and the AASHTO, where the nominal shear resistance is a sum of the inclined cracking load plus the contribution of the stirrups. Another important difference is that EC2 follows the principle of prestressing is preloading. In the first sub-paragraph, the values used for determining the shear resistance are given. In the second sub-paragraph a detailed calculation is done for the shear resistance of the Helperzoom girder. In the last sub-paragraph, a summary for the shear resistances of the other cross-sections is given.

5.6.1. Values used for EC2 draft 2018

Table 5.14 provides the values used for the shear resistance at $x = 1.725$ m.

Table 5.14: Values used for $x = 1.725$ m and $a = 2.903$ m

	Value	Units	Commentary
A_p	3234	mm^2	$= 7 \cdot 462$
A_s	314	mm^2	bottom two layers of tension reinforcement
A_{sw}	157	mm^2	$0.25\pi\phi_v^2 * 2 = 2$ legs per 400 mm
b_w	200	mm	width of the web
d	805	mm	$= \frac{d_s^2 A_s + d_p^2 A_p}{d_s A_s + d_p A_p}$
d_{dg}	39	mm	$= 16 + D_{lower} \cdot \left(\frac{60}{f_{cm}}\right)^2$
D_{lower}	25	mm	assumption for lowest D_{max}
d_s	1065	mm	$h - cover - \phi_v - 0.5\phi_s = 1110 - 30 - 10 - 5$
f_{cm}	62.6	MPa	see Chapter 3.2.1
f_{ywm}	454	MPa	f_{ym} used, see Chapter 3.2.3
s	400	mm	spacing transverse reinforcement
z	725	mm	$= 0.9d$
ρ_l	0.0218	-	$= \frac{d_s A_s + d_p A_p}{b_w \cdot d^2}$

5.6.2. Nominal shear resistance without shear reinforcement

The inclined cracking load is the shear stress resistance of the concrete multiplied by the effective shear area:

$$V_{Rm,c} = \tau_{Rmc} \cdot b_w \cdot d \tag{5.56}$$

For prestressed members the effective depth needs to be replaced by a mechanical shear span a_v in the calculation for the shear stress resistance. This factor includes the positive effect of an axial compressive force N_{Ed} from prestressing. Usually in the design a_{cs} is calculated with Equation 2.47, which depends on the internal forces M_E, N_E and V_E. It is concluded that the external applied load has to be unreasonably large compared to the obtained $V_{Rm,c}$ to obtain $a_{cs} \geq d$. The maximum value for the shear stress resistance is obtained when the effective shear span a_{cd} equals d.

The minimum value for the mechanical shear span a_v:

$$a_v = \sqrt{\frac{a_{cs}}{4} \cdot d} = \sqrt{\frac{1}{4} \cdot 805^2} = 403 \text{ mm} \tag{5.57}$$

This shear stress resistance must be higher than the minimum shear resistance:

$$\tau_{Rmc,min} = 10 \cdot \sqrt{\frac{f_{cm}}{f_{ym}} \cdot \frac{d_{dg}}{a_v}} = 10 \cdot \sqrt{\frac{62.6}{454} \cdot \frac{39}{403}} = 1.155 \text{ MPa} \tag{5.58}$$

The shear stress resistance of the concrete in [MPa] is calculated as follows:

$$\begin{aligned} \tau_{Rm,c} &\geq \tau_{Rmc,min} \\ 0.6 \cdot \left(100\rho_l \cdot f_{cm} \cdot \frac{d_{dg}}{a_v}\right)^{1/3} &\geq 1.155 \\ 0.6 \cdot \left(100 \cdot 0.0218 \cdot 62.6 \cdot \frac{39}{403}\right)^{1/3} &\geq 1.155 \\ \text{CHECK:} \qquad 1.418 &\geq 1.155 \qquad \textbf{OK} \end{aligned} \tag{5.59}$$

The inclined cracking load results in (note that d is used here instead of a_v):

$$V_{Rm,c} = 1.418 \cdot 200 \cdot 805 = 228 \text{ kN} \tag{5.60}$$

When the area of the prestressing A_p is unfavorable for the effective depth d in the calculation of the shear resistance, A_p may be omitted in the calculation for d. The effective depth d then equals $d_s = 1065$ mm according to 8.2.2(5). The inclined cracking load results in:

$$V_{Rm,c} = 1.418 \cdot 200 \cdot 1065 = 302 \text{ kN} \tag{5.61}$$

5.6.3. Nominal shear resistance with shear reinforcement

The calculation of the shear resistance with shear reinforcement is based on a compression field. The range for the inclination of the compression field for prestressed members with a compression zone/chord lower than $0.25d$ equals:

$$19.08° \leq \theta \leq 45° \tag{5.62}$$

According to the sectional analysis for both flexure at ultimate (Chapter 5.4.2) and shear at ultimate (Chapter 4.6.5) the height of the compression chord is lower than $0.25d$. The shear resistance for $\theta_{min} = 19.08°$ with $\nu = 0.5$ for both yielding of the shear reinforcement and crushing/failure of the compression field equals:

$$\begin{aligned} V_R &= \frac{A_{sw}}{s} \cdot z \cdot f_{ywm} \cdot \cot\theta \leq b_w \cdot z \cdot \frac{\nu \cdot f_{cm}}{2} \\ V_R &= \frac{157}{400} \cdot 725 \cdot 454 \cdot \cot(19.08) \leq 200 \cdot 725 \cdot \frac{0.5 \cdot 62.6}{2} \\ V_R &= 373.5 \leq 2266.6 \text{ kN} \end{aligned} \tag{5.63}$$

This results in a shear resistance for the shear reinforcement $V_{Rm,s} = 373.5$ kN. Crushing of the concrete/failure of the compression field occurs at $V_{Rm,max} = 2267$ kN.

5.6.4. Failure of the compression field

Crushing of the concrete is calculated with a predetermined factor $\nu = 0.5$ when the inclination of the compression field is taken between the limits in Equation 5.62. The factor ν can also be calculated on the basis of the state of strains which is based on MCFT. Figure 5.13 shows the development of ν for different values of θ and ε_x. Note that $\theta = 57°$ is not allowed according to EC2 draft 2018, as the maximum value is: $\cot\theta = 1.0 \Rightarrow \theta = 45°$. Also the EC2 draft 2018 does not allow negative longitudinal strains ($\varepsilon_x < 0$) and has no maximum value for the positive longitudinal strains. According to the AASHTO, the values should be in range of: $-0.0002 \leq \varepsilon_x \leq 0.001$.

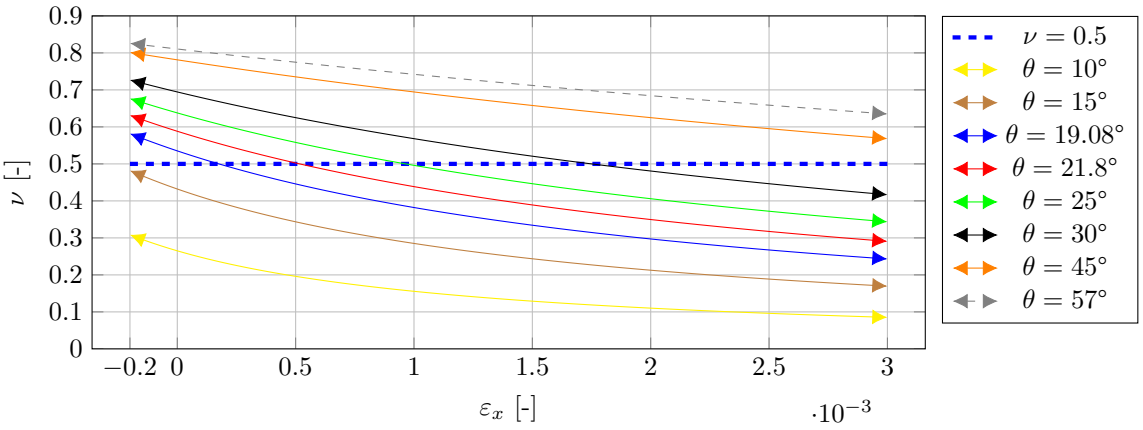

Figure 5.13: Values for ν for different values of θ for $-0.0002 \leq \varepsilon_x \leq 0.003$

The longitudinal strain ε_x is calculated by the average strain between the top ε_{xc} and bottom ε_{xt} chord. Note that in case the flexural compression (top) chord is in compression, the strains ε_{xc} are taken as zero (conservative approach). The strains in the flexural tension (bottom) chord ε_{xt} are calculated by dividing the force in the flexural tension chord F_T by two times the areas multiplied by the modulus of elasticity of the prestressing and longitudinal reinforcement respectively, see Equation 5.64. The internal forces due to the external load, self weight and prestressing are accounted for in M_E, V_E and N_E as the EC2, RBK and EC2 draft 2018 follow the principle of prestressing is preloading. This is different from the AASHTO, where $N_u = 0$ for prestressing. This is added in the term $-A_{ps}f_{po}$ for the calculation of the longitudinal strains at mid depth. The moment and shear forces are not known beforehand so iterations are required. The following procedure is followed:

- Assume a value for $F_{exp,assumed}$ to get the internal moment M_E and shear force V_E;
- Assume a θ (can be lower than $\theta_{min} = 19.08°$);
- Calculate the longitudinal strain ε_x (N_E is negative for compression);

$$\varepsilon_x = \frac{F_T}{2\left(E_sA_s + E_pA_p\left[0.5 + \frac{e_p}{z}\right]\right)} = \frac{\frac{M_E}{z} + 0.5|V_E| \cdot \cot\theta + 0.5N_E}{2\left(E_sA_s + E_pA_p\left[0.5 + \frac{e_p}{z}\right]\right)} \geq 0 \tag{5.64}$$

- With a limit for the force in the flexural tension chord:

$$F_T \leq \frac{M_{E,max}}{z} + 0.5N_E \tag{5.65}$$

- Calculate the factor ν;

$$\nu = \frac{1}{1.2 + 80 \cdot \left(\varepsilon_x + (\varepsilon_x + 0.001) \cdot \cot^2\theta\right)} \leq 1.0 \tag{5.66}$$

- Calculate the force required for failure of the compression field, provided that the stress is lower than the maximum stress calculated in Equation 2.51;

$$V_{R,max} = b_w \cdot z \cdot \frac{\nu \cdot f_{cm}}{2} \tag{5.67}$$

- Calculate the external load with:

$$V_{tot} = F_{exp} \cdot \frac{L_{span} - a}{L_{span}} + V_p + V_{sw} \Rightarrow F_{exp} = \frac{V_{tot} - V_p - V_{sw}}{0.7} \tag{5.68}$$

- Check if the external load equals the assumed $F_{exp,assumed}$, if not repeat until $F_{exp} = F_{exp,assumed}$.

The first calculation is done for $\theta = 19.08°$. The external load is assumed as $F_{exp} = 1890$ kN as this is the failure load for HPZ1. The internal forces follow from the spreadsheet: $M_{E,max} = 3408$ kNm, $M_E = 1926$ kNm, $V_E = 1262$ kN and $N_E = -1598$ kN. $M_{E,max}$ is taken from $x = 2.903$ m as this is the cross-section under the load where the maximum moment in the member occurs. The average eccentricity of the prestressing tendons at $x = 1.725$ m is $e_p = 278$ mm. The longitudinal strain equals:

$$\varepsilon_x = \frac{\frac{1926 \cdot 10^6}{725} + 0.5 \cdot 1262 \cdot 10^3 \cdot \cot(19.08°) - 0.5 \cdot 1598 \cdot 10^3}{2\left(200{,}000 \cdot 314 + 185{,}000 \cdot 3234\left[0.5 + \frac{278}{725}\right]\right)} = 0.00311 \tag{5.69}$$

Note that 89% of the area of the prestressing steel is allowed in the calculation for the longitudinal strain. The force in the flexural tension chord must be lower than the maximum allowed force:

$$\frac{1926 \cdot 10^6}{725} + 0.5 \cdot 1262 \cdot 10^3 \cdot \cot(19.08°) - 0.5 \cdot 1598 \cdot 10^3 \leq \frac{3408 \cdot 10^6}{725} - 0.5 \cdot 1598 \cdot 10^3 \tag{5.70}$$

CHECK: $3683 \leq 3905$ kN **OK**

The value for ν equals:

$$\nu = \frac{1}{1.2 + 80 \cdot \left(0.00311 + (0.00311 + 0.001) \cdot \cot^2(19.08°)\right)} = 0.238 \leq 1.0 \tag{5.71}$$

Check the stress in the compression field:

$$\sigma_c = \frac{1262 \cdot 10^3}{200 \cdot 725} \cdot \left(\cot(19.08°) + \tan(19.08°)\right) \leq 0.238 \cdot 62.6 \tag{5.72}$$

CHECK: $28.20 \leq 14.90$ MPa **NOT OK**

Although the stress exceeds the limit, the procedure is continued. The force required for failure in the compression field results in:

$$V_{R,max} = 200 \cdot 725 \cdot \frac{0.238 \cdot 62.6}{2} = 1080 \text{ kN} \tag{5.73}$$

The external load that corresponds to $V_{R,max}$ is:

$$F_{exp} = \frac{V_{R,max} - V_{p+sw}}{0.7} = \frac{1080 + 56.83}{0.7} = 1628 \text{ kN} \tag{5.74}$$

This means the assumed value of the external load is not equal to the calculated value. New iterations are done and the end result is given. For an assumed external load $F_{exp} = 1733$ kN, the longitudinal strain results in: $\varepsilon_x = 0.00276$. The requirements for the stress in the compression field are still not met: $\sigma_c = 25.74$ MPa vs. $\sigma_{c,max} = 15.91$ MPa. The shear force at which the compression field fails: $V_{R,max} = 1152$ kN, which corresponds to $F_{exp} = 1733$ kN.

Chapter 2.9.2 mentioned that the maximum shear resistance is obtained when yielding of the stirrups occurs simultaneously with failure of the compression field. With the EC2 draft 2018 the rotating strut is allowed to be lower than 21.8°. Solving the inclination of the rotating strut for which $V_R = V_{R,max}$ and $F_{exp,asssumed} = F_{exp,calc}$ holds, results in $\theta = 10.49°$ and $V_R = V_{R,max} = 697$ kN. This corresponds to $F_{exp} = 1081$ kN.

5.6.5. Different procedures for calculating the longitudinal strain

Comparing the longitudinal strain obtained in the previous paragraph with the results from the AASHTO (Chapter 5.3.2), shear at ultimate (Chapter 4.6.5) and the strains obtained from the experiment (Chapter 4.6.4), the value for the longitudinal strain is (much) higher. Therefore different calculations are done:

- The additional tensile axial force $N_V = |V_E| \cdot \cot\theta$ due to shear V_E is partly taken by the shear zone (web). This results in an axial tensile force in the flexural tension chord $N_V = |V_E| \cdot \cot\theta + N_{Ew}$. It is assumed that $N_{Ew} = -N_E$;

– Calculating the resistance according to the longitudinal strains obtained from the analytical solution for shear at ultimate with $F_{exp} = 1890$ kN;

– Calculating the resistance according to the longitudinal strains obtained from the LVDTs (experiment);

The results are given in Table 5.15 and Figure 5.14. The first column gives the result from the calculations in Chapter 5.6.4. The second through fourth column give the results where a part of the additional tensile axial force is taken by the web (N_{Ew}) for $\theta = 19.08°, 17.00°$ and $15.00°$. The fifth column gives the result with the longitudinal strains obtained from the analytical solution. The sixth and seventh column gives the result with the longitudinal strains obtained from the LVDTs for HPZ1 and HPZ2.

Table 5.15: Failure of the compression field with different procedures and values for θ

Procedure:	**Original**	$+N_{Ew}$**(1)**	$+N_{Ew}$**(2)**	$+N_{Ew}$**(3)**	**Analytical**	**LVDTs(1)**	**LVDTs(2)**
$F_{exp,assumed}$ [kN]	1733	1863	1681	1498	1890	1890	1850
θ [°]	19.08	19.08	17.00	15.00	15.11	14.86	18.90
F_T [kN]	3263416	2810843	2536736	2251873			
$F_{T,max}$ [kN]	3465579	3828117	3319213	2807679			
$F_T < F_{T,max}$	TRUE	TRUE	TRUE	TRUE			
ε_{xt} [-]	0.00552	0.00475	0.00429	0.00381			
ε_x [-]	0.00276	0.00238	0.00214	0.00190	0.00110	0.00103	0.00235
ν [-]	0.254	0.274	0.246	0.218	0.278	0.278	0.272
σ_c [MPa]	25.74	27.77	27.54	27.28	34.62	35.14	16.87
$\sigma_{c,max}$ [MPa]	15.91	17.15	15.4	13.64	17.42	17.42	17.03
$\sigma_c < \sigma_{c,max}$	FALSE	FALSE	FALSE	FALSE	FALSE	FALSE	TRUE
$V_{Rm,s}$ [kN]	373	373	423	482	479	487	377
$V_{Rm,max}$ [kN]	1152	1243	1116	988	1262	1262	1234
F_{exp} [kN]	1733	1863	1681	1498	1890	1890	1850

It is important to note that ε_{xt} for all calculations, except from the LVDTs, is calculated at $y = d_p = 770$ mm from the top of the girder. The average longitudinal strain is then calculated at a height of the girder $y = d_p - 0.5 \cdot z = 770 - 0.5 \cdot 725 = 407.5$ mm from the top of the girder. The longitudinal strains for HPZ1: $\mu\varepsilon_{xt,LVDT} = 1796$ are taken from tendon 6, measured at $x = 1658$ mm from the support, but for simplicity considered at $x = 1725$ mm from the support. These strains are measured at $y = 706$ mm and cannot be 'averaged' by just dividing by two. Therefore $\varepsilon_{x,LVDT}$ is calculated as follows (considering a linear strain diagram and the strains at the top of the girder as zero):

$$\mu\varepsilon_{x,LVDT} = \mu\varepsilon_{xt,LVDT} \cdot \frac{407.5}{706} = 1032 \Rightarrow \varepsilon_{x,LVDT} = 0.00103 \tag{5.75}$$

For calculating the longitudinal strains according to the analytical results, the strains in the top chord are not considered zero (although the strains are very small): $\varepsilon_{xc} = -0.000731$ and the strains in the prestressing steel is averaged: $\varepsilon_{xt} = 0.0029$. This results in:

$$\varepsilon_{x,ANALYTICAL} = \frac{-0.000731 + 0.0029}{2} = 0.0011 \tag{5.76}$$

Another note is that in every calculation, except for LVDTs(2), the maximum stress in the compression field is exceeded $\sigma_c > \sigma_{c,max}$. Solving the inclination of the rotating strut for which $V_R = V_{R,max}$ and $F_{exp,asssumed} = F_{exp,calc}$ holds, results in:

Table 5.16: Shear resistance for $V_{Rm,s} = V_{Rm,max}$ with different procedures and values for θ

Procedure:	$N_{Ew} = 0$	$+N_{Ew}$	**Analytical**	**LVDTs(1)**	**LVDTs(2)**
$F_{exp,assumed}$ [kN]	1018	1071	1290	1111	959
θ [°]	11.19	10.60	11.45	10.19	11.91
$V_{Rm,s} = V_{Rm,max}$ [kN]	653	690	843	718	612
F_{exp} [kN]	1018	1071	1290	1111	959

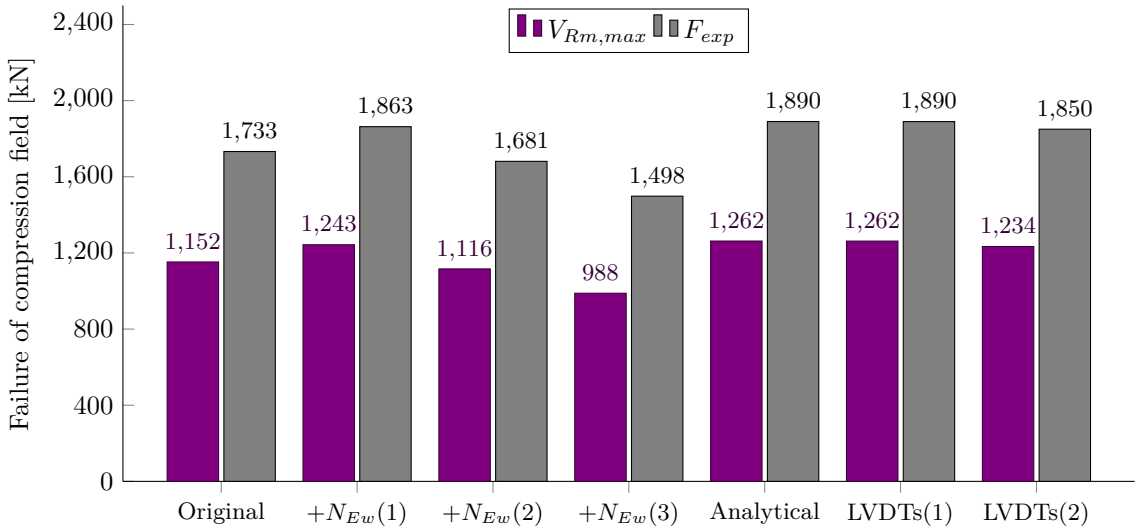

Figure 5.14: Failure of the compression field with different procedures and values for θ

Additional information for Figure 5.14:

- First column: Original, result from the calculations in Chapter 5.6.4 with $\theta = 19.08°$;
- Second column: $+N_{Ew}(1)$, $N_V = |V_E| \cdot \cot\theta - N_E$ with $\theta = 19.08°$;
- Third column: $+N_{Ew}(2)$, $N_V = |V_E| \cdot \cot\theta - N_E$ with $\theta = 17.00°$;
- Fourth column: $+N_{Ew}(3)$, $N_V = |V_E| \cdot \cot\theta - N_E$ with $\theta = 15.00°$;
- Fifth column: Analytical, result with ε_x obtained from the analytical solution with $\theta = 15.11°$;
- Sixth column: LVDTs(1), result with ε_x obtained from the LVDTs (HPZ1) with $\theta = 14.86°$;
- Seventh column: LVDTs(2), result with ε_x obtained from the LVDTs (HPZ2) with $\theta = 18.90°$.

5.6.6. EC2 draft 2018 shear resistance summary

The calculations for the shear resistance according to the EC2 draft 2018 are done for cross-sections $x = 1.725$,..,2.051 m. This code provision states that regions closer than d in mm to the end support **and** a high concentrated load do not have to be checked. The length for $d = 851$ mm is taken from the cross-section where the external load is placed, $x = 2.903$ m. This means that for EC2 draft 2018 the following range of cross-sections are considered: $x = 1.725$,..,2.051 m ($2.903 - 0.851 \approx 2.051$ m).

First two detailed shear strength verifications are done, one for the inclined cracking load and one for the shear resistance of the shear reinforcement. For the calculations of the inclined cracking load, the acting axial compressive force from prestressing is 'hidden' in the mechanical shear span a_v. The effective shear depth d is, in contrary to the 'current' EC2, defined with an expression that takes into account the effective depth of the prestressing tendons. Also the longitudinal tension reinforcement ratio ρ_l is defined in this way. The value for the internal lever arm is taken as $z = 0.9d$ in the calculations for the shear resistance, although the value was higher in the sectional analyses (flexural ultimate and shear ultimate). The values used in the calculations are given in Table 5.17.

Table 5.17: Values used for calculating the shear resistance for $x = 1.725$,..,2.051 m and $a = 2.903$ m

x [m]	**1.725**	**1.8**	**1.85**	**1.9**	**1.95**	**2**	**2.051**
d [mm]	805	809	812	815	817	820	823
z [mm]	725	728	731	733	736	738	741
ρ_l [-]	0.0218	0.0217	0.0216	0.0216	0.0215	0.0214	0.0214
a_{cs} [mm]	805	809	812	815	817	820	823
a_v [mm]	403	405	406	407	409	410	411

The shear resistance for the inclined cracking load, shear reinforcement and crushing of the concrete are given in Table 5.18. For the internal lever arm d including the area of the prestressing steel, the shear *stress* resistance of the concrete is lower for cross-sections closer to the external load. The higher internal lever arm causes the inclined cracking load to be higher for cross-sections closer to the external load. The critical cross-section is $x = 1.725$ m with $V_{Rm,c} = 228$ kN. For the internal lever arm $d = d_s$ the inclined cracking load is higher, but is lowest for cross-section $x = 2.051$ m with $V_{Rm,c} = 298$ kN. Overall, the inclined cracking load is almost constant for every cross-section.

The calculations for the shear reinforcement and failure of the compression chord are done with $\theta_{min} = 19.08°$ and $F_{exp} = 1890$ kN (only to check the stress in the compression field) for cross-sections $x = 1.725$,..,2.051 m, see Table 5.18 and Figure 5.15. The heights of the compression zones x are smaller than $0.25d$ for all cross-sections. The stress in the compression field is lower than $\nu \cdot f_{cm}$ with $\nu = 0.5$. Cross-section $x = 1.725$ m is the most critical cross-section with a $V_{Rm,s} = 373$ kN for yielding of the shear reinforcement and $V_{Rm,max} = 2267$ kN for failure of the compression field.

Table 5.18: Shear resistance for $x = 1.725$,..,2.051 m and $a = 2.051$ m

x [m]	**1.725**	**1.8**	**1.85**	**1.9**	**1.95**	**2**	**2.051**
$\tau_{Rm,c}$ [MPa]	1.418	1.413	1.410	1.407	1.404	1.402	1.398
$\tau_{Rmc,min}$ [MPa]	1.155	1.152	1.150	1.148	1.146	1.144	1.143
$\tau_{Rm,c} > \tau_{Rmc,min}$	TRUE	TRUE	TRUE	TRUE	TRUE	TRUE	TRUE
$V_{Rm,c}$ [d] [kN]	228	229	229	229	230	230	230
$V_{Rm,c}$ [$d = d_s$] [kN]	302	301	300	300	299	299	298
x [mm]	172	170	169	168	167	166	166
$x < 0.25d$	TRUE	TRUE	TRUE	TRUE	TRUE	TRUE	TRUE
σ_c [MPa]	28.20	28.04	27.94	27.85	27.75	27.65	27.55
Check: $\sigma_c < v \cdot f_{cm}$	TRUE	TRUE	TRUE	TRUE	TRUE	TRUE	TRUE
$V_{Rm,s}$ [kN]	373	375	377	378	379	380	382
$V_{Rm,max}$ [kN]	2267	2278	2286	2293	2301	2309	2317

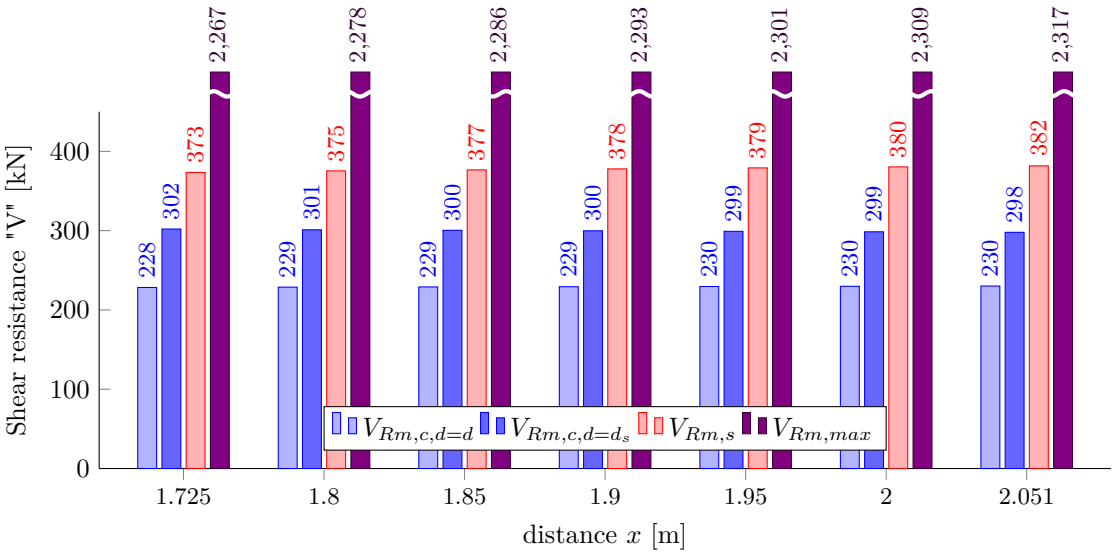

Figure 5.15: Shear resistance for $x = 1.725$,..,2.903 m and $a = 2.903$ m with $\theta = 19.08°$ and $\nu = 0.5$

The EC2 draft 2018 is the only code provision that allows the inclination of the compression field to be lower than $\theta = 19.08°$. It is also the only code provision that includes the inclination of the compression field in the calculation for failure of the compression field/crushing of the concrete. This analysis is only done for cross-section $x = 1.725$ m and shown in the previous paragraph.

5.7. Discussion results analytical analysis

The analytical analysis consists of the Euler-Bernoulli theory (Chapter 5.1) and five code provisions: ACI (Chapter 5.2), AASHTO (Chapter 5.3), EC2 (Chapter 5.4), RBK (Chapter 5.5) and EC2 draft 2018 (Chapter 5.6). First the results from the Euler-Bernoulli theory are summarized. In Chapter 5.7.2 through 5.7.5 the differences and similarities are given for the five considered code provisions. The nominal shear resistances are given in Chapter 5.7.6 and the results for the failure of the compression field are given in Chapter 5.7.7. **All calculations are based on** $N_p = 1598$ kN, under the assumption that the loads on the girder are equal for HPZ1 and HPZ2 and that the failure load for both HPZ1 and HPZ2 is $F_{exp} = 1890$ kN unless specifically stated otherwise.

5.7.1. Results from Euler-Bernoulli theory

The Euler-Bernoulli theory is used to calculate the principal stresses along the height of the girder for multiple cross-sections. Flexural cracking and shear-tension failure can be predicted, because uncracked concrete is in a linear-elastic stage. According to the theory, the first flexural crack occurs at $x = 2.903$ m with $F_{exp} = 714$ kN and $f_{ctm,sp} = 5.4$ MPa and diagonal-tension cracking in the bottom of the web ($\theta = 30°$) at $x = 1.725$ m with $F_{exp} = 1283$ kN and $f_{ctm} = 4.86$ MPa. Considering the results from HPZ1 and HPZ2 the first flexural crack occurred at $F_{exp} \approx 950$,..,1000 kN, which is higher than the calculated 714 kN. Solving for the prestressing force results in $N_p = 2419$,..,2593 kN, instead of the used value $N_p = 1598$ kN.

5.7.2. Effective depth and internal lever arm

The effective depth d and internal lever arm z differs for every code, see Table 5.19. For the ACI, AASHTO and EC2 2018 the effective depth d is calculated by an mean effective depth between the longitudinal reinforcement bars and the prestressing tendons. The EC2 and RBK do not explicitly give an expression to calculate d. However, according to the figures d is taken from the extreme compression fiber to the reinforcement steel in the tension zone. The area of the reinforcement steel is almost negligible to the area of the prestressing tendons ($A_{sl} = 314$ mm^2 vs. $A_p = 3234$ mm^2), therefore the effective depth of the tendons d_p is chosen. The ACI has a minimum value for the effective depth $d = 0.8h = 888$ mm. This value is the highest among the codes (+10-15%) and might be too unconservative.

The internal lever arm z (or effective shear depth d_v in AASHTO) can be calculated with a sectional analysis or can be taken as $0.9d$. According to the calculations $0.9d$ is a bit conservative as the values for the internal lever arm range from $x = 0.91$,..,$0.94d$, but is a good enough approximation. For the EC2 and RBK $0.94d$ is used and for EC2 draft 2018 $0.9d_{mean}$. The AASHTO requires a minimum of $d_v = \max(0.9d_e, 0.72h) = 0.72h = 799$ mm, which is ∼11% higher than the EC2, RBK and EC2 draft 2018. Note that the ACI does not use the internal lever arm z in any of the calculations for the shear resistance.

Table 5.19: Effective depth and effective shear depths for the five code provisions for $x = 1.725$ m

Code	Effective depth d	Min. internal lever arm z	Used internal lever arm z
ACI	$d = 0.8h = 888$ mm	–	–
AASHTO	$d = d_e = 777$ mm	$d_v = 0.72h = 799$ mm	$d_v = 799$ mm
EC2	$d = d_p = 770$ mm	$z = 0.9d = 693$ mm	$z = 0.94d = 721$ mm
RBK	$d = d_p = 770$ mm	$z = 0.9d = 693$ mm	$z = 0.94d = 721$ mm
EC2 2018	$d = d_{mean} = 805$ mm	$z = 0.9d_{mean} = 725$ mm	$z = 0.9d_{mean} = 725$ mm

5.7.3. Critical cross-section

Every code provision has its own position or region for the 'critical cross-section' for the verification of the shear resistance, see Table 5.20. All code provisions state that the critical cross-section is at a certain length away from the face of the support. The EC2 draft 2018 also includes a certain length away from the concentrated load. In the last column the positions or regions are given that are critical to shear. The width of the support is assumed zero.

Table 5.20: Positions or regions for the shear strength verification for the five code provisions

Code	Region/ position	Region or position of the critical cross-section	Region/ position x [m]
ACI	position	$h/2$ from the face of the support (prestressed members)	0.555
AASHTO	position	$\max(d_v, 0.5d_v \cot\theta)$ from the internal face of the support	0.779
EC2	region	between z_{bottom} from the support to the external load	0.618,..,2.903
RBK	region	between z_{bottom} from the support to the external load	0.618,..,2.903
EC2 2018	region	between d_{mean} from the support **and** concentrated load	0.725,..,2.051

For the Helperzoom girders it is not of interest to do a shear strength verification for cross-sections closer than 1.725 m from the end support, because the width of the web is larger and will result in a higher shear resistance. This is the reason that for all code provisions cross-section $x = 1.725$ m is the first assumed critical cross-section. Although shear strength verifications are done for other cross-sections up to $x = 2.903$ m, these results might not be of interest for the critical cross-section. Shear-tension- and flexure-shear failure cannot occur in cross-sections closer than a 45° inclined line from the concentrated load to the centroidal axis and bottom of the girder respectively, as maximum shear will occur at an inclination of the compression field $\theta = 45°$ (which holds for reinforced concrete). This means that, considering an inclination of $\theta = 45°$, shear-tension failure will most likely occur in regions closer than $2.903 - 0.492 = 2.411$ m from the support. Figure 5.1 already showed that the highest principal stresses are at the bottom of the web, which reduces the region of interest even more with $2.903 - 0.680 = 2.223$ m to $x = 1.725$,..,2.223 m.

The ACI and AASHTO give a position for the critical cross-section, $x = 0.555$ and 0.779 m respectively. Both are closer than the first assumed critical cross-section $x = 1.725$ m, therefore only $x = 1.725$ m is considered. EC2, RBK and EC2 draft 2018 give a region for the shear strength verification. The first cross-section for EC2 and RBK is a 45° inclination from the face of the support to the centroid of the member ($= z_{bottom} = 0.618$ m), which results in a region of $x = 0.618$,..,2.903 m. EC2 draft 2018 reduces the region to $2.903 - 805 \approx 2.051$ m which gives the following region of interest for shear failure: $x = 1.725$,..,2.051 m. This range has been the starting point of the potential critical cross-sections, as $x = 2.051$ m is the position where the assumed inclined shear crack $\theta = 30°$ crosses the centroidal axis of the girder, see Figure 3.5.

5.7.4. Inclination of the compression field

Three out of five code provisions either calculates or lets the designer choose the inclination of the compression field θ, see Table 5.21. Every code provision uses θ for the contribution of the shear reinforcement $V_{R,s}$ to the shear resistance. The AASHTO also uses θ indirectly for the calculation of β for aggregate interlocking that is used in the expression for the concrete shear resistance $V_{R,c}$. The EC2 and EC2 draft 2018 are the only code provisions that allow θ to be used for failure of the compression field $V_{R,max}$. For EC2 the prescribed range for θ must be used and for EC2 draft 2018 when the factor ν is calculated on the basis of the state of strains. The last column of Table 5.21 gives the values for θ that are used or calculated for the shear resistance of the member for cross-section $x = 1.725$ m. From this column it can be concluded that the value for θ between the five code provisions differ a lot.

- **ACI:** θ is considered the same for reinforced- and prestressed concrete members. It is conservatively taken as $\theta = 45°$, which is correct for reinforced concrete but not for prestressed concrete members.

- **AASHTO:** Two values for θ are obtained for $f_{po} = 0.27f_{pu}$: 27.57° (tables) and 31.02° (algebraic). It is important to note that the algebraic approach consists of a simplified linear relationship between θ and ε_s. This linear relationship is safely in between the lower limit 'failure of the shear reinforcement' and the upper limit 'crushing of the concrete' and is based on $\nu/f'_c = 0.25$, see Figure 5.6. The values obtained from the tables are based on different ν/f'_c-ratios, which are more accurate but at the cost that the iterations have to be done by hand.

Table 5.21: Range for the inclination for the compression field θ for the five code provisions

Code	Range for inclination compression field θ		Used for	Used/ calculated θ
ACI	45°	(fixed)	$V_{R,s}$	45°
AASHTO	$27.6° \leq \theta \leq 50°$	(algebraic)	$V_{R,c}$ & $V_{R,s}$	31.02°
	$18.1° \leq \theta \leq 37.3°$	(tables)		27.57°
EC2	$21.8° \leq \theta \leq 45°$		$V_{R,s}$ & $V_{R,max}$	21.8°
RBK	30°	(fixed)	$V_{R,s}$	30°
EC2 2018	$19.08° \leq \theta \leq 45°$	(original)	$V_{R,s}$	19.08°
	$\theta \leq \theta_{min} = 19.08°$	(state of strains)	$V_{R,s}$ & $V_{R,max}$	$15° - 19.08°$

– **EC2:** The designer is free to choose the inclination within $21.8° \leq \theta \leq 45°$. Note that mostly the lowest possible θ is chosen, unless crushing of the concrete becomes decisive. The chosen value for θ is 21.8°.

– **RBK:** It is explicitly stated that the expression $V_{Rm,RBK} = V_{Rm,c,RBK} + V_{Rm,s,RBK}$ is only valid if the inclination is taken as $\theta = 30°$.

– **EC2 draft 2018:** Same as EC2, but the range has a lower minimum: $19.08° \leq \theta \leq 45°$. The EC2 draft 2018 even lets the designer choose a lower inclination than the minimum $\theta_{min} = 19.08°$, but this is only allowed if the factor ν is calculated on the basis of the state of strains. According to Figure 5.13 choosing a $\theta < \theta_{min}$ results in a lower value for $\nu = 0.5$ and leads for a lower $V_{R,max}$. For the general procedure the inclination of the compression field is taken as $\theta = 19.08°$ and for the method to assess critical webs the following values are checked: $\theta = 15, 17, 19.08°$. Note that the inclination of the compression field is considered constant along the longitudinal axis of the member. In reality this inclination can vary as observed from the results of the cracking angle from the experimental analysis.

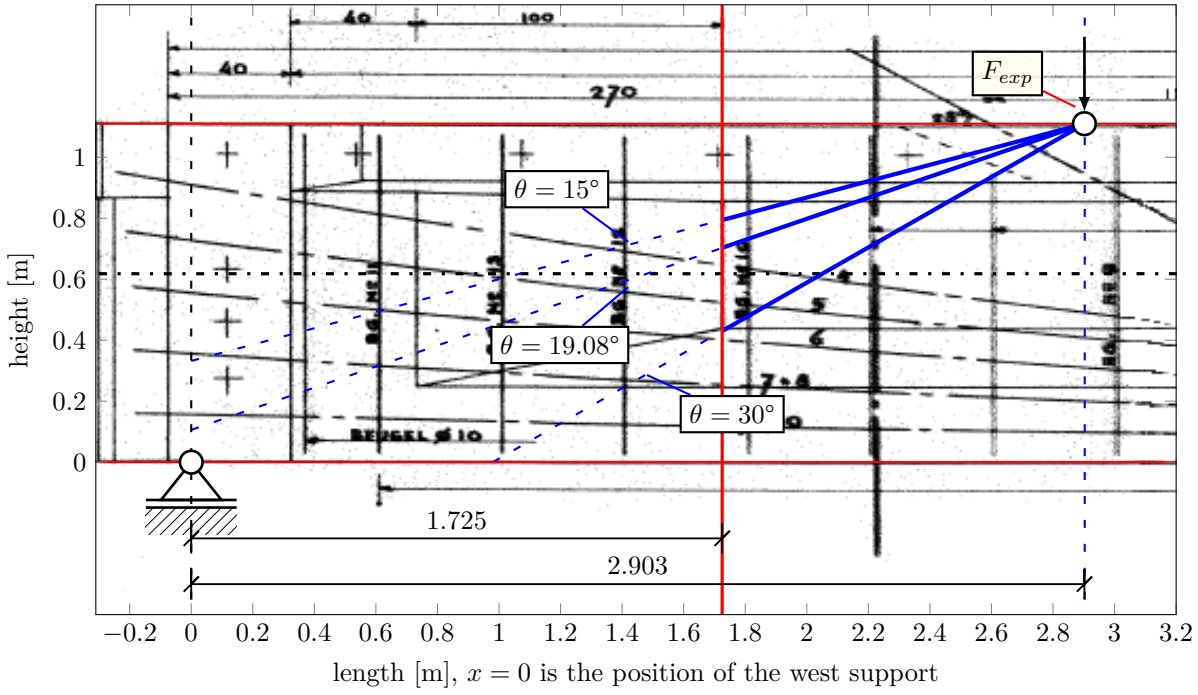

Figure 5.16: Three different inclinations of the compression field θ crossing the critical cross-section $x = 1.725$ m

Excluding the ACI, the range for the inclination of the compression field ranges from 19.08° - 31.02° when the general procedures are followed, see Figure 5.16. This seems to be in line with the assumed $\theta = 30°$ in Chapter 3.4 and the results from the experiments in Chapter 4.6.1. The EC2 draft 2018 is used to assess the web of the girder for failure of the compression field.

5.7.5. Other important differences or similarities between the codes

Next to the differences between the effective depth, critical cross-sections and inclination of the compression field, other important differences between the code provisions are worth mentioning:

- **Prestressing is preloading:** According to the EC2, RBK and EC2 draft 2018 prestressing should be accounted for in the load combination to determine the acting bending moments $M_E = M_F + M_{sw} + M_p$, shear forces $V_E = V_F + V_{sw} + V_p$ and axial forces $N_E = N_p$. This is different from the ACI and AASHTO, where prestressing is considered as an internal action and is not included in the load combination to determine $M_E = M_u = M_F + M_{sw}$, $V_E = V_u = V_F + V_{sw}$ and $N_E = N_u = 0$.
- **Nominal shear resistance:** For the ACI, AASHTO and RBK the nominal shear resistance consists of three components. It is the sum of the inclined cracking load V_c, the contribution of the shear reinforcement V_s and the vertical component of the prestressing force V_p. For the EC2 and EC2 draft 2018 the highest shear resistance of the two defines the shear resistance. This means that if concrete is cracked, the contribution of the cracked and uncracked part of the concrete is zero (no aggregate interlock) and the shear reinforcement is the only part resisting the external load.
- **Failure mechanism:** According to the ACI the lowest calculated shear resistance, flexure-shear or web-shear, is the shear resistance of the member. For the EC2 the member must be checked if it is uncracked or cracked in bending, for the calculation of shear-tension or flexural-shear failure. The other three codes do not distinguish between the shear failure modes.
- **Aggregate size:** Only the EC2 draft 2018 takes into account the effect of the aggregate size to the shear resistance.
- **Shear transfer mechanisms:** All considered code provisions account for aggregate interlock. The ACI is empirically derived and states that it accounts for all shear transfer mechanism, but without any explanation how this is incorporated or accounted for. The AASHTO is based on a simplified version of the MCFT. One model is derived to calculate the shear resistance of a (prestressed) concrete member and is based on only the longitudinal strain. A decrease of the longitudinal strain increases aggregate interlocking. Dowel action is not accounted for in this simplified version. The rest of the code provisions are based on the variable angle truss model, which takes into account both aggregate interlock and dowel action. This is indirectly accounted for with a lower inclination for the compression field θ than 45°.
- **Uncracked concrete:** None of the code provisions take into account parts of the cross-section that are uncracked, for example the top flange, when the member is cracked in bending.
- **Cross-sectional forces:** The ACI, AASHTO and EC2 draft 2018 take into account the internal forces due to the external load and self-weight (and prestressing) for the calculation of the shear resistance. The EC2 and RBK do not include these internal forces, which results in a constant shear resistance for all considered cross-sections (apart from a varying internal lever arm). Apart from the EC2 draft 2018, all codes **do not consider** the external load for the calculation for shear-compression failure.
  - The ACI only takes into account the ratio between the moment and shear forces due to the external load and self-weight for flexure-shear failure. Omitting the self-weight from M_u and V_u, the ratio becomes constant and requires no iterations, although including the self-weight hardly changes the V_u/M_u-ratio. Therefore it can be concluded that the value of the external load has **no influence** on the shear resistance.
  - The AASHTO takes into account the moment- (M_u), shear- (V_u, V_p) and axial forces ($A_{ps} \cdot f_{po}$) in the calculation for the longitudinal strains. The value for aggregate interlocking and

the inclination of the compression field depend on these strains. This results in iterative calculations, so it can be concluded that the external load **has influence** on the nominal shear resistance.

* The EC2 draft 2018 takes into account the moment- (M_E), shear- (V_E) and axial forces (N_E) for the calculation of the effective shear span a_{cs}, which is used for the shear resistance of the concrete. It was observed that these internal forces had no influence on the effective shear span, as it must be taken higher or equal to d. Unless the external load was taken more than three times higher than the shear stress resistance of the concrete $\tau_{Rm,c}$, the external load had **no influence** on the resistance. For failure of the compression field the external load influences the chord forces in the calculation for the longitudinal strains. For this shear failure the external load **has influence** on the resistance.

It can be concluded that for the EC2, RBK and EC2 draft 2018 (general procedure) other cross-sections are not worth verifying for the shear resistance when the cross-sectional properties do not or barely change in the region where a shear strength verification must be done.

– The AASHTO provides two methods for the shear resistance, an algebraic and table method. The algebraic method is a simplification that inaccurately calculates the values for β and θ for low values of the longitudinal strain ε_s. Although the two methods almost predict the same nominal shear resistance, the simplified version underestimates the contribution of the transverse reinforcement and overestimates the contribution of aggregate interlock as can be seen in Figure 5.17.

– The calculations based on the state of strains (AASHTO and EC2 draft 2018) conservatively take $\varepsilon_c = 0$ for the longitudinal strains at the tension reinforcement ε_s or at mid depth of the girder ε_x. Although the value for the strains at the compression chord are very small, neglecting these compressive strains result in higher strains in the calculations. Subsequently this results in a lower shear resistance.

5.7.6. Nominal shear resistance

It is of interest to compare the experimentally observed external load with the nominal shear resistance of the girder. The previous paragraph already concluded that only two codes (AASHTO and EC2 draft 2018) are influenced by the external load. When $F_{exp} = 1890$ kN (failure load for HPZ1) is used in these design codes, so without the use of iterations, the nominal shear resistance reaches such a low value that the use of iterations are inevitable to obtain an accurate value for the nominal shear resistance.

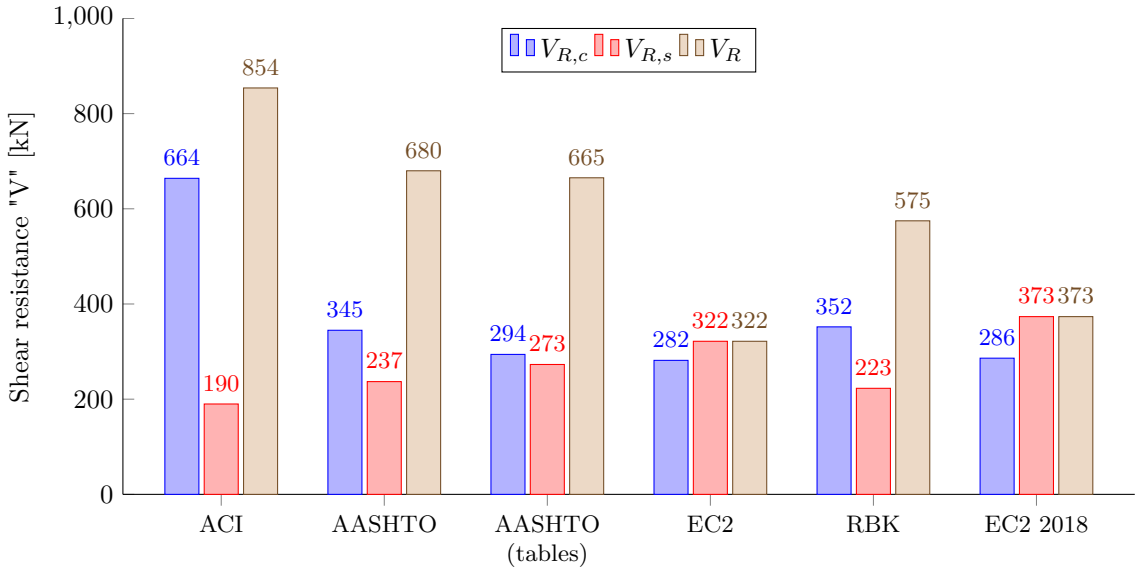

Figure 5.17: Nominal shear resistance for $x = 1.725$ m for the five code provisions

In Chapters 5.2 through 5.6 the nominal shear resistances are calculated for cross-sections between $x = 1.725$,..,2.903 m. In the previous paragraphs the critical cross-sections, the inclination of the compression field and other important differences between the code provisions are summarized. From these conclusions and the results from the experiments it can be concluded that the critical cross-section is at $x = 1.725$ m, as the inclinations of the compression field $\theta = 30°, 19.08°$ and $15°$ all cross the web at $x = 1.725$ m. The shear resistances for this critical cross-section are given in Figure 5.17.

The shear failure mode according to the ACI is web-shear failure $V_c = 664$ kN and for EC2 flexural-shear failure $V_c = 282$ kN when not considering shear reinforcement. The other three codes do not consider different shear failure modes. None of the code provisions either give the correct shear failure mode or a value close to the failure load for HPZ1 and HPZ2. The lowest value for the nominal shear resistance is given by EC2: $V_R = 322$ kN ($F_{exp} = 541$ kN) and the highest value by ACI: $V_R = 854$ kN ($F_{exp} = 1305$ kN), which is a difference of 165%. The values for the shear resistance of the concrete V_c for AASHTO (tables), EC2, RBK and EC2 draft 2018 are close to each other $V_c = 282$,..,352 kN. The general procedure from the AASHTO give a higher value than the table approach, at the cost for the contribution of the shear reinforcement. The ACI gives more or less twice the value compared to the last four codes. The contribution of the shear reinforcement to the shear resistance is related to the calculated or used value for θ. The higher the value, the higher the contribution of the shear reinforcement: EC2 draft 2018 $\theta = 19.08° \rightarrow V_s = 373$ kN and ACI $\theta = 45° \rightarrow V_s = 190$ kN.

5.7.7. Failure of the compression field

The failure load for failure of the compression field is a lot higher than the nominal shear failure and was not further checked at first. According to the experimental results of HPZ1 and HPZ2, the failure mode for both girders is shear-compression failure and not the assumed shear-tension failure. Therefore the failure of the compression field is considered for three code provisions: AASHTO, EC2 and EC2 draft 2018, see Figure 5.18.

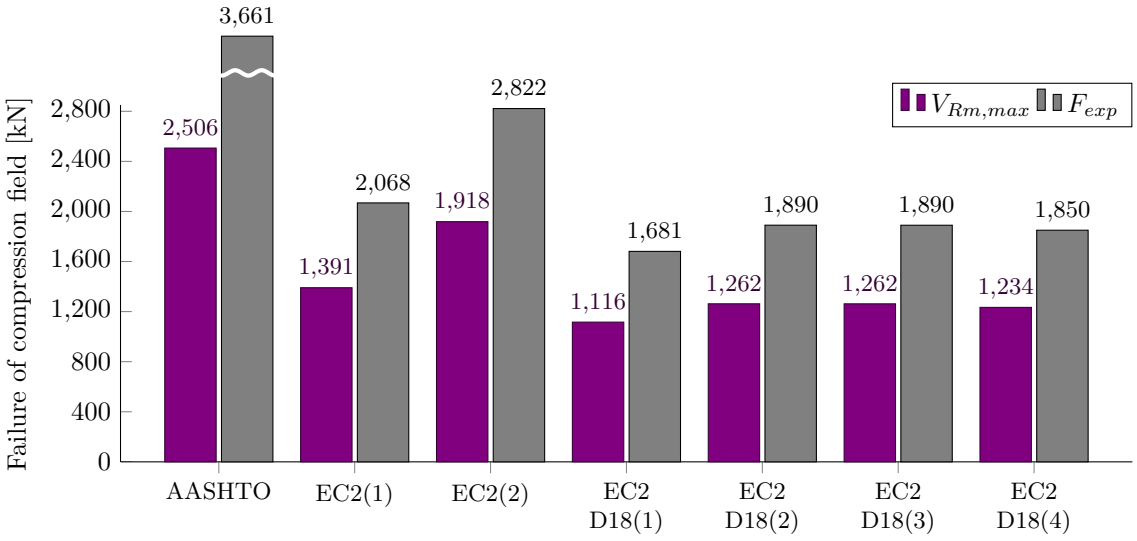

Figure 5.18: Failure of the compression field for $x = 1.725$ m with different code provisions

Additional information for Figure 5.18:

- First column: AASHTO, $V_{Rm,max} = 0.25 f'_c \cdot b_v \cdot d_v$;
- Second column: EC2(1), $V_{Rm,max} = \dfrac{\alpha_{cw} \cdot b_w \cdot z \cdot v_1 \cdot f_{cm}}{\cot\theta + \tan\theta}$ with $\theta = 15°$;

  Note: not allowed according to EC2, but calculated as a reference
- Third column: EC2(2), $V_{Rm,max} = \dfrac{\alpha_{cw} \cdot b_w \cdot z \cdot v_1 \cdot f_{cm}}{\cot\theta + \tan\theta}$ with $\theta = 21.8°$;

– Fourth column: EC2 D18(1), $V_{Rm,max} = 0.5 \cdot \nu \cdot f_{cm} \cdot b_w \cdot z$ with $\theta = 17°$ and $N_V = N_{Ew} + V_E \cot\theta$ with $N_{Ew} = -N_E = -N_p$;

  Note: when $\nu = 0.5$ it is the same expression as AASHTO, but calculated with slightly different internal lever arm and concrete compressive strength;

– Fifth column: EC2 D18(2), $V_{Rm,max} = 0.5 \cdot \nu \cdot f_{cm} \cdot b_w \cdot z$ with $\theta = 15.11°$ and ε_x taken from the sectional analysis (analytical) for shear at ultimate $F_{exp} = 1890$ kN;

– Sixth column: EC2 D18(3), $V_{Rm,max} = 0.5 \cdot \nu \cdot f_{cm} \cdot b_w \cdot z$ with $\theta = 14.86°$ and ε_x taken from the results from LVDTs of HPZ1;

– Seventh column: EC2 D18(4), $V_{Rm,max} = 0.5 \cdot \nu \cdot f_{cm} \cdot b_w \cdot z$ with $\theta = 18.90°$ and ε_x taken from the results from LVDTs of HPZ2.

The general procedure according to the AASHTO and EC2 (EC2(2) in the figure) lead to very unrealistic values for failure of the compression field and are not further discussed. As a reference the EC2 has been used for $\theta = 15°$, which comes close to the observed failure loads of HPZ1 and HPZ2, see EC2(1) in the figure. The EC2 draft 2018 allows for lower inclinations of θ.

The fourth through the sixth column in the figure give the results that are closest to the failure load of HPZ1. The seventh column in the figure gives the result that is closest to the failure load of HPZ2. It is important to note that these results are based on three different approaches to obtain the longitudinal strain at mid depth ε_x: with calculations based on EC2, sectional analysis (analytical) for shear at ultimate $F_{exp} = 1890$ kN given in Chapter 4.6.5 and from the LVDTs of HPZ1 and HPZ2 (experiment) given in Chapter 4.6.4.

The stress in the compression chord is mostly exceeded, but it may be questioned that this calculated stress is realistic. It is also not clear in the draft if the expression must be satisfied when using angles of the compression field inclination lower than θ_{min}. Ignoring this verification, the results for all three approaches with EC2 draft 2018 for $\theta = 14.86° - 17°$ and $F_{exp} = 1890$ kN are in line with the experimentally observed failure load and -mode for HPZ1. For HPZ2, the results are not in line with the observed inclination of the compression field: $\theta = 18.9°$ (EC2 draft 2018) vs. $\theta = 34°$ (experiment HPZ2).

For EC2 and EC2 draft 2018, yielding of the stirrups is set equal to crushing of the concrete/failure of the compression field: $V_{Rm,s} = V_{Rm,max}$, see Chapters 5.4.4 and 5.6.6. In this procedure not only the inclination of the compression field, but also the failure load is set as a variable. This procedure leads to lower results for the failure load than the procedure where the failure load is set equal to the observed failure load of HPZ1 or HPZ2 in the experiments and only considering a rotating strut in the truss model, see Table 5.22. Note that in order to obtain a solution for EC2, the inclination θ needs to be lower than the allowed limit of 21.8°. For the EC2 draft 2018 the first column gives the result from the calculations with the state of strains with $N_{Ew} = 0$ (zero contribution of the shear zone). For this results the force in the tension chord exceeds the maximum allowed force: $F_T > F_{T,max}$. The second column gives the result where a part of the additional tensile axial force is taken by the web (assumed: $N_{Ew} = -N_E$) for $\theta = 19.08°, 17.00°$ and $15.00°$. The third column gives the result with the longitudinal strains obtained from the analytical solution. The fourth and fifth column give the results with the longitudinal strains obtained from the LVDTs for HPZ1 and HPZ2.

Table 5.22: Shear resistance for $V_{Rm,s} = V_{Rm,max}$ with different procedures and values for θ

	EC2	**EC2 draft 2018**				
Procedure:	**Original**	$\boldsymbol{N_{Ew} = 0}$	$\boldsymbol{+N_{Ew}}$	**Analytical**	**LVDTs(1)**	**LVDTs(2)**
$F_{exp,assumed}$ [kN]	1282	1018	1071	1290	1111	959
θ [°]	8.67	11.19	10.60	11.45	10.19	11.91
$V_{Rm,s} = V_{Rm,max}$ [kN]	838	653	690	843	718	612
F_{exp} [kN]	1282	1018	1071	1290	1111	959

The shear capacity is calculated with five (inter)national standards and the results are discussed in the previous subsections. Both the ultimate shear capacity and failure mode are not in line with the observed test results, which is why failure of the compression field is also considered. Only three codes consider this type of failure: AASHTO, EC2 and EC2 draft 2018. The measured angles of the shear crack of HPZ1 and HPZ2 and failure load are compared with these three codes. The AASHTO and EC2 do not give representative values for failure of the compression field; the AASHTO does not consider the inclination θ in the expression to calculate failure of the compression field and EC2 has a lower limit of $\theta = 21.8°$. The EC2 draft 2018 is the only code that allows the inclination θ to be lower than 19.08°, resulting in lower values for the shear capacity. Calculating the shear capacity with various inclinations and ways that the longitudinal strain ε_x is obtained show that the shear capacities are close to the observed failure load. The lower limit of the shear capacity is obtained when the inclination θ is lowered until failure of the compression field occurs simultaneously with yielding of the stirrups.

6

Numerical analysis with Response-2000

Response-2000 is a free to use, non-linear cross-sectional analysis program and is developed at the University of Toronto by E. Bentz (2000). It calculates the strength and ductility of reinforced and prestressed concrete that is subjected to shear, moment and axial loads [59]. This makes Response-2000 distinctive in it's area, because normally in a cross-sectional program shear is not included in the models. Response-2000 uses the Modified Compression Field Theory (MCFT). This theory is originally derived for membrane elements, although Response-2000 uses the MCFT to analyze beam behavior. Input of the geometry of the girder of one cross-section together with the material properties is needed to calculate a full load-deformation cross-sectional analysis. This program can determine the ultimate strength and both shear-failure mechanisms, flexural-shear failure and shear-tension failure.

6.1. Modified Compression Field Theory (MCFT)

The Modified Compression Field Theory (MCFT) [15] [16] is a model that describes the load-deflection response for concrete membranes. The code provisions AASTHO and CSA are based on this theory. The MCFT can both be used for members with and without transverse reinforcement for determining the shear resistance and assumes that cracked concrete is a different material than uncracked concrete. It uses relationships between the average stresses and strains for both concrete and reinforcement. A total of 15 expressions are used for the MCFT and shown in Table 6.1.

Concrete in a cracked state is modeled in principal stress directions, tensile stresses σ_1 and compressive stresses σ_2. The reinforcement steel is modeled in axial directions, longitudinal direction σ_{sx} and transverse direction σ_{sz}. The expressions that relate to cracked concrete are empirically determined from 30 membrane shear tests performed by Vecchio & Collins [15] and take into account shear transfer mechanisms and influencing factors on the shear resistance (see Chapter 2.2 and 2.3). The mechanisms and influencing factors are: stresses between cracks, stresses at cracks, interface shear on cracks (aggregate interlocking) and dowel action [10] [19].

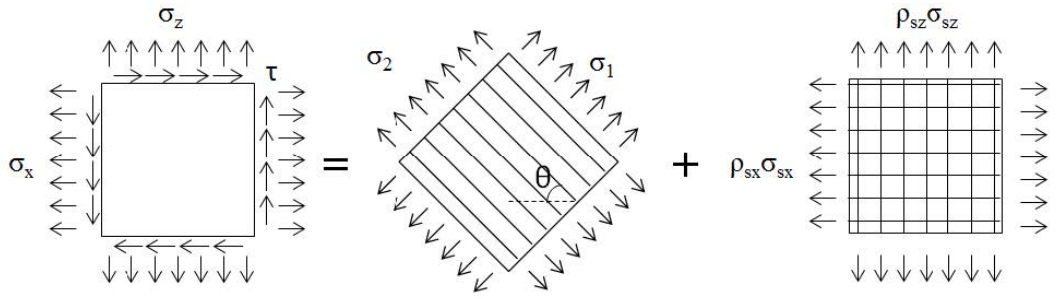

Figure 6.1: Equilibrium conditions for concrete and reinforcement according to MCFT [16]

Table 6.1: Failure mechanisms with corresponding mode of diagonal cracking [16]

FAILURE MECHANISMS		
GLOBAL EQUILIBRIUM AVERAGE STRESSES	GEOMETRIC CONDITIONS AVERAGE STRAINS	STRESS-STRAIN RELATIONSHIPS REINFORCEMENT:
1. $\sigma_x = \rho_x\sigma_{sx} + \sigma_1 - \tau\cot\theta$ 2. $\sigma_z = \rho_z\sigma_{sz} + \sigma_1 - \tau\tan\theta$ 3. $\tau = \dfrac{\sigma_1+\sigma_2}{\tan\theta+\cot\theta}$	6. $\tan^2\theta = \dfrac{\varepsilon_x+\varepsilon_2}{\varepsilon_z+\varepsilon_2}$ 7. $\varepsilon_1 = \varepsilon_x+\varepsilon_z+\varepsilon_2$ 8. $\gamma_{xz} = 2(\varepsilon_x+\varepsilon_2)\cot\theta$	12. $\sigma_{sx} = E_s\varepsilon_x \le f_{yx}$ 13. $\sigma_{sz} = E_s\varepsilon_z \le f_{yz}$ CRACKED CONCRETE: 14. $\sigma_2 = \dfrac{f_c}{0.8+170\varepsilon_1}\left[2\dfrac{\varepsilon_2}{\varepsilon_c} - \left(\dfrac{\varepsilon_2}{\varepsilon_c}\right)^2\right]$ 15. $\sigma_1 = \dfrac{0.33\sqrt{f_c}}{1+\sqrt{500}\varepsilon_1}$
CRACK CONDITIONS		
LOCAL EQUILIBRIUM STRESSES AT CRACKS	CRACK WIDTHS	SHEAR STRESS ON CRACK
4. $\sigma_{sx,cr} = \dfrac{\sigma_x+\tau\cot\theta+\tau_{ci}\cot\theta}{\rho_x}$ 5. $\sigma_{sz,cr} = \dfrac{\sigma_z+\tau\tan\theta+\tau_{ci}\tan\theta}{\rho_z}$	9. $w = s_\theta\varepsilon_x$ 10. $s_\theta = \dfrac{1}{\dfrac{\sin\theta}{s_x}+\dfrac{\cos\theta}{s_z}}\varepsilon_x$	11. $\tau_{ci} = \dfrac{0.18\sqrt{f_c}}{0.31+\dfrac{24w}{d_{max}+16}}$

The derivation of the expressions shown in Table 6.1 are made on the following assumptions [19]:

- The strain state has no influence of the loading history;
- Stresses and strains are averaged over an area;
- There is perfect bond between the concrete and reinforcement, identical strains $\varepsilon_s = \varepsilon_c = \varepsilon$;
- The reinforcement in x- and z-directions are uniformly distributed in an orthogonal grid;
- The angle for principal stresses and -strains are the same;
- There is no interaction between concrete and reinforcement for the stress-strain relationship.

6.1.1. Failure mechanism and crack condition expressions for MCFT

Expressions 1 - 3 - (GLOBAL EQUILIBRIUM - AVERAGE STRESSES)
An external load causes stresses inside a membrane element, which consists of concrete and reinforcement. Equilibrium must be made and is provided by expressions 1 to 3 in Table 6.1. MCFT makes the assumption that the reinforcement has no shear component, $\tau = \tau_{cx} = \tau_{cz}$. The tensile and compressive stresses in the concrete are calculated in the principal directions and by substituting σ_{cx}, σ_{cz} and σ_2 into the equilibrium conditions give Equations 1 to 3, see Equation 6.1.

$$\text{EQUILIBRIUM} \begin{cases} \sigma_x = \sigma_{cx} + \rho_x\sigma_{sx} \text{ HORIZONTAL} \\ \sigma_z = \sigma_{cz} + \rho_z\sigma_{cz} \text{ VERTICAL} \\ \tau = \tau_{cx} + \rho_x\tau_{sx} = \tau_{cz} + \rho_z\tau_{sz} \text{ SHEAR} \end{cases} \quad \text{WITH} \begin{cases} \sigma_{cx} = \sigma_1 - \tau\cot\theta \\ \sigma_{cz} = \sigma_1 - \tau\tan\theta \\ \sigma_2 = \sigma_1 - \tau(\tan\theta+\cot\theta) \end{cases} \tag{6.1}$$

Expressions 4 & 5 - (Local equilibrium - stresses at cracks)
Inside the crack the stresses are different for both concrete and steel compared to outside the crack. This means that when the concrete is in the cracked state, there are local differences in stresses for concrete and steel. The concrete stresses are lower and reinforcement stresses are higher inside a crack. Between cracks the concrete stresses are higher and reinforcement stresses are lower than average. This means local equilibrium must also be satisfied, in the cracks and between the cracks. From Figure 6.2 the expressions in for local equilibrium are found:

$$\text{Section B} \begin{cases} \sigma_x = \rho_x \sigma_{sx} \sin\theta + f_{ci} \sin\theta \\ \sigma_z = \rho_z \sigma_{sz} \cos\theta + \sigma_1 \cos\theta \end{cases} \tag{6.2}$$

$$\text{Section C} \begin{cases} \sigma_x = \rho_x \sigma_{sx,cr} \sin\theta - f_{ci} \sin\theta - \tau_{ci} \cos\theta \\ \sigma_z = \rho_z \sigma_{sz,cr} \cos\theta - f_{ci} \cos\theta + \tau_{ci} \sin\theta \end{cases} \tag{6.3}$$

By equating section B and section C and assuming $f_{ci} = 0$, the stresses in the reinforcement and the shear stress across the cracks are obtained. These two expressions $\sigma_{sx,cr}$ and $\sigma_{sz,cr}$ are Equations 4 and 5 from Table 6.1. When the shear stress in the crack τ_{ci} exceeds the maximum resistance, the average principal tensile stress σ_1 is reduced until the condition is met. The reinforcement stresses in the crack, $\sigma_{sx,cr}$ and $\sigma_{sz,cr}$ can exceed the tensile strength of the steel f_{yx} and f_{yz}, where the average principal tensile stress σ_1 is reduced until this condition is met [10] [19].

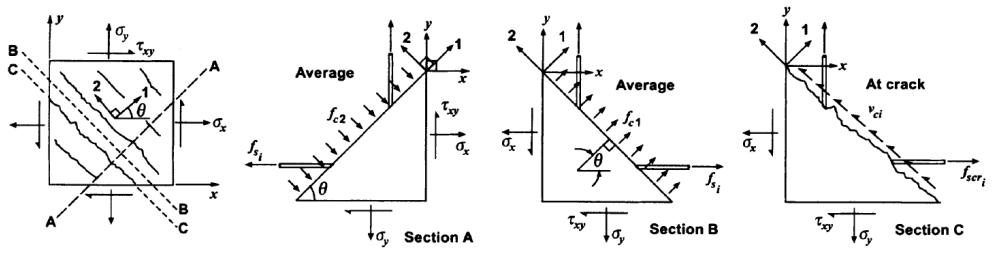

Figure 6.2: Global and local equilibrium conditions according to MCFT [80]

Expressions 6 - 8 - (Geometric conditions - average strains)
A relation between the average strains $\varepsilon_x, \varepsilon_z, \gamma_{xz}$ and the principal strains $\varepsilon_1, \varepsilon_2, \theta_\varepsilon$ is needed to make the strains in the steel and concrete compatible with each other. The strains in the concrete are equal to $\varepsilon_1, \varepsilon_2$ and the strains in the reinforcement steel are equal to the longitudinal and transverse average strains $\varepsilon_x, \varepsilon_z$, see Figure 6.3. The relation for the average strains, principal strains and cracking angle θ can be found by using the Mohr's circle for average strains. This will result in Equations 6 - 8 in Table 6.1.

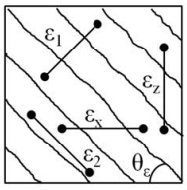

Figure 6.3: Compatibility for the geometric conditions of the MCFT [10]

Expressions 9 - 11 - (Crack widths & shear stress on crack)
According to the MCFT, concrete in cracked state can still transfer forces due to the transfer mechanism aggregate interlocking. This transfer mechanism is explained in Chapter 2.2.3. Based on experiments done by Walraven, the shear stress at a crack τ_{ci} is related to both aggregate interlocking and the average crack width w. When a crack grows in width the contribution of the interlocking is less, because the sides along the crack are further apart. If the aggregate size increases, the area of the aggregate is bigger and provides more roughness and resistance to the crack. If a concrete compressive strength higher than $f_c = 70$ MPa is used, a_g should be taken as zero as the cracks break through the aggregate instead of going around the aggregates.

$$\text{Shear transfer} \begin{cases} \tau_{ci} \leq \dfrac{0.18\sqrt{f_c}}{0.31 + \dfrac{24w}{a_g + 16}}, & \text{with } a_g = \text{ max aggregate size} \\ w = s_\theta \, \varepsilon_1, & \text{with } s_\theta = \dfrac{1}{\dfrac{\sin\theta}{s_x} + \dfrac{\cos\theta}{s_z}} \end{cases} \tag{6.4}$$

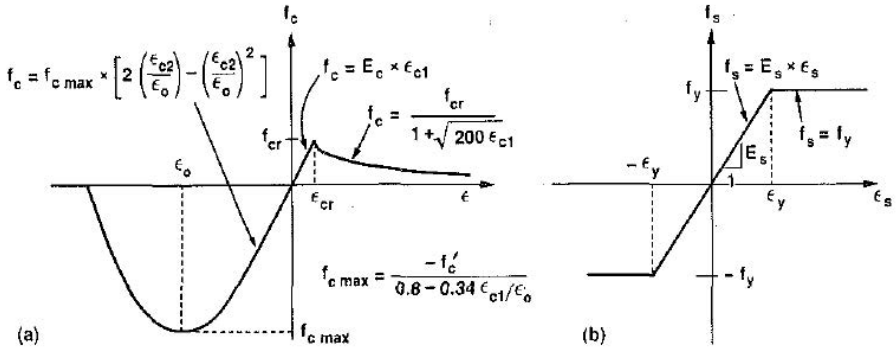

Figure 6.4: Stress-strain relationship for the concrete and reinforcement for MCFT [81]

Expressions 12 & 13 - (Stress-strain relationship - reinforcement)
The MCFT uses a bi-linear stress-strain relationship for the reinforcement. The stresses for the concrete and reinforcement are linked to the strains with the stress-strain diagram, see Figure 6.4. The model assumes that no interaction takes place between concrete and reinforcement.

Expressions 14 & 15 - (Stress-strain relationship - cracked concrete)
The MCFT assumes that cracked concrete is treated as a new material. Equations 14 and 15 are empirically determined for concrete in cracked state. Equation 14 is a constitutive expression for the principal compressive stresses σ_2, which depends on both the principal compressive strain ε_2 and the principal tensile strain ε_1. Equation 15 is a constitutive expression for the principal tensile stresses for cracked concrete σ_1, $\varepsilon_1 > \varepsilon_{cr}$. Before the cracking moment of concrete, between σ_1 - f_{cr}, the principal tensile stress increases linearly with the principal strain, see Figure 6.4. The principal stresses for cracked concrete are:

$$\text{Cracked concrete} \begin{cases} \sigma_1 = \dfrac{0.33\sqrt{f_c}}{1+\sqrt{500\varepsilon_1}}, & \text{(if uncracked } \sigma_1 = E_c\ \varepsilon_1) \\ \sigma_2 = \dfrac{f_c}{0.8+170\varepsilon_1}\left[2\dfrac{\varepsilon_2}{\varepsilon_c} - \left(\dfrac{\varepsilon_2}{\varepsilon_c}\right)^2\right] \end{cases} \tag{6.5}$$

For the case $\varepsilon_1 = 0$, σ_2 only depends on ε_2 and the basic stress-strain relation is obtained of concrete cylinder tests. For higher values of ε_1 the compressive strength of concrete is reduced $f_c = f_{c,red}$, which results from a bi-axial stress/strain state of concrete. This also applies to a value ε_2, σ_2 is lower.

6.1.2. Physical conditions failure cracked concrete

For cracked concrete three failure mechanisms are possible according to MCFT [15]

- Slipping of the crack: σ_1 limited by τ_{ci}:

  $\Rightarrow \sigma_1 = \rho_x(\sigma_{sx,cr} - \sigma_{sx}) - \tau_{ci,max}\cot\theta = \rho_z(\sigma_{sz,cr} - \sigma_{sz}) + \tau_{ci,max}\tan\theta$

- Crushing or shear failure: σ_2 limited by $\sigma_{2,max}$:

  $$\Rightarrow \sigma_2 = \sigma_1 - \tau(\tan\theta + \cot\theta) < \frac{f_c}{0.8+170\varepsilon_1}\left[2\frac{\varepsilon_2}{\varepsilon_c} - \left(\frac{\varepsilon_2}{\varepsilon_c}\right)^2\right]$$

- Yielding of longitudinal reinforcement at the crack: σ_1 limited by requirement $\sigma_{sx,cr} \leq f_{yx}$:

  $\Rightarrow \sigma_{sx,cr} = f_{yx}$

The first failure is slipping of the crack, which limits the principal tensile stress σ_1 by τ_{ci}. This influences the principal compressive stress and can eventually lead to the second failure mode: crushing failure of the concrete. Crushing of the concrete can happen with or without yielding of the transverse reinforcement. If high ratios of stirrups is present, crushing will happen without yielding of the reinforcement. The last failure is yielding of the longitudinal or transversal reinforcement near the cracks if the reinforcement ratio is low. The failure mechanism that occurs with the lowest external load is the governing failure mode [10] [19] [15].

6.1.3. Procedure for calculating one load step

Calculating the shear resistance with MCFT requires a lot of iterative calculations and is a complex procedure. For every load step different relations between the shear stress and -strain must be calculated. The use of programs like `MS Excel` and `Response-2000` are inevitable for calculating multiple load steps. In Figure 6.5 the procedure for one load step is given [19]:

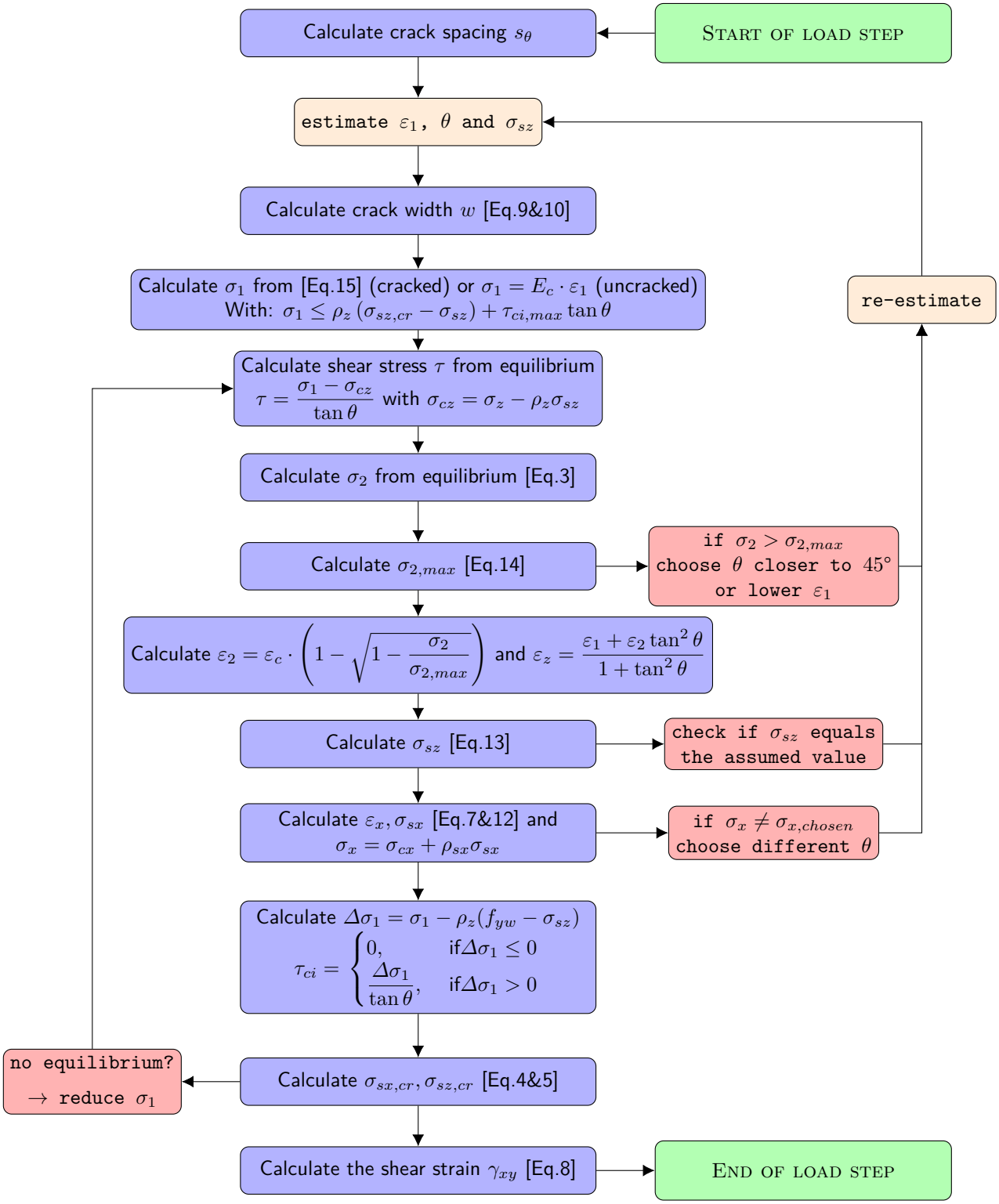

Figure 6.5: Procedure of one load step for the MCFT [15]

6.2. Introduction to Response-2000

Response-2000 is an excellent cross-sectional analysis program to calculate multiple load steps of a concrete member. It is based on the MCFT and distinguishes shear failure in flexural-shear and shear-tension failure. To calculate the load-deformation diagram of a member, Response-2000 needs input of the initial value of the axial force (by prestressing) and the ratio between the shear force and moment in the considered cross-section. Every load step it calculates the relation between stresses and strains over the height of the girder [59].

6.2.1. Background of Response-2000 iterative load steps

The background of Response-2000 is based on a series of bi-axial nodes along a line in the cross-section of a member. First a global strain state is estimated in the first load step (step 0), consisting of a longitudinal strain at the gravity center of the cross-section $\varepsilon_{x,0}$, a curvature ϕ_0 and an average shear strain $\gamma_{xz,0}$. The shear strain varies over the height of the girder, so a numerical outline is made to modify the average shear strain $\gamma_{xz,0}$. This outline is used to make a desired shape. For the following load steps (step i = 1,2,3,..,n), the calculated strains from previous steps to estimate a new global strain state. One load step requires four nested loops after which the load step is finished [10]:

1. Assumption $\sigma_z = 0$. In the bi-axial nodes the transverse strain $\varepsilon_{z,i}$ is calculated, where-after from the global stress state and shear strains the longitudinal strain $\varepsilon_{x,i}$ and shear strain $\gamma_{xz,i}$ are obtained for each bi-axial node;
2. From the global strain state the cross-sectional forces are calculated;
3. An iterative calculation is used for the global strain state until it is equal or close enough to the global load ratio;
4. An iterative calculation is used for the shear strain profile until it is equal or close enough to the assumed shear strain.

6.2.2. Setup of a model

To calculate the cross-sectional forces, stresses and strains of a concrete member, Response-2000 needs input of the geometry of the cross-section, material properties, external load(s), shear span and cross-sectional forces of the member. The simplicity of the program is that every cross-section with pre-stressing, transverse- and longitudinal reinforcement and concrete properties can be easily inserted. With Response-2000 it is possible to define a cross-section with a quick define wizard, although only commonly used and simple cross-sections can be made. Also it is easy to define the material properties and cross section outside this quick define option.

Latest (Beta) version Response-2000

Several versions have been released after the official release of Response-2000 version 1.0.5. The latest release is Response-2010 beta-version 1.9.7. With this version the program is much more stable and several important changes have been made:

- Instead of one cross-section more different cross-sections can be defined in the Catalog of Elements;
- A more advanced full member calculation;
- Length of the member can be defined;
- Location and type of the bearings can be defined;
- Changes in cross-section over the full member can be defined;
- Detailed live-load and dead-load with moment and shear-lines can be defined;
- Graphs for AASHTO and CSA code provisions are made;

This sub-paragraph is used to guide the user through the steps required to calculate the shear resistance of a concrete member the general way. In this guide the material properties and cross-sectional forces are taken from data available of the Helperzoom bridge, see Chapter 3. The cross-section at x = 2.453 m from the left bearing is considered with a = 2.903 m.

1. A new file needs to be created:

   `File` → `New` → `Save as (*.rsp)-file`.

   The title of the file, author, date, crack spacing and moment axis can be defined:

   `Define` → `Edit General`

2. The material properties of the concrete, reinforcement steel and prestressing steel is done with:

   `Define` → `Material Properties` → `Concrete / Non-Prestressed Reinforcement / Prestressed Reinforcement`

   The material properties can be defined with basic properties or with a detailed f'_c, f_y or f_{pu} for a more precise stress-strain curve or if more than one material of the same type is used (composite girder, different reinforcement strengths, etc). A detailed f'_c, f_y and f_{pu} is used:

   (a) Concrete Details f'_c, CONCRETE 1:

   Cylinder Strength [60.2 MPa], Tension Strength [4.86 MPa], Aggregate Size [32 mm]

   (b) Rebar Details f_y, STEEL 1:

   Elastic Modulus [200,000 MPa], Yield Strength [454 MPa], Rupture Strain [120 mm/m], Ultimate Strength [655 MPa]

   (c) Prestressing Steel Details f_{pu}, PSTEEL 1:

   Ramberg-Osgood [Standard Values: A=0.025, B=118, C=10], Elastic Modulus [185,000 MPa], Ultimate Strength [1824 MPa], Rupture Strain [60.0 mm/m]

3. The cross-section of the prestressed concrete girder is done with:

   `Define` → `Concrete Section` → `User Defined`

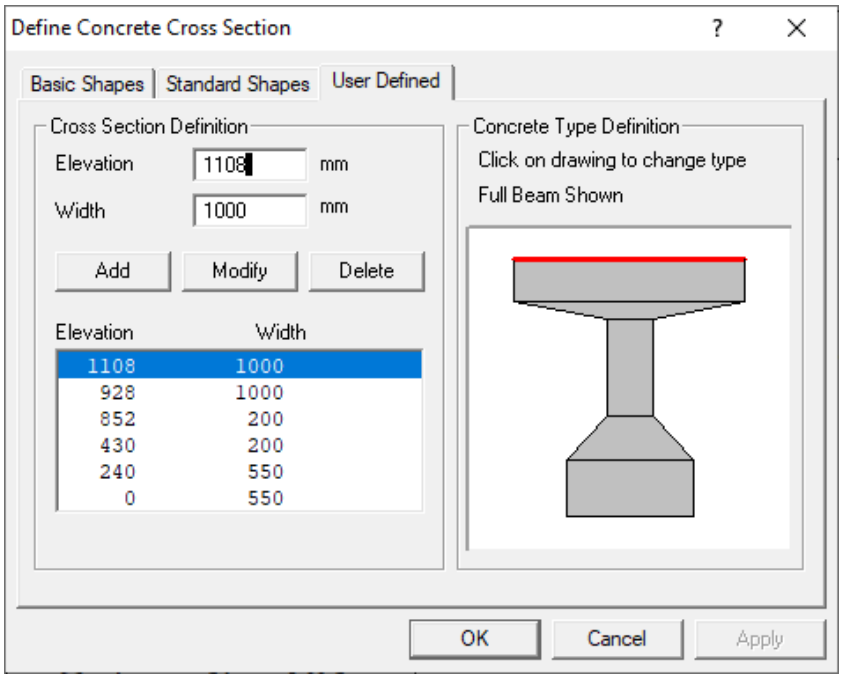

Figure 6.6: Step 4: geometry of cross-section

4. The location of the transverse and longitudinal reinforcement and the prestressing tendons need to be defined. To add/delete/modify layers for the reinforcement or prestressing cables, simply give the layer a name and click Add. The concrete cover for the both transversal and longitudinal reinforcement is automatically defined with distance to bottom and/or top (Note: in `Response-2010` reinforcement cannot be aligned along the geometry of the cross-section):

`Define → Transverse Reinforcement / Longitudinal Reinforcement / Tendons`

`Define a new layer → Name → Add/Modify → Select Steel/Tendon Type`

(a) Transverse reinforcement (INDIVIDUAL LAYERS):

A "closed stirrup" is used to account for the two legs. The stirrup spacing is 400 mm, the "select bar by area" is ticked with $\varnothing = 10$ mm, $A_{sw} = 78.54$ mm^2 per leg. The height of the transverse reinforcement is given in "distance to bottom and top". All transverse reinforcement bars are defined as (STEEL 1).

(b) Longitudinal reinforcement (INDIVIDUAL LAYERS):

The longitudinal reinforcement is defined per layer. Over the height of the girder seven layers of two to four reinforcement bars are present. This is inserted in "number of bars". All longitudinal reinforcement bars are defined as (STEEL 1).

(c) Tendons:

The girder has seven tendons in the shear span, named cable 4 through 10. One cable consists of 12 strands, each with $A_{p,strand} = 38.5$ mm^2 with a total area $A_p = 462$ mm^2. The axial compressive force from prestressing is defined as the prestrain in the cables. The axial force of one cable is 228,228 N ($= 0.27 \cdot 1824 \cdot 462$). The prestrain is calculated with the axial force, area of the cable and elastic modulus of the prestressing steel. The slope of the tendon is calculated from the inclination α of the cables given in Table 3.7.

$$
\begin{aligned}
N_p &= 228{,}228 \text{ N} \\
\sigma_p = \frac{N_p}{A_p} &= \frac{228{,}228}{462} = 494 \text{ MPa} \\
\varepsilon_p = \frac{\sigma_p}{E_p} &= \frac{494}{185{,}000} = 0.00267 \text{ m/m} \\
&= 2.67 \text{ mm/m prestrain}
\end{aligned}
\tag{6.6}
$$

$$\text{Slope of Tendon (9)} = 1 \cdot \sin\alpha_9 = \sin(0.84°) = 0.01466 \text{ m/m} = 1.47\%$$

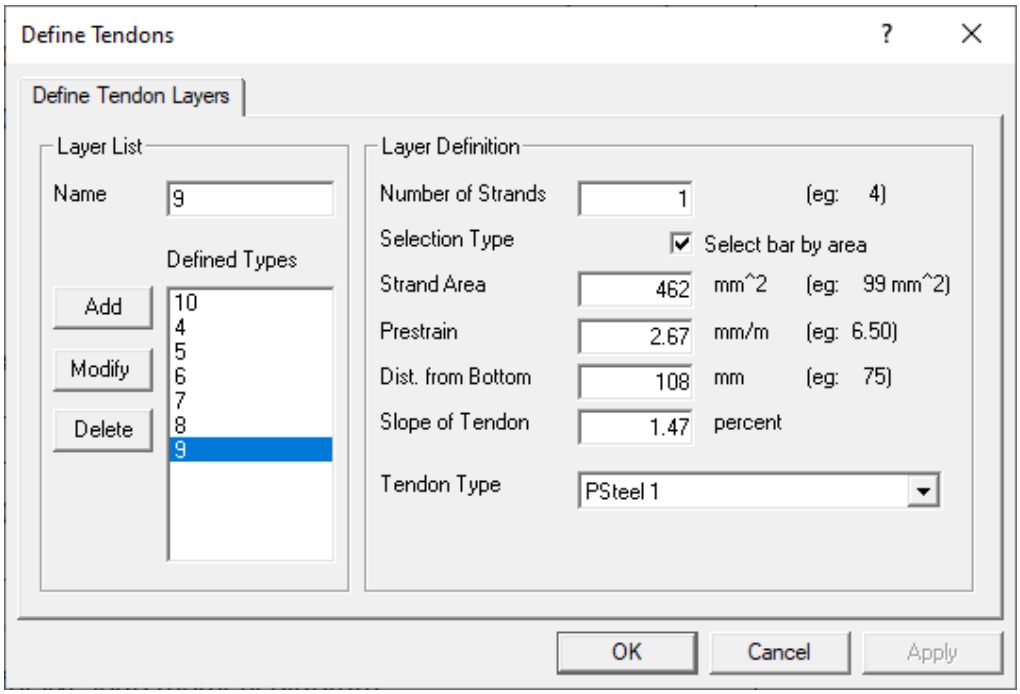

Figure 6.7: Step 5: Defining the prestressing tendons

5. After defining the cross-section, material properties and position of the reinforcement and prestressing tendons, the cross-sectional forces "Loads" are defined.

   Loads → Loads

   For one load analysis only the left column is used. For multiple load analyses the right column with increments is used as well. The prestressing force is already defined with the prestrain in step 4, therefore $N_u = 0$ kN. The moment and shear forces from self-weight and the external load must be defined, which is calculated with either `MatrixFrame` or with the use of a `MS Excel`-sheet. The moment and shear forces due to self-weight are accounted for in the left column, with $V_{sw} = 31.75$ kN and $M_{sw} = 121.12$ kNm for $x = 2.453$ m. The moment and shear forces due to the external load are accounted for in the right column (increments) with a unique M/V-ratio for every cross-section. For $x = 2.453$ m the values are $M = 1.71, V = 0.7$.

6.2.3. Overview of input `Response-2010`

Once the setup of the model is complete, the overview of the cross-section should look similar to Figure 6.8. The geometric properties are shown at the top left. The 'Full Member Properties' are not used for a cross-sectional analysis, so these can be ignored. Below these properties the crack spacing and the input of the loads are given. Three graphs are given for the material properties of the concrete, reinforcement bars and prestressing steel. Note that the ultimate strength of the prestressing steel $f_{pu} = 1824$ MPa is shown a bit lower in the overview, because of the standard parameters used for Ramberg-Osgood. In the middle the cross-section is given with the geometry and the position, area and slope of the prestressing steel, stirrups and longitudinal reinforcement. On the right the 'Element Catalog' is shown with all defined cross-sections. The defined cross-sections are: $x = 1.725, 1.800, 1.900, 2.051, 2.453$ m.

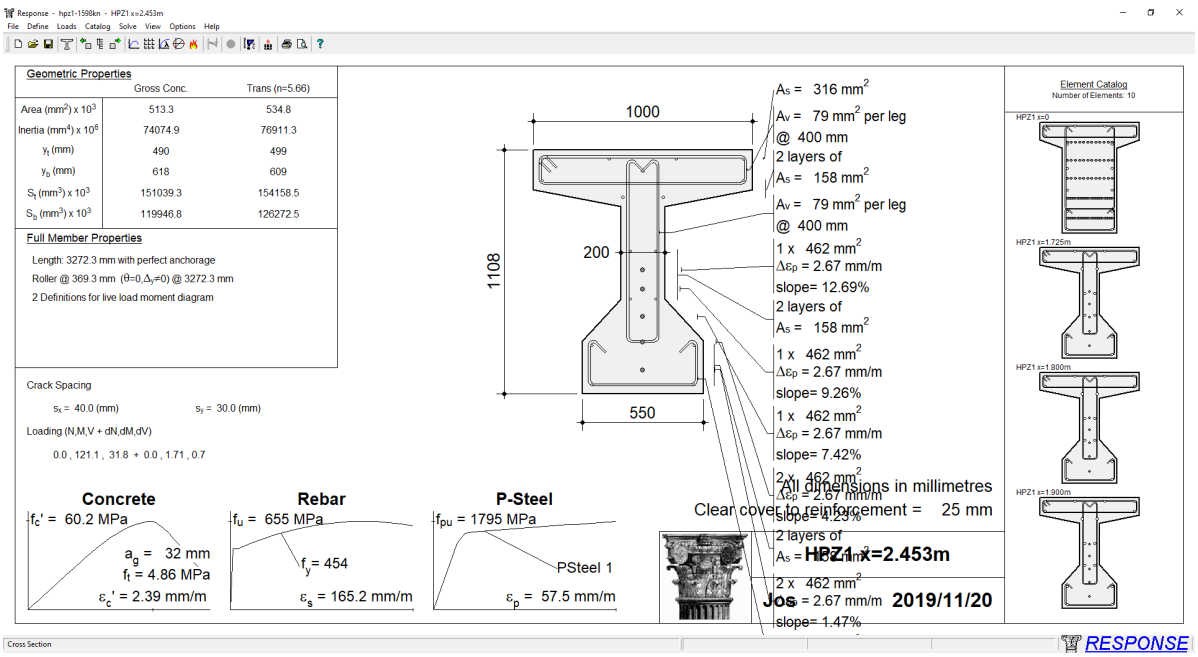

Figure 6.8: Overview of all the input for `Response-2010`

`Response-2010` also provides information about the area of the reinforcement and prestressing steel, reinforcement-ratio, lever arm and the nominal shear strength according to the AASHTO 2000 and CSA 2014. This information can be accessed by double click on the white area. The results from the CSA code provision are used to check if the vertical component of the prestressing force V_p is inputted correctly in `Response-2010`, see Figure 6.9. Table 6.2 shows that the values for V_p calculated by `Response-2010` and `MS Excel` are identical.

```
CSA-2014 Shear Strength
-----------------------

HPZ1 x=2.453m
M_r = 1415.0 kNm  V_r = 561.5 kN
|e_x =  0.72 mm/m  s_z_e =   207 mm
V_c = 256.9 kN   V_s = 211.9 kN
V_p =  92.7 kN
d_v =   798 mm  b_w =   200 mm
|f_c = 1.00  |f_s = 1.00  |f_p = 1.00
```

Figure 6.9: Overview of the CSA 2014 nominal shear resistance according to Response-2010

Table 6.2: Comparison between V_p from output Response-2010 and MS Excel with 2.67 mm/m prestrain ($N_p = 1598$ kN)

$x =$	**1.725 m**	**1.800 m**	**1.900 m**	**2.051 m**	**2.453 m**
MS Excel	98.21	97.63	96.87	95.72	92.65
Response-2010 (CSA)	98.2	97.6	96.8	95.7	92.7

The CSA-2014 shear strengths of the considered cross-sections are given in Table 6.3. The output gives the effective shear depth d_v (is 798 mm for all cross-sections), the longitudinal strains that are calculated at mid depth ε_x, the contribution of the concrete V_c, contribution of the shear reinforcement V_s and the vertical prestressing force V_p. According to these results the critical cross-section is $x = 2.453$ m with $V_R = 561.5$ kN.

Table 6.3: CSA-2014 shear strength from output Response-2010 with 2.67 mm/m prestrain ($N_p = 1598$ kN)

$x =$	**1.725 m**	**1.800 m**	**1.900 m**	**2.051 m**	**2.453 m**
ε_x [mm/m]	0.47	0.50	0.53	0.58	0.72
V_c [kN]	314.6	305.1	296.2	284.5	256.9
V_s [kN]	226.3	224.6	222.5	219.6	211.9
V_p [kN]	98.2	97.6	96.8	95.7	92.7
V_R [kN]	639.0	627.3	615.6	599.7	561.5

The results are compared with the AASHTO results $f_{po} = 0.27 f_{pu}$ ($N_p = 1598$ kN) see Table 6.4. These values are taken from Table 5.7. Note that the longitudinal strains in AASHTO are calculated at the tension reinforcement ε_s instead of the mid depth of the girder. Comparing the results from both code provisions, the nominal shear resistance according to the AASHTO is a bit higher than the CSA. This can be explained by a higher calculated longitudinal strain for CSA-2014 (effective shear depth AASHTO: $d_v = 799$ mm vs. CSA: $d_v = 798$ mm, so the longitudinal strain at the tension reinforcement can be divided by two to obtain the strains at the same height as CSA: $\varepsilon_x = 0.5\varepsilon_s$). Although Response-2010 does not give information about the inclination of the compression field θ, the expression to calculate V_s is the same in both code provisions. Comparing the values for V_s, a lower value for θ is calculated in CSA-2014, resulting in a lower V_c and V_s.

Table 6.4: AASHTO shear strength from output MS Excel for $f_{po} = 0.27 f_{pu}$ ($N_p = 1598$ kN)

$x =$	**1.725 m**	**1.800 m**	**1.900 m**	**2.051 m**	**2.453 m**
ε_s [mm/m]	0.58	0.63	0.69	0.78	1.02
V_c [kN]	345	336	326	312	280
V_s [kN]	237	235	233	230	223
V_p [kN]	98.2	97.6	96.8	95.7	92.7
V_R [kN]	680	669	656	638	595

6.3. Sectional response with Response-2010

The results from the cross-sectional analysis with Response-2010 (Solve → Sectional Response) are in the form of plots. At the left side the plots from the control section are given for V-γ_{xy} and M-ϕ-diagrams. The green line shows the current load stage and is always positioned at the failure load when the sectional response is calculated. If no increments are defined at 'Loads' (only a constant moment and shear force) only one load stage is given. When increments are defined, to go to the previous or next load stage simply press Pg Dn or Pg Up respectively. At the right side nine graphs are shown, based on the drop down menu at the left side. The most important ones are: "Cracking, General & Reinforcement", see Figures 6.10, 6.11 and 6.12.

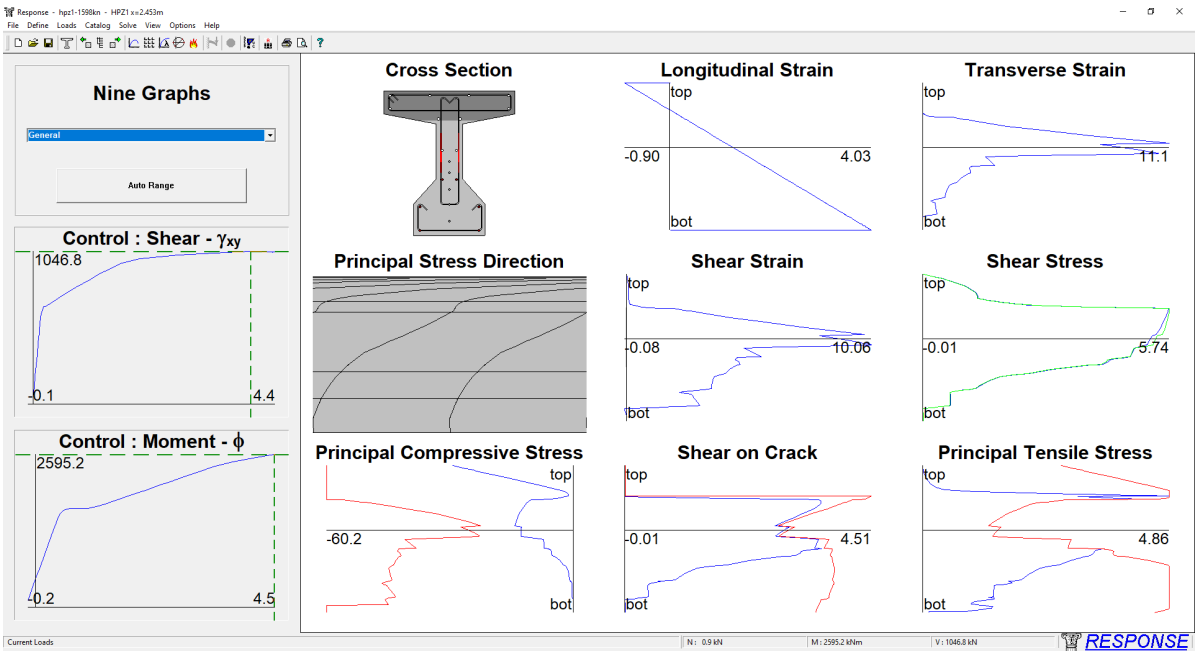

Figure 6.10: Sectional Response - General for $x = 2.453$ m with Response-2010

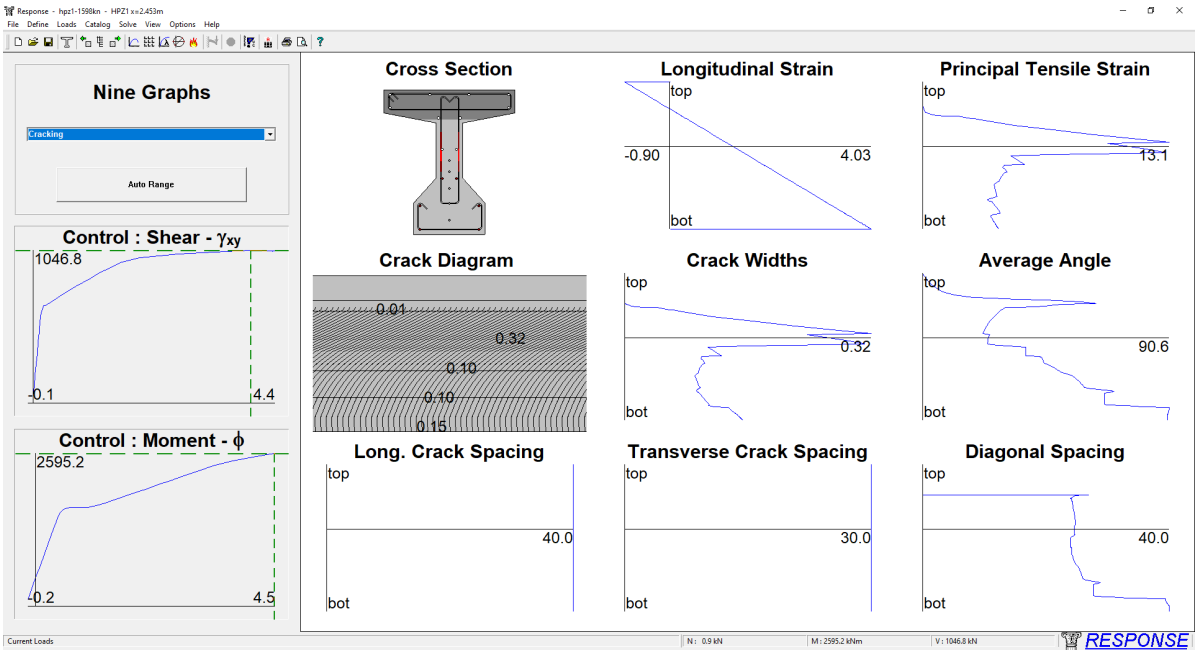

Figure 6.11: Sectional Response - Cracking for $x = 2.453$ m with Response-2010

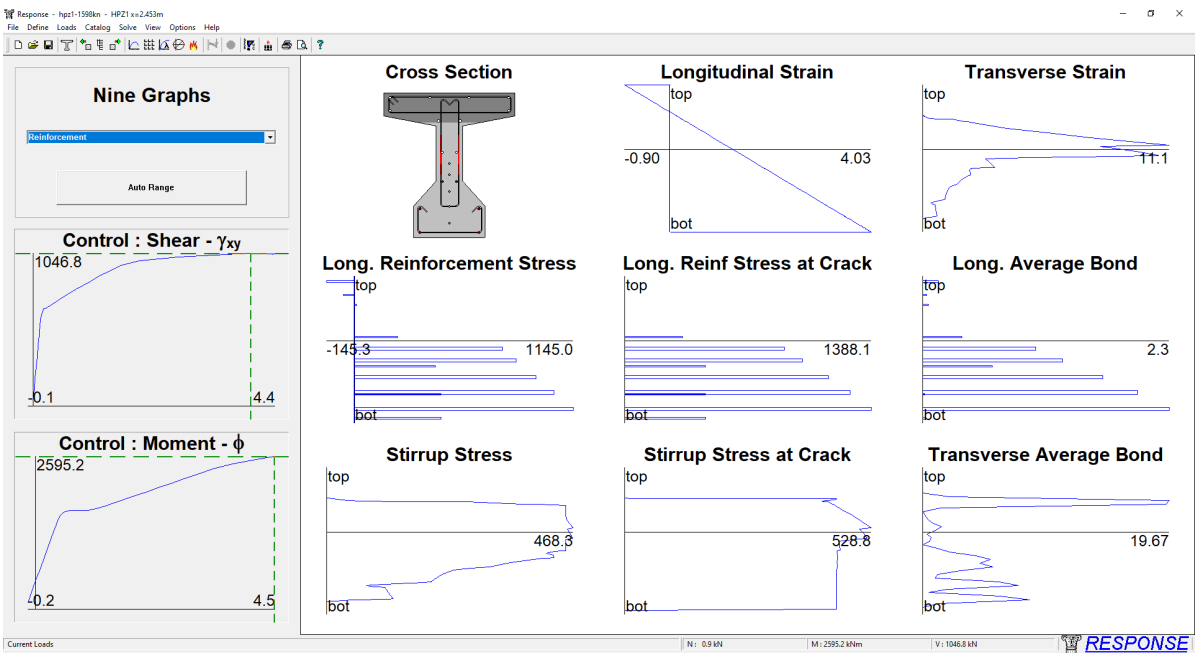

Figure 6.12: Sectional Response - Reinforcement for $x = 2.453$ m with Response-2010

6.3.1. Background of the plots from Response-2010

The nine plots from "General" are explained in more detail below [59]:

1. **Cross Section:** gives information about the concrete and reinforcement. The *light grey* areas present the cracked areas. When the reinforcement is colored *dark red* it means that the reinforcement is yielding, *red* means the reinforcement is in strain hardening stage and *green* means the reinforcement is yielding in compression.

2. **Longitudinal Strain:** gives the longitudinal strain ($\varepsilon_x \cdot 10^3$) along the height of the member. Assumption: plane sections remain plane. *Calculated from iterative method.*

3. **Transverse Strain:** gives the bulging strain ($\varepsilon_z \cdot 10^3$) along the height of the member. Assumption: $\sigma_z = 0$. *Calculated from iterative method.*

4. **Crack Diagram/Principal Stress Direction:** gives information about the crack pattern and crack width. The principal stress direction can be shown by right clicking on the plot and click toggle mode. *Pink* means crushing of the concrete and *purple* means failure due to slipping of the reinforcement.

5. **Shear Strain:** gives the shear strain $\gamma_{xy} \cdot 10^3$ along the height of the member. *Calculated from iterative method.*

6. **Shear Stress:** gives the shear stress (τ in MPa) along the height of the member. The *green* line gives the shear stress calculated with the longitudinal stiffness method and *blue* gives the shear stress calculated from the strain state. *Calculated from iterative method.*

7. **Principal Compressive Stress:** gives the principal compressive stress (σ_2 in MPa) along the height of the member. The *red* line gives the maximum allowable compressive stress capacity and is reduced when concrete is cracked. The *blue* line gives the calculated compressive stress.

   Maximum allowable stress: $\sigma_2 = \dfrac{f_c}{0.8 + 170\varepsilon_1} \cdot \left[2\dfrac{\varepsilon_2}{\varepsilon_c} - \left(\dfrac{\varepsilon_2}{\varepsilon_c}\right)^2\right]$

   Actual stress: $\sigma_2 = \tau \cdot (\tan\theta + \cot\theta) - \sigma_1$

8. **Shear on Crack:** gives the shear stress on the crack (τ_{ci} in MPa) along the height of the member. The *red* line gives the maximum allowed shear on the crack and the *blue* line gives the calculated shear on the crack.

To calculate the shear stress on the crack τ_{ci} and the maximum shear stress on the crack $\tau_{ci,max}$ a so-called "crack check" is done. The first step is to check if the steel is able to take up the tensile stresses in both directions:

$$\Delta f_{c1x} = \sigma_1 - \rho_x(f_{sxy} - \sigma_{sx})$$
$$\Delta f_{c1z} = \sigma_1 - \rho_z(f_{szy} - \sigma_{sz})$$

After cracking of the concrete, four different situations can occur in the crack-checks that are done in `Response-2010` for the calculation of τ_{ci}:

(a) Transverse reinforcement does not yield ($\Delta f_{c1z} < 0$):

Shear stress on crack: $\tau_{ci} = 0$

(b) Transverse reinforcement is yielding ($\Delta f_{c1z} > 0$):

Shear stress on crack: $\tau_{ci} = \dfrac{\sigma_1 - \rho_z(f_{yw} - \sigma_{sz})}{\tan\theta}$

(c) Transverse reinforcement is yielding and maximum shear stress on the crack is reached ($\Delta f_{c1z} > 0$ and $\tau_{ci} = \tau_{ci,max}$):

Maximum allowable shear stress on crack: $\tau_{ci,max} = \dfrac{0.18\sqrt{f_c}}{0.31 + \dfrac{24w}{a_g + 16}}$

(d) Transverse and longitudinal reinforcement are yielding ($\Delta f_{c1z} > 0$ and $\Delta f_{c1x} > 0$):

Shear stress on crack: $\tau_{ci} = \big(\rho_x(\sigma_{sx,cr} - \sigma_{sx}) - \rho_z(\sigma_{sz,cr} - \sigma_{sx})\big) \cdot \sin\theta \cdot \cos\theta$

9. **Principal Tensile Stress:** gives the principal tensile stress (σ_1 in MPa) along the height of the member. The *red* line gives the maximum allowed principal tensile stress, which is equal to the tensile strength of the concrete. The *blue* line gives the calculated principal tensile stress.

The same four situations can occur in the crack-checks that are done in `Response-2010` for the calculation of σ_1. The governing situation gives the value for σ_1:

(a) Transverse reinforcement does not yield ($\Delta f_{c1z} < 0$):

Principal tensile stress: $\sigma_1 = \dfrac{0.33\sqrt{f_c}}{1 + \sqrt{3.6\dfrac{A_c}{\Sigma d_b \cdot \pi} \cdot \varepsilon_1}}$

(b) Transverse reinforcement is yielding ($\Delta f_{c1z} > 0$):

Shear stress on crack: $\sigma_1 = \rho_z(\sigma_{sz,cr} - \sigma_{sx}) + \tau_{ci}\tan\theta$

(c) Transverse reinforcement is yielding and maximum shear stress on the crack is reached ($\Delta f_{c1z} > 0$ and $\tau_{ci} = \tau_{ci,max}$), σ_1 is reduced because of slipping of the crack:

Maximum allowable shear stress on crack: $\sigma_1 = \rho_z(\sigma_{sz,cr} - \sigma_{sx}) + \tau_{ci,max}\tan\theta$

(d) Transverse and longitudinal reinforcement are yielding ($\Delta f_{c1z} > 0$ and $\Delta f_{c1x} > 0$):

Shear stress on crack: $\sigma_1 = \rho_x(\sigma_{sx,cr} - \sigma_{sx}) \cdot \cos^2\theta - \rho_z(\sigma_{sz,cr} - \sigma_{sx}) \cdot \sin^2\theta$

The following plots from "Cracking" and "Reinforcement" are also of interest and are also explained in more detail below [59]:

1. **Average Angle:** gives the average angle of the inclination of the compression field (θ in degrees) along the height of the member.

Average angle: $\tan^2\theta = \dfrac{\varepsilon_x + \varepsilon_2}{\varepsilon_z + \varepsilon_2}$

2. **Long. Reinforcement Stress:** gives the stress in the longitudinal reinforcement (σ_{sx} in MPa) for both the reinforcement bars and prestressing tendons along the height of the member.

Stress in the longitudinal reinforcement: $\sigma_{sx} = E_s \cdot \varepsilon_x$

3. **Long. Reinf Stress at Crack:** gives the stress in the longitudinal reinforcement at the crack ($\sigma_{sx,cr}$ in MPa) for both the reinforcement bars and prestressing tendons along the height of the member.

   Stress in the longitudinal reinforcement at crack: $\sigma_{sx,cr} = \dfrac{\sigma_1 + \tau_{ci} \cot\theta}{\rho_x} + \sigma_{sx}$

4. **Stirrup Stress at Crack:** gives the stress in the transverse reinforcement at the crack ($\sigma_{sz,cr}$ in MPa) along the height of the member.

   Stress in the transverse reinforcement at crack: $\sigma_{sz,cr} = \dfrac{\sigma_1 + \tau_{ci} \tan\theta}{\rho_z} + \sigma_{sz}$

6.3.2. Contribution of the components to the total shear resistance

The V-γ_{xy} plot on the left side only gives the shear resistance at failure, which is $V_R = 1046.8$ kN in the figures above. This total shear resistance can be divided into:

- $V_{c,AI}$ is the contribution of the aggregate interlock of the cracked concrete;
- V_{cc} is the contribution of the uncracked concrete;
- V_s is the contribution of the transverse reinforcement;
- V_p is the contribution of the vertical component of the prestressing force;

The following notations are used for the total contribution of the components:

$$V_R = V_{tot} + V_p \quad \text{with} \quad V_{tot} = V_{c,AI} + V_{cc} + V_s \tag{6.7}$$

Where V_R is the shear resistance according to Response-2010. If the slope of the prestressing tendons is zero, the vertical component of the prestressing force V_p is also zero, which results in $V_{tot} = V_R$.

The models used in all code provisions neglect the contribution of the uncracked concrete once concrete is cracked, although this component can be of quite the influence to the total shear resistance. The contribution of every component can be calculated with the RAW-data provided by Response-2010. By right-clicking on one of the plots and click "Copy Chart Data", the data can be extracted to a spreadsheet. The plots that of interest are: Shear stress (τ); Shear on Crack (τ_{ci}); Average Angle (θ); Stirrup Stress at Crack ($\sigma_{sz,cr}$) and Long. Reinforcement Stress (σ_{sx}).

The RAW-data of the plots give the stress at several points of the height of the cross-section. Multiplying the stress by the width at the calculated point and integrating the distribution of $\tau \cdot b$ over the height gives the shear force [19]:

$$V = \sum_{i=1}^{n} \left(\frac{\tau_i \cdot b_i + \tau_{i+1} \cdot b_{i+1}}{2} \cdot \Delta h \right) \tag{6.8}$$

This expression is used to calculate the total contribution V_{tot} and the contribution of each of the components $V_{c,AI}, V_{cc}$ and V_s. The components are calculated from the RAW-data with Equation 6.8 as follows:

- $V_{tot} \rightarrow \tau$;
- $V_{c,AI} \rightarrow \tau_{ci}$;
- $V_{cc} \rightarrow \tau$, where $\tau_{ci} = 0$ and $\tau_{sz,cr} = 0$;
- $V_s \rightarrow \tau_{sz,cr}$;
- $V_p \rightarrow \sigma_{sx}$.

The shear stress in the transverse reinforcement is calculated as follows:

$$\tau_{sz,cr} = \frac{\sigma_{sz,cr} \cdot \rho_z}{\tan\theta} \quad \text{with} \quad \rho_z = \frac{A_{sw}}{b \cdot s} \tag{6.9}$$

The vertical component of the prestressing force V_p is calculated as the sum of all vertical forces $V_{p,i}$ per cable:

$$V_p = \sum V_{p,i} \quad \text{with} \quad V_{p,i} = \sigma_{sx,i} \cdot A_p \cdot \sin\alpha_i \tag{6.10}$$

6.3.3. In-depth summary at a certain depth of the girder

The tab "Mohr's Circles", shown in Figure 6.13, gives an in-depth summary at a certain depth of the girder, including two Circles of Mohr (strains and stresses), longitudinal strains ε_x, inclination of the compression field θ, principal compressive stress σ_2 (f_2 in Response-2010), maximum allowed principal compressive stress $\sigma_{2,max}$, shear stress at crack τ_{ci} (ν_{ci} in Response-2010) and maximum allowed shear stress at crack $\tau_{ci,max}$. The "Vital Signs" bar plot visualizes the actual vs. the maximum allowed stresses of the concrete and reinforcement steel. When increments are defined, the previous or next load stage can be checked by simply pressing Pg Dn or Pg Up respectively.

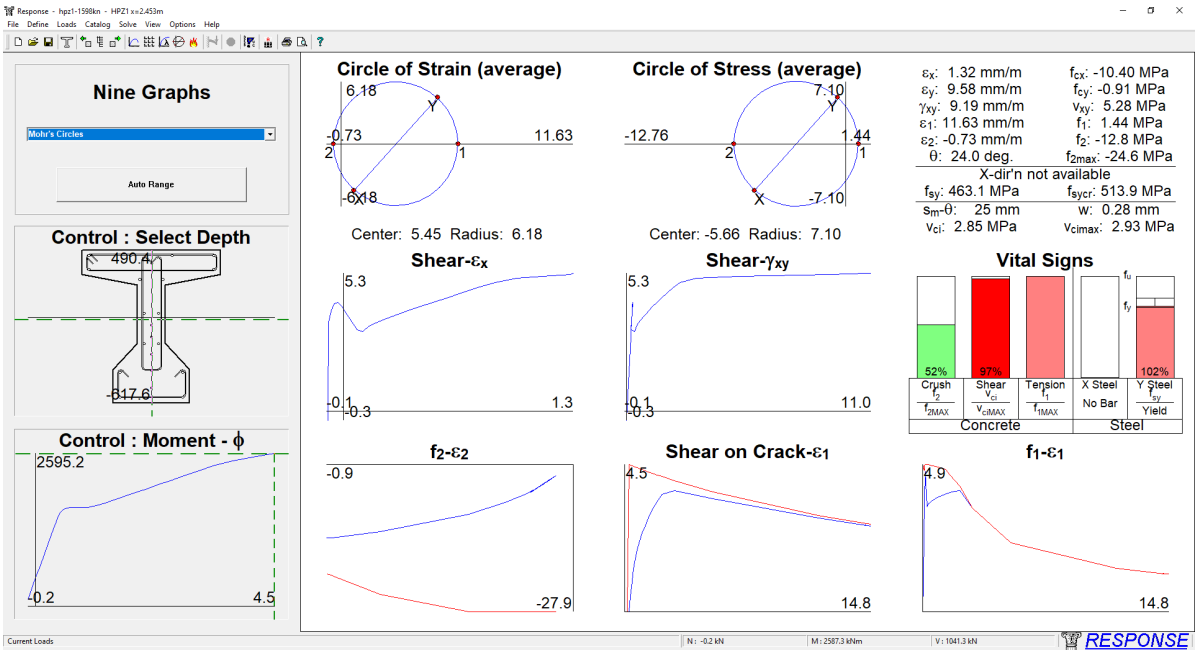

Figure 6.13: Sectional Response - Mohr's Circles for $x = 2.453$ m with Response-2010

6.4. Numerical results Response-2010

The numerical analysis for HPZ1 is done for two values for the prestressing force, 2.67 mm/m prestrain ($N_p = 1598$ kN) and 4.69 mm/m prestrain ($N_p = 2808$ kN). The maximum shear force calculated by Response-2010 is divided into components given in Chapter 6.3.2.

6.4.1. Detailed results for a = 2.903 m, N_p = 1598 kN and x = 1.725 m

Figure 6.14 shows the shear-shear strain-plot (V-γ_{xy}) for $x = 1.725$ m. The maximum shear is $V = 913.1$ kN. Figure 6.15 shows the six plots of interest to calculate the contribution of each component.

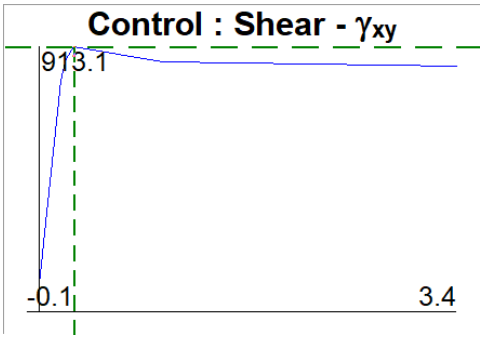

Figure 6.14: V-γ_{xy}-plot for $a = 2.903$ m, $x = 1.725$ m and $N_p = 1598$ kN

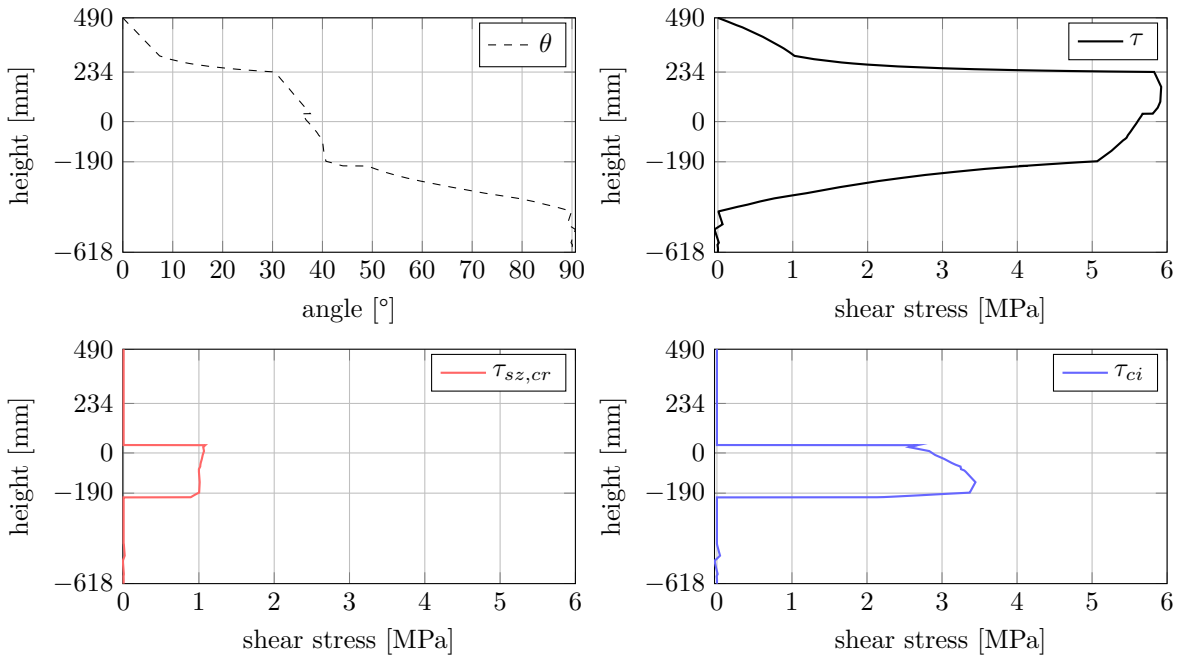

Figure 6.15: Plots with stresses for $V_R = 913.1$ kN with $a = 2.903$ m, $x = 1.725$ m and $N_p = 1598$ kN

Table 6.5: Longitudinal reinforcement stress σ_{sx} for $x = 1.725$ m

Long. Reinforcement Stress σ_{sx}				
Cable	σ_{sx} [MPa]	$N_{p,i}$ [N]	α_i[°]	$V_{p,i}$ [N]
4	476	219908	7.62	29167
5	488	225272	5.70	22387
6	501	231356	4.43	17881
7	514	237621	2.55	10589
8	514	237621	2.55	10589
9	529	244246	0.91	3893
10	529	244246	0.91	3893
			$\sum$	98399

The results from the RAW-data are shown in Figure 6.16. The shear stress τ, shear stress at crack τ_{ci} and average shear stress from the stirrups at crack $\tau_{sz,cr}$, given in Figure 6.15, are plotted together at the left side. The cross-section is shown at the right side of the figure. In the Helperzoom girder an additional shear force was found, denoted as ΔV, and is the difference between V_{tot} and the other components: $\Delta V = V_{tot} - V_{c,AI} - V_{cc} - V_s$. This additional component ΔV was not present in a simple girder with prestressing.

Plot (left): The centroidal axis of the girder is taken as $h = 0$ mm. The area between the horizontal dashed black lines correspond to the web of the girder, which is between $h = -190,..,234$ mm. The black line is the total shear stress τ, which gives the total shear V_{tot}. This total shear is divided in four components: uncracked concrete V_{cc} (light blue), cracked concrete $V_{c,AI}$ (blue), stirrups V_s (red) and additional shear force ΔV (green). ΔV is the difference between the black line (τ) and the red line ($\tau_{ci} + \tau_{sz,cr}$) multiplied by the width and integrated over the height. The shear contribution of each component is given inside the graph together with the percentage to the shear resistance V_R given by Response-2010.

Cross-section (right): The cross-section shows two colors, dark grey and light grey. The dark grey color represents the uncracked part of the member, where $\tau_{ci}, \tau_{sz,cr} = 0$. The top flange is fully uncracked, a part of the web is uncracked $h = 37,..,234$ mm and a part of the bottom flange is uncracked $h = -429,.., -210$ mm. The light grey color represents the cracked part of the member, where $\tau_{ci}, \tau_{sz,cr} > 0$. The bottom part of the web is cracked $h = -210,..,37$ mm and a part of the bottom flange is cracked $h = -617,.., -429$ mm.

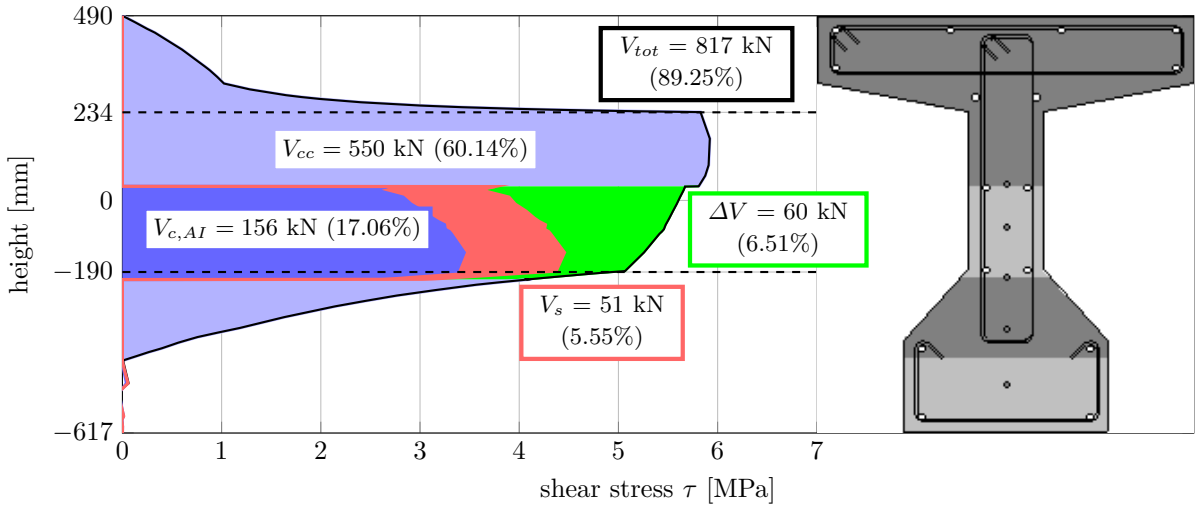

Figure 6.16: Contribution of each component to the shear resistance for $a = 2.903$ m, $x = 1.725$ m and $N_p = 1598$ kN

The results from Table 6.5 (σ_{sx}) and Figure 6.16 give a total shear resistance V_R of:

$$\begin{aligned} V_{tot} &= V_{c,AI} + V_{cc} + V_s + \Delta V = 156 + 51 + 550 + 60 = 817 \text{ kN} \\ V_R &= V_{tot} + V_p = 817 + 98.4 = 915.3 \text{ kN} \end{aligned} \tag{6.11}$$

This is a difference of +2.2 kN (+0.2%) with the shear resistance of the V-γ_{xy}-plot given in Figure 6.14.

6.4.2. Summarized results for a = 2.903 m and N_p = 1598 kN

The detailed results for five cross-sections with $a = 2.903$ m and $N_p = 1598$ kN are shown in Appendix B. In Figure 6.17 the contribution of each component to the shear resistance is given for the considered cross-sections. Figure 6.18 shows the shear resistance calculated with the sum of all components and the shear resistance given by Response-2010. Table 6.6 gives the failure mode for the cross-sections according to Response-2010.

The cross-sections given in Figure 6.17 can be separated into two regions, a region with a mostly uncracked member and a region with a mostly cracked member:

Region 1: $x = 1.725, 1.800, 1.900$ m with a cracked web and cracked bottom part of the bottom flange. A large part of the girder is uncracked: 60.14%, 74.56% and 62.07%.

- high contribution uncracked;
- low(er) contribution cracked;
- low contribution stirrups;
- contribution of ΔV;
- V_p remains almost constant.

Region 2: $x = 2.051, 2.453$ m with a cracked web and bottom flange. A low part of the girder is uncracked: 35.15% and 28.78%.

- low(er) contribution uncracked;
- high contribution cracked;
- high contribution stirrups;
- almost no contribution of ΔV;
- V_p is higher than the input value and V_p from the CSA output in Response-2010.

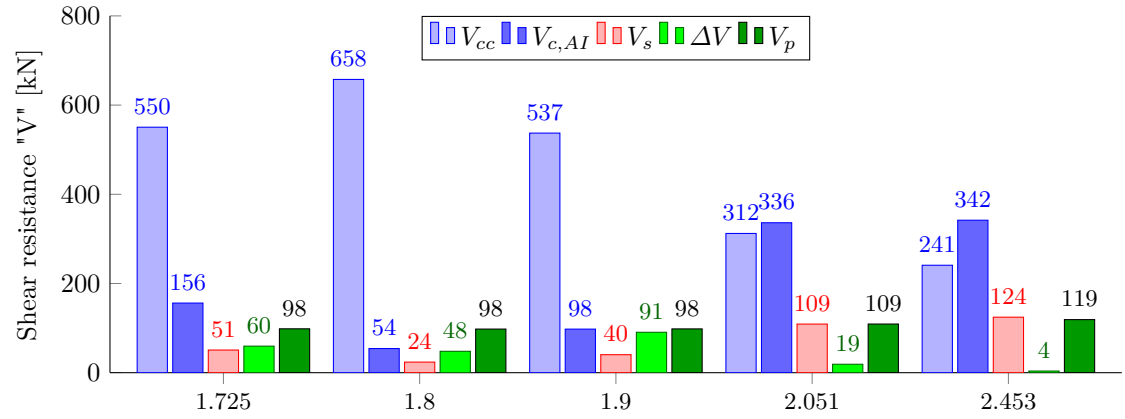

Figure 6.17: Contribution of each component to the shear resistance for $a = 2.903$ m and $N_p = 1598$ kN for different cross-sections

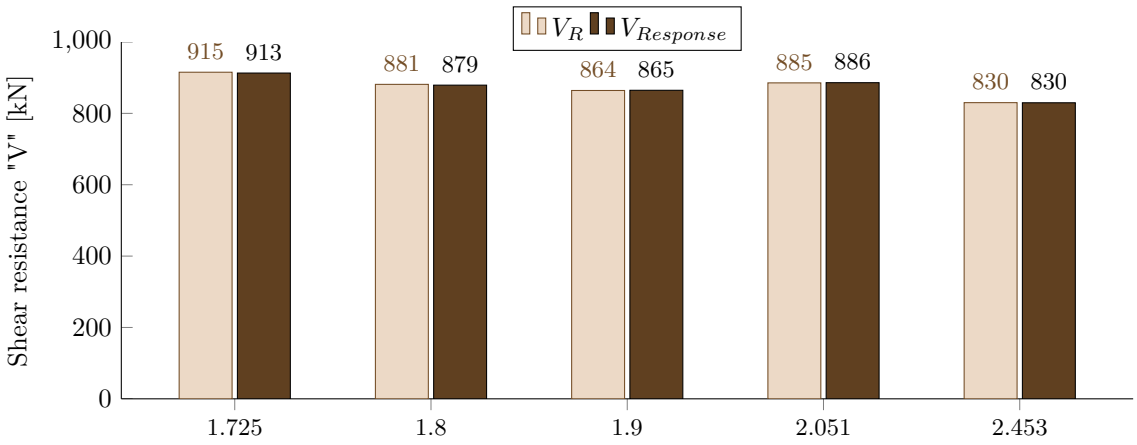

Figure 6.18: Shear resistance for $a = 2.903$ m and $N_p = 1598$ kN for different cross-sections

Table 6.6 gives the failure mode, the shear force at the first flexural crack V_{flex} and the shear force at diagonal tension cracking in the web V_{DTC}. For cross-section $x = 2.453$ m, the first flexural-shear cracks occur at $V = 746.9$ kN. The value for the first flexural crack for cross-section $x = 2.903$ m is $V_{flex} = 743$ kN. Table 6.7 shows the calculated internal lever arm z at maximum capacity and at failure.

Table 6.6: Failure mode V_{flex} and V_{DTC} for $x = 1.725$,..,2.453 m, $N_p = 1598$ kN

Cross-section [m]	**Failure mode**	V_{flex} **[kN]**	V_{DTC} **[kN]**
1.725	Crushing of the concrete	817.4	913.1
1.800	Crushing of the concrete	780.3	879.1
1.900	Crushing of the concrete	752.4	863.4
2.051	Crushing of the concrete / Buckling of the top flange	702.3	813.3
2.453	Crushing of the concrete	598.5	-

Table 6.7: Internal lever arm z for $x = 1.725$,..,2.453 m, $N_p = 1598$ kN

	1.725 m	**1.800 m**	**1.900 m**	**2.051 m**	**2.453 m**
Max load [mm]	679	688	695	717	739
Failure [mm]	616	625	664	668	673

6.4.3. Summarized results for a = 2.903 m and N_p = 2808 kN

The detailed results for all cross-sections with $a = 2.903$ m and $N_p = 2808$ kN are shown in Appendix C. In Figure 6.19 the contribution of each component to the shear resistance is given for the considered

cross-sections. Figure 6.20 shows the shear resistance calculated with the sum of all components and the shear resistance given by Response-2010. Table 6.8 gives the failure mode for the cross-sections according to Response-2010.

The cross-sections given in Figure 6.19 are mostly uncracked. **Region:** $x = 1.725,..,2.453$ m with a cracked web and cracked bottom part of the bottom flange. A large part of the girder is uncracked: 75.22%, 75.71%, 84.48%, 72.20% and 62.79%.

- high contribution uncracked;
- low contribution cracked;
- low contribution stirrups;
- low contribution of ΔV;
- V_p remains almost constant, although it decreases a bit towards the external load.

Cross-section $x = 1.900$ m is almost fully uncracked, resulting in zero contribution of aggregate interlock V_c, the shear reinforcement at the crack V_s and ΔV.

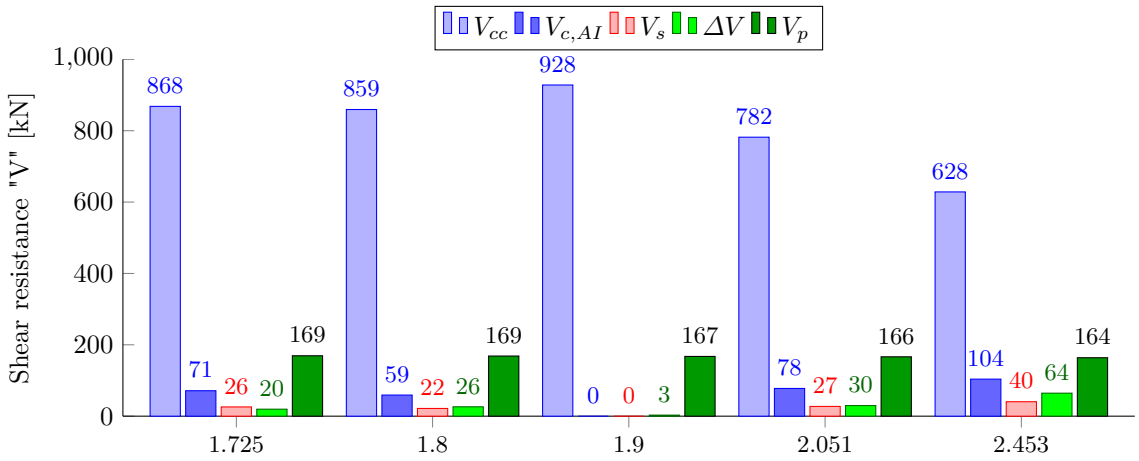

Figure 6.19: Contribution of each component to the shear resistance for $a = 2.903$ m and $N_p = 2808$ kN for different cross-sections

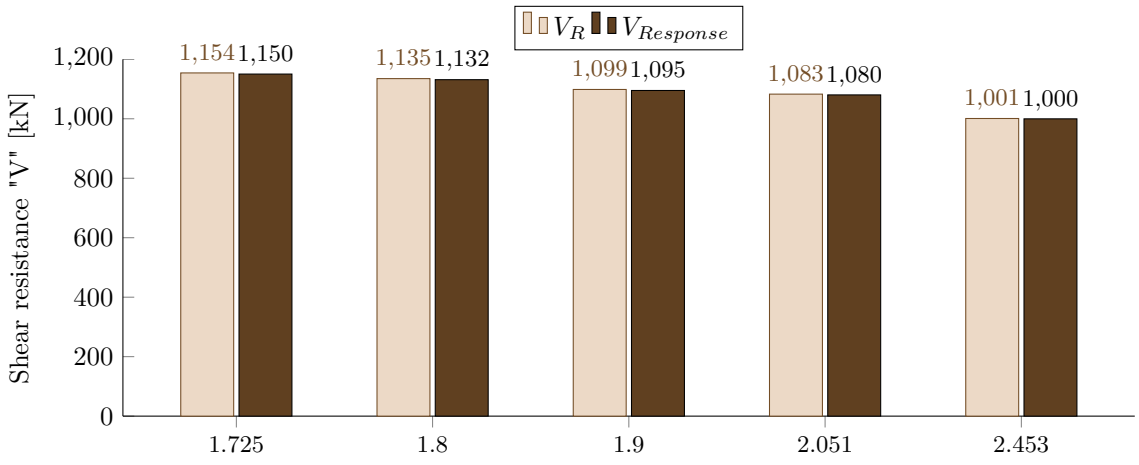

Figure 6.20: Shear resistance for $a = 2.903$ m and $N_p = 2808$ kN for different cross-sections

Table 6.8 gives the failure mode, the shear force at the first flexural crack V_{flex} and the shear force at diagonal tension cracking in the web V_{DTC}. The value for the first flexural crack for cross-section $x = 2.903$ m is $V_{flex} = 1055.7$ kN. Table 6.9 shows the calculated internal lever arm z at maximum capacity and at failure.

Table 6.8: Failure mode V_{flex} and V_{DTC} for $x = 1.725$,..,2.453 m, $N_p = 2808$ kN

Cross-section [m]	Failure mode	V_{flex} [kN]	V_{DTC} [kN]
1.725	Crushing of the concrete	1150.4	1150.4
1.800	Crushing of the concrete	1131.5	1131.5
1.900	Crushing of the concrete	1095.2	1095.2
2.051	Crushing of the concrete	1007.8	1080.3
2.453	Crushing of the concrete	915.4	999.8

Table 6.9: Internal lever arm z for $x = 1.725$,..,2.453 m, $N_p = 2808$ kN

	1.725 m	**1.800 m**	**1.900 m**	**2.051 m**	**2.453 m**
Max load [mm]	632	642	653	667	696
Failure [mm]	552	565	578	591	644

6.5. Discussion results Response-2010

The results for the numerical analysis are given in Chapter 6.4, Appendix B and Appendix C. In this section the results are discussed and divided in two sections: the use of Response-2010 and the results obtained with Response-2010.

6.5.1. Use of Response-2010

- Response-2010 is an quick and easy to use program to calculate the maximum shear force and failure mode of a cross-section. The five tabs, each with nine plots (General, Cracking, Mohr's Circles, No Shear and Reinforcement), present information about the distribution of stresses and strains of the reinforcement-, prestressing steel and the concrete for multiple load steps (if increments are defined).
- Response-2010 can be used for a cross-sectional- or a full member response. The full member analysis does not give detailed information about the distribution of the stresses and strains. For the cross-sectional response only the (unique) shear/moment-ratio and shear and moments from self-weight are defined. The influence of the length subjected to shear and the type of supports is not taken into account.
- In Response-2010 only one tension strength can be defined, there is no difference between the axial tensile strength f_{ctm} and the splitting tensile strength $f_{ctm,sp}$ as used in Chapter 5.1.
- The type of stirrup (closed, open, single, etc.) in the web had no influence on the maximum shear force, as long as the area of the shear reinforcement A_v is kept constant.
- The transverse reinforcement for the Helperzoom girders are following the shape of the girder as addressed in Chapters 3.1 and 4.1. This shape can not be modeled in Response-2010. However, it is observed that this will most likely not influence the capacity of the Helperzoom girder in Response-2010:
  1. The stirrups are always activated (yielding) in the web of the girder and not in the transition of the web to the flange, even when increasing the depth of the stirrups;
  2. Response-2010 is not able to give a failure mechanism of stirrups bursting out.
- If tendons are defined under an angle (slope in Response-2010), a vertical component of the prestressing force V_p is present. The input in the model is checked with the output of the CSA code provision given by Response-2010.
- The prestressing force is inputted as a prestrain $\Delta\varepsilon_p$. The axial compressive force N is zero from prestressing at the input for the sectional loads.
- There is no direct way to obtain the contribution of each component ($V_{cc}, V_{c,AI}, V_s, V_p$ and ΔV) from the maximum shear force given by Response-2010. The RAW-data (stresses) can be extracted from the plots and put into, for example, a spreadsheet program. The input of the model

makes a cross-section unique, which means that the amount of calculated nodes (data points / layers) differ for every cross-section. Therefore the procedure cannot be fully automated. To obtain the results presented in this Chapter for the different components, together with the complex geometry of the Helperzoom girders, it takes effort to create a spreadsheet that gives the results quickly, with as few manual actions as possible.

- It is observed that the maximum shear force calculated by Response-2010, denoted as "V_R", for members without prestressing cables is equal to the shear stress τ multiplied by the width b and integrated along the height of the cross-section, denoted as "V_{tot}" (see Equation 6.8). For members with prestressing and sloped tendons, V_{tot} is not equal to V_R. By adding the vertical component of the prestressing force $V_p = N_p \cdot \sin\alpha$ with $N_p = \sigma_{sx} \cdot A_p$ to V_{tot}, the difference between $V_{tot} + V_p$ and V_R lies between 0 and 0.9% for the calculated cross-sections. This (negligible) difference can be explained by the use of the expression for the linear stress distribution given in Equation 6.8.
- The values for V_p from the CSA results (Response-2010) and spreadsheet calculations (Chapter 3.7) are identical, for both $N_p = 1598$ and $N_p = 2808$ kN, and decrease for cross-sections closer to the external load. This is because the angle of the prestressing cables decreases, resulting in a lower value for the vertical component V_p. The calculated V_p with the longitudinal reinforcement stress σ_{sx} shows an increase for cross-sections closer to the external load, because the stress in the prestressing cables is higher than the stress inputted with the prestrain ($\sigma_{p\infty} = 0.00267 \cdot 185{,}000 = 494$ MPa $\rightarrow N_p = 1598$ kN and $\sigma_{p\infty} = 0.00469 \cdot 185{,}000 = 868$ MPa $\rightarrow N_p = 2808$ kN). This means that in the calculated V_p, a 'hidden' part is present due to elongation of the prestressing cables (if $\sigma_{sx} > \sigma_{p\infty}$), resulting in an increase of the vertical component of the prestressing force.

6.5.2. Results with Response-2010

- All cross-sections, for both $N_p = 1598$ and $N_p = 2808$ kN, had the same failure mode: crushing of the concrete. At failure the stirrups were yielding, but did not rupture as the stress in the stirrups did not reach its ultimate capacity: $f_y < f_u = 655$ MPa. The only cross-section that is different is at $x = 2.051$ m with $N_p = 1598$ kN, which also had buckling of the top flange at the last load step.
- Failure is taken at the depth of the girder where Response-2010 gives crushing of the concrete in the "crack diagram" in the "general tab" of the results. Crushing only takes place at one depth. At other depths $f_{2,max}$ is not reached, but v_{ci} is almost equal to $v_{ci,max}$.
- Before crushing of the concrete, the shear capacity is almost reached $v_{ci} \approx v_{ci,max}$ as observed in the "Mohr's Circle" tab. At further load steps f_2 rapidly approaches $f_{2,max}$.
- With increasing load steps the principal tensile strain ε_1 increases. The acting and maximum shear force v_{ci} and $v_{ci,max}$, the acting and maximum compressive force in the compression field/strut f_2 and $f_{2,max}$, the acting and maximum tensile force f_1 and $f_{1,max}$ and the inclination of the compression field θ decreases.
- The lowest inclination θ does not have to be at the depth taken where crushing of the concrete occurs. Also at the load step before failure, θ has a lower value than the load step at failure, at the depth where crushing of the concrete occurs.
- The internal lever arm z increases for cross-sections closer to the external load, because of the sloped tendons. It is lower at failure than at maximum load ($x = 1.725$ m): 679 mm at maximum load and 616 mm at failure. The prestressing force has influence on z: a higher prestressing force results in a lower z in order to make equilibrium between the compression- and tension chord forces.
- It is remarkable that the first flexural crack is not occurring at the cross-section under the external load at $x = 2.903$ m for both values for N_p. Cross-section $x = 2.453$ m has the lowest V_{flex}.
- At maximum shear force: For $N_p = 1598$ kN cross-sections $x = 1.725, 1.800, 1.900$ are mostly uncracked and $x = 2.051, 2.453$ are mostly cracked. For $N_p = 2808$ kN all cross-sections are mostly uncracked. Increasing the prestressing level results in a higher area of the girder that is uncracked, a higher failure load and flexural cracks occurring at a higher external load.

- The inclined cracking load is the maximum capacity of the girder, for all cross-sections. Increasing the area of the stirrups A_v by **two**, the girder builds up extra capacity after the onset of the first inclined crack and the failure mode stays crushing of the concrete.
- For both values of N_p the cross-section $x = 2.453$ m has the lowest maximum shear force: 830 kN for $N_p = 1598$ kN and 1001 kN for $N_p = 2808$ kN.
- At the depth where crushing of the concrete occurred all cross-sections had a value for the inclination of $\theta \approx 17°$, even for the cross-sections close to the external load. Figure 5.16 shows that for a (constant) inclination of $\theta = 15°$, this virtual crack crosses the intersection between the top flange and the web at $x \approx 2.0$ m and $x \approx 2.15$ m for $\theta = 19.08°$. Considering a constant inclination of $\theta = 17°$ this crack is still in the top flange of the girder, with a width of the top flange $b \approx 1$ m, for cross-sections between ≈ 2.075 and 2.903 m. It is unlikely that crushing of the concrete will occur in the top flange. For cross-sections between $x = 1.725$ and ≈ 2.075 m crushing of the concrete should occur at the top half of the web, although according to Response-2010 the depth at which crushing of the concrete occurred is at the lower half of the web. The measured angles of the shear cracks for HPZ1 and HPZ2, shown in Figure 4.7, show that the inclination varies along the crack. For cross-section $x = 2.453$ m this means that an inclination of $\theta = 45°$ is needed, see Figure 6.21. At $x = 2.453$ m the inclination has to abruptly change from $\theta \approx 45°$ to $\theta = 18.1°$, which is why this cross-section should be questioned as the critical cross-section.

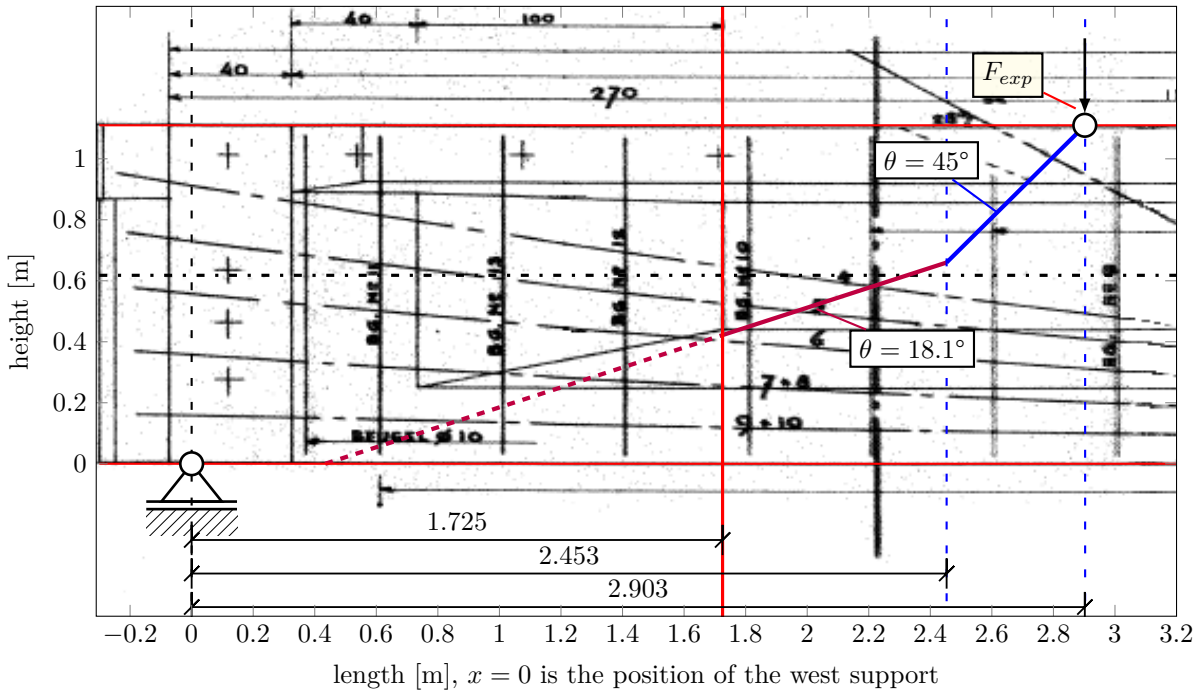

Figure 6.21: Three different inclinations of the compression field θ crossing the critical cross-section $x = 1.725$ m

- For $N_p = 2808$ kN, flexural- and diagonal tension cracking in the web occurs at the same shear force for $x = 1.725, 1.800, 1.900$ m, while for $N_p = 1598$ kN all cross-sections are cracked in bending before diagonal tension cracking occurs.
- The additional shear force component ΔV is not directly calculated from the plots/data provided by Response-2010. This shear force only occurs in a cracked area of the Helperzoom girder and in particular in cross-sections that have the following pattern: cracked bottom flange - uncracked bottom flange - cracked (bottom half) web. The cross-sections that have this pattern are (at maximum load):

  $N_p = 1598$ kN: $x = 1.725, 1.800, 1,900$ m

  $N_p = 2808$ kN: $x = 1.725, 1.800, 2.051, 2.453$ m

Replacing τ_{ci} with $\tau_{ci,max}$ for these cross-sections it was found that $\Delta V \approx 0$ and the following expression holds: $V_{tot} = V_{c,AI} + V_{cc} + V_s$, see Figure 6.22. Using $\tau_{ci,max}$ means that the maximum allowed shear stress is used, instead of actual stress τ_{ci}. Using $\tau_{ci,max}$ might not explain the additional component ΔV, because the shear stress τ is overestimated in the bottom part of the cracked zone in the web and underestimated in the upper part of the cracked zone in the web, shown in green in the figure below.

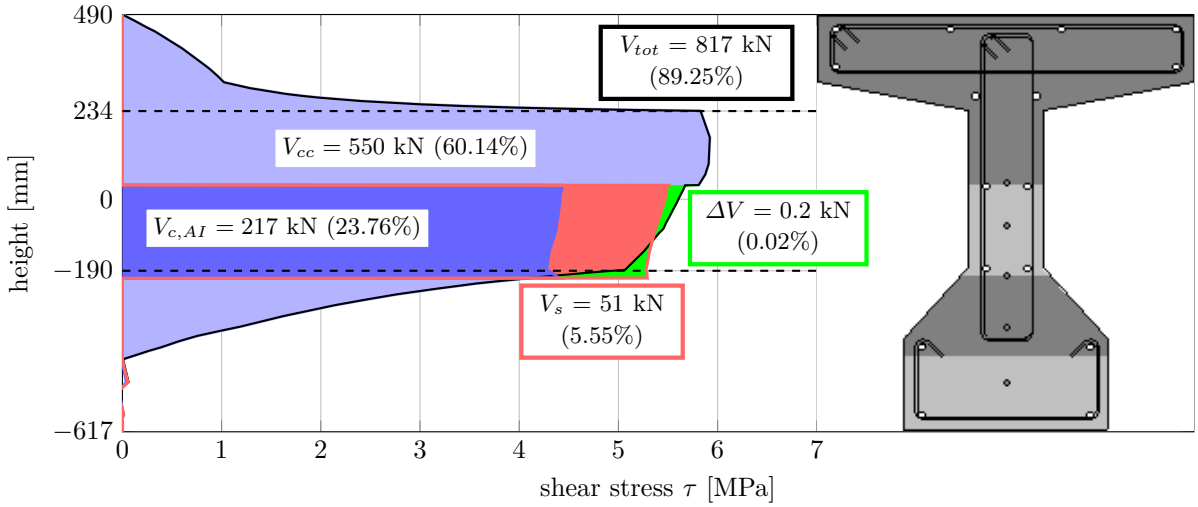

Figure 6.22: Contribution of each component to the shear resistance for $a = 2.903$ m, $x = 1.725$ m and $N_p = 1598$ kN using $\tau_{ci,max}$ instead of τ_{ci}

In this research ΔV is calculated as the difference between V_{tot} (calculated from the shear stress τ) minus the contribution of uncracked concrete V_{cc} (calculated from the shear stress τ, where $\tau_{ci}, \tau_{sz,cr} = 0$), cracked concrete $V_{c,AI}$ (calculated from the shear stress at crack of the concrete τ_{ci}) and the contribution of the stirrups V_s (calculated from the stirrup stress at crack $\sigma_{sz,cr}$).

7

Discussion results analytical, numerical and experimental analyses

In this chapter the results between Chapters 4, 5 and 6 are discussed. The results of the individual chapters for the experimental-, analytical- and numerical analysis with `Response-2010` are already given in their respective chapters. In the first paragraph the inclined cracking load is addressed. The second paragraph gives the observed and calculated shear capacities of the Helperzoom girder. Next the shear capacities for failure of the compression field are given. Lastly the results are evaluated between the three analyses.

7.1. Inclined cracking load

The results regarding the inclined cracking load from the experiments, analytical and numerical analyses for cross-section $x = 1.725$ m are compared in Figure 7.1. All the results are based on $N_p = 1598$ kN, except for **Response(2)** where $N_p = 2808$ kN. For the experimental and numerical analysis, the sectional shear force is used for which the first shear crack occurs. For the analytical analysis only the code provisions that distinguish between the flexural-shear capacity and shear-tension capacity are presented. The following additional information is given for Figure 7.1:

- **Black dashed line:** average value of the failure load of HPZ1 and HPZ2;
- **HPZ1:** sectional shear force for the first shear crack in the first experiment;
- **HPZ2:** sectional shear force for the first shear crack in the second experiment;
- **E-B:** shear-tension capacity according the the Euler-Bernoulli beam theory;
- **ACI (FS):** flexural-shear capacity according to ACI (V_{ci});
- **ACI (ST):** shear-tension capacity according to ACI (V_{cw});
- **EC2 (FS):** flexural-shear capacity according to EC2;
- **EC2 (ST):** shear-tension capacity according to EC2;
- **RBK:** flexural-shear capacity according to RBK1.1;
- **Response(1):** sectional shear force for which diagonal tension cracking occurs in the web according to `Response-2010` with $N_p = 1598$ kN;
- **Response(2):** sectional shear force for which diagonal tension cracking occurs in the web according to `Response-2010` with $N_p = 2808$ kN.

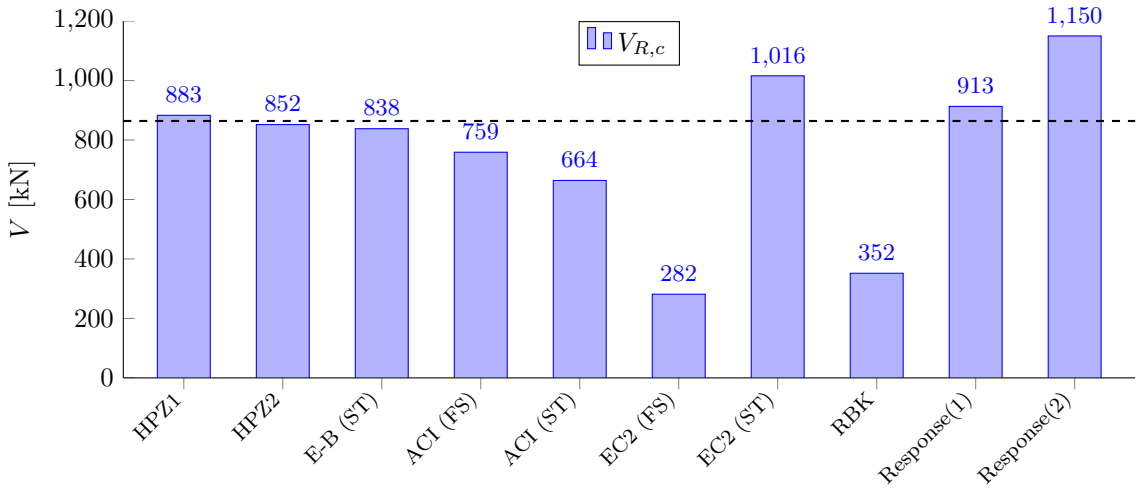

Figure 7.1: Inclined cracking load for the observed shear crack load for HPZ1 and HPZ2, Euler-Bernoulli beam theory and the five code provisions

7.2. Calculated shear capacities

The observed ultimate shear capacity from the experiments and the predicted shear resistances for the analytical and numerical analyses for cross-section $x = 1.725$ m are compared in Figure 7.2. All the results are based on $N_p = 1598$ kN, except for **Response(2)** where $N_p = 2808$ kN. For the analytical analysis the nominal shear resistance is used and differs per code provision. The nominal shear resistance in the EC2 and EC2 draft 2018 is the highest value of the concrete capacity and the capacity of the stirrups. In the ACI and AASHTO it is the sum of the contribution of the concrete, stirrups and prestressing force. The RBK sums the contribution of the concrete and the stirrups. In the numerical analysis with `Response-2010` the maximum shear force is used, which is given by the shear-shear strain plot. This shear force is the sum of the contribution of the cracked concrete, uncracked concrete, contribution of the stirrups at the crack, contribution of the vertical component of the prestressing force in the cracked area and the contribution of the vertical component of the prestressing force from the given prestrain. The following additional information is given for Figure 7.2:

- **Black dashed line:** average value of the failure load of HPZ1 and HPZ2;
- **HPZ1:** sectional shear force at failure in the first experiment ($V_{exp,HPZ1}$);
- **HPZ2:** sectional shear force at failure in the second experiment ($V_{exp,HPZ2}$);
- **ACI:** nominal shear resistance according to ACI for web-shear cracking/shear-tension failure ($V_{cw} + V_s$);
- **AASTHO:** nominal shear resistance according to AASHTO (algebraic equations) ($V_c + V_s + V_p$);
- **AASTHO (tables):** nominal shear resistance according to AASHTO (tables) ($V_c + V_s + V_p$);
- **EC2:** nominal shear resistance according to EC2 (yielding stirrups) (V_s);
- **RBK:** nominal shear resistance according to RBK1.1 (flexure-shear + yielding stirrups) ($V_c + V_s$);
- **EC2 2018:** nominal shear resistance according to EC2 draft 2018 (yielding stirrups) (V_s);
- **Response(1):** sectional shear force for which failure occurs in the web according to `Response-2010` with $N_p = 1598$ kN (crushing of the concrete) ($V_{c,AI} + V_{cc} + V_s + V_p + \Delta V$);
- **Response(2):** sectional shear force for which failure occurs in the web according to `Response-2010` with $N_p = 2808$ kN (crushing of the concrete) ($V_{c,AI} + V_{cc} + V_s + V_p + \Delta V$).

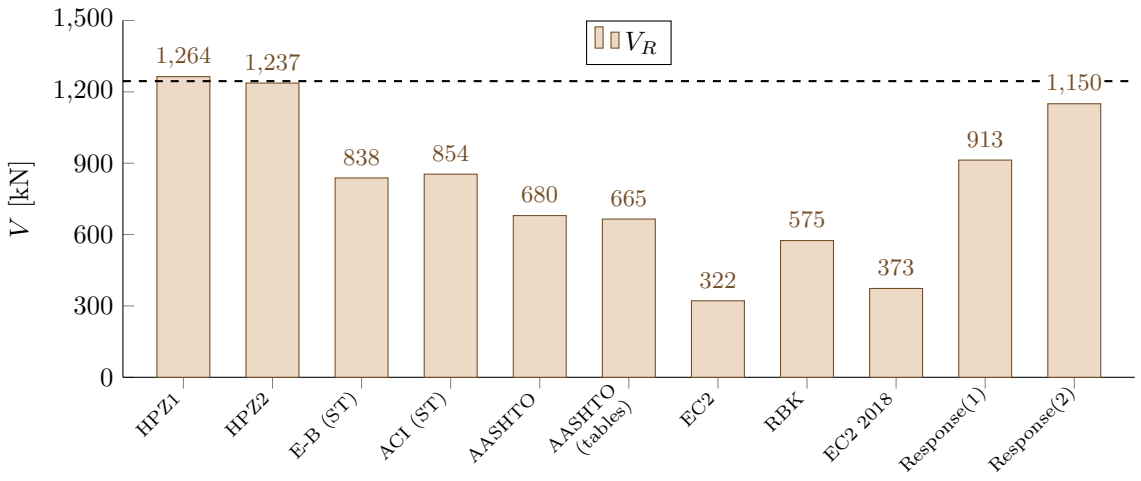

Figure 7.2: Shear capacities for the observed failure load for HPZ1 and HPZ2, Euler-Bernoulli, the five code provisions and `Response-2010`

7.3. Failure of the compression field

Next to the observed and calculated shear capacities, given in the previous paragraph, other calculations are made with the EC2 and EC2 draft 2018 as the observed failure mode was shear-compression failure for HPZ1 and HPZ2. These calculations are based on the maximum compressive capacity of the compression field with a certain inclination of the strut θ. In the first section calculations are made with a fixed (chosen) value for θ and in the second section with θ as a variable (rotating strut) until a solution was found, where the compressive capacity of the compression field is equal to the capacity of the stirrups (see Table 5.22).

In Chapter 5.7.7 three code provisions are checked for failure of the compression field: AASHTO, EC2 and EC2 draft 2018. For the AASHTO the calculation is based on a "hidden" and fixed value for θ, while for the EC2 and EC2 draft 2018 θ is included in the expression and can be chosen by the user. As the observations from the experiments are compared with the analytical and numerical results and the AASHTO does not include θ in the calculation, this code provision is not further considered. At the end of Chapter 5 the results are already thoroughly discussed, so only the results are presented, see Figures 7.3 and 7.4. Additional information for Figure 7.3:

- **Black dashed line:** average value of the failure load of HPZ1 and HPZ2;

First and second column (EC2): $V_{Rm,max} = \dfrac{\alpha_{cw} \cdot b_w \cdot z \cdot v_1 \cdot f_{cm}}{\cot\theta + \tan\theta}$

- **EC2(1)**, $V_{Rm,max}$ with $\theta = 15°$;
- **EC2(2)**, $V_{Rm,max}$ with $\theta = 21.8°$;

Third through ninth column (EC2 draft 2018): $V_{Rm,max} = 0.5 \cdot \nu \cdot f_{cm} \cdot b_w \cdot z$

- **EC2 D18(1)**, $V_{Rm,max}$, ν based on state of strains with $\theta = 19.08°$ and $N_{Ew} = 0$;
- **EC2 D18(2)**, $V_{Rm,max}$, ν based on state of strains with $\theta = 19.08°$ and $N_{Ew} = -N_E$;
- **EC2 D18(3)**, $V_{Rm,max}$, ν based on state of strains with $\theta = 17°$ and $N_{Ew} = -N_E$;
- **EC2 D18(4)**, $V_{Rm,max}$, ν based on state of strains with $\theta = 15°$ and $N_{Ew} = -N_E$;
- **EC2 D18(5)**, $V_{Rm,max}$, ν based on state of strains with $\theta = 15.11°$ and ε_x taken from the sectional analysis (analytical) for shear at ultimate $F_{exp} = 1890$ kN;
- **EC2 D18(6)**, $V_{Rm,max}$, ν based on state of strains with $\theta = 14.86°$ and ε_x taken from the results from LVDTs of HPZ1;
- **EC2 D18(7)**, $V_{Rm,max}$, ν based on state of strains with $\theta = 18.90°$ and ε_x taken from the results from LVDTs of HPZ2.

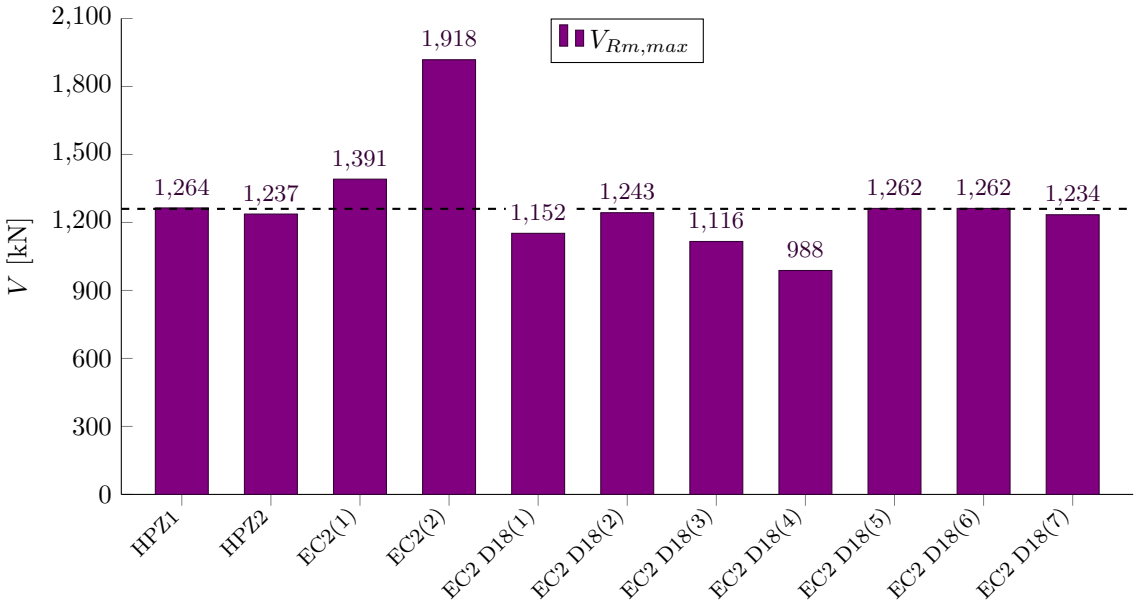

Figure 7.3: Shear capacities for failure of the compression field with EC2 and EC2 draft 2018

Additional information for Figure 7.4:

- **Black dashed line:** average value of the failure load of HPZ1 and HPZ2;
- **EC2**, $V_{Rm,max} = V_{Rm,s}$ with $\theta = 8.67°$;
- **EC2 D18(1)** $N_{Ew} = 0$, $V_{Rm,max} = V_{Rm,s}$ with $\theta = 11.19°$;
- **EC2 D18(2)** $+N_{Ew}$, $V_{Rm,max} = V_{Rm,s}$ with $\theta = 10.60°$;
- **EC2 D18(3)** Analytical, $V_{Rm,max} = V_{Rm,s}$ with $\theta = 11.45°$;
- **EC2 D18(4)** LVDTs HPZ1, $V_{Rm,max} = V_{Rm,s}$ with $\theta = 10.19°$;
- **EC2 D18(5)** LVDTs HPZ2, $V_{Rm,max} = V_{Rm,s}$ with $\theta = 11.91°$.

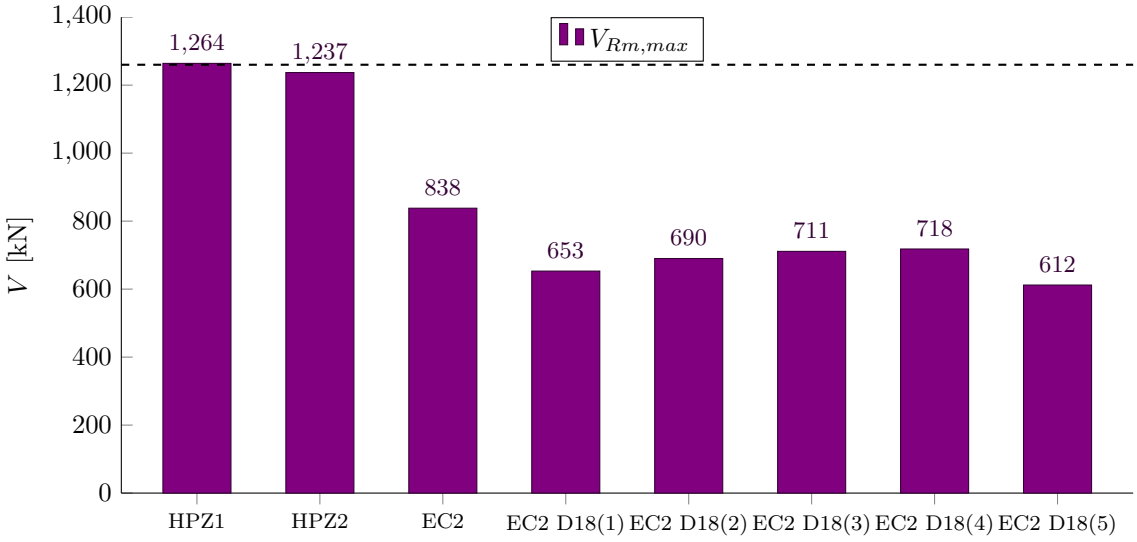

Figure 7.4: Shear capacities where failure of the compression field occurs simultaneously with yielding of the stirrups with EC2 and EC2 draft 2018

Based on the results given in Figures 7.1 through 7.4 the EC2 draft 2018 expression for $V_{Rm,max}$ with ν based on the state of strains give the shear capacity that is most in line with the observed failure loads of HPZ1 and HPZ2 and in particular with the longitudinal strains ε_x calculated with $N_{Ew} = -N_E$ ($\theta = 19.08°$), obtained from the sectional analysis for shear ($\theta = 15.11°$) and obtained from the LVDTs of HPZ1 ($\theta = 14.86°$) and HPZ2 ($\theta = 18.90°$).

7.4. Evaluation between the analyses

In this section the results of the shear capacities from the experimental, analytical and numerical analyses, given in the previous paragraphs, are discussed. Next to the shear capacities, the results regarding the internal lever arm z in mm, the critical position at x in m and the inclination of the compression field θ in degree are summarized in Table 7.1. For `Response-2010` two different z are given, at maximum load and at failure. The critical position $x = 1.725$ m is used for all analyses in order to compare the results.

7.4.1. Evaluation between the inclined cracking loads and shear capacities

Figures 7.1 through 7.4 are evaluated below:

- **Figure 7.1**: the results from Euler-Bernoulli, ACI (FS) and Response(1) are close to the onset of the first inclined crack observed in the two experiments of HPZ1 and HPZ2. The ACI (ST) and especially the EC2 (FS) and RBK underestimate the value for the inclined cracking load, while the EC2 (ST) and Response(2) overestimate it.
- **Figure 7.2**: all calculated shear capacities in the analytical and numerical analyses underestimate the observed failure load for HPZ1 and HPZ2. Response(2) is the closest result to the failure load, but is based on a high level of the prestressing force. The occurring failure mode for the analytical results presented in the figure are not in line with the observed failure mode in the experiments. The failure mode given by `Response-2010` is in line with the failure mode observed in the experiments.
- **Figure 7.3**: the calculations are based on the expressions given by EC2 and EC2 draft 2018 for failure of the compression field. The EC2 result with the lower limit of the inclination: EC(2) with $\theta = 21.8°$ results in a high capacity: $V = 1918$ kN and is overestimated compared to the results of HPZ1 and HPZ2. Ignoring this limit and lowering the inclination to $\theta = 15°$ results in a closer result: $V = 1391$ kN. The EC2 draft 2018 result EC2 D18(4), with ν based on the state of strains, using $\theta_{HPZ1} = 15°$ and $+N_{Ew}$ underestimates the capacity: $V = 988$ kN. The shear capacities of: EC2 D18(2) with an inclination of $\theta = 19.08°$ and $+N_{Ew}$ and EC2 D18(4,5&6) with analytically obtained and experimentally observed longitudinal strains from the LVDTs, are in line with the results of the experiments. The calculated inclination θ is compared with the measured cracking angle from the photographs and calculated inclination θ from the LVDTs, see Chapter 4.6.1 and 4.6.2. For HPZ1, the analytically calculated inclination from EC2 draft 2018 is close to the lowest measured cracking angle: $\theta_{EC2D18} = 19.08°$ vs. $\alpha_{photo} = 15°$ and calculated inclination from the LVDTs: $\theta_{EC2D18} = 19.08°$ vs. $\theta_{LVDT,XY} = 22.43°$. For HPZ2: $\theta_{EC2D18} = 18.90°$ vs. $\alpha_{photo} = 18°$, $\theta_{LVDT,XY} = 27°$ and $\theta_{LVDT,rosette} = 12°$.
- **Figure 7.4**: lowering the inclination θ until crushing of the concrete occurs simultaneously with yielding of the stirrups results in a lower shear capacity according to EC2 and EC2 draft 2018. The calculated inclinations are lower than the measured angles for the critical shear crack α_{photo} and calculated inclinations from the LVDT measurements θ_{LVDT}. Also the calculated shear capacities are not in line with the observed failure load. Comparing Figure 7.3 with Figure 7.4 and the discussion of the results in Chapter 5.7 might indicate that failure of the compression field does not occur simultaneously with yielding of the stirrups.

7.4.2. Evaluation of the differences between the analyses

In this section the calculated internal lever arms z, critical positions x and inclinations of the compression field θ between the three analyses are compared.

Table 7.1: Summarized results of the three analyses: experimental, analytical and numerical

	Calculated z [mm]		Critical position x [m]		Inclination θ [°]
	Max load	Failure	Calculated	Used	
HPZ1	-		1.828[8]	1.725	22° – 37° [5] (avg:27°) 18° – 26° [6] (avg:23°)
HPZ2	-		1.873[8]	1.725	29° – 36° [5] (avg:33°) 20° – 30° [6] (avg:27°) 12° – 18° [7] (avg:14°)
ACI	888[1]		0.555	1.725	45°
AASHTO	799		0.779	1.725	31.02° (algebraic) 27.57° (tables)
EC2	721		0.618,..,2.903	1.725	21.08°
RBK	721		0.618,..,2.903	1.725	30°
EC2 2018	725		0.725,..,2.051	1.725	19.08° (original) 15° – 19.08° (strains)
R(1)[3]	679	616	2.453	1.725	17.1° [2]
R(2)[4]	632	552	2.453	1.725	17.1° [2]

[1] ACI does not define z, only the effective depth d is calculated.
[2] Inclination at failure.
[3] `Response-2010` results with $N_p = 1598$ kN.
[4] `Response-2010` results with $N_p = 2808$ kN.
[5] Measured angle of the **critical** shear crack in the experiments from the DIC results (photos).
[6] Calculated inclination from the LVDTs results with XY-method.
[7] Calculated inclination from the LVDTs results with Rosette-method for "LVDTs 3-11-15, 5-6-11-14 and 1-2-5-6-11-14" (HPZ2 only).
[8] Measured critical position x from photographs taken after failure for the shear crack.

– The internal lever arm is lowest for `Response-2010`: 679 mm [$0.88d_p$] ($N_p = 1598$ kN and at maximum load) and highest for ACI: 888 mm [$1.15d_p$]. The ACI and AASHTO have a minimum value for the internal lever arm, $0.8h$ [$1.15d_p$] and $0.72h$ [$1.04d_p$] respectively. This is the reason why the internal lever arms for these two code provisions is higher than the other codes and `Response-2010`. The EC2, RBK and EC2 draft 2018 state that z can be assumed as $0.9d_p$ and have no minimum value like the ACI and AASHTO. The internal lever arm can also be calculated with a flexural analysis, which is done in the analytical analysis: $z \approx 0.94d_p$. These codes are closest to the value calculated by `Response-2010`. It is important to note that z stays constant for the codes, while in `Response-2010` it decreases at increasing load steps.

– None of the design codes nor `Response-2010` predicted the critical position x correctly. For the ACI and AASHTO, the calculated cross-section is in the region where the web is thicker: $x < 1.725$ m. For the EC2, RBK and EC2 draft 2018 a region is calculated and the cross-section with the lowest shear capacity is the critical position. For all three code provisions $x = 1.725$ m is the cross-section with the lowest shear capacity, although the shear capacities for all cross-sections are close to each other. The results from `Response-2010` state that $x = 2.453$ m is the critical cross-section, but this could be questioned as done in Chapter 6.5. From the results of the analytical analysis (EC2, RBK and EC2 draft 2018) it could be concluded that the critical position is between $x = 1.725$,..,2.051 m and from the numerical analysis (`Response-2010`) at $x = 1.900$ m. Based on these conclusions and the measured critical position of both experiments, it can be concluded that the critical positions are predicted correctly. Also the critical position $x = 1.725$ m with $\theta = 30°$ used in Chapter 3 is considered as a good assumption. To compare the results between the three analyses, $x = 1.725$ m is used as the critical cross-section.

– The calculated inclinations of the compression field θ (or measured angle of the **critical** shear crack α from the photographs) differ a lot between the three analyses and even between the results of the individual analyses. For the experimental results the minimum angle of the critical shear crack is $\alpha_{photo} = 22°$ for HPZ1 and $\alpha_{photo} = 29°$ for HPZ2. The minimum inclinations from the LVDTs (XY-method) are $\theta_{LVDT,XY} = 18°$ for HPZ1 and $\theta_{LVDT,XY} = 20°$ for HPZ2 and the average inclinations are $\theta_{LVDT,XY} = 23°$ for HPZ1 and $\theta_{LVDT,XY} = 27°$ for HPZ2. For the Rosette-method the inclination of "LVDTs 3-11-15" is $\theta_{LVDT,rosette} = 12°$. The angle of the shear crack α, measured from the photographs, is usually higher than the (internal) inclination of the compression field. The inclination θ_{LVDT}, calculated from the measured displacements of the LVDTs, are based on a grid of 500x320 mm and are calculated at an infinitesimal plane element, at the intersection of the vertical - horizontal (- diagonal) LVDTs. The calculated θ_{LVDT} are averaged over an area around this very small plane element, locally at or around the crack θ could be lower. For the analytical results the way to obtain θ differs for most of the design codes, resulting in a wide range: $\theta = 15° - 45°$. For the numerical results with `Response-2010` the inclination at maximum load ranges from $\theta = 31.3° - 47.8°$ for $N_p = 1598$ kN and $\theta = 33.5° - 39.7°$ for $N_p = 2808$ kN. At failure the inclination is $\theta = \approx 17°$ for all cross-sections and the two levels of the prestressing force. Considering all results, the EC2, EC2 draft 2018 and `Response-2010` are close to the measured angles of the critical shear crack α_{photo} and calculated inclinations from the LVDT results θ_{LVDT} for HPZ1. For HPZ2 the measured angles of the critical shear crack α_{photo} are higher than the analytical and numerical results. The inclinations obtained with $\theta_{LVDT,XY}$ and $\theta_{LVDT,rosette}$ are more in line with the analytical and numerical results. The XY-method gives higher values for θ, while the Rosette-method gives values that are most in line with the values obtained with the EC2 draft 2018.

7.4.3. Other noteworthy differences/observations

– For two design codes the shear capacity was influenced/based on the value of the external load F_{exp}: AASHTO and EC2 draft 2018. When $F_{exp} = 1890$ or $F_{exp} = 1850$ kN is used, so without the use of iterations, the nominal shear resistance reaches a much lower value. It is concluded that the use of iterations are inevitable to obtain an accurate value for the nominal shear resistance. For the other three design codes: ACI, EC2 and RBK the external load had no influence on the shear capacity, see also Chapter 5.7.5.

– Increasing N_p results in flexural cracks occuring at a higher external load and results in a higher failure load for both analytical (flexural analysis) and numerical analyses.

– The additional vertical force ΔV_p is not implemented in the design codes. It can be added separately as an increase of the shear capacity of the girder. However, in AASHTO it is possible to increase the value of f_{po} in the calculation for the longitudinal strains at mid-depth ε_x, to account for the elongation of the tendons during loading (see Appendix A with $f_{po} = 0.342 f_{pu}$). Although ΔV_p is analytically calculated in Chapter 4.6.5, this contribution is not implemented in the shear capacities calculated in Chapter 5. The increase of the shear capacity is also almost negligible ($\Delta V_p \approx 43$ kN). In `Response-2010` this additional component ΔV_p is included in the component V_p.

– Arching action is not considered in the analytical analysis, because the span-to-depth ratio is greater than the ratios given in the design codes. For the EC2 arching action can increase the value for $V_{R,c}$ by **four** for low a/d-ratios ($\beta_{EC2} < 4$). In the analysis and measurement reports [72] [73] it was concluded that a direct strut did not develop. Simulating arching action in the numerical analysis is not possible, because a cross-section analysis is done with `Response-2010`.

– For the three analyses the contribution of the stirrups is calculated in different ways. For the experimental analysis the contribution of the stirrups is based on the intact stirrups after failure. For HPZ1 three stirrups were still intact and one was broken after failure of the girder. For HPZ2 all stirrups were intact, so all contributed to the shear capacity. The design codes use a maximum contribution of the stirrups based on the inclination θ and the yield strength of the mild steel f_{ym}. For `Response-2010` the contribution of the stirrups depends on the calculated stress in the stirrups. The stress in in the stirrups did not reach ultimate strength $f_u = 655$ MPa ($\sigma \approx 600$ MPa).

- The acting and maximum allowed compressive force in the compression field decreases with increasing load steps/strain in `Response-2010` and varies along the depth of the girder. In the design codes the compressive force is constant over the depth of the girder. The calculations of EC2 draft 2018 exceed the maximum allowed compressive force in the compression field. The acting and maximum allowed compressive force do not match the results from `Response-2010`.
- For the calculations where the capacity for crushing of the concrete is equal to yielding of the stirrups, the mean yield strength of the stirrups is used $f_{ywm} = 454$ MPa. After yielding of the stirrups there is extra capacity of the steel until failure (rupture of the stirrups) at ultimate strength f_u. According to `Response-2010` the ultimate strength $f_u = 655$ MPa is not reached, the stress peaks around 600 MPa. Using a higher stress than the yield stress in the analytical analysis will result in a higher shear capacity. In the experiments,
- According to the numerical results presented in Chapter 6 the contribution of the uncracked zone of the concrete is accounted for in the total shear capacity and can be large: up to 75% for $N_p = 1598$ kN and up to 85% for $N_p = 2808$ kN, while all the design codes assume zero contribution of the uncracked zone.

8

Conclusions and recommendations

The intended result of this research is to predict the shear capacity and failure mode for the Helperzoom prestressed T-girders according to the (inter)national design codes and `Response-2010`. These type of girders do not get approved (unity check (UC) > 1.0) by arithmetic models in the current standards: the edge girders have a UC of 1.69 and the middle girders of 1.05 according to the road layout provided in the RBK 1.1. Next to the analytical and numerical models used in this research, four Helperzoom girders have been tested at Stevinlab II. Due to limited time available only the first two girders, HPZ1 and HPZ2, are analyzed in this thesis. The results of the analytical, numerical and experimental analysis give answers to the research question:

What is the predicted shear capacity and governing shear-failure mode of the post-tensioned T-beams taken from the Helperzoom Bridge (KW 17)?

The sub-questions are related to the research question and should give a basis to verify the shear capacity, if possible the governing failure mode and the differences and similarities between the analyses and is done in the first paragraph. With this thesis the view on prestressed T-girders of this type can be reconsidered, because a new code provision (EC2 draft 2018) is used to calculate the shear capacity for failure of the compression field and gives results that are in line with the observed failure load of HPZ1 and HPZ2. This new insight can be used to verify similar existing bridges in the Netherlands and to give the start for further research on this topic. The recommendations for practice and future work are given in the second and third paragraph.

8.1. Conclusions

Prior to this thesis and the experiments, a preliminary report was made by Roosen [1]. In this report a recommended set-up was given and calculations were made for the Helperzoom girders to see how and whether shear-tension failure could occur during the experiments. Many assumptions have been made: the inclination of the compression field θ, level of the prestressing force, tensile strength of the mild steel and prestressing steel, and the compressive- and tensile strength of the concrete. Most of these assumptions were based on the RBK, the Dutch code for existing structures. The preliminary report has been the basis for this research and is made more extensive, whereby multiple cross-sections are considered, the material properties taken from test results and the internal forces are updated with the set-up used in the experiments, see Chapter 3. The most important results of the two experiments have been combined and summarized in the experimental analysis, such as the failure load, the failure mechanism, the load at which the first inclined crack occurred, the cracking angles of the observed cracks, the contribution of the shear reinforcement and the contribution of the prestressing cables to the shear capacity. This data is used in the analytical and numerical analysis to validate the results obtained from the experiments.

Which codes can be used for (existing) structures?

A total of five, national and international, (design) codes are used to check the shear capacity and the associated failure mechanism is if the code in question gives it. The five codes are: ACI 318-14, AASHTO LRFD 8th edition, EC2 (NEN-EN 1992-1-1:2011), RBK 1.1 (2013) and EC2 draft 2018 (prEN 1992-1-1 2018 D3), have been studied in Chapter 2 and used in Chapter 5. In section 5.7 it appeared that there are many differences between the design codes.

What are the significant differences between the code provisions for the calculation of the shear resistance of prestressed concrete members?

The differences are the models used (experimentally or analytically obtained), the calculated shear capacities and the given failure mechanism. Only the ACI and the EC2 provide a failure mechanism between flexure-shear and shear-tension failure. The used and/or calculated variables can also vary considerably, such as the internal lever arm z, inclination of the compression field θ and the critical position x. The lowest calculated capacity is the shear capacity according to the design codes, but it has been found that these capacities are not realistic and give too low values compared to the test results.

Which codes predict the critical shear capacity and associated failure mode the most accurately?

The load for which the first inclined crack (shear-tension or flexure-shear crack) occurs varies enormously between the models and standards: $\approx 33\% - 133\%$ of the average inclined cracking load of HPZ1 and HPZ2. It can be concluded that the Euler-Bernoulli beam theory (shear-tension), ACI (flexure-shear) and EC2 (shear-tension) give representative values for the inclined cracking load. However, for the ultimate shear capacity, none of the design codes provide a representative value that matches the results of the experiments. According to the EC2 (shear-tension) the capacity after the first inclined crack is zero (inclined crack = failure) and according to the ACI (flexure-shear and shear-tension), AASHTO and RBK the extra capacity is (a part of) the contribution of the shear reinforcement. The results of EC2 (flexure-shear) and EC2 draft 2018 show that the capacity of the concrete is lower than the capacity of the shear reinforcement, meaning that only the capacity of the shear reinforcement is considered for the shear capacity of the girder. According to the Eurocodes, the contribution of the uncracked zone(s) in the cross-section is zero. From this it is concluded that there is no general agreement as to what happens to a concrete girder after the first inclined crack has occurred.

Observations from the two tests, HPZ1 and HPZ2, showed that shear-tension failure did not occur, but another failure mechanism: shear-compression failure. As previously mentioned the calculated shear capacities are not in line with the observed failure load and -mode. Shear-compression failure cannot be calculated with the codes, because of arch action between the external load and the support. This is the reason why the capacity for failure of the compression field is calculated.

What is the influence of the inclination of the compression field θ and how do the results change if θ changes? (analytical)

The values obtained for failure of the compression field $V_{Rm,max}$ are much closer to the results of the tests and in particular the values that are calculated with the EC2 draft 2018. The EC2 draft 2018 is one of two design codes, wherein the angle of the strut θ can be entirely chosen by the user with the condition that the capacity of the compression field is greater than the capacity of the shear reinforcement (yielding). The inclination θ in the EC2 draft 2018 can be much lower than the limit prescribed by the current EC2, with $\theta = 21.8° - 45°$. In addition, calculations are made by lowering the inclination of the compression field to the point where yielding of the shear reinforcement is equal to the failure of the compression field: $V_{Rm,s} = V_{Rm,max}$ (lower limit of the shear capacity), see Figure 7.4. This results in a lower shear capacity and a lower capacity than the results from the experiments. Comparing the inclination θ_{LVDT}, obtained from the LVDT measurements, with the used θ in EC2 draft 2018 for $V_{Rm,max}$, it can be concluded that the inclinations are almost the same. The obtained θ for $V_{Rm,s} = V_{Rm,max}$ in EC2 draft 2018 is much lower than $\theta_{LVDT,XY}$ for both girders. The inclinations obtained with the Rosette-method $\theta_{LVDT,rosette}$ for HPZ2 are close to θ obtained with $V_{Rm,s} = V_{Rm,max}$. Comparing the observed failure load of the experiments V_{exp} with the shear capacity calculated with $V_{Rm,max}$, the capacity for failure of the compression field is higher than that of the shear reinforcement: $V_{Rm,max} > V_{Rm,s}$. However, in the experiments it was observed that some

stirrups were broken after failure. This implicates that failure of the compression field occurred at the same time as failure of the shear reinforcement $V_{Rm,s} = V_{Rm,max}$. Based on this contradiction arching action occurred between the external load and the support, but according to the DIC and LVDTs results this did not appear to be present during the experiments. Arching action is not considered in the analytical analysis, because the span-to-depth ratios for the experiments are higher than the ratios given for arching action in the design codes.

What additional insights do the numerical calculations give to the contributions of the various components to the total shear resistance?

In addition to the analytical calculations, a numerical model is made in `Response-2010` to calculate the shear force capacity and to determine the failure mode. The advantages of this program is that the calculations are made relatively quickly and that the contributions of all components ($\Delta V_c, V_c, V_s, V_p, \Delta V$) can be evaluated separately. The disadvantage is that calculations are done per cross-section, which means that the adjacent cross-sections have no influence and that the girder cannot be modeled as a whole. After evaluating the contributions of all components, it can be concluded that the contribution of the uncracked zone is significant to the total shear capacity. For the model with the prestressing force $N_p = 1598$ kN, which is also used in the analytical analysis, cross-sections close to the support ($x = 1.725 - 1.900$ m) have a high contribution of the uncracked zone to the total shear resistance (60% - 75%). For the model with a higher prestressing force $N_p = 2808$ kN the contribution of the uncracked zone is high for all cross-sections (63% - 85% of the total shear capacity). Thus the higher the prestressing force N_p, the higher the contribution of the uncracked zone to the total shear resistance. The contribution of the other components are generally speaking low, except for cross-sections $x = 2.051$ and $x = 2.453$ m for $N_p = 1598$ kN where most of the cross-section is cracked.

What is the influence of the inclination of the compression field θ and how do the results change if θ changes? (numerical)

The results of this model show that at maximum load V_R the inclination θ ranges from $31.3° - 47.8°$. At increasing load steps the maximum load decreases together with the inclination θ. The acting and allowable compressive force in the compression field is related to this inclination and decreases as well. At failure, the last load step, the results show that failure of the compression field occurs for all considered cross-sections, with an angle $\theta \approx 17°$. This also applies to cross-sections close to the external load. At these cross-sections the calculated angle does not correspond at all to the depth at which failure occurs in the model; with the calculated angle crushing of the concrete should occur at the top of the web instead of at the bottom half of the web. For that reason and to compare the results with the analytical and experimental results, only the critical cross-section at 1.725 m is considered.

How do the analytical and numerical calculations relate to the results of the test?

and

What is the predicted shear capacity and governing shear-failure mode of the post-tensioned T-beams taken from the Helperzoom Bridge (KW 17)?

National- and international design codes are a tool for a safe and conservative design of a structure, but are based on simplifications and assumptions of complex theories or a number of experiments. This means that when a (part of a) bridge or other type of structure is designed, assessed or checked with experimental results, these tools can provide a good basis and insight for an engineer. Relatively quick calculations can be made to see if a certain element meets the prescribed requirements given by the design codes. It can be questioned that every civil structure can be based on simplified calculations and standards.

So the question is; is this realistic and is this applicable for the girders taken from the Helperzoom bridge? This will most likely suffice for a large number of structures, especially for "simple" structures. If these structures differ geometrically from the standard or become complex, like the Helperzoom girders, it may be possible that it cannot simply be validated with current regulations. According to the analytical results provided in this research, none of the design codes give a corresponding result with the experimental results, except for EC2 draft 2018: "failure of the compression field, $V_{Rm,max}$" with ν based on the state of strains, $\theta \leq 19.08°$ and where (a part of) the compressive force is taken by the web, denoted as N_{Ew}. Four results, each with a different way the longitudinal strain ε_x is obtained,

are very close to the observed shear capacity in the experiments of HPZ1 and HPZ2. Comparing the results for the inclination of the compression field θ obtained from the experimental results, the calculated inclinations $\theta_{LVDT,XY}$ for the "XY-method" are a bit higher than the used inclinations in the EC2 draft 2018. The calculated inclinations $\theta_{LVDT,rosette}$ with the "Rosette-method" (HPZ2 only) for combinations "LVDTs 3-11-15, 5-6-11-14 and 1-2-5-6-11-14" are a bit lower than the used inclinations in the EC2 draft 2018 for $V_{Rm,max}$.

Fortunately, there are powerful numerical programs to model and calculate these structures in 2D and 3D. `Response-2010` is a 2D sectional analysis program that is used in this thesis to calculate the shear resistance of the Helperzoom girders. The remarkable thing is that the inclined cracking load (diagonal tension cracking, shear-tension) and the occurring failure mechanism (crushing of the concrete) from the model corresponds to the test results, with a prestressing force of $N_p = 1598$ kN. However, no additional capacity is built up after the occurrence of the inclined crack in the model as observed in the experiments. The inclined cracking load is therefore the maximum capacity of the girder and is not in line with the observed failure loads for HPZ1 and HPZ2. Crushing of the concrete occurs at a lower capacity than the inclined cracking load/maximum capacity, a few load steps further, without rupture of the stirrups.

For both the analytical and numerical analyses it can be concluded that the output remains dependent on the user's input and the results must always be critically examined and judged from an civil engineering perspective. "Engineering judgment" will therefore play a major role in this involving insight, knowledge and experience.

8.2. Recommendation for practice

This section gives a recommendation to determine the shear capacity of bridges with similar T-girders as the Helperzoom girders that are still in use. An analytical analysis, with five (inter)national standards, and a numerical analysis, with `Response-2010`, has been conducted to check the shear capacity of the Helperzoom girders. It is easy to model the girder in `Response-2010` and the shear capacity is calculated relatively quickly. It can be said without doubt that the result obtained with `Response-2010` gives a good (first) estimate, although the calculated shear capacity was found to be conservative compared to the observed failure load. The analytical analysis shows that the EC2 draft 2018 gives the best result for the Helperzoom girders, whereby the shear capacity is determined on the basis of the state of strains. In this code provision, the inclination of the compression field can be chosen completely freely. The limit of this inclination is the moment that failure of the compression field occurs simultaneously with yielding of the stirrups, which is also the lower limit of the shear capacity of the girder. The actual shear capacity is likely to be higher than this limit, as shown in this study, but that cannot be proven without conducting experiments. To determine the minimum shear capacity, data such as the longitudinal strain obtained from the sectional analysis (analytical) and LVDTs from both tests cannot be used, so the longitudinal strain must be determined using the expression given in EC2 draft 2018. The longitudinal strain ε_x is determined in two ways, the first being based on the shear zone (web) making no contribution: $N_{Ew} = 0$ and the second being based on the shear zone making a contribution. In this research it is assumed that this contribution is equal to $N_{Ew} = -N_p$. The difference in the shear force capacity between these two methods is 7.3% for failure of the compression field and around 5% when failure of the compression field equals yielding of the stirrups. Without a contribution of the shear zone the longitudinal strains are higher, resulting in a lower value for ν and a lower shear capacity. In the EC2 draft 2018 no expression was given how N_{Ew} should be calculated or determined, just an upper limit: $-N_{Ew} \leq |V_E| \cdot \cot\theta$. In other words, the axial tensile force N_V must be greater than zero. This upper limit did not apply to the Helperzoom girders using $N_{Ew} = -N_p$, because the value of $|V_E| \cdot \cot\theta$ was quite high. For the Helperzoom girders, HPZ1 and HPZ2, the second method gave the best results regarding the shear capacity and the inclination of the compression field. For the assessment of similar T-girders this can be different, so it is recommended to calculate the longitudinal strains with $N_{Ew} = 0$ as this gives a more conservative (lower) value for the shear capacity.

8.3. Future work

The following recommendations are given for possible future work:

- Check if the value for the level of the prestressing force N_p used in this research coincides with the HPZ3 and HPZ4. At the time of writing this thesis a realistic value was needed for N_p to conduct the analytical and numerical analysis. This value is based on tests performed on HPZ2: $N_p = 0.27 f_{pu}$ (or $0.57 N_{p,RBK}$), see Chapter 4.3.2.
- Only HPZ1 and HPZ2 are analyzed and calculated with the design codes and `Response-2010`, since the experiments were postponed and it takes time to analyze the test results. The test configurations were the same for HPZ1 and HPZ2, and changed for HPZ3 and HPZ4. It would be interesting to make the analytical- and numerical calculations for HPZ3 and HPZ4 and then compare the results with HPZ1 and HPZ2 given in this thesis.
- With the EC2 draft 2018 and ν based on state of strains, it is assumed that the web takes the full compressive normal force: $N_{Ew} = -N_E$. The reason behind this assumption is that the force F_T in the calculation for the longitudinal strain ε_x (see Equation 5.64) would be identical to the expression given by the AASHTO (see Equation 5.32).
- With `Response-2010` the maximum shear capacity is divided into four components: $V_{c,AI}, V_{cc}, V_s$ and V_p. For cross-sections that have the following pattern (from bottom to top): "cracked part bottom flange - uncracked part bottom flange - cracked part web - rest of the web and top flange uncracked", the sum of these four components did not result in the total shear force given by `Response-2010`. An additional shear force was found, denoted as ΔV. The value for the "additional" component in the cracked area ΔV is calculated by subtracting the other four components from the maximum shear capacity. No possibility was found to extract this value directly from the results of `Response-2010` during this research. For future work it is recommended to look at the tension stresses (f_{ctm}) at the crack tips of the crack in the web, which is surrounded by two uncracked parts of the cross-section.

Bibliography

[1] M. Roosen. Bijlage 1 ontwerp experiment liggers helperzoom. Technical report, Delft University of Technology, 2017.

[2] T. Dinges. The history of prestressed concrete: 1888 to 1963. Master's thesis, Kansas State University, 2009. URL http://krex.k-state.edu/dspace/handle/2097/1439.

[3] Ministerie van Verkeer en Waterstaat. Inventarisatie kunstwerken. Technical report, Rijkswaterstaat, September 2007. URL https://www.rijksoverheid.nl/documenten/rapporten/2007/09/26/inventarisatie-kunstwerken-bruggen-tunnels-en-viaducten.

[4] J. Calavera; A. De Chefdebien; D. Fernandez-Ordonez; A. Gasperi; J. Ley; F. Monnig; P. Passeman; C. Quartel; L. Sasek; G. Tootell; A. Van Acker. Precast concrete bridges. Technical Report Bulletin 29, CEB-FIP, November 2004. URL https://www.fib-international.org/publications/fib-bulletins/precast-concrete-bridges-pdf-detail.html.

[5] J.C. Walraven; C.R. Braam. *Prestressed Concrete CIE4160*. Faculty of Civil Engineering and Geosciences, Delft University of Technology, 2019.

[6] D. Gasparini. The prestressing of structures: a historical review. *Proceedings of the Second International Congress on Construction History*, 2:1221–1232, 2006. URL https://www.arct.cam.ac.uk/Downloads/ichs/vol-2-1221-1232-gasparini.pdf/view.

[7] A. Bleijenberg. De staat van onze bruggen. Technical report, TNO, 2017. URL https://www.tno.nl/nl/tno-insights/artikelen/de-staat-van-onze-bruggen/.

[8] JCSS. *JCSS Probabilistic Model Code*. Joint Committee on Structural Safety, Zurich, 2001. ISBN 978-3-909386-79-6.

[9] S. Foster; F. Minelli; G. Plizzari; V. Sigrist. Shear and punching shear in RC and FRC elements. techreport Bulletin 57, fib - Federation Internationale du Beton, October 2010. URL https://www.fib-international.org/publications/fib-bulletins/shear-and-punching-shear-in-rc-and-frc-elements-detail.html.

[10] M. Roosen; C. van der Veen; D. Hordijk. Suitability of shear tension code requirements for the assessment of existing structures build-up with prestressed I- and T-Shape girders. *High Tech Concrete: Where Technology and Engineering Meet*, pages 786–793, 2018. doi: https://doi.org/10.1007/978-3-319-59471-2_92. URL https://pure.tudelft.nl/portal/en/publications/suitability-of-shear-tension-code-requirements-for-the-assessment-of-existing-structures-buildup-with-prestressed-i-and-tshape-girders(a0ef448f-66be-441a-afcf-2f9872310a26).html.

[11] K.W. Ritter. *Die Bauweise Hennebique*. Drck Z & F, 1899. URL https://books.google.nl/books?id=VbsncgAACAAJ.

[12] E. Mörsch. *Concrete-steel construction (Der Eisenbetonbau)*. New York, The Engineering News Pub. Co., 1909. URL https://babel.hathitrust.org/cgi/pt?id=wu.89080447535&view=1up&seq=1.

[13] J.C. Walraven; N. Lehwalter. Die tragfähigkeit von betondruckstreben in fachwerkmodellen am beispiel von gedrungenen balken [bearing capacity of concrete compression struts in strut and tie models, considering the example of short compact beams]. *Beton- und Stahlbetonbau*, 84(4):81–87, 1989. doi: 10.1002/best.198900130. URL https://onlinelibrary.wiley.com/doi/abs/10.1002/best.198900130.

[14] M.P. Collins. Towards a rational theory for RC members in shear. *Journal of the Structural Division*, 104(4):649–666, 1978. URL https://cedb.asce.org/CEDBsearch/record.jsp?docky=0008018.

[15] F.J. Vecchio; M.P. Collins. The modified compression-field theory for reinforced concrete elements subjected to shear. *ACI Journal Proceedings*, 83(2):219–231, 1986. doi: 10.14359/10416. URL https://www.concrete.org/publications/internationalconcreteabstractsportal/m/details/id/10416.

[16] E.C. Bentz; F.J. Vecchio; M.P. Collins. Simplified modified compression field theory for calculating shear strength of reinforced concrete elements. *ACI Structural Journal*, 103(4):614–624, 2006. doi: 10.14359/16438. URL https://www.concrete.org/publications/internationalconcreteabstractsportal.aspx?m=details&ID=16438.

[17] Y. Yang; J.C. Walraven; J. den Uijl. Shear behavior of reinforced concrete beams without transverse reinforcement based on critical shear displacement. *Journal of Structural Engineering*, 143(1):1–13, January 2017. doi: 10.1061/(ASCE)ST.1943-541X.0001608. URL https://ascelibrary.org/doi/10.1061/(ASCE)ST.1943-541X.0001608.

[18] M.J. Kraczla. Analytical and numerical analysis of the shear tension critical prestressed beams. Master's thesis, Delft University of Technology, 2016. URL https://repository.tudelft.nl/islandora/object/uuid%3A27cebe1c-6d9b-4980-8a3d-e28f27c9a940.

[19] M. Vergeer. Shear tension resistance of prestressed concrete beams with shear reinforcement. Master's thesis, Delft University of Technology, 2019. URL https://repository.tudelft.nl/islandora/object/uuid%3A1ecc58a0-b907-440c-b9fc-74952f1c6f57.

[20] L. Xie. The influence of axial load and prestress on the shear strength of web-shear critical reinforced concrete elements. Master's thesis, University of Toronto, September 2009. URL https://tspace.library.utoronto.ca/handle/1807/17846.

[21] E.G. Nawy. *Prestressed Concrete: A Fundamental Approach (ACI, AASHTO, IBC 2009 Codes Version)*. Pearson Education, 5th edition edition, 2009. ISBN 0-13-608150-9.

[22] C.R. Braam; P. Lagendijk. *Constructieleer Gewapend Beton*. AEneas, uitgeverij van vakinformatie bv, 7th edition edition, July 2011. ISBN 978-94-6104-006-0.

[23] R. Sarkhosh. *Shear Resistance of Reinforced Concrete Beams without Shear Reinforcement under Sustained Loading*. PhD thesis, Delft University of Technology, April 2014. URL https://repository.tudelft.nl/islandora/object/uuid%253A3273b5ee-bd17-4586-bba0-da5ee04a75c4?collection=research.

[24] M. Roosen. Literature review shear tension resistance of prestressed beams. Unpublished, 2018.

[25] ASCE-ACI Committee 426. The shear strength of reinforced concrete members. *ACI Journal Proceedings*, 70(7), 1973. doi: 10.14359/11224.

[26] ASCE-ACI Committee 445. Recent approaches to shear design of structural concrete. *Journal of Structural Engineering*, 124(12):1375–1417, dec 1998. doi: 10.1061/(asce)0733-9445(1998)124:12(1375). URL https://ascelibrary.org/doi/10.1061/%28ASCE%290733-9445%281998%29124%3A12%281375%29.

[27] S. Jung and K.S. Kim. Knowledge-based prediction of shear strength of concrete beams without shear reinforcement. *Engineering Structures*, 30(6):1515–1525, jun 2008. doi: 10.1016/j.engstruct.2007.10.008. URL https://www.sciencedirect.com/science/article/pii/S0141029607003768.

[28] M.D. Kotsovos and M.N. Pavlovic. *Ultimate Limit-state Design of Concrete Structures: A New Approach*. Thomas Telford Ltd, 1998. ISBN 9780727726650. URL https://www.amazon.com/Ultimate-Limit-state-Design-Concrete-Structures/dp/072772665X?SubscriptionId=AKIAIOBINVZYXZQZ2U3A&tag=chimbori05-20&linkCode=xm2&camp=2025&creative=165953&creativeASIN=072772665X.

[29] Sarkhosh; Uijl; R. Braam; Walraven. Shear capacity of concrete without shear reinforcement under sustained loads. *Stevin Laboratory Report 25.5.10-16*, 2010. URL https://repository.tudelft.nl/islandora/object/uuid%3A45476ff2-450d-46cd-84ba-9f4b1aafb4bc?collection=research.

[30] T. Baumann; H. Rüsch. *Versuche zum Studium der Verdübelungswirkung der Biegezugbewehrung eines Stahlbetonbalkens.* Deutscher Ausschuss für Stahlbeton: 210. Berlin : Ernst, 1970.

[31] Y. Yang. *Shear Behavior of Reinforced Concrete Members without Shear Reinforcement.* PhD thesis, Delft University of Technology, April 2014. URL https://repository.tudelft.nl/islandora/object/uuid%3Aac776cf0-4412-4079-968f-9eacb67e8846.

[32] G.I. Zarate Garnica. Analysis of shear transfer mechanisms in concrete members without shear reinforcement based on kinematic measurements. Master's thesis, Delft University of Technology, 2018. URL https://repository.tudelft.nl/islandora/object/uuid%3A9b40b743-73b3-4698-9e9b-c6ac05f5f99c.

[33] P.E. Regan; A. Al-Hussaini; K-E Ramdane; H-Y Xue. Behaviour of high strength concrete slabs. *Concrete 2000. Proceedings of International Conference*, 1:761–773, 1993. URL https://www.researchgate.net/publication/273205811_Behaviour_of_High_Strength_Concrete_Slabs.

[34] E.A.P. Liberati. *Handbook of Materials Failure Analysis: With Case Studies from the Chemicals, Concrete and Power Industries*, chapter 5: Failure analysis of reinforced concrete structures, pages 93–121. Elsevier, 2016. ISBN 978-0-08-100116-5. URL https://www.sciencedirect.com/book/9780081001165/handbook-of-materials-failure-analysis-with-case-studies-from-the-chemicals-concrete-and-power-industries.

[35] H.P.J. Taylor. Shear strength of large beams. *Journal of the Structural Division*, 98(11):2473–2490, 1972. URL https://cedb.asce.org/CEDBsearch/record.jsp?dockey=0127926.

[36] N.M. Hawkins, D.A. Kuchma, R.F. Mast, M.L. Marsh, and K.H. Reineck. *Simplified Shear Design of Structural Concrete Members: Appendixes.* The National Academies Press, Washington, DC, 2005. doi: 10.17226/22070. URL https://www.nap.edu/catalog/22070/simplified-shear-design-of-structural-concrete-members-appendixes.

[37] M.P. Collins and D. Mitchell. *Prestressed Concrete Structures.* Response Publications, 1997. ISBN 9780968195802. URL https://www.amazon.com/Prestressed-Concrete-Structures-Michael-Collins/dp/0968195806?SubscriptionId=AKIAIOBINVZYXZQZ2U3A&tag=chimbori05-20&linkCode=xm2&camp=2025&creative=165953&creativeASIN=0968195806. 152–349.

[38] J.C. Walraven; E. Vos; H.W. Reinhardt. Experiments on shear transfer in cracks in concrete. part i: Description of results. Technical Report Report 25.5-79-10, Delft University of Technology, December 1979. URL https://repository.tudelft.nl/islandora/object/uuid%3A97fbae46-94e6-4cf5-901c-4ba76f28e682.

[39] J.C. Walraven. *Aggregate Interlock: A Theoretical and experimental analysis.* PhD thesis, Delft University of Technology, October 1980. URL https://repository.tudelft.nl/islandora/object/uuid:c33a2890-f9c1-4176-929e-6988f0f23640/datastream/OBJ.

[40] J.C. Walraven. Fundamental analysis of aggregate interlock. *Journal of the Structural Division*, 107 (11):2245–2270, 1981. URL https://cedb.asce.org/CEDBsearch/record.jsp?dockey=0010563.

[41] E.O.L. Lantsoght. *Shear in Reinforced Concrete Slabs under Concentrated Loads close to Supports.* PhD thesis, Delft University of Technology, 2013. URL https://repository.tudelft.nl/islandora/object/uuid%3A3c0045dc-66b2-4151-b778-c318a96b22bc.

[42] Z.P. Bažant; J.K. Kim. Size effect in shear failure of longitudinally reinforced beams. *ACI Journal Proceedings*, 81(5):456–468, 1984. doi: 10.14359/10696. URL https://www.concrete.org/publications/internationalconcreteabstractsportal/m/details/id/10696.

[43] S.D.B. Alexander and S.H. Simmonds. Bond model for concentric punching shear. *ACI Structural Journal*, 89(3), 1992. doi: 10.14359/3246.

[44] R. Park and T. Paulay. *Reinforced Concrete Structures*. Wiley, jul 1975. doi: 10.1002/9780470172834.

[45] W. Kim and J.P. Jeong. Non-bernoulli-compatibility truss model for RC members subjected to combined action of flexure and shear. *KSCE Journal of Civil Engineering*, 15(1):101–117, dec 2011. doi: 10.1007/s12205-011-0662-6.

[46] D. Angelakos; E.C. Bentz; M.P. Collins. Effect of concrete strength and minimum stirrups on shear strength of large members. *ACI Structural Journal*, 98(3), 2001. doi: 10.14359/10220.

[47] K.G. Moody; M. Viest; R.C. Elstner; E. Hognestad. Shear strength of reinforced concrete beams part 1: Tests of simple beams. *ACI Journal Proceedings*, 51(12):317–332, 1954. doi: 10.14359/11680. URL https://www.concrete.org/publications/internationalconcreteabstractsportal/m/details/id/11680.

[48] G.N.J. Kani. Basic facts concerning shear failure-part 1. *ACI Journal Proceedings*, 63(6):675–692, 1966. doi: 10.14359/7644. URL https://www.concrete.org/publications/internationalconcreteabstractsportal/m/details/id/7644.

[49] G.N.J. Kani. How safe are our large reinforced concrete beams? *ACI Journal Proceedings*, 64(3):128–141, March 1967. doi: 10.14359/7549. URL https://www.concrete.org/publications/internationalconcreteabstractsportal/m/details/id/51685189.

[50] J.C. Walraven. *The influence of depth on the shear strength of lightweight concrete beams without shear reinforcement*. Delft University of Technology, 1978. URL https://www.worldcat.org/title/influence-of-depth-on-the-shear-strength-of-lightweight-concrete-beams-without-shear-reinforcement/oclc/271051572.

[51] Z. P. Bažant and Y. Xi. Statistical size effect in quasi-brittle structures: II. nonlocal theory. *Journal of Engineering Mechanics*, 117(11):2623–2640, November 1991. doi: 10.1061/(asce)0733-9399(1991)117:11(2623). URL https://ascelibrary.org/doi/10.1061/%28ASCE%290733-9399%281991%29117%3A11%282623%29.

[52] J.C. Walraven and N. Lehwalter. Size effects in short beams loaded in shear. *ACI Structural Journal*, 91(5):585–593, 1994. doi: 10.14359/4177. URL https://www.concrete.org/publications/internationalconcreteabstractsportal/m/details/id/4177.

[53] M. Roosen; C. van der Veen; D. Hordijk; M. Hendriks. Shear tension resistance of prestressed girders with a low stirrup ratio. *SEMC 2019 Cape Town*, 2019.

[54] AASHTO. *AASHTO LRFD bridge design specifications. SI units.* American Association of State Highway and Transportation Officials, 4th edition edition, 2007. ISBN 978-1-56051-355-1. URL https://app.knovel.com/web/toc.v/cid:kpAASHTOL2/viewerType:toc/.

[55] J.C. Walraven. *Background document for prENV 1992-1-1:2002*. Delft University of Technology, 2002. URL https://pure.tudelft.nl/portal/en/publications/background-document-for-prenv-1992112002-62-shear(23a63ece-1445-4606-8824-75812e9839b0)/export.html.

[56] J.C. Walraven. Shear in prestressed concrete members: a state-of-the-art report. *Comité Euro-International du Beton*, 1987. URL https://www.fib-international.org/publications/ceb-bulletins/shear-in-prestressed-concrete-members-detail.html.

[57] N. Hawkins, D. Kuchma, and K. Kim. NCHRP project 12-56, application of load and resistance factor design specifications to high-strength structural concrete: Shear provisions. *Transportation Research Record: Journal of the Transportation Research Board*, 11s:87–97, jan 2005. doi: 10.3141/trr.11s.3t3qlrxm0h1r8262.

[58] ACI committee 318. *ACI 318-14 Building Code Requirements for Structural Concrete and Commentary*. American Concrete Institute, September 2014. ISBN 978-0-87031-930-3. URL https://www.amazon.com/Building-Requirements-Structural-Concrete-Commentary/dp/0870319302?SubscriptionId=AKIAIOBINVZYXZQZ2U3A&tag=chimbori05-20&linkCode=xm2&camp=2025&creative=165953&creativeASIN=0870319302.

[59] E.C. Bentz. *Sectional Analyses of Reinforced Concrete Members*. PhD thesis, University of Toronto, 2000. URL https://tspace.library.utoronto.ca/bitstream/1807/13811/1/NQ49840.pdf.

[60] J.G. MacGregor; M.A. Sozen; C.P. Siess. Strength and behavior of prestressed concrete beams with web reinforcement. Technical report, University of Illinois, August 1960. URL https://www.ideals.illinois.edu/handle/2142/13780.

[61] A.H. Elzanaty; A.H. Nilson; F.O. Slate. Shear capacity of prestressed concrete beams using high-strength concrete. *ACI Journal Proceedings*, 83(3):359–368, 1986. doi: 10.14359/10436. URL https://www.concrete.org/publications/internationalconcreteabstractsportal/m/details/id/10436.

[62] AASHTO. *AASHTO LRFD Bridge Design Specifications: Customary U.S. Units 2017*. Amer Assn of State Hwy, 8th edition edition, January 2017. ISBN 978-1560516545. URL https://www.amazon.com/Aashto-Lrfd-Bridge-Design-Specifications/dp/1560516542?SubscriptionId=AKIAIOBINVZYXZQZ2U3A&tag=chimbori05-20&linkCode=xm2&camp=2025&creative=165953&creativeASIN=1560516542.

[63] NEN. *Eurocode 2: Ontwerp en berekening van betonconstructies: Deel 1-1: Algemene regels en regels voor gebouwen*. Nederlands Normalisatie-instituut, 2011. URL https://connect.nen.nl/portal/Abonnementen/Standaard/Bouw/Eurocodes/Eurocodes-Gebouwen-Beton-en-metselwerk.

[64] A; Hedman, O.; Losberg. Design of concrete structures with regard to shear forces. *CEB Bulletin d'Information*, (126):184–209, 1978.

[65] Comité Euro-International du Béton;. *Ceb-Fip Model Code 1990: Design Code*. Thomas Telford Ltd, 1993. ISBN 978-0-7277-1696-5. URL https://www.amazon.com/Ceb-Fip-Model-Code-1990-Design/dp/0727716964?SubscriptionId=AKIAIOBINVZYXZQZ2U3A&tag=chimbori05-20&linkCode=xm2&camp=2025&creative=165953&creativeASIN=0727716964.

[66] J.C. Walraven; N. Al-Zubi. Shear capacity of lightweight concrete beams with shear reinforcement. In *International symposium, Structural lightweight aggregate concrete*, volume 1, pages 91–104, Oslo, 1995. Norwegian Concrete Association. URL https://www.tib.eu/en/search/id/BLCP%3ACN011589030/Shear-Capacity-of-Lightweight-Concrete-Beams-with/.

[67] J.C.Walraven; J. Stroband. Shear capacity of high strength concrete beams with shear reinforcement. In *International symposium; 5th, Utilization of high strength/high performance concrete*, volume 1, pages 693–700, Oslo, 1999. Norwegian Concrete Association. URL https://www.tib.eu/en/search/id/BLCP%3ACN033790119/Shear-Capacity-of-High-Strength-Concrete-Beams/.

[68] RWS. Richtlijnen beoordeling kunstwerken (RBK1.1). Technical report, Dutch Ministry of Infrastructure and Watermanagement, 2013. URL http://publicaties.minienm.nl/documenten/richtlijnen-beoordeling-kunstwerken-rbk-1-1.

[69] NEN. Eurocode 2: Design of concrete structures - part 1-1: General rules, rules for buildings, bridges and civil engineering structures. Final draft by Project Team SC2.T1, April 2018.

[70] J. Linssen. Wat gaat er veranderen aan de eurocodes? *Cement*, (8):58–61, 2018. URL https://www.cementonline.nl/wat-gaat-er-veranderen-aan-de-eurocodes.

[71] E. Veenstra. Werkplan cluster 3 - verdiepte ligging. Buitendienststelling 7-2019 - Slopen KW17.02, January 2019.

[72] E.O.L. Lantsoght; F. Zhang; G. Zarate Garnica; Y. Yang; R. Braam. Measurement report of prestressed beams for helperzoom viaduct. Technical Report Stevin Report 25.5-19-03, Delft University of Technology, 2019. Version 0.3.

[73] E.O.L. Lantsoght; F. Zhang; G. Zarate Garnica; Y. Yang; R. Braam. Analysis report of prestressed beams from helperzoom viaduct. Technical Report Stevin Report 25.5-19-04, Delft University of Technology, 2019. Version 0.2.

[74] F.G.A. Linthorst and E.A.H. Teunissen. BDX-9002 materiaalonderzoek 64 kunstwerken 07d-105-01 noordelijk viaduct over de spoorlijn assen-groningen. 2009.

[75] H. Welleman and C. Hartsuijker. Constructiemechanica 3 CTB2210 module: spanningsleer en bezwijkmodellen, January 2018. TU Delft.

[76] F.L. Marques dos Santos, B. Peeters, W. Desmet, and L.C.S. Góes. Strain-based experimental modal analysis on planar structures: Concepts and practical aspects. In *Topics in Modal Analysis & Testing, Volume 10*, pages 335–346. Springer International Publishing, 2016. doi: 10.1007/978-3-319-30249-2_30.

[77] A. Simone. Lecture notes in analysis of slender structures CIE4190. Delft University of Technology, 2011.

[78] C. van der Veen and F.B.J. Gijsbers. Working set factors for existing concrete bridges. Delft University of Technology, 2011. in Dutch.

[79] E.C. Bentz. Summary of development and use of CSA 2004 shear design provisions. In *Advances in Engineering Structures, Mechanics & Construction*, pages 67–80. Springer Netherlands, 2006. doi: 10.1007/1-4020-4891-2_5.

[80] G.D. Sciascio. Use of the pushover method for the seismic analysis of mixed frame-wall structures. In *International CAE Conference*, 2018. URL `http://www.disciasciosrl.com/images/pubblicazioni/Cae_Conference_2018_Di_Sciascio_srl.pdf`.

[81] F. J. Vecchio. Reinforced concrete membrane element formulations. *Journal of Structural Engineering*, 116(3):730–750, mar 1990. doi: 10.1061/(asce)0733-9445(1990)116:3(730).

A

AASHTO with different f_{po}

A.1. AASHTO shear resistance with f_{po}=0.342f_{pu}

This procedure requires iterative calculations, therefore only the end result is given. The iterations are done with the `MS Excel Solver package`. The following values are used to calculate ε_s:

$$\begin{aligned} F_{exp,assumed} &= 1{,}017{,}752 \text{ N} = 1018 \text{ kN} \\ V_u = \frac{L_{span}-a}{L_{span}} \cdot F_{exp,assumed} + V_{sw} &= 0.70 \cdot 1018 + 41.38 = 751.69 \approx 752 \text{ kN} \\ M_u = \frac{L_{span}-a}{L_{span}} \cdot F_{exp,assumed} \cdot a + M_{sw} &= 1.20 \cdot 1018 + 94.50 = 1319.5 \text{ kNm} \\ \theta_{assumed} &= 30.01^\circ \end{aligned} \tag{A.1}$$

Check if M_u is greater than the allowed minimum (note that $V_u - V_p$ equals $V_{tot} = V_F + V_{sw} - V_p$):

$$\begin{aligned} M_u &> |V_u - V_p| d_v \\ 1320 \cdot 10^6 &> |752 \cdot 10^3 - 98.21 \cdot 10^3| \cdot 799 = 522 \text{ kNm} \\ \text{CHECK:} \qquad 1320 &\leq 522 \text{ kNm} \qquad \textbf{OK} \end{aligned} \tag{A.2}$$

During loading of the girder, the stress in the prestressing steel will increase. The analytical procedure for the increase in stress **at ultimate shear capacity** shown in Chapter 4.6.5 is done for $F_{exp} = 1890$ kN. The average increase of stress in the prestressing steel equals $\Delta\sigma_p = 470.6$ MPa. A re-calculation with $F_{exp} = 1100$ kN gives $\Delta\sigma_p \approx 130$ MPa for $x = 1.725$ m. For the calculation given in this paragraph, the value is set to $f_{po} = \sigma_{p\infty} + \Delta\sigma_p = 494 + 130 = 624$ MPa. This results in a value of ε_s:

$$\begin{aligned} \varepsilon_s &= \frac{\left(\frac{|M_u|}{d_v} + 0.5N_u + 0.5|V_u - V_p| \cot\theta - A_{ps} f_{po}\right)}{E_s A_s + E_p A_{ps}} = 0.000287 \\ &= \frac{\left(\frac{1320 \cdot 10^6}{799} + 0 + 0.5 \cdot |(752 - 98.21) \cdot 10^3| \cdot \cot(30.01) - 3234 \cdot 624\right)}{200{,}000 \cdot 314 + 185{,}000 \cdot 3234} \end{aligned} \tag{A.3}$$

This results in a value for θ and β of:

$$\begin{aligned} \beta &= \frac{4.8}{1 + 750\varepsilon_s} = \frac{4.8}{1 + 750 \cdot 0.000287} = 3.95 \\ \theta_{calc} &= 29 + 3500 \cdot 0.000287 = 30.01^\circ \end{aligned} \tag{A.4}$$

The inclined cracking load and contribution of the stirrups follow from the results of Equations A.3 and A.4:

$$\begin{aligned} V_c &= 0.083\beta\sqrt{f'_c}b_v d_v = 0.083 \cdot 3.95 \cdot 7.76 \cdot 200 \cdot 799 = 407 \text{ kN} \\ V_s &= \frac{A_v f_y d_v \cot\theta}{s} = \frac{157 \cdot 454 \cdot 799 \cot(30.01)}{400} = 247 \text{ kN} \end{aligned} \tag{A.5}$$

The external load that the girder can resist equals:

$$F_{exp,AASHTO} = (V_n - V_{sw}) \cdot \frac{L_{span}}{L_{span} - a} = \frac{407 + 247 + 98 - 41.38}{0.7} = 1017.8 \text{ kN} \tag{A.6}$$

Check if the constraints are met:

$$\begin{aligned} \theta_{assumed} &= \theta_{calc} \\ \text{CHECK:} \qquad 30.01° &= 30.01° \qquad \textbf{OK} \\ F_{exp,assumed} &= F_{exp,AASHTO} \\ \text{CHECK:} \qquad 1017.8 &= 1017.8 \text{ kN} \qquad \textbf{OK} \end{aligned} \tag{A.7}$$

The nominal shear resistance according to the AASHTO for $x = 1.725$ m equals:

$$V_n = V_c + V_s + V_p = 407 + 247 + 98 = 752 \text{ kN} \tag{A.8}$$

The calculated nominal shear resistance V_n must be smaller than the shear force required for the crushing of concrete in the web. When the nominal shear resistance calculated in Equation A.1 is smaller, the stirrups will yield before crushing of the web:

$$\begin{aligned} V_n &< 0.25 f'_c b_v d_v + V_p \\ 786 &< 0.25 \cdot 60.3 \cdot 200 \cdot 799 + 98.21 \\ \text{CHECK:} \qquad 786 &\leq 2506 \text{ kN} \qquad \textbf{OK} \end{aligned} \tag{A.9}$$

Procedure with tables

The same procedure is followed as with the algebraic equations, except that a table is used to obtain θ and β. First θ and F_{exp} are assumed to calculate the longitudinal strains at mid depth. Again, only the end result is given with $\theta = 25.22°$ and $F_{exp,assumed} = 975$ kN:

$$\begin{aligned} \varepsilon_x &= \frac{\left(\frac{|M_u|}{d_v} + 0.5N_u + 0.5|V_u - V_p|\cot\theta - A_{ps}f_{po}\right)}{2(E_s A_s + E_p A_{ps})} = 0.000175 \\ &= \frac{\left(\frac{1268 \cdot 10^6}{799} + 0 + 0.5 \cdot |(624) \cdot 10^3| \cdot \cot(25.22) - 3234 \cdot 624\right)}{200{,}000 \cdot 314 + 185{,}000 \cdot 3234} \end{aligned} \tag{A.10}$$

The ratio between the shear stress in the concrete equals:

$$\frac{\nu_u}{f'_c} = \frac{\left(\frac{V_u - V_p}{d_v b_v}\right)}{f'_c} = \frac{\left(\frac{624}{799 \cdot 200}\right)}{60.3} = 0.065 \tag{A.11}$$

According to Table 2.4 with $\varepsilon_x < 0.000125$ and $\nu_u/f'_c < 0.075$, the values are $\theta = 24.3°$ and $\beta = 3.24$. For $\varepsilon_x < 0.00025$ and $\nu_u/f'_c < 0.075$, the values are $\theta = 26.6°$ and $\beta = 2.94$. Interpolation for $\varepsilon_x = 0.000175$ results in:

$$\begin{aligned} \theta &= 24.3 + \frac{26.6 - 24.3}{0.00025 - 0.000125} \cdot (0.000175 - 0.000125) = 25.22° \\ \beta &= 3.24 - \frac{3.24 - 2.94}{0.00025 - 0.000125} \cdot (0.000175 - 0.000125) = 3.12 \end{aligned} \tag{A.12}$$

The inclined cracking load and contribution of the stirrups equals to:

$$\begin{aligned} V_c &= 0.083 \cdot 3.12 \cdot 7.76 \cdot 200 \cdot 799 = 321 \text{ kN} \\ V_s &= \frac{157 \cdot 454 \cdot 799 \cot(25.22)}{400} = 303 \text{ kN} \end{aligned} \tag{A.13}$$

Check if the external load that the girder can resist equals to the applied external load:

$$\begin{aligned} F_{exp,AASTHO} &= \frac{V_c + V_s + V_p + V_{sw+p}}{0.7} = \frac{321 + 303 + 98 - 41.38}{0.7} = 975.4 \text{ kN} \\ \text{CHECK:} \qquad & 975.4 \approx 975 \text{ kN} \qquad \textbf{OK} \end{aligned} \tag{A.14}$$

The nominal shear resistance becomes:

$$V_n = 321 + 303 + 98 = 722 \text{ kN} \tag{A.15}$$

The result for the nominal shear resistance is almost the same for both approaches:

$$V_{n,algebraic} = 752 \approx V_{n,tables} = 722 \text{ kN} \tag{A.16}$$

This might implicate that the two approaches for Method 2 may be considered equivalent. As shown in the detailed calculations, this statement is not true for the calculations performed in this paragraph. The β and θ values are not the same $\theta = 30.01°$ vs. $25.22°$ and $\beta = 3.95$ vs. 3.12. This means that the inclined cracking loads for both methods are not equal $V_c = 407$ kN vs. 321 kN and the same holds for the contribution of the stirrups $V_s = 247$ kN vs. 303 kN. Subsequently, the value of the applied external load found from the procedure with tables is lower than the procedure with algebraic equations $F_{exp} =$ 1018 kN vs. 975 kN.

A.2. Summary with f_{po}=0.342f_{pu}, 0.52f_{pu} and 0.7f_{pu}

The nominal shear resistances of the cross-sections between $x = 1.725$,..,2.903 m are calculated with the **algebraic equations only** and $f_{po} = 0.342 f_{pu}$, $0.52 f_{pu}$ and $0.7 f_{pu}$ in MPa. The results of the calculations are shown in Tables A.1, A.2 and A.3. The nominal shear resistances are given in Figures A.1, A.2 and A.3. Cross-section $x = 2.903$ m is the most critical cross-section for shear failure for all considered values for f_{po}:

- $f_{po} = 0.342 f_{pu} = 624$ MPa:

  The angles for the compression chord range between 30.00° and 30.41° and the longitudinal strains in the tension chord range from $0.286 \cdot 10^{-3}$ to $0.404 \cdot 10^{-3}$. The nominal shear resistance is $V_n = 711$ kN.

- $f_{po} = 0.52 f_{pu} = 948$ MPa (RBK value):

  The angles for the compression chord range between 28.83° and 30.15° and the longitudinal strains in the tension chord range from $-0.05 \cdot 10^{-3}$ to $-0.327 \cdot 10^{-3}$. The nominal shear resistance is $V_n = 731$ kN.

- $f_{po} = 0.7 f_{pu} = 1277$ MPa (AASHTO value):

  The angles for the compression chord range between 28.48° and 28.90° and the longitudinal strains in the tension chord range from $-0.148 \cdot 10^{-3}$ to $0.029 \cdot 10^{-3}$. The nominal shear resistance is $V_n = 853$ kN.

Table A.1: Results of the nominal shear resistance for $x = 1.725$,..,2.903 m, $a = 2.903$ m and $f_{po} = 0.342 f_{pu}$

x [m]	**1.725**	**1.8**	**1.85**	**1.9**	**1.95**	**2**	**2.051**	**2.453**	**2.903**
$F_{assumed}$ [kN]	1019	1015	1013	1010	1008	1006	1004	990	983
$\theta_{assumed}$ [°]	30.01	30.04	30.07	30.09	30.11	30.14	30.16	30.31	30.42
$\varepsilon_s(\times 10^3)$ [-]	0.286	0.297	0.304	0.310	0.317	0.323	0.329	0.373	0.404
$\varepsilon_s > 0$	TRUE	TRUE	TRUE	TRUE	TRUE	TRUE	TRUE	TRUE	TRUE
β [-]	3.95	3.93	3.91	3.89	3.88	3.86	3.85	3.75	3.68
θ_{calc} [°]	30.00	30.04	30.06	30.09	30.11	30.13	30.15	30.31	30.41
V_c [kN]	407	404	402	401	399	398	396	386	379
V_s [kN]	247	246	246	246	246	245	245	244	243
V_p [kN]	98	98	97	97	96	96	96	93	89
F_{exp} [kN]	1019	1015	1013	1010	1008	1006	1004	990	983
V_n [kN]	752	748	746	743	741	739	737	722	711

Table A.2: Results of the nominal shear resistance for $x = 1.725$,..,2.903 m and $a = 2.903$ m with $0.52 f_{pu}$

x [m]	**1.725**	**1.8**	**1.85**	**1.9**	**1.95**	**2**	**2.051**	**2.453**	**2.903**
$F_{assumed}$ [kN]	1188	1184	1181	1178	1176	1173	1170	1103	1011
$\theta_{assumed}$ [°]	28.83	28.85	28.87	28.89	28.91	28.92	28.94	29.4	30.15
$\varepsilon_s(\times 10^3)$ [-]	−0.05	−0.042	−0.037	−0.032	−0.027	−0.022	−0.016	0.113	0.327
$\varepsilon_s > 0$	FALSE	FALSE	FALSE	FALSE	FALSE	FALSE	FALSE	TRUE	TRUE
β [-]	4.99	4.96	4.94	4.92	4.9	4.88	4.86	4.42	3.85
θ_{calc} [°]	28.83	28.85	28.87	28.89	28.91	28.92	28.94	29.4	30.15
V_c [kN]	513	510	508	506	504	502	500	456	397
V_s [kN]	259	259	258	258	258	258	258	253	245
V_p [kN]	98	98	97	97	96	96	96	93	89
F_{exp} [kN]	1188	1184	1181	1178	1176	1173	1170	1103	1011
V_n [kN]	871	867	864	861	859	856	854	801	731

Table A.3: Results of the nominal shear resistance for $x = 1.725$,..,2.903 m and $a = 2.903$ m with $0.7 f_{pu}$

x [m]	**1.725**	**1.8**	**1.85**	**1.9**	**1.95**	**2**	**2.051**	**2.453**	**2.903**
$F_{assumed}$ [kN]	1254	1249	1246	1243	1239	1236	1233	1209	1185
$\theta_{assumed}$ [°]	28.48	28.51	28.53	28.55	28.56	28.58	28.6	28.74	28.9
$\varepsilon_s(\times 10^3)$ [-]	−0.148	−0.14	−0.135	−0.13	−0.124	−0.119	−0.114	−0.073	−0.029
$\varepsilon_s > 0$	FALSE	FALSE	FALSE	FALSE	FALSE	FALSE	FALSE	FALSE	FALSE
β [-]	5.4	5.36	5.34	5.32	5.29	5.27	5.25	5.08	4.91
θ_{calc} [°]	28.48	28.51	28.53	28.55	28.56	28.58	28.6	28.74	28.9
V_c [kN]	556	552	550	548	545	543	541	523	505
V_s [kN]	263	262	262	262	262	262	261	260	258
V_p [kN]	98	98	97	97	96	96	96	93	89
F_{exp} [kN]	1254	1249	1246	1243	1239	1236	1233	1209	1185
V_n [kN]	917	912	909	906	903	900	898	875	853

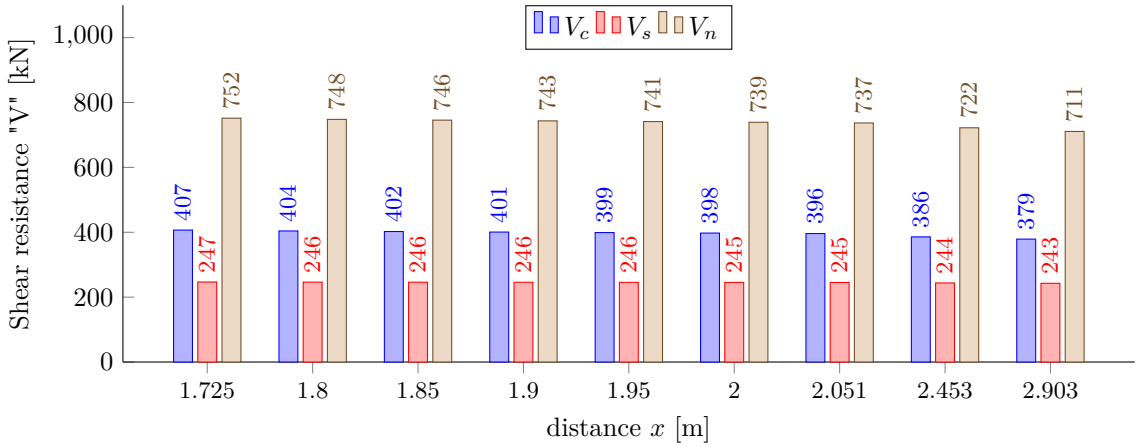

Figure A.1: Shear resistance for $x = 1.725,..,2.903$ m and $a = 2.903$ m with $f_{po} = 0.342 f_{pu}$

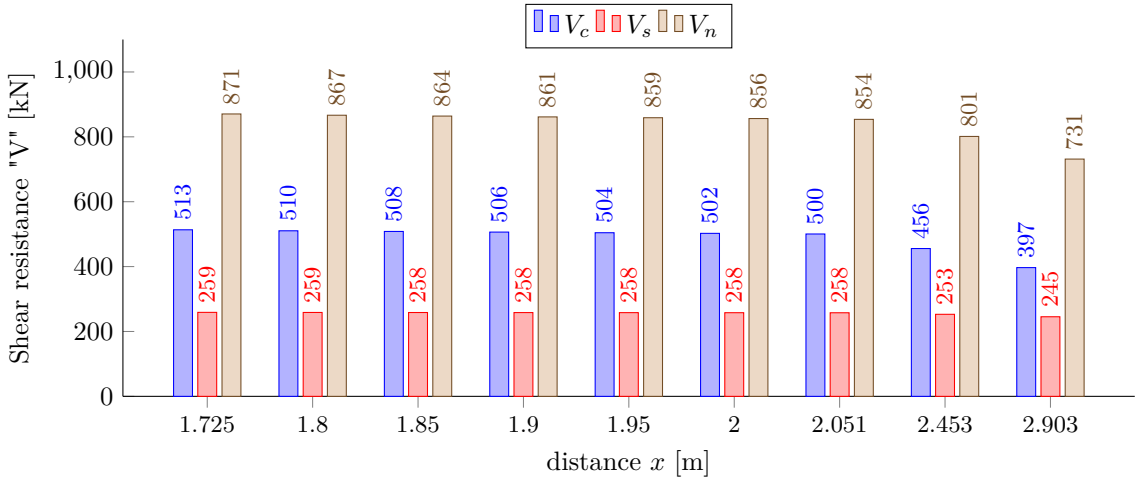

Figure A.2: Shear resistance for $x = 1.725,..,2.903$ m and $a = 2.903$ m with $f_{po} = 0.52 f_{pu}$

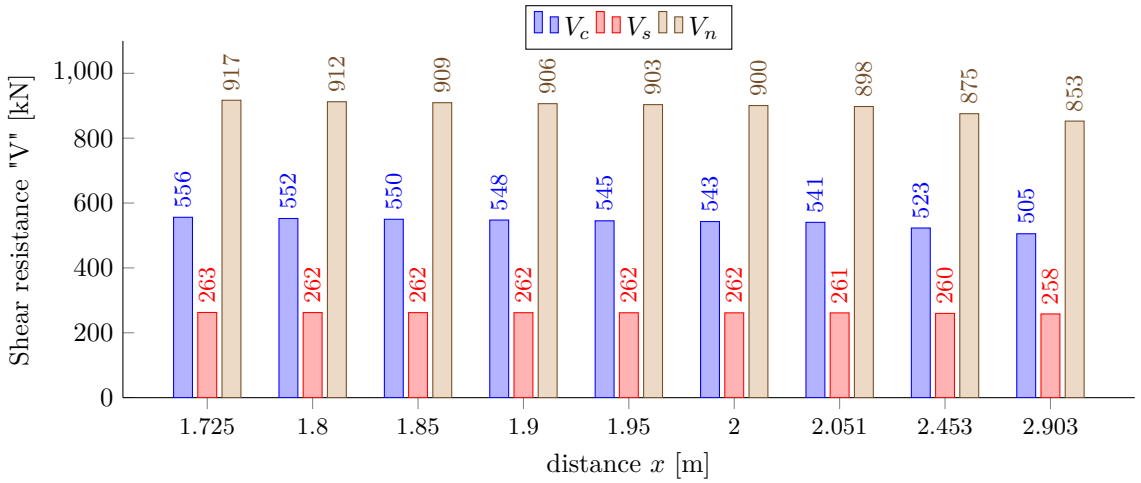

Figure A.3: Shear resistance for $x = 1.725,..,2.903$ m and $a = 2.903$ m with $f_{po} = 0.7 f_{pu}$

B

Response-2010 results
a = 2.903 m, N = 1598 kN

The black dashed line is the sum of the shear stress on the crack and transverse reinforcement. The contribution of the components to the total shear resistance V_R in % are also shown in the plot. ΔV is the difference between the blue line (τ) and the black dashed line ($\tau_{ci} + \tau_{sz,cr}$) multiplied by the width and integrated over the height.

B.1. Summary cross-section x = 1.725 m

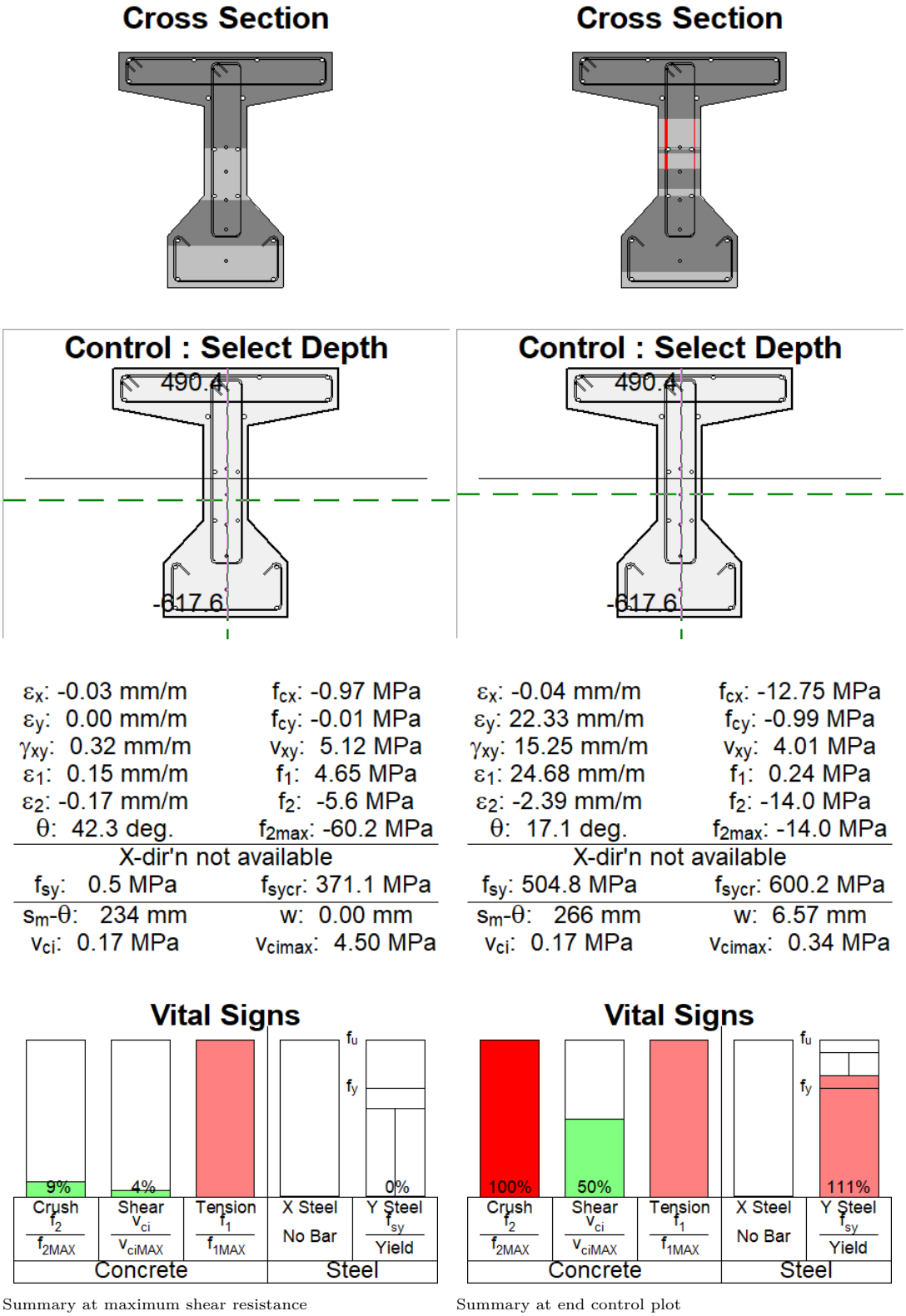

Summary at maximum shear resistance

Summary at end control plot

Figure B.1: Summary from 'Mohr's Circles' tab $x = 1.725$ m

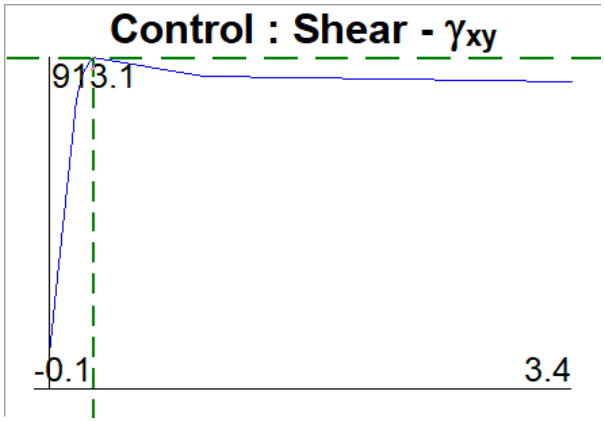

Figure B.2: Control plot for $x = 1.725$ m

Flexural cracking occurs at $V = 817.4$ kN, because the principal tensile capacity is reached at the extreme tension fiber (bottom flange). As the load increases, the height of the cracked zone in the bottom flange increases up to the point where the principal tensile capacity is exceeded in the web at $V = 913.1$ kN. At this point a part of the bottom flange is cracked in bending and diagonal tension cracking occurs in the bottom part of the web. After diagonal tension cracking (next load step) the load drops, the stirrups at the crack immediately yield, slipping of the crack occurs ($\tau_{ci} = \tau_{ci,max}$), the principal compressive capacity decreases and the average angle decreases in the top part of the web. The web and bottom flange are fully cracked at this step. As the shear force further decreases the principal compressive capacity decreases, the principal compressive stress increases, the average angle decreases and the stirrup stress at the crack increases. At the last load stage the principal compressive stress reaches the maximum capacity in the web ($\sigma_2 = \sigma_{2,max} = -14.0$ MPa), with an average angle $\theta = 17.1°$. The stirrup stress at the crack does not rupture ($\sigma_{sz,cr} = 600.2 < 655$ MPa). The failure mechanism is crushing of the concrete. The shear-shear strain plot of this failure is given in Figure B.2.

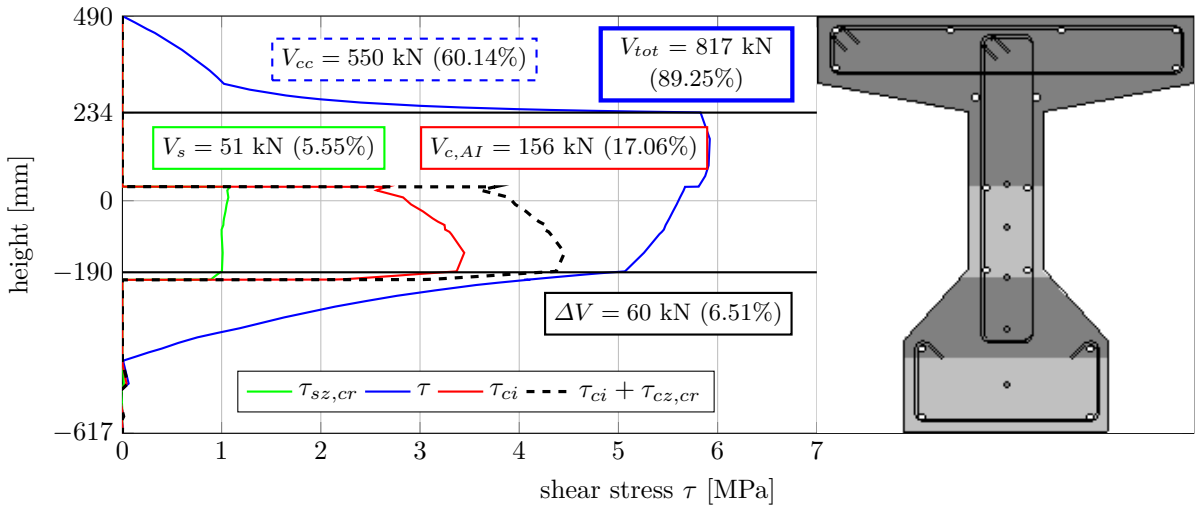

Figure B.3: Contribution of each component to the shear resistance for $a = 2.903$ m, $x = 1.725$ m and $N_p = 1598$ kN

The results from Figure B.3 give a total shear resistance V_R of:

$$V_R = V_{tot} + V_p = 816.9 + 98.4 = 915.3 \text{ kN} \tag{B.1}$$

This is a difference of +2.2 kN (+0.2%) with the shear resistance of the V-γ_{xy}-plot given in Figure B.2.

B.2. Summary cross-section x = 1.800 m

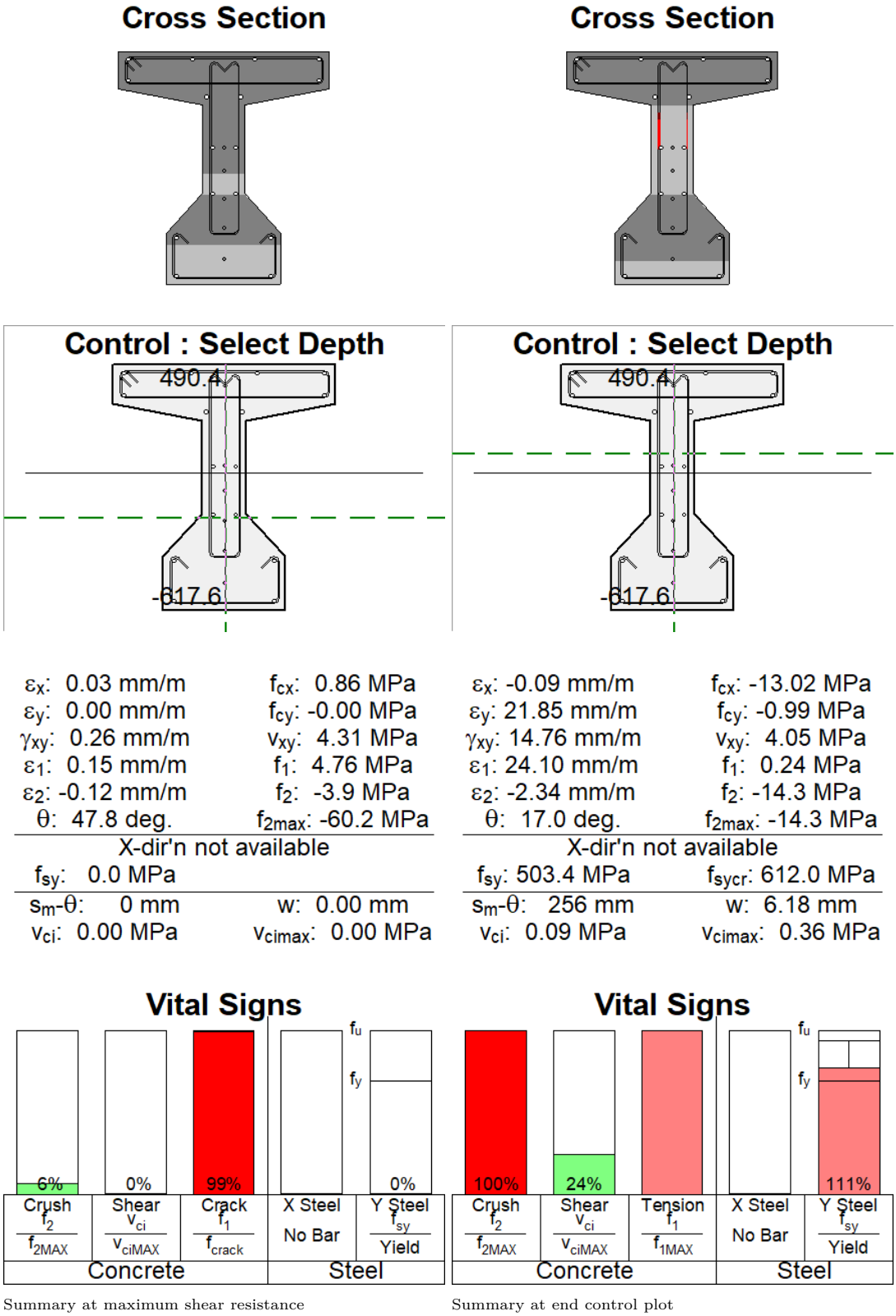

Summary at maximum shear resistance

Summary at end control plot

Figure B.4: Summary from 'Mohr's Circles' tab $x = 1.800$ m

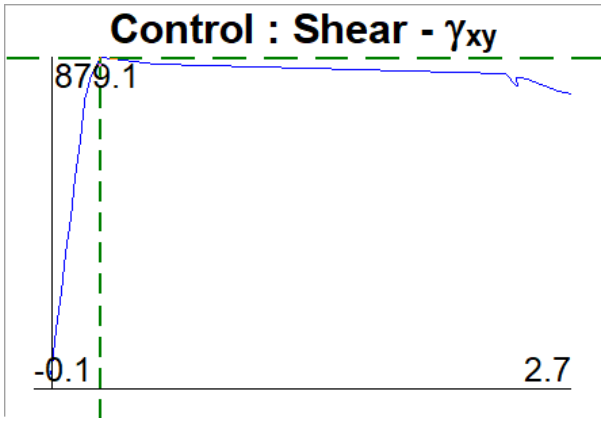

Figure B.5: Control plot for $x = 1.800$ m

Flexural cracking occurs at $V = 780.3$ kN, because the principal tensile capacity is reached at the extreme tension fiber (bottom flange). As the load increases, the height of the cracked zone in the bottom flange increases up to the point where the principal tensile capacity is exceeded in the web at $V = 879.1$ kN. At this point a part of the bottom flange is cracked in bending and diagonal tension cracking occurs in the bottom part of the web. After diagonal tension cracking (next load step) the load drops, the stirrups at the crack immediately yield, slipping of the crack occurs ($\tau_{ci} = \tau_{ci,max}$), the principal compressive capacity decreases and the average angle decreases in the top part of the web. The web and bottom flange are fully cracked at this step. As the shear force further decreases the principal compressive capacity decreases, the principal compressive stress increases, the average angle decreases and the stirrup stress at the crack increases. At the last load stage the principal compressive stress reaches the maximum capacity in the web ($\sigma_2 = \sigma_{2,max} = -14.3$ MPa), with an average angle $\theta = 17.0°$. The stirrup stress at the crack does not rupture ($\sigma_{sz,cr} = 612.0 < 655$ MPa). The failure mechanism is crushing of the concrete. The shear-shear strain plot of this failure is given in Figure B.5.

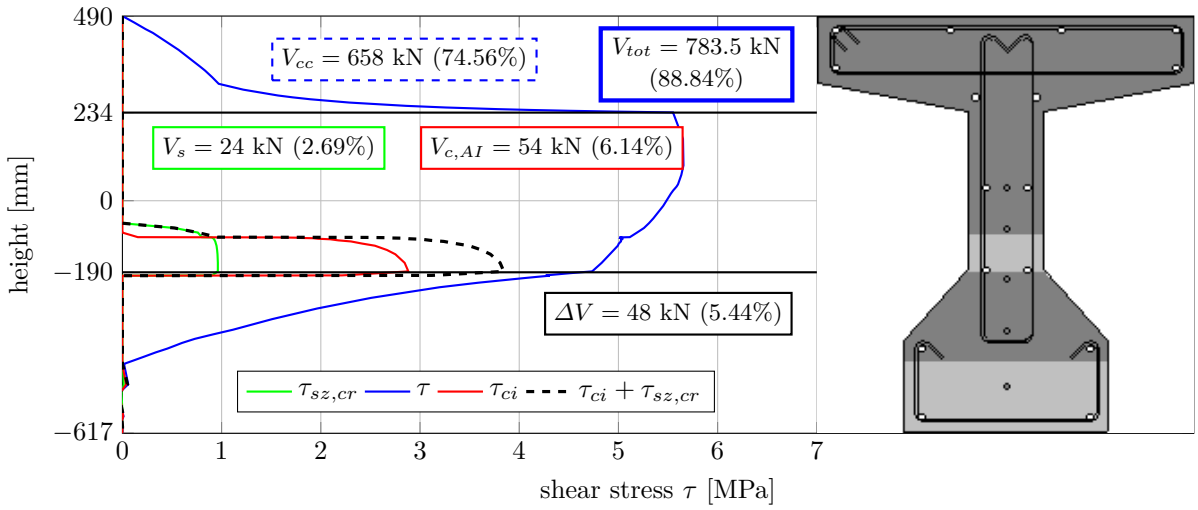

Figure B.6: Contribution of each component to the shear resistance for $a = 2.903$ m, $x = 1.800$ m and $N_p = 1598$ kN

The results from Figure B.6 give a total shear resistance V_R of:

$$V_R = V_{tot} + V_p = 783.5 + 98.4 = 881.9 \text{ kN} \tag{B.2}$$

This is a difference of +2.8 kN (+0.3%) with the shear resistance of the V-γ_{xy}-plot given in Figure B.5.

B.3. Summary cross-section x = 1.900 m

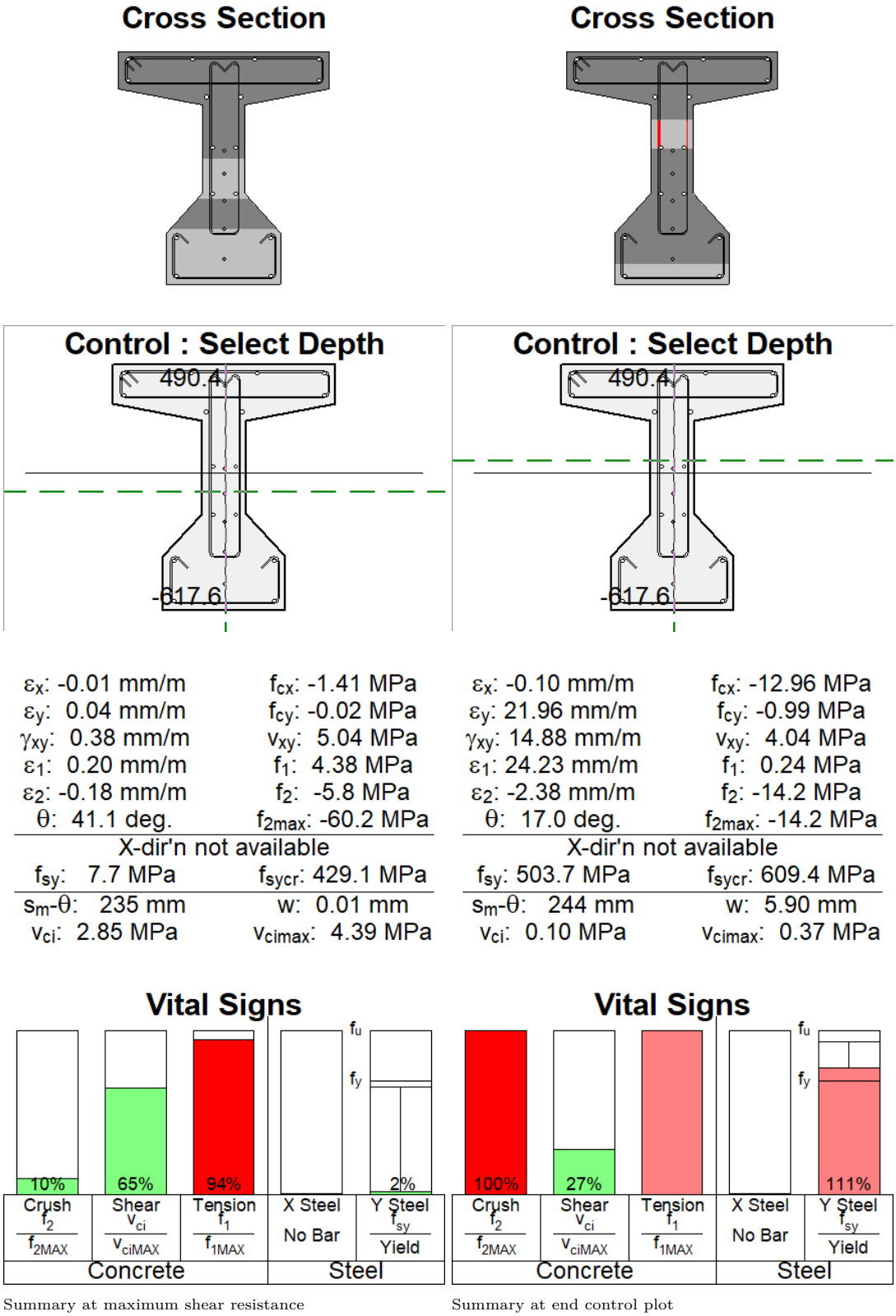

Summary at maximum shear resistance

Summary at end control plot

Figure B.7: Summary from 'Mohr's Circles' tab $x = 1.900$ m

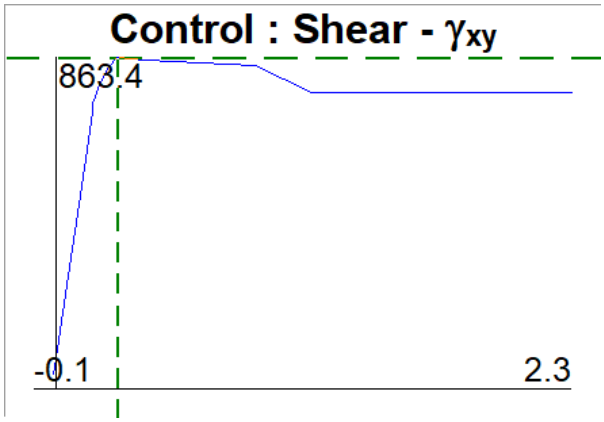

Figure B.8: Control plot for $x = 1.900$ m

Flexural cracking occurs at $V = 752.4$ kN, because the principal tensile capacity is reached at the extreme tension fiber (bottom flange). As the load increases, the height of the cracked zone in the bottom flange increases up to the point where the principal tensile capacity is exceeded in the web at $V = 863.4$ kN. At this point a part of the bottom flange is cracked in bending and diagonal tension cracking occurs in the bottom part of the web. After diagonal tension cracking (next load step) the load drops, the stirrups at the crack immediately yield, slipping of the crack occurs ($\tau_{ci} = \tau_{ci,max}$), the principal compressive capacity decreases and the average angle decreases in the top part of the web. The web and bottom flange are fully cracked at this step. As the shear force further decreases the principal compressive capacity decreases, the principal compressive stress increases, the average angle decreases and the stirrup stress at the crack increases. At the last load stage the principal compressive stress reaches the maximum capacity in the web ($\sigma_2 = \sigma_{2,max} = -14.2$ MPa), with an average angle $\theta = 17.0°$. The stirrup stress at the crack does not rupture ($\sigma_{sz,cr} = 609.4 < 655$ MPa). The failure mechanism is crushing of the concrete. The shear-shear strain plot of this failure is given in Figure B.8.

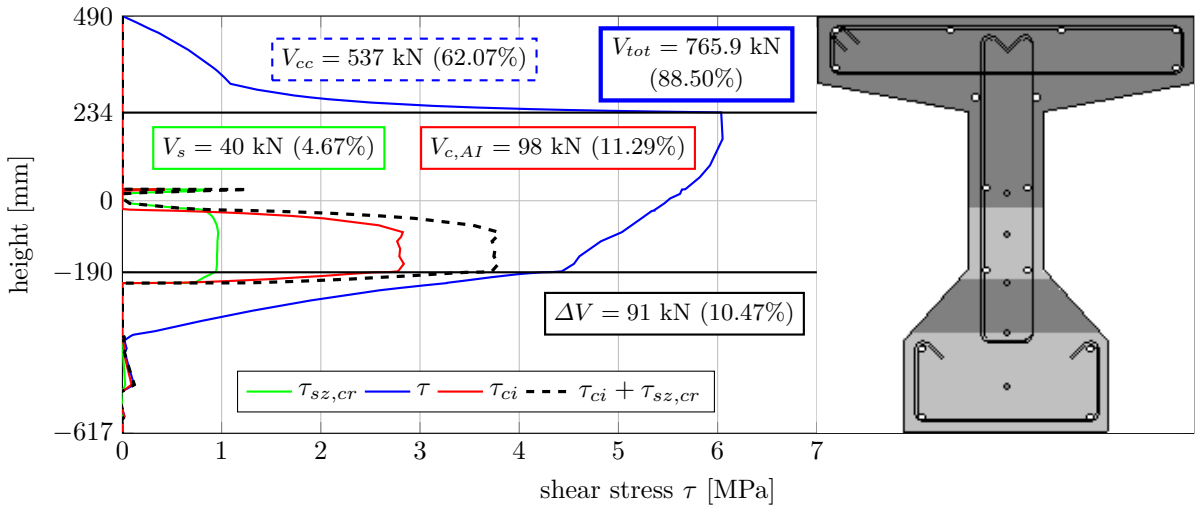

Figure B.9: Contribution of each component to the shear resistance for $a = 2.903$ m, $x = 1.900$ m and $N_p = 1598$ kN

The results from Figure B.9 give a total shear resistance V_R of:

$$V_R = V_{tot} + V_p = 765.9 + 99.6 = 865.5 \text{ kN} \tag{B.3}$$

This is a difference of +0.8 kN (+0.09%) with the shear resistance of the V-γ_{xy}-plot given in Figure B.8.

B.4. Summary cross-section x = 2.051 m

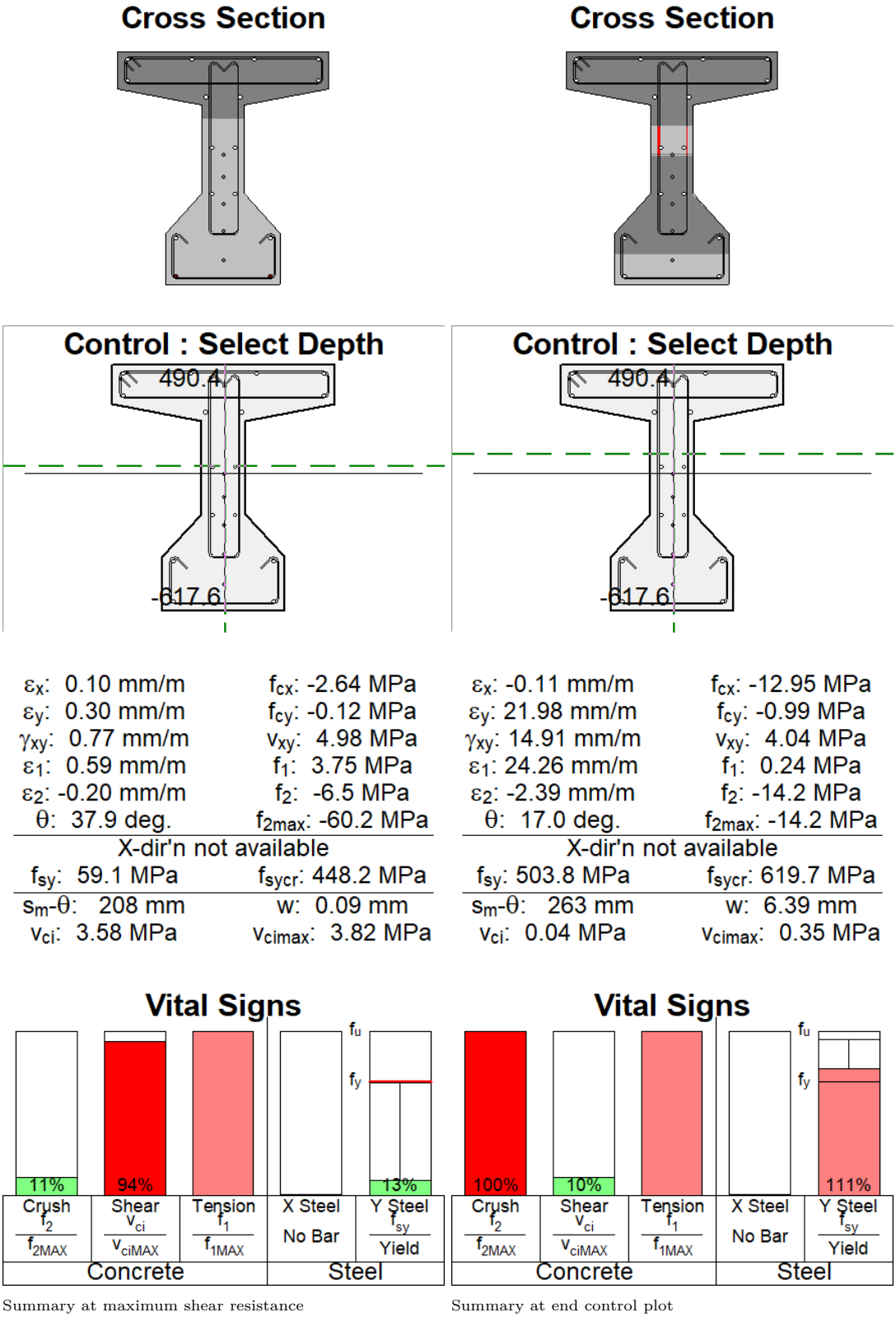

Summary at maximum shear resistance

Summary at end control plot

Figure B.10: Summary from 'Mohr's Circles' tab $x = 2.051$ m

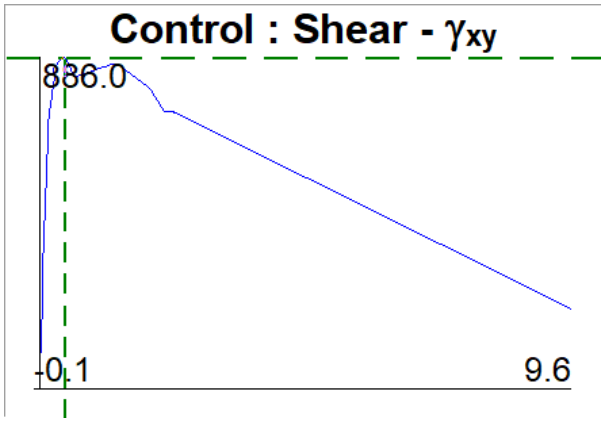

Figure B.11: Control plot for $x = 2.051$ m

Flexural cracking occurs at $V = 702.3$ kN, because the principal tensile capacity is reached at the extreme tension fiber (bottom flange). As the load increases, the height of the cracked zone in the bottom flange increases up to the point where the principal tensile capacity is exceeded in the web at $V = 813.3$ kN. At this point a part of the bottom flange is cracked in bending and diagonal tension cracking occurs in the bottom part of the web. After diagonal tension cracking the load further increases and the stirrups at the crack immediately yield. The maximum load is reached at $V = 886.0$ kN and the web and bottom flange are fully cracked. After reaching this maximum load, slipping of the crack occurs ($\tau_{ci} = \tau_{ci,max}$), the principal compressive capacity decreases and the average angle decreases in the top part of the web. As the shear force further decreases the principal compressive capacity decreases, the principal compressive stress increases, the average angle decreases and the stirrup stress at the crack increases. Just before the last load stage at $V = 739.5$ kN, the principal compressive stress reaches the maximum capacity in the web ($\sigma_2 = \sigma_{2,max} = -14.2$ MPa), with an average angle $\theta = 17.0°$. The stirrup stress at the crack does not rupture ($\sigma_{sz,cr} = 619.7 < 655$ MPa). At the last load stage the buckling of the top flange occurs. The failure mechanism is crushing of the concrete and buckling of the top flange. The shear-shear strain plot of this failure is given in Figure B.11.

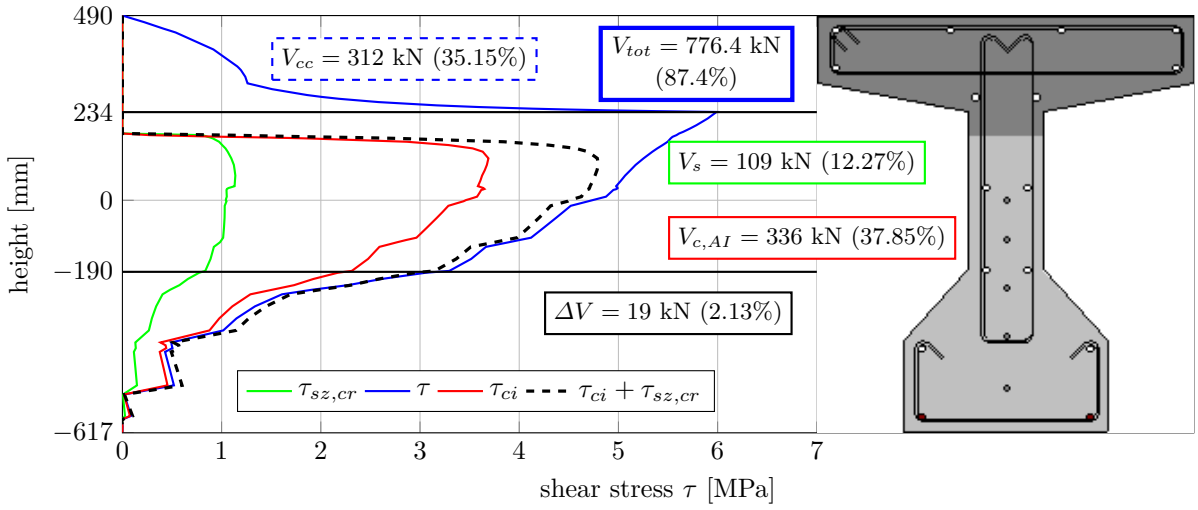

Figure B.12: Contribution of each component to the shear resistance for $a = 2.903$ m, $x = 2.051$ m and $N_p = 1598$ kN

The results from Figure B.12 give a total shear resistance V_R of:

$$V_R = V_{tot} + V_p = 776.3 + 112 = 888.3 \text{ kN} \tag{B.4}$$

This is a difference of +2.3 kN (+0.3%) with the shear resistance of the V-γ_{xy}-plot given in Figure B.11.

B.5. Summary cross-section x = 2.453 m

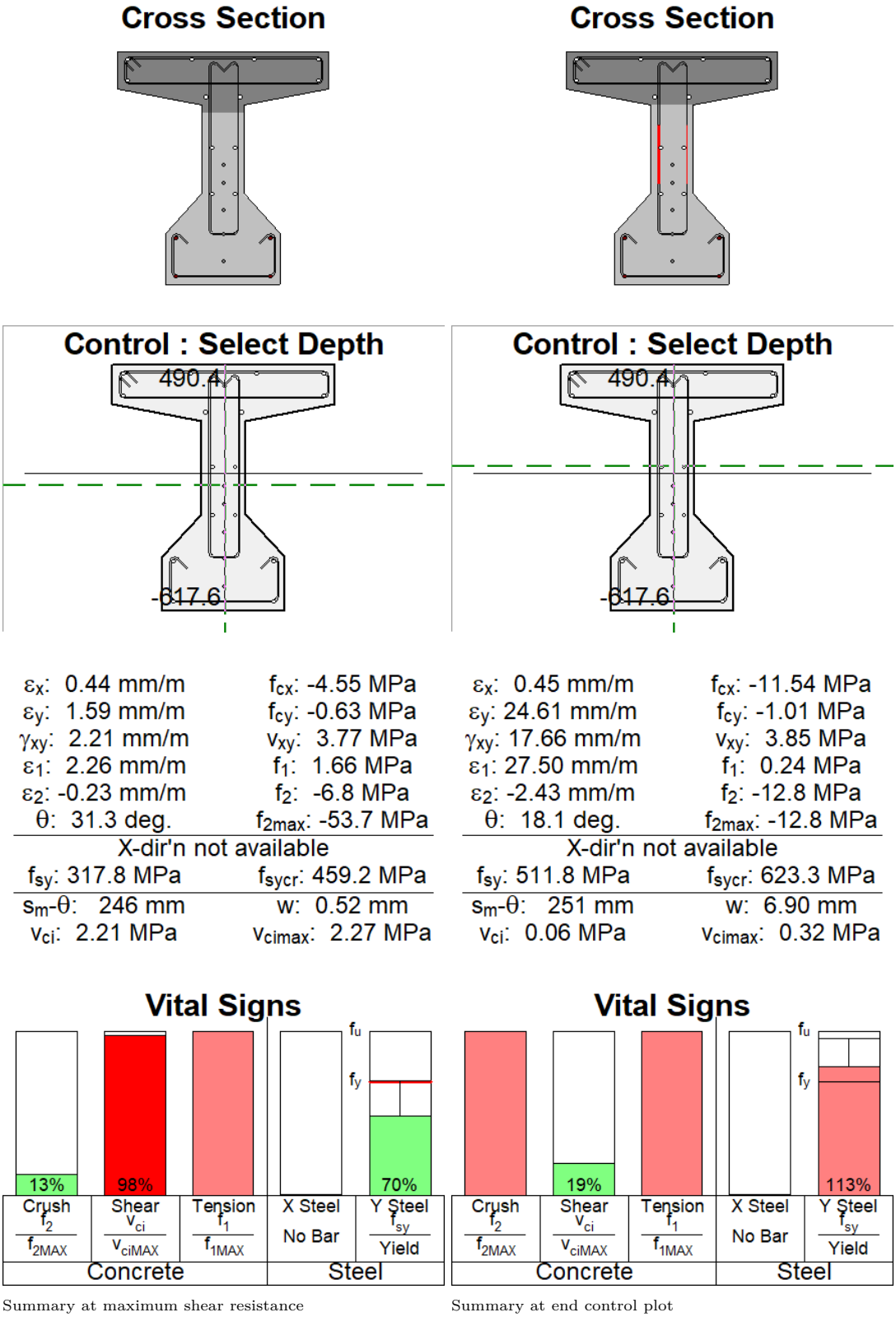

Summary at maximum shear resistance

Summary at end control plot

Figure B.13: Summary from 'Mohr's Circles' tab $x = 2.453$ m

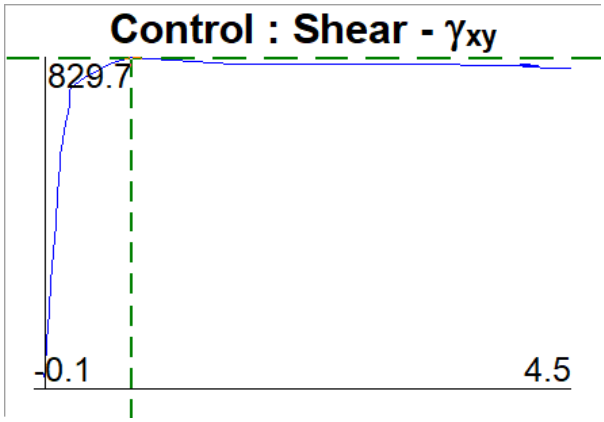

Figure B.14: Control plot for $x = 2.453$ m

Flexural cracking occurs at $V = 598.5$ kN, because the principal tensile capacity is reached at the extreme tension fiber (bottom flange). As the load increases, the height of the cracked zone increases and the stirrups at the crack immediately yield. The maximum load is reached at $V = 829.7$ kN and the web and bottom flange are fully cracked. After reaching the maximum load the load drops, slipping of the crack occurs ($\tau_{ci} = \tau_{ci,max}$), the principal compressive capacity decreases and the average angle decreases in the top part of the web. As the shear force further decreases the principal compressive capacity decreases, the principal compressive stress increases, the average angle decreases and the stirrup stress at the crack increases. At the last load stage the principal compressive stress reaches the maximum capacity in the web ($\sigma_2 = \sigma_{2,max} = -12.8$ MPa), with an average angle $\theta = 18.1°$. The stirrup stress at the crack does not rupture ($\sigma_{sz,cr} = 623.3 < 655$ MPa). The failure mechanism is crushing of the concrete. The shear-shear strain plot of this failure is given in Figure B.14.

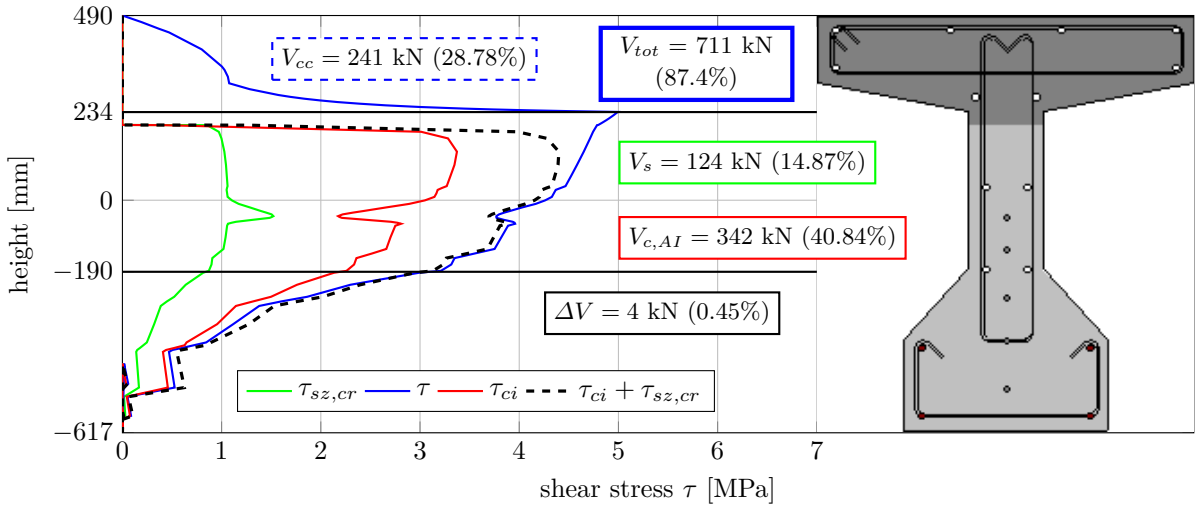

Figure B.15: Contribution of each component to the shear resistance for $a = 2.903$ m, $x = 2.453$ m and $N_p = 1598$ kN

The results from Figure B.15 give a total shear resistance V_R of:

$$V_R = V_{tot} + V_p = 711 + 126.2 = 837.2 \text{ kN} \tag{B.5}$$

This is a difference of +7.5 kN (+0.9%) with the shear resistance of the V-γ_{xy}-plot given in Figure B.14.

C

Response-2010 results
a = 2.903 m, N = 2808 kN

C.1. Summary cross-section x = 1.725 m

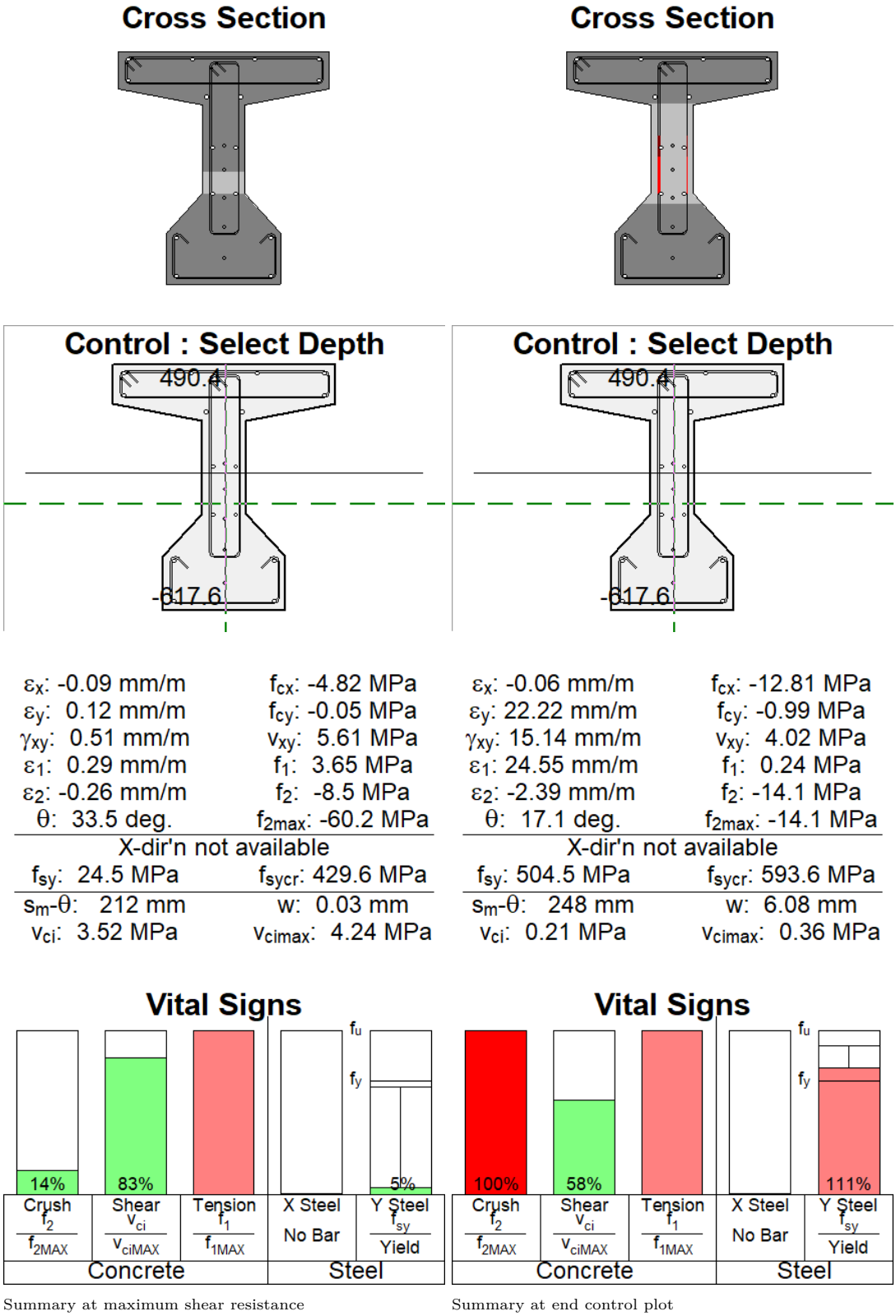

Summary at maximum shear resistance

Summary at end control plot

Figure C.1: Summary from 'Mohr's Circles' tab $x = 1.725$ m

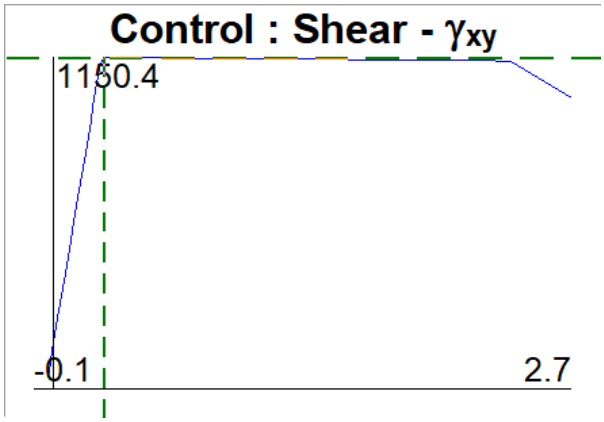

Figure C.2: Control plot for $x = 1.725$ m

Diagonal tension cracking occurs at $V = 1150.4$ kN, because the principal tensile capacity is exceeded in the bottom part of the web. At this step the maximum load is reached, although the stirrups are not yielding ($\sigma_{sz,cr} = 430.4 < 454$ MPa). After reaching the maximum load, flexural cracks occur at the extreme tensile fiber and the height of the cracked zone increases in the web. The stirrups at the crack immediately yield, slipping of the crack occurs ($\tau_{ci} = \tau_{ci,max}$), the principal compressive capacity decreases and the average angle decreases in the top part of the web. At the last load stage the principal compressive stress reaches the maximum capacity in the web ($\sigma_2 = \sigma_{2,max} = -14.1$ MPa), with an average angle $\theta = 17.1°$. The stirrup stress at the crack does not rupture ($\sigma_{sz,cr} = 593.6 < 655$ MPa). The failure mechanism is crushing of the concrete. The shear-shear strain plot of this failure is given in Figure C.2.

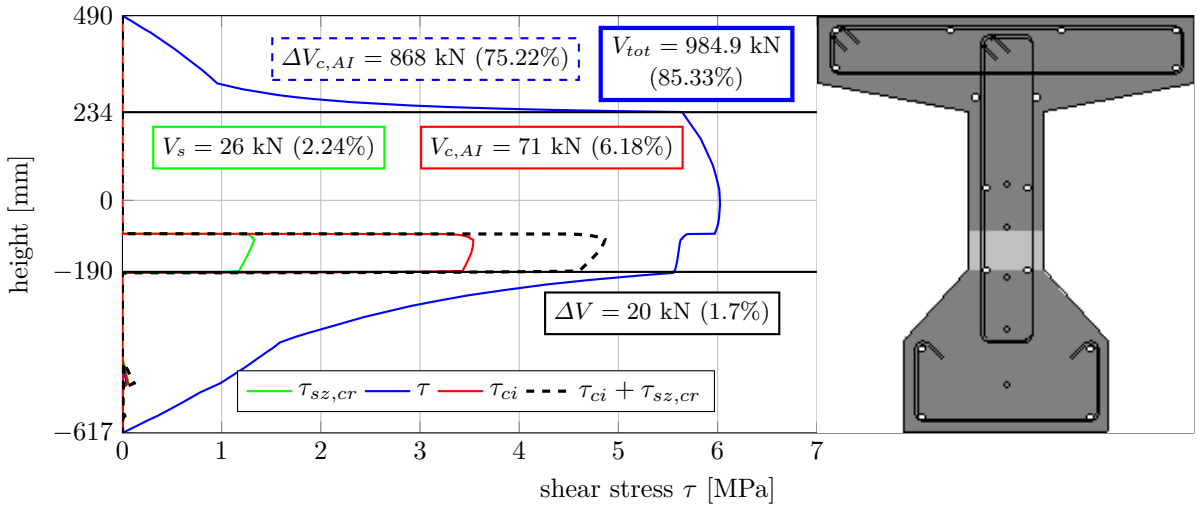

Figure C.3: Contribution of each component to the shear resistance for $a = 2.903$ m, $x = 1.725$ m and $N_p = 2808$ kN

The results from Figure C.3 give a total shear resistance V_R of:

$$V_R = V_{tot} + V_p = 984.9 + 169.3 = 1154.2 \text{ kN} \tag{C.1}$$

This is a difference of +3.8 kN (+0.33%) with the shear resistance of the V-γ_{xy}-plot given in Figure C.2.

C.2. Summary cross-section x = 1.800 m

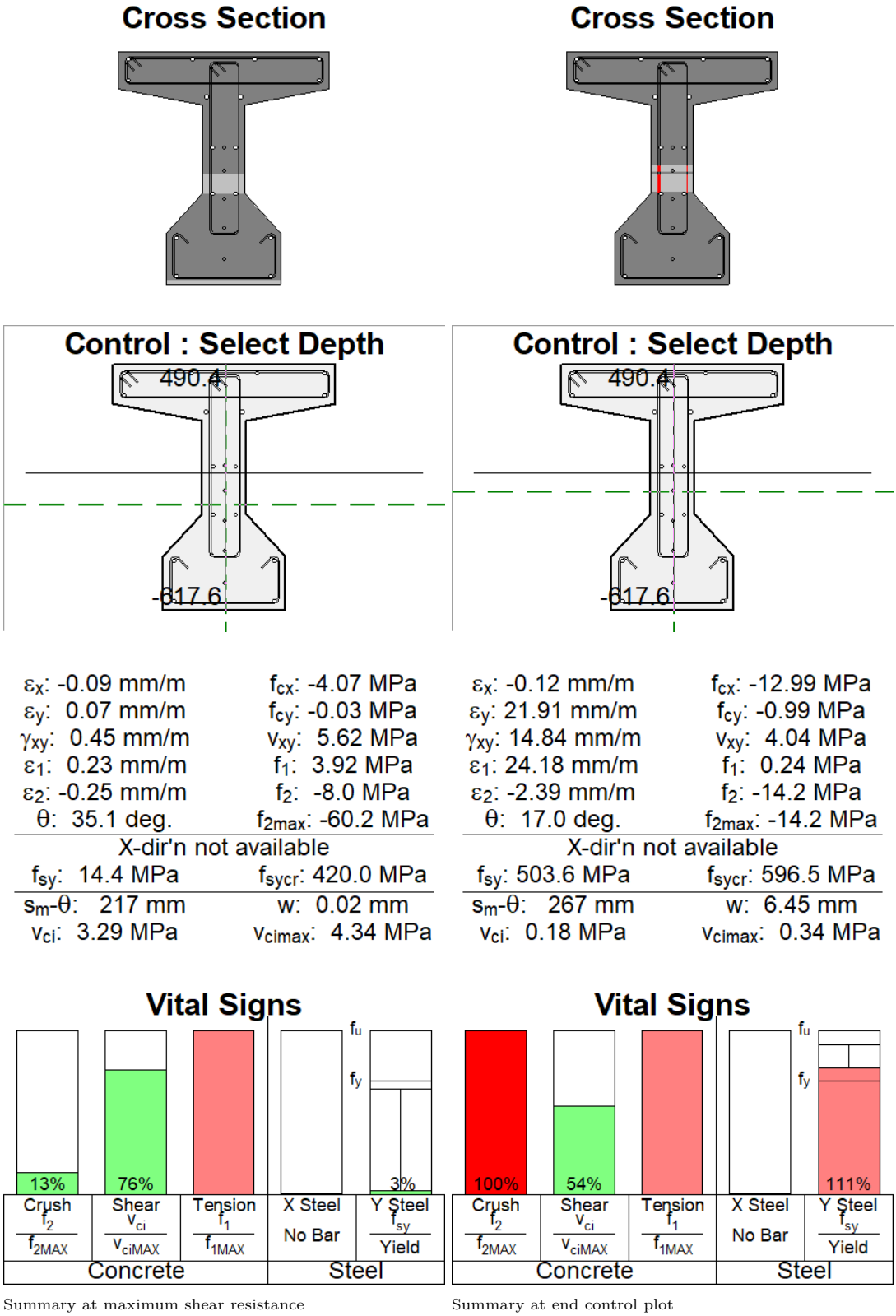

Summary at maximum shear resistance

Summary at end control plot

Figure C.4: Summary from 'Mohr's Circles' tab $x = 1.800$ m

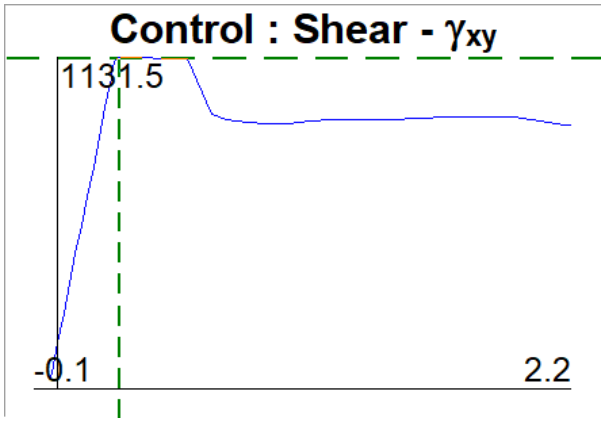

Figure C.5: Control plot for $x = 1.800$ m

Diagonal tension cracking occurs at $V = 1131.5$ kN, because the principal tensile capacity is exceeded in the bottom part of the web. At this step the maximum load is reached, although the stirrups are not yielding ($\sigma_{sz,cr} = 420.6 < 454$ MPa). After reaching the maximum load, flexural cracks occur at the extreme tensile fiber and the height of the cracked zone increases in the web. The stirrups at the crack immediately yield, slipping of the crack occurs ($\tau_{ci} = \tau_{ci,max}$), the principal compressive capacity decreases and the average angle decreases in the top part of the web. At the last load stage the principal compressive stress reaches the maximum capacity in the web ($\sigma_2 = \sigma_{2,max} = -14.2$ MPa), with an average angle $\theta = 17.0°$. The stirrup stress at the crack does not rupture ($\sigma_{sz,cr} = 596.5 < 655$ MPa). The failure mechanism is crushing of the concrete. The shear-shear strain plot of this failure is given in Figure C.5.

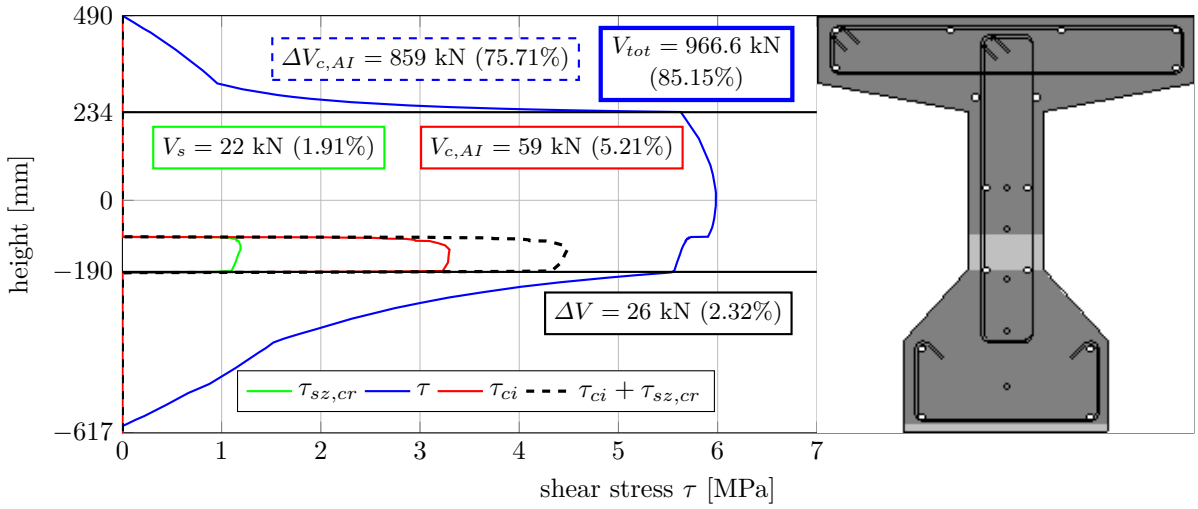

Figure C.6: Contribution of each component to the shear resistance for $a = 2.903$ m, $x = 1.800$ m and $N_p = 2808$ kN

The results from Figure C.6 give a total shear resistance V_R of:

$$V_R = V_{tot} + V_p = 966.6 + 168.5 = 1135.1 \text{ kN} \tag{C.2}$$

This is a difference of +3.6 kN (+0.32%) with the shear resistance of the V-γ_{xy}-plot given in Figure C.5.

C.3. Summary cross-section x = 1.900 m

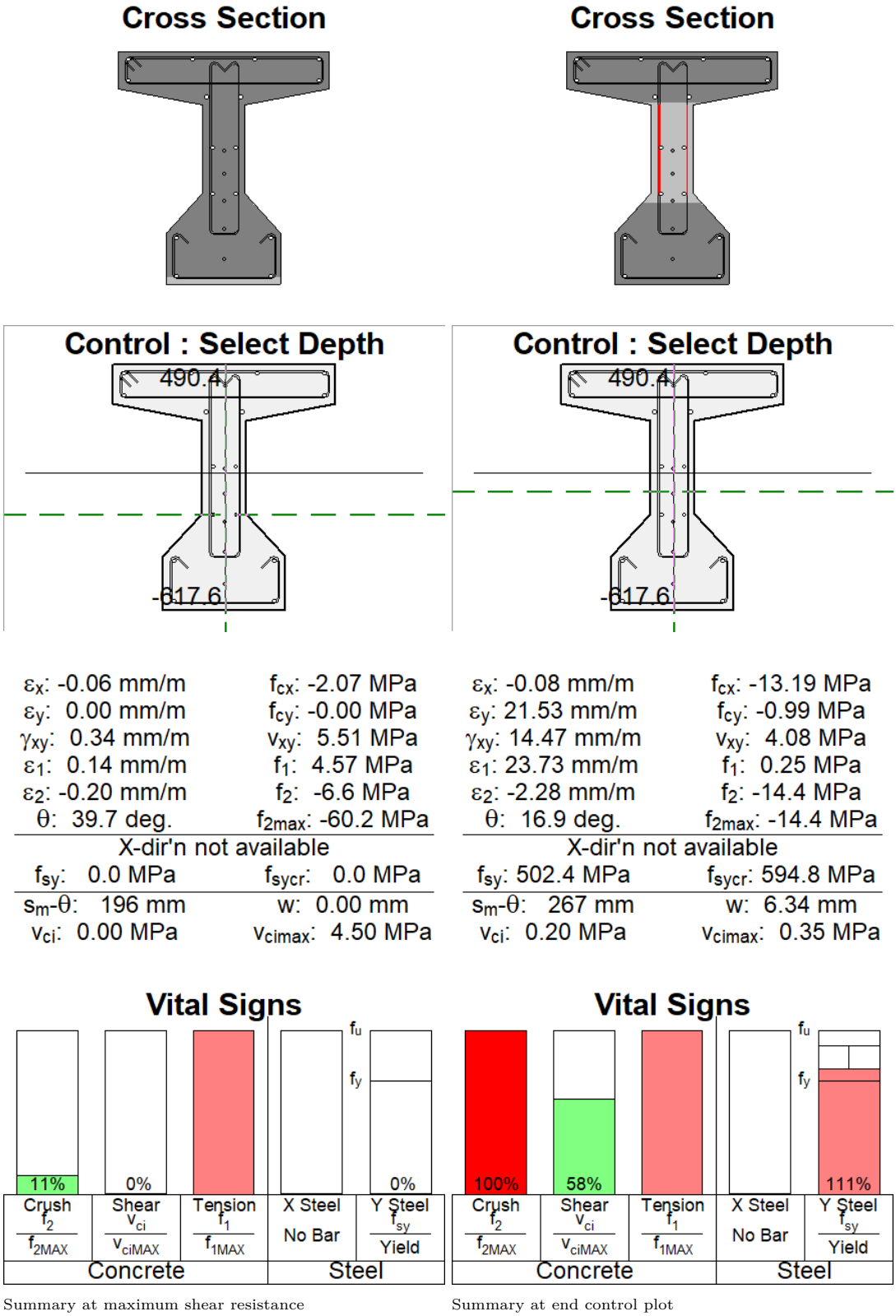

Summary at maximum shear resistance

Summary at end control plot

Figure C.7: Summary from 'Mohr's Circles' tab $x = 1.900$ m

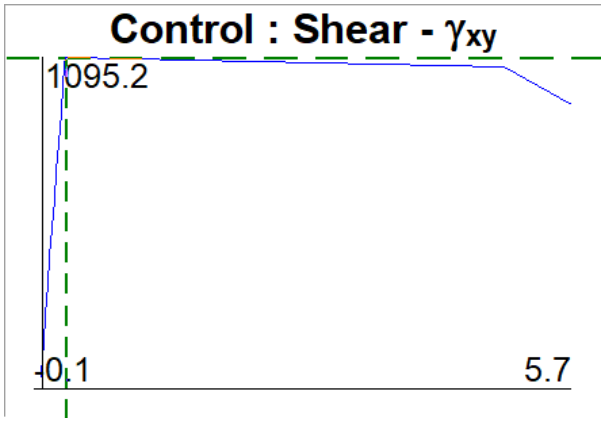

Figure C.8: Control plot for $x = 1.900$ m

Diagonal tension cracking occurs at $V = 1095.2$ kN, because the principal tensile capacity is exceeded in the bottom part of the web (not visible in the cross-section given by `Response-2010`, but it is visible from the Vital Signs graph). At this step the maximum load is reached, although the stirrups are not yielding ($\sigma_{sz,cr} = 0 < 454$ MPa). After reaching the maximum load, flexural cracks occur at the extreme tensile fiber and the height of the cracked zone increases in the web. The stirrups at the crack immediately yield, slipping of the crack occurs ($\tau_{ci} = \tau_{ci,max}$), the principal compressive capacity decreases and the average angle decreases in the top part of the web. At the last load stage the principal compressive stress reaches the maximum capacity in the web ($\sigma_2 = \sigma_{2,max} = -14.4$ MPa), with an average angle $\theta = 16.9°$. The stirrup stress at the crack does not rupture ($\sigma_{sz,cr} = 594.8 < 655$ MPa). The failure mechanism is crushing of the concrete. The shear-shear strain plot of this failure is given in Figure C.8.

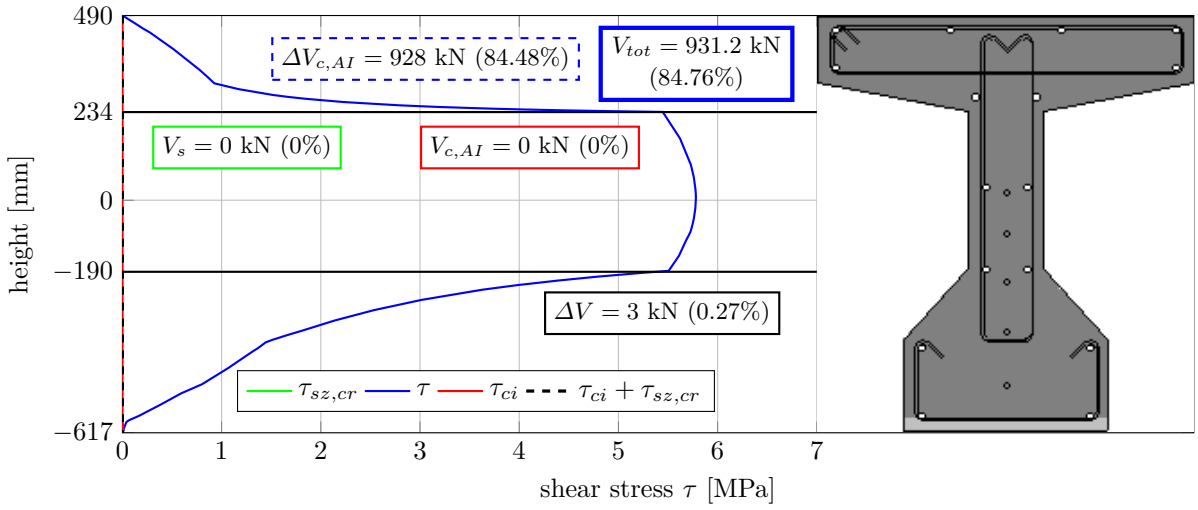

Figure C.9: Contribution of each component to the shear resistance for $a = 2.903$ m, $x = 1.900$ m and $N_p = 2808$ kN

The results from Figure C.9 give a total shear resistance V_R of:

$$V_R = V_{tot} + V_p = 931.2 + 167.4 = 1098.6 \text{ kN} \tag{C.3}$$

This is a difference of +3.4 kN (+0.31%) with the shear resistance of the V-γ_{xy}-plot given in Figure C.8.

C.4. Summary cross-section x = 2.051 m

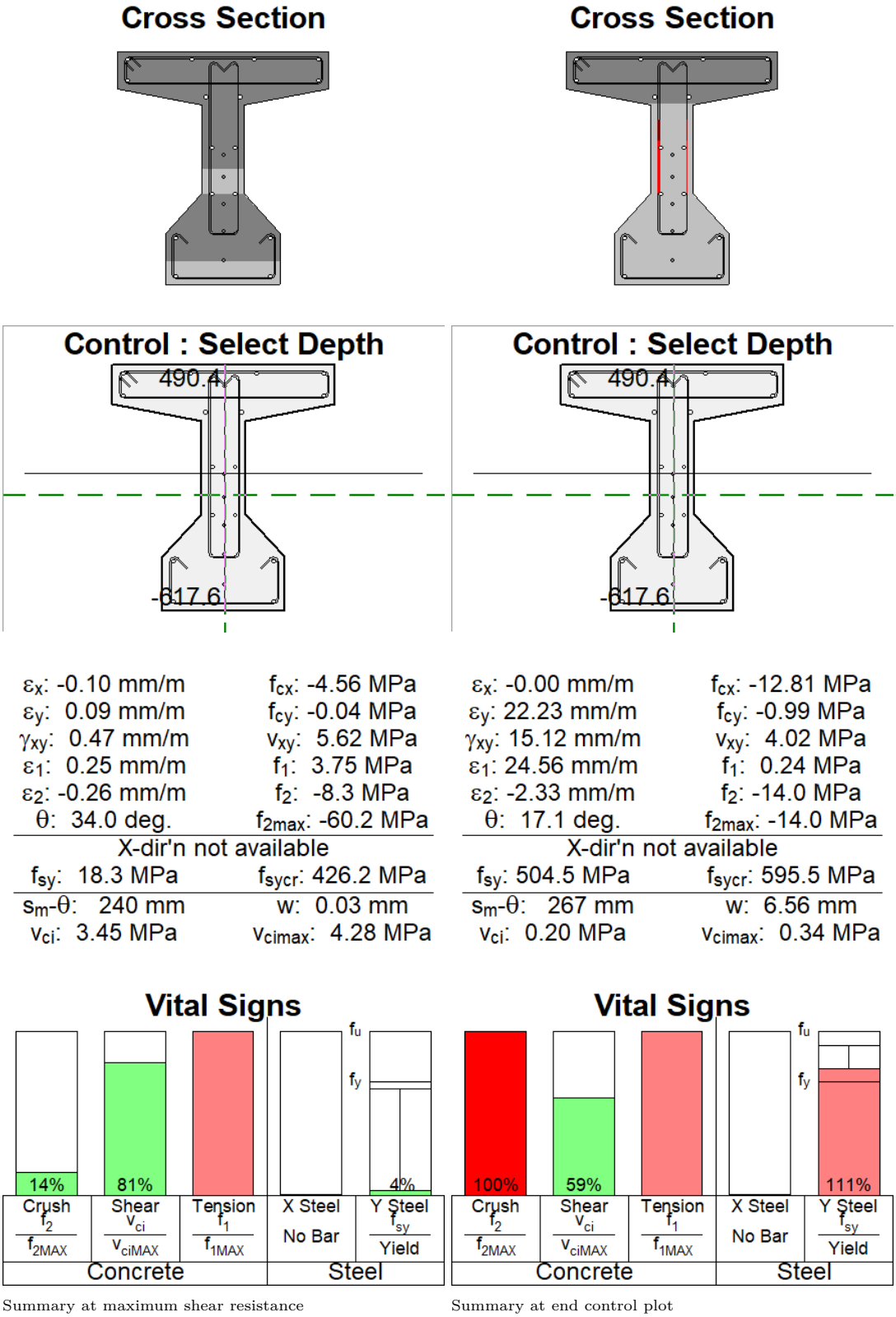

Summary at maximum shear resistance

Summary at end control plot

Figure C.10: Summary from 'Mohr's Circles' tab $x = 2.051$ m

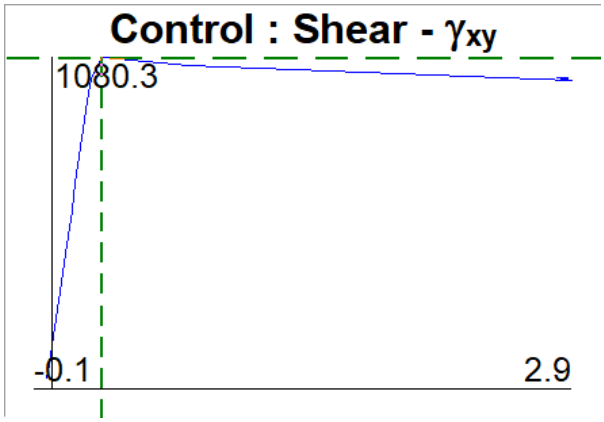

Figure C.11: Control plot for $x = 2.051$ m

Flexural cracking occurs at $V = 1007.8$ kN, because the principal tensile capacity is reached at the extreme tension fiber (bottom flange). As the load increases, the height of the cracked zone in the bottom flange increases up to the point where the principal tensile capacity is exceeded in the web at $V = 1080.3$ kN. At this point a part of the bottom flange is cracked in bending and diagonal tension cracking occurs in the bottom part of the web. After diagonal tension cracking (next load step) the load drops, the stirrups at the crack immediately yield, slipping of the crack occurs ($\tau_{ci} = \tau_{ci,max}$), the principal compressive capacity decreases and the average angle decreases in the top part of the web. The web and bottom flange are fully cracked at this step. As the shear force further decreases the principal compressive capacity decreases, the principal compressive stress increases, the average angle decreases and the stirrup stress at the crack increases. At the last load stage the principal compressive stress reaches the maximum capacity in the web ($\sigma_2 = \sigma_{2,max} = -14.0$ MPa), with an average angle $\theta = 17.1°$. The stirrup stress at the crack does not rupture ($\sigma_{sz,cr} = 595.5 < 655$ MPa). The failure mechanism is crushing of the concrete. The shear-shear strain plot of this failure is given in Figure C.11.

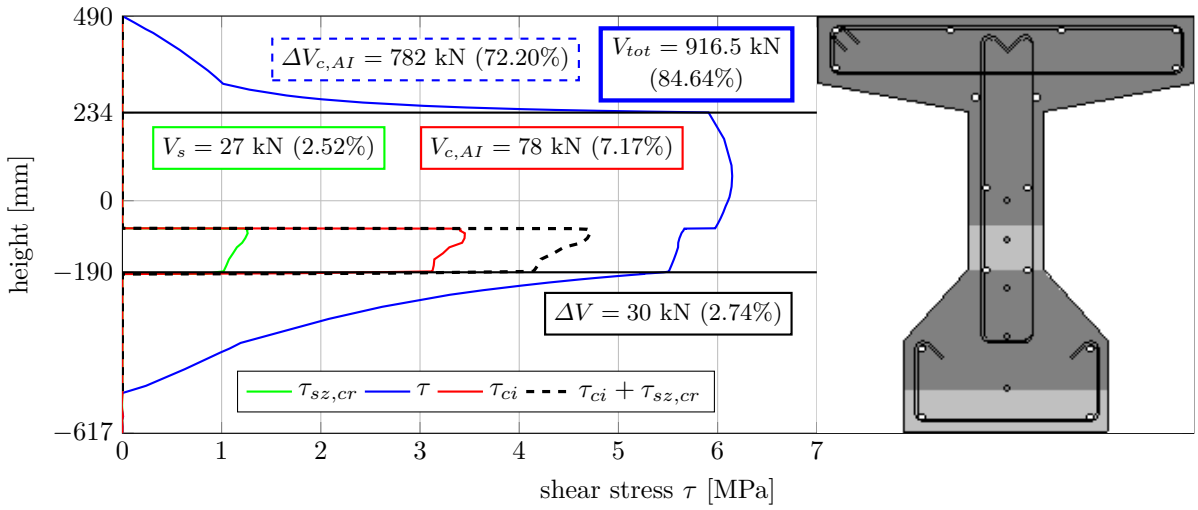

Figure C.12: Contribution of each component to the shear resistance for $a = 2.903$ m, $x = 2.051$ m and $N_p = 2808$ kN

The results from Figure C.12 give a total shear resistance V_R of:

$$V_R = V_{tot} + V_p = 916.5 + 166.4 = 1082.9 \text{ kN} \tag{C.4}$$

This is a difference of +2.6 kN (+0.24%) with the shear resistance of the V-γ_{xy}-plot given in Figure C.11.

C.5. Summary cross-section x = 2.453 m

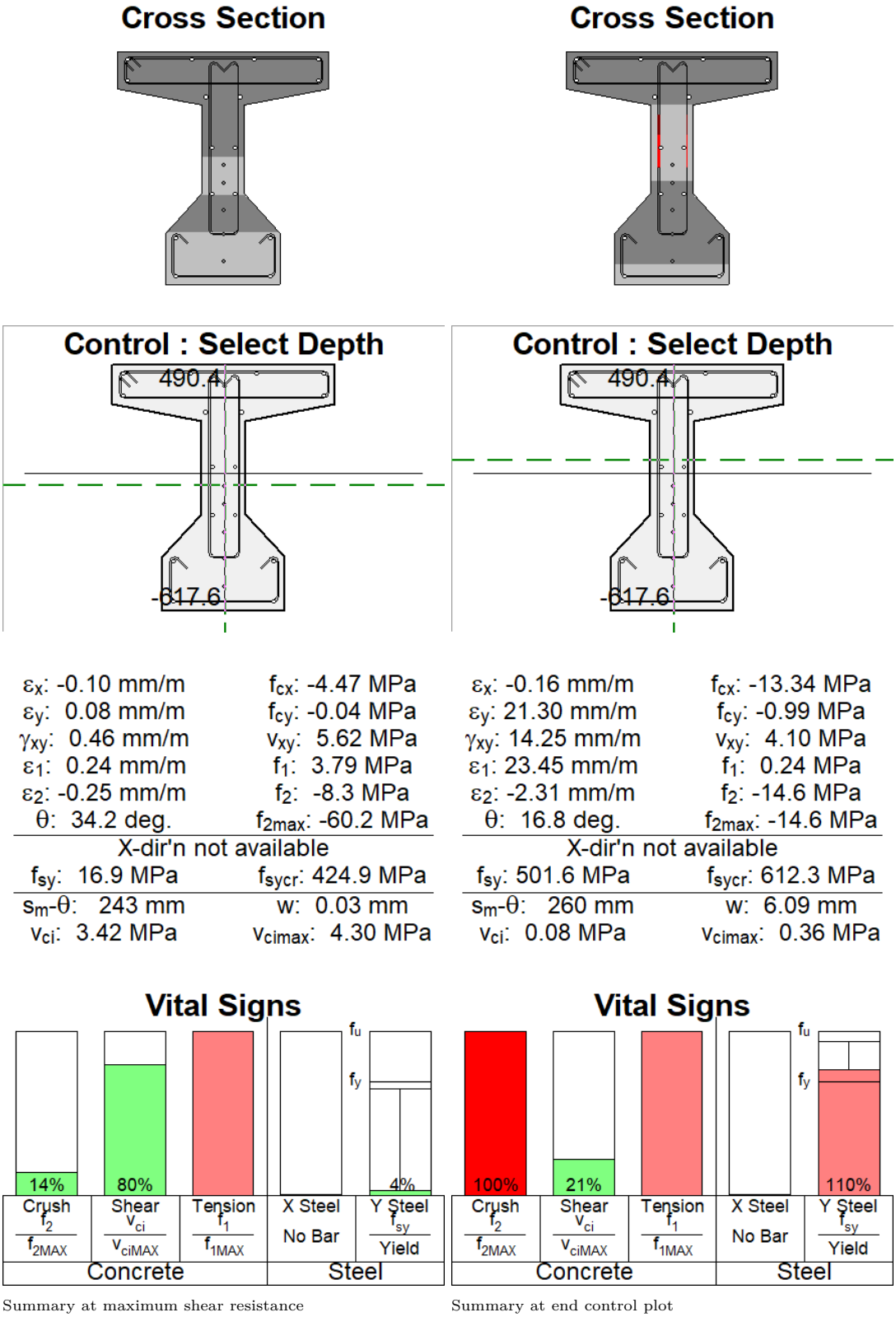

Summary at maximum shear resistance

Summary at end control plot

Figure C.13: Summary from 'Mohr's Circles' tab $x = 2.453$ m

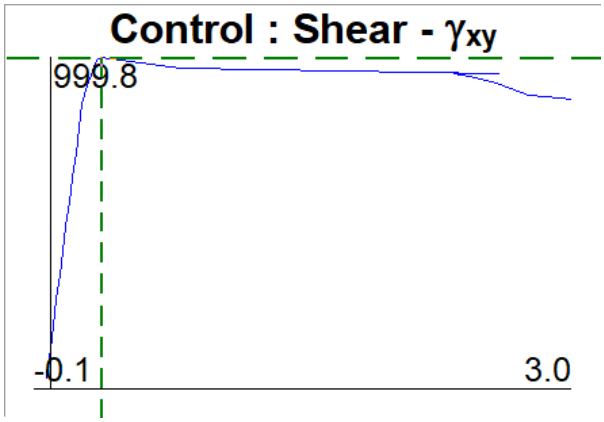

Figure C.14: Control plot for $x = 2.453$ m

Flexural cracking occurs at $V = 915.4$ kN, because the principal tensile capacity is reached at the extreme tension fiber (bottom flange). As the load increases, the height of the cracked zone in the bottom flange increases up to the point where the principal tensile capacity is exceeded in the web at $V = 999.8$ kN. At this point a part of the bottom flange is cracked in bending and diagonal tension cracking occurs in the bottom part of the web. After diagonal tension cracking (next load step) the load drops, the stirrups at the crack immediately yield, slipping of the crack occurs ($\tau_{ci} = \tau_{ci,max}$), the principal compressive capacity decreases and the average angle decreases in the top part of the web. The web and bottom flange are fully cracked at this step. As the shear force further decreases the principal compressive capacity decreases, the principal compressive stress increases, the average angle decreases and the stirrup stress at the crack increases. At the last load stage the principal compressive stress reaches the maximum capacity in the web ($\sigma_2 = \sigma_{2,max} = -14.6$ MPa), with an average angle $\theta = 16.8°$. The stirrup stress at the crack does not rupture ($\sigma_{sz,cr} = 612.3 < 655$ MPa). The failure mechanism is crushing of the concrete. The shear-shear strain plot of this failure is given in Figure C.14.

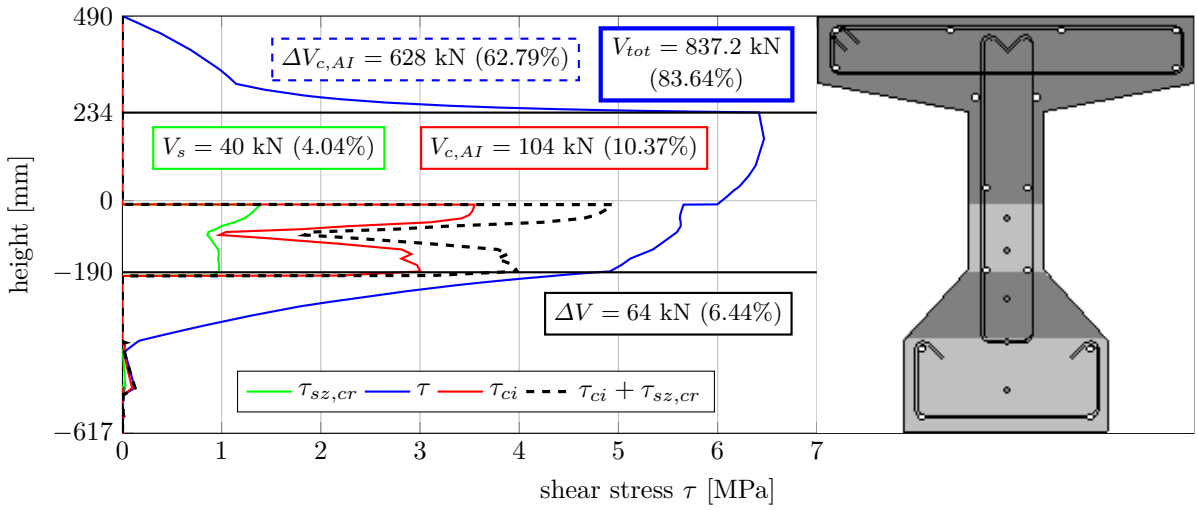

Figure C.15: Contribution of each component to the shear resistance for $a = 2.903$ m, $x = 2.453$ m and $N_p = 2808$ kN

The results from Figure C.15 give a total shear resistance V_R of:

$$V_R = V_{tot} + V_p = 837.2 + 163.8 = 1001 \text{ kN} \tag{C.5}$$

This is a difference of +1.2 kN (+0.12%) with the shear resistance of the V-γ_{xy}-plot given in Figure C.14.